(2)

RESEARCH CENTER FOR THE

PENNSTATE ENGINEERING OF ELECTRONIC & ACOUSTIC MATERIALS

College of Engineering/Materials Research Laboratory
149 Hammond Building
University Park, PA 16802

(814) 863-4210
(814) 865-2481
FAX (814) 865-3052
Co-Directors:
V.K. Varadan
L.E. Cross

August 10, 1990

Dr. R. C. Pohanka
Office of Naval Research
Code 1131
800 N. Quincy Street
Arlington, VA 22217-5000

Dear Dr. Pohanka:

Please find enclosed two copies of the Final Report for Contract Number: N0014-87-K-0031, Work Unit Number: 431d010, Scientific Officer: Dr. Wallace Smith.

This contract supports theoretical research in "Wave Material Interaction and Design of Composite Materials: and is complemented by ongoing experimental work in the Research Center for the Engineering of Electronic and Acoustic Materials. A major focus for theoretical and experimental research has been in the area of chiral composite materials. This has resulted in the publication of the first monograph on the subject by Springer Verlag and on the experimental side, we have been able to measure for the very first time the chirality parameter of chiral materials in the 8 - 40 GHz frequency range. ONR Materials Division can take credit for their vision and foresight in funding research in this exciting new field. Equally strong strides have been taken in the area of piezoelectric composites for active acoustic absorbers and active vibration control, as well as in the field of microwave processing and joining of ceramics.

We wish to express our sincere appreciation for your support and interest. Due to an unfortunate misunderstanding, this report which was prepared in December 1989 was never mailed out. We apologize for the delay. With best regards,

Sincerely,

Vasundara V. Varadan
Distinguished Alumni Professor of Engr.
Professor, Engr. Science & Electrical Engr.

Vijay K. Varadan
Distinguished Alumni Professor of Engr.
Professor, Engr. Science & Electrical Engr.
Co-Director, Research Center for the Engineering of Electronic and Acoustic Materials

VVV/akh

enclosures

cc: W. Smith

ONR CONTRACT INFORMATION

Contract Title: Studies in wave-material interaction and design of composite materials.

Contract Number: N00014-87-K-0031

Work Unit Number: 431d010

Scientific Officer: Wallace Smith

STATEMENT "A" per Dr. Wallace Smith
ONR/Code 1131F
TELECON 8/30/90 VG

A. DESCRIPTION OF THE SCIENTIFIC RESEARCH GOALS

The thrust of this project is to come up with the design and specification of advanced composite materials using dielectric ceramics, chiral polymers or piezoelectric materials as inclusions with polymer-based materials as the binders. The research is theoretical and complements the associated experimental and developmental programs on such materials at the Research Center for the Engineering of Electronic and Acoustic Materials and the Materials Research Laboratory. Basic research on the interaction of electromagnetic and acoustic fields with composite materials at wavelengths comparable to inclusion size and spacing were to be studied to come up with structure- property relations that offer better possibilities for controling material behavior than those permitted by simple mixing rules. Emphasis was on chiral composites, piezoelectric composites, fractal composites, and ferrite composites.

B. SIGNIFICANT RESULTS IN THE PAST YEAR

Much progress has been achieved during the three years of this program as evidenced by the numerous publications in refereed journals.

Basic research on the electromagnetics of chiral media have now been applied to chiral waveguides, chiral mirrors and their applications, Green's functions for chiral media which were then used in the solution of several problems of practical interest. The first monograph on this subject entitled " *Time Harmonic Electromagnetic Fields in Chiral Media* " , co–authored by Lakhtakia, Varadan and Varadan was published by Springer – Verlag in 1989. Multiple scattering calculations have been extended to composites containing chiral inclusions, as well as anisotropic inclusions. We have demonstrated that chirality significantly alters the absorption characteristics of an otherwise low loss composite. This has also been verified by experiments on chiral composites designed and prepared at our laboratory and measured in the 8 – 18 GHz frequency range. The chirality parameter β has been measured for the first time for chiral materials. This parameter has not been measured for optically active materials, although that phenomenon has been known and studied for over one hundred years.

Composites containing anisotropic inclusions have been modeled, treating for the first time

the effects of inclusion anisotropy. A new coupled dipole model was formulated and implemented numerically to compute the single scatterer response. These were then included in the multiple scattering computations. The results were then compared with models which neglect the anisotropy of the inclusions. The differences are tremendous and wrong approximations can lead to gross errors.

The phenomenon of back scattering enhancement is of great practical interest because it may permit imaging through composite media. This particular problem is engaging the interest of several theorists and experimentalists. Using our multiple scattering formulation, we have been able to obtain good agreement with enhancement observed experimentally on random systems in the optical region.

The theoretical problems associated with the microwave sintering of ceramics fit very well into the scope of our multiple scattering studies. Green ceramics in the form of porous pellets have a high dielectric loss tangent, leading to absorption of microwave power and resulting increase of temperature and loss tangent. This creates a condition for rapid increase of temperature often referred to as temperature runaway. By theoretically analyzing the effective properties of the porous ceramic, the thermal runaway condition can be predicted by including thermal effects via a diffusion equation and hot wall boundary conditions correlated with experimental observations. Research is ongoing in this area.

Inverse problems associated with ferrite composites have been studies. Ferrite composites have both dielectric and magnetic properties which are complex and frequency dependent. From measurements of the propagation constant, it is not possible to infer both properties. An inverse procedure has been proposed and has been tested against experimental data. It can be used to infer constituent properties from the data. This is a convenient way of obtaining constituent properties, especially for constituents in powder form.

C. PLANS FOR NEXT YEAR'S RESEARCH

This is the final report for the three year program. The Center will continue development of further applications of novel chiral composite as well as piezoelectric composite coatings for various types of sensors and coatings.

D. LIST OF PUBLICATIONS, REPORTS, PRESENTATIONS

1. Papers Published in Refereed Journals

T.R. Howarth, 'Book Review of Power Sonic and Ultrasonic Transducers Design,' *J. Acoust. Soc. Am.* **85**, 1989, 520-521 (B).

T.R. Howarth, 'Experimental studies using chiral composites as acoustic energy attenuators,' *J. Acoust. Soc. Am.* **84**, 1988, 1557 (T).

A. Lakhtakia, R. Messier, V.V. Varadan & V.K. Varadan, 'Incommensurate numbers, continued fractions, and fractal immittances,' *Z. Naturforsch. A* **43**, 1988, 943 - 955.

A. Lakhtakia, V.K. Varadan & V.V. Varadan, 'Excitation of a planar achiral/chiral interface by near fields,' *J. Wave-Mater. Interact.* **3**, 1988, 231 - 241.

A. Lakhtakia, V.V. Varadan & V.K. Varadan, 'What happens to plane waves at the planar interfaces of mirror-conjugated chiral media,' *J. Opt. Soc. Am. A* **6**, 1989, 23 - 26.

A. Lakhtakia, V.K. Varadan & V.V. Varadan, 'Green's functions for acoustic propagation of sound in a simply moving fluid,' *J. Acoust. Soc. Am.* **85**, 1989, 1852 - 1856.

A. Lakhtakia, V.V. Varadan & V.K. Varadan, 'Time-harmonic and time-dependent dyadic Green's functions for some uniaxial gyroelectromagnetic media,' *Appl. Opt.* **28**, 1989, 1049 - 1052.

A. Lakhtakia, V.K. Varadan & V.V. Varadan, 'Eigenmodes of a chiral sphere with a perfectly conducting coating,' *J. Phys. D* **22**, 1989, 825 - 828.

A. Lakhtakia, V.K. Varadan & V.V. Varadan, 'Influence of impedance mismatch between a chiral scatterer and the surrounding chiral medium,' *J. Mod. Opt.* **36**, 1989, 1385 - 1392.

Y. Ma, V.K. Varadan & V.V. Varadan, 'Effective properties of microwave composites,' *J. Wave-Mater. Interact.* **3**, 1988, 243 - 248.

V.K. Varadan, A. Lakhtakia & V.V. Varadan, 'Propagation in a parallel-plate waveguide wholly filled with a chiral medium,' *J. Wave-Mater. Interact.* **3**, 1988, 267 - 272.

V.V. Varadan, A. Lakhtakia & V.K. Varadan, 'Scattering by three-dimensional anisotropic scatterers,' *IEEE Trans. Antennas Propagat.* **37**, 1989, 800 - 802. *J. Wave-Mater. Interact.* 3, 1988, 243 - 248.

2. Technical Reports

3a. Invited Presentations

V.K. Varadan, Y. Ma and V.V. Varadan, 'Modelling of dielectric properties of porous ceramics during microwave sintering,' *91st Annual Meeting of American Ceramic Society*, Indianapolis, Indiana, April 23-27, 1989.

3b. Contributed Presentations

X.Q. Bao, J.H. Jeng, V.V. Varadan and V.K. Varadan, 'Designing and analyzing the performance of PZT/polymer composite probes. II,' *91st Annual Meeting of American Ceramic Society*, Indianapolis, Indiana, April 23-27, 1989.

X.Q. Bao, V.V. Varadan and V.K. Varadan, 'Additional damping and wave attenuation in 1-3 piezoelectric composites due to electric conductivity,' *91st Annual Meeting of American Ceramic Society*, Indianapolis, Indiana, April 23-27, 1989.

T.R. Howarth, X.-Q. Bao, V.K. Varadan, V.V. Varadan, 'Large area sensors for active acoustic control systems,' *117th Meeting of the Acoustical Society of America*, Syracuse, New York, May 22-26, 1989.

T.R. Howarth, X.-Q. Bao, V.K. Varadan, V.V. Varadan, 'Passive and active acoustic absorbing materials for underwater applications,' *International Conference on Coatings and Sensors for Acoustic and Electromagnetic/Optical Applications* , University Park, Pennsylvania, May 9-11, 1989.

J.H. Jeng, X.Q. Bao, V.V. Varadan and V.K. Varadan, 'Designing and analyzing the performance of PZT/polymer composite probes. I,' *91st Annual Meeting of American Ceramic Society*, Indianapolis, Indiana, April 23-27, 1989.

A. Lakhtakia, V.V. Varadan & V.K. Varadan, 'On left- and right-circularly polarized waves in isotropic noncentrosymmetric elastic media,' *Second Joint Meeting of the Acoustical Society of America and the Acoustical Society of Japan*, Honolulu, Hawaii, USA, November 14-18, 1988.

A. Lakhtakia, V.K. Varadan & V.V. Varadan, 'Review of recent progress in the electromagnetic theory of chiral media,' *First Progress in Electromagnetics Research Symposium*, Boston, Massachusetts, USA, July 25-26, 1989.

Y. Ma, R. Ro & V.V. Varadan, 'Wave scattering from rough surfaces using the facet-ensemble approach,' *Second Joint Meeting of the Acoustical Society of America and the Acoustical Society of Japan*, Honolulu, Hawaii, USA, November 14-18, 1988.

Y. Ma, V.K. Varadan & D.K. Ghodgaonkar, 'Inverse problems for ferromagnetic composites,' *91st Annual Meeting of American Ceramic Society*, Indianapolis, Indiana, April 23-27, 1989.

Y. Ma, V.K. Varadan & V.V. Varadan, 'Enhanced absorption due to dependent scattering,' 1989 *CRDEC Scientific Conference on Obscuration and Aerosol Research*, Aberdeen Proving Ground, Maryland, June 26-30, 1989.

V.K. Varadan, Y. Ma, V.V. Varadan & A. Lakhtakia, 'Electromagnetic wave propagation in chiral composite materials,'*First Progress in Electromagnetics Research Symposium*, Boston, Massachusetts, USA, July 25-26, 1989.

V.V. Varadan, A. Lakhtakia, Y. Ma & V.K. Varadan, 'Long and intermediate wavelength models for the effective properties of a chiral composite material,' *URSI International Symposium on Electromagnetic Theory*, Stockholm, Sweden, August 14-17, 1989.

S.K. Yang, V.V. Varadan, V.K. Varadan & S. Moghe, 'Transverse waves in structurally chiral media,' *IEEE 1988 Ultrasonics Symposium*, Chicago, Illinois, October 2-5, 1988.

S.K. Yang, V.V. Varadan & V.K. Varadan, 'Characterization and thickness measurement of a ceramic coating using an ultrasonic technique,' *91st Annual Meeting of American Ceramic Society*, Indianapolis, Indiana, April 23-27, 1989.

S.K. Yang, V.V. Varadan & V.K. Varadan, 'Acoustical activity in structurally chiral composites,' *117th Meeting of the Acoustical Society of America*, Syracuse, New York, May 22-26, 1989

4. Books (and sections thereof)

A. Lakhtakia, V.K. Varadan and V.V. Varadan, *Time-Harmonic Electromagnetic Fields in Chiral Media*, Heidelberg: Springer-Verlag, 1989.

V.K. Varadan, Y. Ma, A. Lakhtakia and V.V. Varadan, 'Microwave sintering of ceramics,' in *Microwave Processing of Materials* (Eds.: W.H. Sutton, M.H. Brooks & I.J. Chabinski), Pittsburgh: MRS, 1988.

V.K. Varadan, V.V. Varadan and A. Lakhtakia, 'Principles of microwave interaction with poymeric and organic materials,' in *Microwave Processing of Materials* (Eds.: W.H. Sutton, M.H. Brooks & I.J. Chabinski), Pittsburgh: MRS, 1988.

E. LIST OF AWARDS

Name of Person Receiving Award	Recipient's Institution	Name of Award	Sponsor of Award
T.R. Howarth	Penn State University	1988 Authors Award	Raytheon Company

F. PARTICIPANTS AND THEIR STATUS

V.K. VARADAN (Principal Investigator), Professor

V.V. VARADAN (Principal Investigator), Professor

A. LAKHTAKIA, Assistant Professor

Y. MA, Assistant Professor

T.R. HOWARTH, Graduate Student

Y.W. KIM, Graduate Student

R.-Y. RO, Graduate Student

G. OTHER SPONSORED RESEARCH DURING FY89

	Item	Amount	V.K. Varadan	V.V. Varadan
1.	1989 Center Memberships	$225,000	11.0%	17.0%
2.	Ben Franklin State Support +PA Industrial Support for projects in Materials Research	$320,000	24.5%	27.5%
3.	ONR Contract #N00014-82-K-0339 (Global-local sensing of fluid-structure interactions)	$85,000	0.0%	2.0%
4.	ONR Contract #N00014-89-J-3102 (Global-local SAW sensors for turbulence)	$105,000	3.0%	3.0%

H. PUBLICATIONS / PATENTS / PRESENTATIONS / HONORS REPORT

(Number Only)

Papers Submitted to Refereed Journals (and not yet published):

Papers Published in Refereed Journals: 12

Books (and sections thereof) Submitted for Publications: 0

Books (and sections thereof) Published: 3

Patents Filed: 1

Patents Granted: 0

Invited Presentations at Topical or Scientific / Technical Society Conferences: 1

Contributed Presentations at Topical or Scientific / Technical Society Conferences: 15

Honors / Awards / Prizes: 1

Technical Reports Published or Non-Journal Publications:0

Number of Graduate Students: 3

Number of Post-Docs: 0

BRIEF RESEARCH REPORTS

Electromagnetic Response of Chiral Media

Electromagnetic waves in a chiral medium are circularly birefringent. In other words, left- and right-circularly polarized waves, with different phase velocities, exist in this class of media. In order to describe the electromagnetic properties of *isotropic* chiral media, the usual constitutive equations, $\mathbf{D} = \varepsilon\mathbf{E}$ and $\mathbf{B} = \mu\mathbf{H}$, are inadequate because they admit to a single phase velocity. Instead, $\mathbf{D} = \varepsilon\,[\mathbf{E} + \beta\nabla\times\mathbf{E}]$ and $\mathbf{B} = \mu\,[\mathbf{H} + \beta\nabla\times\mathbf{H}]$; these constitutive relations are symmetric under time-reversality. For a right-handed medium, the chirality parameter $\beta > 0$; while for a left-handed medium, $\beta < 0$. Several theoretical aspects of electromagnetic wave propagation and scattering in isotropic chiral media have been explored, and have been described in the previous Annual Report.

A major activity during the present period was the publication of a book on electromagnetic chirality in the *Lecture Notes in Physics* series published by Springer-Verlag. This is the first book on the subject, and it aims to summarize the recent developments in this exciting new area. Undertook as a service to the electromagnetics community, this book lays down the foundations of electromagnetic theory as applicable to chiral media. [A. Lakhtakia, V.K. Varadan and V.V. Varadan, *Time-Harmonic Electromagnetic Fields in Chiral Media*, Heidelberg: Springer-Verlag, 1989.]

In general, when a wave propagating in a homogeneous isotropic chiral medium encounters a homogeneous isotropic chiral scatterer, both the scattered and the internally induced fields contain LCP and RCP components regardless of the state of polarization of the incident field. In the previous Annual Report, we had shown that the reflected and the transmitted plane waves across the planar interface of a mirror-conjugated chiral media have the same handedness as the incident plane wave. It has now been proved that the scattered as well as the internal fields have the same state of polarization as the incident field, if the scatterer and the surrounding medium are impedance-matched; this conclusion holds regardless of the two chiral parameters involved as well as the geometry of the scatterer. [A. Lakhtakia, V.K. Varadan & V.V. Varadan, 'Influence of impedance mismatch between a chiral scatterer and the surrounding chiral medium,' *J. Mod. Opt.* **36**, 1989, 1385 - 1392.]

A fully vector treatment of the problem of scattering by singly periodic interfaces between

chiral and achiral media was developed. Using an improved T-matrix method of solution, this treatment is able to bypass the restrictions imposed by the Rayleigh hypothesis. In addition, several other related problems have their solutions embedded in the method developed. The specific features of the solution procedure allow it be easily converted for doubly periodic interfaces. The analysis may be useful for developing new surface-relief gratings made using chiral materials. [A. Lakhtakia, V.K. Varadan & V.V. Varadan, 'Scattering by periodic achiral-chiral interfaces,' accepted for publication in *J. Opt. Soc. Am. A*]. Furthermore, the excitation of a planar achiral-chiral interface by near fields was also examined. [A. Lakhtakia, V.K. Varadan & V.V. Varadan, 'Excitation of a planar achiral/chiral interface by near fields,' *J. Wave-Mater. Interact.* 3, 1988, 231 - 241.]

Wave propagation in unidirectionally inhomogeneous chiral media was examined, i.e., the constitutive properties of the chiral media vary along the z axis. It was also assumed that the electromagnetic field was a function of the z coordinate alone. It was shown that the electromagnetic field, in this arrangement, can be decomposed into two mutually-independent circularly-polarized states. Coupled first-order differential equations were derived to describe the fields, and various solution procedures discussed. Extension was made to the case when the medium inhomogeneity is periodic, for which case a perturbational solution was explicitly given.[A. Lakhtakia, V.K. Varadan & V.V. Varadan, 'Propagation along the direction of inhomogeneity in an inhomogeneous chiral medium,' accepted for publication in *Int. J. Engg. Sci.*]

In the previous Annual Report, we had described spherical chiral resonators. Continuing on the same lines, propagation of electromagnetic waves in a parallel-plate waveguide wholly filled with a chiral medium was examined. The dispersion equation derived leads to two sets of modes, and the propagation constants for the two sets were numerically obtained. [V.K. Varadan, A. Lakhtakia & V.V. Varadan, 'Propagation in a parallel-plate waveguide wholly filled with a chiral medium,' *J. Wave-Mater. Interact.* 3, 1988, 267 - 272.]

In another effort to utilize the geometric foundations of chirality, the reflection and the transmission characteristics of a structurally chiral slab had been investigated in the previous year. This effort has been further extended this year. By stacking up unit cells made of (identical) structurally chiral slabs, a periodically inhomogeneous medium was constructed. Each structurally

chiral slab was made up of a certain number of identical uniaxially anisotropic plates, the consecutive optic axes describing either a right- or a left-handed spiral. When the unit cell thickness is very small compared to the principal wavelengths in the uniaxial plates, the periodically inhomogeneous uniaxial medium was shown to be equivalent to a homogeneous biaxial medium, the two optic axes of the equivalent medium being dependent on the handedness of the periodic medium. [V.V. Varadan, A. Lakhtakia & V.K. Varadan, 'Propagation through a periodic chiral arrangement of identical uniaxial dielectric layers and its effective properties,' accepted for publication in *Optik*] A similar result was also obtained when the uniaxial plates were replaced by biaxial plates. [A. Lakhtakia, V.K. Varadan & V.V. Varadan, 'Effective properties of a periodic chiral arrangement of identical biaxially dielectric plates,' accepted for publication in *J. Mater. Res.*]

When particles of considerable concentration are dispersed in a host medium to form a composite, multiple scattering dominates the scattered energy when waves are impinging upon them. While this effect is known and shown for various dense systems, it has never been examined for chiral composites. Therefore, preliminary investigations were undertaken this year. The scattering response of a single chiral particle is cast in terms of a T-matrix. The circular birefringence of chiral media does not generate any difficulties in the present multiple scattering formulation, if and only if the composite medium is assumed to be achiral (or weakly chiral). Although a rigorous multiple scattering formalism needs to be introduced when the effective medium is chiral, at least in the low frequency regime, using Maxwell-Garnett Approximation (MGA), we have derived the dispersion equation for an effectively chiral composite medium. [V.V. Varadan, Y. Ma & V.K. Varadan, 'Effects of chiral microstructure on EM wave propagation in a lossy dielectric composite material,' accepted for publication in *Radio Science*] The low frequency expressions of the dispersion equation using the Bruggeman approximation were also obtained. [V.V. Varadan, A. Lakhtakia, Y. Ma & V.K. Varadan, 'Long and intermediate wavelength models for the effective properties of a chiral composite material,' *URSI International Symposium on Electromagnetic Theory*, Stockholm, Sweden, August 14 - 17, 1989]. Finally, computed results of microwave properties of chiral composite materials, were obtained by the numerical solution of the dispersion equations. [V.K. Varadan, Y. Ma, V.V. Varadan & A. Lakhtakia, 'Electromagnetic wave propagation in chiral composite materials,' *First Progress in Electromagnetics*

Research Symposium, Boston, Massachusetts, USA, July 25 - 26, 1989]

Acoustic Chirality

The premise for acoustic chirality in elastic solids has been investigated by us in the past, and was reported in the Previous Annual Reports. In an effort to synthesize structurally chiral media, layered composites were examined. These are made up by stacking identical uniaxial plates, their consecutive symmetric axes describing either a right- or a left-handed spiral. The field equations governing the harmonic motions of the layered composite were written as a first order matrix ordinary differential equation, where the field variable is a 6-vector consisting of the displacement and traction components. A matrix representation method was used for solving the reflection and transmission characteristics of the layered composites; it is noteworthy that this method is not affected by the number of layers. Numerical results of the plane wave reflection and transmission characteristics were obtained for these chiral arrangements. It was observed that the co-polarized characteristics are unaffected by the structural chirality, while the cross-polarized reflected and transmitted electromagnetic fields are greatly influenced by it. These investigations will shortly be submitted for publication.

Experimental research on the use of chiral composites for acoustic attenuation continued during the present period. The composites were constructed by embedding piezoelectric springs in a polymeric material. Each chiral inclusion was also backed by an air-filled cavity, while echo reduction and insertion loss were measured in an acoustic pulse tube. The results of our investigations demonstrated that underwater sound attenuation could be enhanced by embedding chiral-shaped inclusions in polymeric materials. Further research is in progress.

Effective Properties of Ferromagnetic Composites

Ferrite composite materials as well as other ferromagnetic, carbonyl iron composites have recently received wide attention due to their various applications over quite a broad microwave band. Electromagnetic shielding ability and wave absorbing efficiency are just two of their popular characteristics. In order to use these materials in different environments and to optimize their

capabilities, we must carefully tailor their properties. In this context, we have developed a direct formalism which can be used to predict the effective electromagnetic properties of ferrite composite materials [Y. Ma, V.K. Varadan & V.V. Varadan, 'Prediction of electromagnetic properties of ferrite composites,' submitted for publication in *Progress in Electromagnetic Research*].

In addition, for many types of ferrites, it is hard to directly measure the frequency dependent complex permittivity and permeability due to their high electric conductivities. We have developed a new technique to predict these complex properties using the effective property measurements done for a high (or low) porosity ferrite composite, as well as our mutiple scattering formalism. [Y. Ma, V.K. Varadan & D.K. Ghodgaonkar, 'Inverse problems for ferromagnetic composites,' *91st Annual Meeting of American Ceramic Society*, Indianapolis, Indiana, April 23-27, 1989].

Modified Flux Models and Their Applications to Coating Design

In two- and four- flux models of radiative transfer theory, the scattering coefficients or efficiencies of non-emitting media are commonly computed using the single-scattering albedo, while the interactions among particles are neglected. The flux models are modified by considering multiple scattering. One application of the modified flux model is to predict the opacity of high pigment volume concentration paint coatings. Therefore, we introduced the multiple scattering formalism and have shown from the resulting equations how the multiple scattering albedo can be calculated from the effective propagation constant K. The multiple scattering albedo so obtained can be used in the flux model to compute the diffuse reflectance of the corresponding paint film.

Because the refractive index of pigment particles used in the measurements is direction-dependent, the modeling of an anisotropic scatterer wass introduced. For an unpolarized light source, illuminated anisotropic particles of random orientation can be thought of as having an average refractive index over the optical axes within the particles in most of the visible spectrum. This information is used to compute scattering cross section or the T-matrix.

We also reviewed the existing formalisms of the flux models. The coupled differential equations for the diffuse reflectance and transmittance are solvable in general. However, the coefficients in the equations were modified by incorporating multiple scattering. The boundary

conditions for the real paint films cannot be ignored and we considered two different diffuse substrates in order to justify the opacity through the contrast ratio. Though in most cases theoretical results compare favorably well with those measured, the discrepancies in some case due to either the anisotropic modeling or inaccuracy in the values used for the substrate are discussed [Y. Ma, V.V. Varadan & V.K. Varadan, 'Modified flux models considering multiple scattering - application to opacity of coatings,' submitted, *Applied Optics*].

Enhanced Absorption due to Dependent Scattering

In a recent series of studies on light scattering from pigmented surface coatings or by radiative heat transfer in powder insulators, it has been shown that for densely populated heterogeneous media dependent scattering as well as dependent absorption have to be considered. As a result, for paint opacity, the dependent scattering-absorption can greatly affect the diffuse reflectance as it does the overall thermal radiation resistance of the powder insulation composites. Analogous to the aforementioned applications, chemical and nuclear reactors, fuel combustors, cryogenic insulation, microwave and laser coatings, artificial obscuration materials and many other commercial and military systems usually involve a high concentration of particles. In order to analyze the energy transport characteristics, the dependent scattering and absorption properties cannot be ignored.

The role of multiple scattering on dependent scattering as well as on dependent absorption was investigated for heterogeneous media containing a high concentration of particles. The decrease of scattering and increase of absorption for lossy (with intrinsic absorption) particles in a lossless matrix was quantitatively described by the use of a Rayleigh region solution derived from a multiple scattering formalism. For smaller wavelengths, dependent scattering and absorption was obtained through numerically solving the resulting dispersion equation. Numerical results were computed for lossless particles in a lossy matrix which models an optical coating system. [(i) Y. Ma, V.K. Varadan & V.V. Varadan, 'Enhanced absorption due to dependent scattering,' accepted for publication in *ASME Journal of Heat Transfer;* (ii) Y. Ma, V.K. Varadan & V.V. Varadan, 'Enhanced absorption due to dependent scattering,' *1989 CRDEC Scientific Conference on Obscuration and Aerosol Research*, Aberdeen Proving Ground, Maryland, June 26-30, 1989]

Modeling of Dielectric Properties of Porous Ceramic Materials

In our experimental studies on the microwave sintering of ceramics, it has been observed that the (initial) porosity of the green sample predetermines the subsequent sintering rate [V.K. Varadan, Y. Ma, A. Lakhtakia and V.V. Varadan, 'Microwave sintering of ceramics,' in *Microwave Processing of Materials* (Eds.: W.H. Sutton, M.H. Brooks & I.J. Chabinski), Pittsburgh: MRS, 1988].The change in porosity during sintering is a complex thermodynamic process, rooted in the absorbed microwave energy; the instantaneous absorption depends on the temperature-dependent dielectric loss of the porous sample.

We have proposed a model to quantitatively describe the change in the dielectric properties using the effective two-body inter-particle potentials. These potentials depend on the porosity as well as on the temperature. At the critical porosity (or ,the critical temperature), a phase switch can thus be predicted [V.K. Varadan, Y. Ma and V.V. Varadan, 'Modeling of dielectric properties of porous ceramics during microwave sintering,' *91st Annual Meeting of American Ceramic Society*, Indianapolis, Indiana, April 23-27, 1989]. In addition, using analytical expressions [Y. Ma, V.K. Varadan & V.V. Varadan, 'Effective properties of microwave composites,' *J. Wave-Mater. Interact.* 3, 1988, 243 - 248] we have predicted dielectric properties of some sintered ceramic materials. The computed results compare quite well with those measured which were provided by Georges Roussy from Universite' de Nancy 1, France.

The Journal of the Acoustical Society of America
Vol. 85 (1), January 1989, pp. 520-521.

BOOK REVIEWS

Power Sonic and Ultrasonic Transducers Design

B. Harmonic and J. N. Decarpigny, Eds.

Springer, New York, 1988.
x+249 pp. Price $59.40.

The subject of power sonic and ultrasonic transducers has been rapidly expanding on an international scale over the last several years. This book is a collection of papers resulting from the Proceedings of the International Workshop on the Design of Power Sonic and Ultrasonic Transducers, as held in Lille, France, on 26 and 27 May 1987. A presentation of some of the latest transducer design techniques, applications, and available materials are given. The complete text includes 222 figures and is written in English.

The contents of the book begin with an introductory lecture by B. Tocquet and follows with the 13 papers written by each of the invited Workshop contributors. Each chapter is an individual paper, and, as such, they can stand on their own.

The first chapter is entitled "Power Limitations of Piezoelectric Length Expander Transducers," by Oscar B. Wilson of the U.S. Naval Postgraduate School in Monterey, California. This paper discusses some of the internal and external power limiting factors of electroacoustic transducers. Effective use of an equivalent network is provided with the example discussion of a longitudinal vibrator.

L. Eyraud of the Laboratoire de Genie Electrique et Ferroelectricite in Villeurbanne, France authors the second paper "The Material for Piezoelectric Power Transducers" and coauthors the third paper "Characterization of Piezoelectric Ceramics for High Power Transducers" with P. Gonnard and P. Champ of the same address. Chapter 2 discusses the mechanisms of piezoceramic stability as a function of aging and polarization through a discussion of chemical compositions, while Chap. 3 characterizes various ferroelectric parameters. An analysis of piezoceramics under cw and pulsed conditions is presented with the limiting factors of each detailed.

The fourth chapter is titled "Highly Magnetostrictive Rare Earth Compounds for High Power Acoustic Projectors," by Arthur E. Clark from the Naval Surface Weapons Center (NSWC) in Silver Spring, Maryland. This paper is a reproduction of a chapter (7) written in 1980 in the book *Ferromagnetic Materials*, Volume 1, published by North-Holland, Amsterdam. It presents a background and detailed discussion of magnetostrictive lanthanide compounds. Although the discussion appears complete, much of the literature is dated and does not include the excellent recent work done by Clark and his colleagues at NSWC.

D. Boucher of Groupe d'Etude et de Recherche en Detection Sous-Marine in Toulon, France penned Chap. 5 "Trends and Problems in Low Frequency Sonar Projectors Design." A discussion on various classical sonar transducer designs is presented along with an effective briefing on array interaction effects. Unfortunately several of his comments on specific transducer designs are quite misleading. For example, when he states "...the work in this field (Class IV flextensional design) has been pursued as far as possible," he ignores the recent resurgence of the Class IV flextensional design utilizing lanthanide drivers, high strength epoxy shell composites, and new multidimensional array designs. On the other hand, his summary is an accurate portrayal of the present problems being encountered in low-frequency sonar transducers.

"Frequency, Power and Depth Performance of Class IV Flextensional Transducers" is the title of Chap. 6 as cowritten by J. Oswin and J. Dunn of British Aerospace, Underwater Research and Engineering Unit in Weymouth, United Kingdom. This paper gives an excellent overview of the Class IV flextensional transducers from the original patents to present. Discussions on depth, power, and frequency performance are given along with simple design guidelines. A correction on the dates of the two Toulis patents (references 6.1 and 6.11) must be clarified though. The authors incorrectly listed the patents as being granted in 1963 but in actuality the patents were first filed in 1963 and granted in 1966. A minor point but one that should be quantified to establish an accurate historical setting.

Chapter 7 is titled "Opportunities and Challenges in the Use of Terfenol for Sonar Transducers," by J. M. Sewell and P. M. Kuhn of Martin Marietta Aerospace in Baltimore, Maryland. This paper begins with a brief comparison between piezoceramic and terfenol, and is then followed with a discussion of terfenol transducer performance characteristics. Even though the authors found several positive points in the designs presented, the technology shown here is antiquated. Their methods for applying both the dc (magnetic) and the mechanical bias are ineffective and will result in low-efficiency devices. The educated reader will readily notice that the latest reference given is 1977, despite the literature and patents published by the Naval Underwater Systems Center (NUSC), Raytheon Company, and Image Acoustics, among others, that have advanced this technology much further along.

"Application of the Finite Element Method to the Design of Power Piezoelectric Sonar Transducers" and "Determination of the Power limits of a High Frequency Transducer Using the Finite Element Method" are the titles to Chaps. 8 and 9, respectively. The first one, authored by B. Harmonic (one of the two book editors) of the Institut Superieur d'Electronique du Nord, Laboratoire d'Acoustique, in Lille, France, presents FEM analysis (with ATILA code) on several sonar transducer designs. Chapter 9, cowritten by W. Steichen, G. Vanderborck, and Y. Lagier of Thomson-Sintra in Valbonne, France, explains a multiprocedure FEM analysis that includes acoustic radiation and thermal and dielectric losses. Although this method appears rather tedious, the experimental and computed examples are in general agreement.

The next two chapters present discussions on novel new ultrasonic transducer designs for industrial applications. Chapter 10 is entitled "High Power Ultrasonic Transducers for Use in Gases and Interphases," by J. A. Gallego-Juarez of the Instituto de Acustica in Madrid, Spain, while Chap. 11 is entitled "Design of High Power Ultrasonic Transducers for Use in Macrosonics," by P. Tierce of Sinaptec Sarl and J. N. Decarpigny (the second editor of the book) of the Institut Superieur d'Electronique du Nord, Laboratoire d'Acoustique, both in Lille, France.

The functions and architecture of a sonar emitting system are presented in Chap. 12 under the heading "Power Electronic Devices for Sonar Systems," by C. Pohlenz of Groupe d'Etude et de Recherche en Detection Sous-Marine (GERDSM) in Toulon, France. This paper offers several methods for solving difficult impedance matching problems in a sonar system. Disappointingly, it is the only paper that did not offer any references for further study. The final paper in the book, Chap. 13, is "The Electronic Driving Sources for Ultrasonic Machining," by B. Thirion of Slice Sarl in Lille, France.

 0001-4966/89/01520-02$00.80

In summary, although I found several papers reporting on "past glories," I feel that most transducer designers and material scientists will benefit from this book. It offers a rare glimpse of the international transducer world with a wide variety of useful global references. It is not limited to the underwater sonar designer since it additionally offers innovative ultrasonic devices that may be found in use in the private sector.

THOMAS R. HOWARTH
Department of Engineering Science and Mechanics
Research Center for the Engineering of Electronic and Acoustic Materials
The Pennsylvania State University
University Park, Pennsylvania 16802

The Journal of the Acoustical Society of America
Vol. 84 (4), October 1988, p. 1557.

TECHNICAL NOTES AND RESEARCH BRIEFS

Advanced-degree dissertations in acoustics

Experimental studies using chiral composites as acoustic energy attenuators [43.30.Ky]—Thomas R. Howarth, *The Research Center for Engineering of Electronic and Acoustic Materials, Department of Engineering Science and Mechanics, The Pennsylvania State University, University Park, PA 16802, May 1988 (M.S.).* The area of underwater acoustic attenuation has been a subject of much research since the 1940s. The Germans first investigated the use of air-rubber baffles to camouflage their submarines for active sonar. In their study they also developed a water-filled acoustic pulse tube device for determining air-rubber performance characteristics under various hydrostatic pressures and temperatures. In the late 1970s and into the 1980s other types of designs have been sought. It was found by using the concept of a T matrix in conjunction with multiple scattering theory that the use of piezoelectric chiral-shaped elements could replace the air pockets of the previous designs and offer new mechanisms for acoustic energy attenuation. This thesis investigates experimental studies using piezoelectric chiral composities for acoustic attenuation. A discussion of the theoretical concepts is given followed by the techniques used for fabrication of test samples. Background and operation of the pulse tube measurement system are provided followed by a discussion of measured results. Recommendations for future investigations conclude the presentation.

Thesis Advisor: Vijay K. Varadan.

Incommensurate Numbers, Continued Fractions, and Fractal Immittances

A. Lakhtakia*, R. Messier*,**, V. V. Varadan*, and V. K. Varadan*
The Pennsylvania State University, University Park, PA 16802 (USA)

Z. Naturforsch. 43a, 943–955 (1988); received June 10, 1988

Continued fractions have a rich tradition in the theory of numbers; e.g., non-terminating continued fractions represent irrational numbers. It will be shown that a class of continued fractions possess the property of self-referential decomposition, and their interpretation in the form of non-terminating ladder circuits gives rise to fractal immittances with potential analogies to rough surfaces, thin cermet films, as well as to the internal void network structure of thick films.

Introduction

The motivation for this work comes from number theory: the representation of irrational numbers in the Stieltjes continued fraction form, and which has already inspired the development of ladder circuits [1]. Continued fractions have recently been used in understanding fractal quantization of particles in one-dimensional potentials with incommensurate periods [2], as well as in two-dimensional electron gases [3]: a particularly appealing and simple interpretation of the relevant Hamiltonian has been given by Chao [4]. Continued fractions have also been applied in examining the frustrated instabilities of active optical resonators [5].

Although continued fractions have seen some use in the characterisation of the rough surfaces of real materials [6, 7], they have not been applied yet to the inhomogeneous internal structure of materials. It will be shown that specific examples of the resulting ladder circuits have fractal immittances with potential analogies to both cermet thin films and films with internal void networks; and, hence, to the related film properties.

* Department of Engineering Science and Mechanics.
** Materials Research Laboratory.

Reprint requests to Prof. R. Messier, Engineering Science and Mechanics, 265 Materials Research Labroatory, The Pennsylvania State University, University Park, PA 16802, USA

Continued Fractions and Quadratic Irrational Numbers

Any rational or irrational number can be written down in the continued fraction form as [8]

$$\langle a_0, a_1, a_2, a_3, \ldots \rangle = a_0 + \cfrac{1}{a_1 + \cfrac{1}{a_2 + \cfrac{1}{a_3 + \ldots}}}, \qquad (1)$$

with a_0, a_1, etc. being positive integers [but see Appendix]. The continued fraction is finite in size when it represents any rational number p/q, with a_0 being the integral part of the ratio p/q; it turns out that every *rational* number has exactly two such representations [9]. On the other hand, *irrational* numbers have continued fraction representations which are infinite in size. Of these irrational numbers, there is a class of *quadratic irrational* numbers which are solutions of a quadratic equation. A theorem due to Lagrange [10] states that the continued fraction expansion of any quadratic irrational is periodic after a certain state, e.g.,

$$\sqrt{15} = \langle 3, 1, 6, 1, 6, 1, 6, \ldots \rangle,$$

$$\sqrt{31} = \langle 5, 1, 1, 3, 5, 3, 1, 1, 10, 1, 1, 3, 5, 3, 1, 1, 10, 1, 1, 3, 5, 3, 1, 1, 10, \ldots \rangle,$$

$$\{24 - \sqrt{15}\}/17 = \langle 1, 5, 2, 3, 2, 3, 2, 3, \ldots \rangle.$$

It is the representation of quadratic irrational numbers which is of particular interest in the present context. The simplest example is the number

$$Q(\mu) = \langle 0, \mu, \mu, \mu, \ldots \rangle; \quad \mu > 0, \qquad (2)$$

0932-0784 / 88 / 1100-0943 $ 01.30/0. – Please order a reprint rather than making your own copy.

in which we will accept μ as any rational number; Q can achieve two numerical values *via* the equation $Q = 1/(\mu + Q)$. The next example is the number

$$Q(\mu_1, \mu_2) = \langle 0, \mu_1, \mu_2, \mu_1, \mu_2, \ldots \rangle; \quad \mu_1, \mu_2 > 0, \tag{3}$$

which too can achieve two numerical values *via* the quadratic equation $\mu_1 Q^2 + \mu_1 \mu_2 Q - \mu_2 = 0$.

This latter function $Q(\mu_1, \mu_2)$ forms the basis of the work reported here. We will remove the restriction that μ_1 and μ_2 be real positive rational numbers, and let them represent (complex) impedances Z and admittances Y; we will also assume [see Appendix] that all continued fractions are either finite in size or they converge. The first fundamental form comes out when we set $\mu_1 = Y_b = 1/Z_b$ and $\mu_2 = Z_a = 1/Y_a$, so that

$$Q(Y_b, Z_a) = 0 + \cfrac{1}{Y_b + \cfrac{1}{Z_a + \cfrac{1}{Y_b + \ldots}}}, \tag{4}$$

and $Q(Y_b, Z_a) + Z_a$ can be interpreted as the *impedance* of the "series-parallel" circuit shown in Figure 1a. The second fundamental form comes around when $\mu_1 = Z_b$ and $\mu_2 = Y_a$ so that

$$Q(Z_b, Y_a) = 0 + \cfrac{1}{Z_b + \cfrac{1}{Y_a + \cfrac{1}{Z_b + \ldots}}}, \tag{5}$$

and $Q(Z_b, Y_a) + Y_a$ can be interpreted as the *admittance* of the "parallel-series" circuit shown in Figure 1b.

From the preceding paragraph, it is immediately obvious that $Q(Y_b, Z_a) + Z_a$ and $Q(Z_b, Y_a) + Y_a$ are nothing but the immittances of ladder circuits [1]. Usually, however, ladder circuits are terminated in some prescribed fashion; thus, their immittances are "closer" to rational numbers than to irrational numbers.

Circuits of Infinite Size: Impedances

There is no restriction on ladder circuits that they be terminated after some number of stages, and we seize upon that idea to generalize $Q(Y_b, Z_a) + Z_a$. Our basic building blocks are two impedances $Z_a = 1/Y_a$ and $Z_b = 1/Y_b$, and the circuit will be constructed in a sequential manner. At the zeroth stage, these impedances are connected in series, and

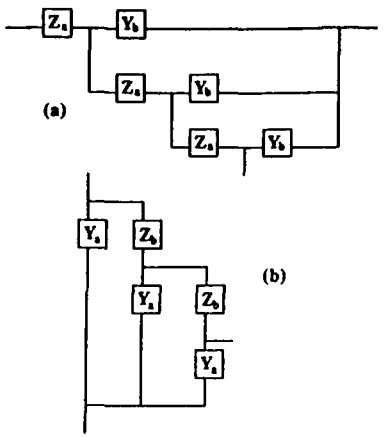

Fig. 1. Ladder circuit representation of (a) $Q(Y_b, Z_a) + Z_a$ in the "series-parallel" form, and (b) $Q(Z_b, Y_a) + Y_a$ in the "parallel-series" form.

$$Z^{(0)} = Z_a + Z_b. \tag{6a}$$

Then Z_b is shorted by N_1 parallel branches, each of which carries an impedance $p_1 Z_a$ and $q_1 Z_b$, where p_1 and q_1 are appropriate numbers such that $p_1 Z_a$ and $q_1 Z_b$ are realizable. Consequently, the impedance of the circuit at this stage can be represented by

$$Z^{(1)} = Z_a + \cfrac{1}{Y_b + \cfrac{N_1}{p_1 Z_a + q_1 Z_b}}. \tag{6b}$$

In the next stage of growth each of the impedances $q_1 Z_b$ is shorted out by N_2 parallel branches, each having an impedance $p_2 Z_a + q_2 Z_b$. Thus, the circuit impedance at this stage is given as

$$Z^{(2)} = Z_a + \cfrac{1}{Y_b + \cfrac{N_1}{p_1 Z_a + \cfrac{1}{Y_b/q_1 + \cfrac{N_2}{p_2 Z_a + q_2 Z_b}}}}. \tag{6c}$$

This process continues *ad infinitum*. Provided the real and the imaginary parts of the sequence $\{Z^{(i)}\}$ converge, it can be said that

$$Z^{(\infty)} = \lim_{i \to \infty} Z^{(i)} \tag{6d}$$

will be the impedance of the circuit so obtained. There is a pattern immediately obvious in the development of this circuit. As an example, let $N_i = N$ and $p_i = q_i = a^i \; \forall i \geq 1$. Then, it is easy to verify that

$$Z^{(i)} = Z_a + 1/[Y_b + (N/a)\, Y^{(i-1)}]; \quad i > 0, \tag{7a}$$

in which $Y^{(i)} = 1/Z^{(i)} \; \forall i \geq 0$. Provided (6d) holds, then it can be easily seen that $Z^{(\infty)}$ can be obtained as a solution of the quadratic equation

$$[Z^{(\infty)}]^2\, Y_b + [Z^{(\infty)}]\,\{N/a - Z_a Y_b - 1\} - Z_a N/a = 0. \tag{7b}$$

This scheme for generating $Z^{(\infty)}$ can be easily randomised by randomizing the selection of N_i, p_i and q_i. It may be that some of the circuits will turn out to be fractal, and others may not be so; and we are *a priori* unable to decisively rule on the outcome. Instead, we will give four examples which will be shown to have *fractal* impedances in the frequency domain, provided some specific conditions have been satisfied. These cases are:

Circuit ZRC: $\forall i \geq 1, N_i = N, p_i = a^i, q_i = 1$; $a > 1$; $Z_a = R$ and $Z_b = [j\omega C]^{-1}$.

For this circuit, by substitution of these conditions in (6) and computing $Z^{(\infty)}$ it can be shown that the following *scaling* relationships in the frequency domain arise:

$$Z^{(\infty)}(\omega) = R + a\, Z^{(\infty)}(a\omega) \cdot [N + a[j\omega C]\, Z^{(\infty)}(a\omega)]^{-1}, \tag{8a}$$

$$Z^{(\infty)}(\omega/a) = R + a\, Z^{(\infty)}(\omega) \cdot [N + [j\omega C]\, Z^{(\infty)}(\omega)]^{-1}. \tag{8b}$$

Circuit ZCR: $\forall i \geq 1, N_i = N, p_i = a^i, q_i = 1$; $a > 1$; $Z_a = [j\omega C]^{-1}$ and $Z_b = R$.

$$Z^{(\infty)}(\omega) = [j\omega C]^{-1} + a\, Z^{(\infty)}(\omega/a) \cdot [N + R^{-1}\, Z^{(\infty)}(\omega/a)]^{-1}, \tag{9a}$$

$$a\, Z^{(\infty)}(a\omega) = [j\omega C]^{-1} + a\, Z^{(\infty)}(\omega) \cdot [N + R^{-1}\, Z^{(\infty)}(\omega)]^{-1}. \tag{9b}$$

Circuit ZRL: $\forall i \geq 1, N_i = N, p_i = a^i, q_i = 1$; $a > 1$; $Z_a = R$ and $Z_b = j\omega L$.

$$Z^{(\infty)}(\omega) = R + a\, Z^{(\infty)}(\omega/a) \cdot [N + a[j\omega L]^{-1}\, Z^{(\infty)}(\omega/a)]^{-1}, \tag{10a}$$

$$Z^{(\infty)}(a\omega) = R + a\, Z^{(\infty)}(\omega) \cdot [N + [j\omega L]^{-1}\, Z^{(\infty)}(\omega)]^{-1} \tag{10b}$$

Circuit ZLR: $\forall i \geq 1, N_i = N, p_i = a^i, q_i = 1$; $a > 1$; $Z_a = j\omega L$ and $Z_b = R$.

$$Z^{(\infty)}(\omega) = j\omega L + Z^{(\infty)}(a\omega) \cdot [N + R^{-1}\, Z^{(\infty)}(a\omega)]^{-1}, \tag{11a}$$

$$a\, Z^{(\infty)}(\omega/a) = j\omega L + a\, Z^{(\infty)}(\omega) \cdot [N + R^{-1}\, Z^{(\infty)}(\omega)]^{-1}, \tag{11b}$$

It should be noted that in all of these four cases, the parameter a assumes a special status: as the discriminant for scale over the frequency range ω. To further elucidate the self-referential character of such circuits, consider the case when $N = 1$ and when Z_a as well as Z_b are arbitrary impedances. Then, it is possible to see that while $Z^{(0)} = Z_a + Z_b$, the higher order approximants can be set down compactly as

$$Z^{(i)} = [Z^{(0)}\, z_{1,i} + a\, Z_a\, Z^{(0)} + Z_a Z_b] \cdot [a\, Z_a + Z_b + z_{1,i}]^{-1}, \quad i \geq 1, \tag{12}$$

in which

$$z_{1,1} = Z_b, \tag{13a}$$

but

$$z_{1,i} = Z_b[a^2 Z_a + z_{2,i}] \cdot [a^2 Z_a + Z_b + z_{2,i}]^{-1}, \quad i \geq 2. \tag{13b}$$

But the impedance functions $z_{2,i}$, $i \geq 2$, can themselves be further simplified with the help of the impedance functions $z_{3,i}$, $i \geq 3$, as

$$z_{2,2} = Z_b, \tag{14a}$$

but

$$z_{2,i} = Z_b[a^3 Z_a + z_{3,i}] \cdot [a^3 Z_a + Z_b + z_{3,i}]^{-1}, \quad i \geq 3. \tag{14b}$$

It then becomes possible to observe the self-affinity of these circuits by defining the functions

$$z_{i,i} = Z_b, \tag{15a}$$

$$z_{j,i} = 0; \quad \text{if} \quad i < j, \tag{15b}$$

$$z_{j,i} = Z_b[a^{j+1} Z_a + z_{j+1,i}] \cdot [a^{j+1} Z_a + Z_b + z_{j+1,i}]^{-1}; \quad i \geq j+1. \tag{15c}$$

Circuits of Infinite Size: Admittances

The aforementioned circuits are of the "series-parallel" form such as $Q(Y_b, Z_a) + Z_a$ in (4). Because of duality, it is easy to visualise "parallel-series" forms such as $Q(Z_b, Y_a) + Y_a$ in (5). Our building blocks here

will be two admittances $Y_a = 1/Z_a$ and $Y_b = 1/Z_b$. In the zeroth-stage these admittances are connected in parallel; then,

$$Y^{(0)} = Y_a + Y_b. \tag{16a}$$

Next, N_1 branches connected in series are inserted into the branch containing Y_b, each branch of admittance $p_1 Y_a + q_1 Y_b$. Consquently, the admittance of the circuit at this stage can be represented by

$$Y^{(1)} = Y_a + \cfrac{1}{Z_b + \cfrac{N_1}{p_1 Y_a + q_1 Y_b}}, \tag{16b}$$

where $Z_b = 1/Y_b$. In the second stage, N_2 branches connected in series are inserted into the branches containing $q_1 Y_b$, each branch of admittance $p_2 Y_a + q_2 Y_b$; hence,

$$Y^{(2)} = Y_a + \cfrac{1}{Z_b + \cfrac{N_1}{p_1 Y_a + \cfrac{1}{Z_b/q_1 + \cfrac{N_2}{p_2 Y_a + q_2 Y_b}}}}, \tag{16c}$$

This process also continues *ad infinitum*. Provided the real and the imaginary parts of the sequence $\{Y^{(i)}\}$ converge, it can be said that

$$Y^{(\infty)} = \lim_{i \to \infty} Y^{(i)} \tag{16d}$$

will be the admittance of the circuit so obtained. As a counterpart to (7a), if $N_i = N$ and $p_i = q_i = a^i \; \forall i \geq 1$, then

$$Y^{(i)} = Y_a + 1/[Z_b + (N/a)\, Z^{(i-1)}]; \quad i > 0, \tag{17}$$

where $Z^{(i)} = 1/Y^{(i)} \; \forall i \geq 0$.

The "parallel-series" counterparts of the circuits identified above as ZRC, etc., along their respective frequency scaling relationships, are as follows:

Circuit YRC: $\forall i \geq 1$, $N_i = N$, $p_i = a^i$, $q_i = 1$; $a > 1$; $Y_a = R^{-1}$ and $Y_b = j\omega C$.

$$Y^{(\infty)}(\omega) = R^{-1} + a\, Y^{(\infty)}(\omega/a) \cdot [N + a[j\omega C]^{-1}\, Y^{(\infty)}(\omega/a)]^{-1}, \tag{18a}$$

$$Y^{(\infty)}(a\omega) = R^{-1} + a\, Y^{(\infty)}(\omega) \cdot [N + [j\omega C]^{-1}\, Y^{(\infty)}(\omega)]^{-1}. \tag{18b}$$

Circuit YCR: $\forall i \geq 1$, $N_i = N$, $p_i = a^i$, $q_i = 1$; $a > 1$; $Y_a = j\omega C$ and $Y_b = R^{-1}$.

$$Y^{(\infty)}(\omega) = j\omega C + Y^{(\infty)}(a\omega) \cdot [N + R\, Y^{(\infty)}(a\omega)]^{-1}, \tag{19a}$$

$$a\, Y^{(\infty)}(\omega/a) = j\omega C + a\, Y^{(\infty)}(\omega) \cdot [N + R\, Y^{(\infty)}(\omega)]^{-1}, \tag{19b}$$

Circuit YRL: $\forall i \geq 1$, $N_i = N$, $p_i = a^i$, $q_i = 1$; $a > 1$; $Y_a = R^{-1}$ and $Y_b = [j\omega L]^{-1}$.

$$Y^{(\infty)}(\omega) = R^{-1} + a\, Y^{(\infty)}(a\omega) \cdot [N + a[j\omega L]\, Y^{(\infty)}(a\omega)]^{-1}, \tag{20a}$$

$$Y^{(\infty)}(\omega/a) = R^{-1} + a\, Y^{(\infty)}(\omega) \cdot [N + [j\omega L]\, Y^{(\infty)}(\omega)]^{-1}, \tag{20b}$$

Circuit YLR: $\forall i \geq 1$, $N_i = N$, $p_i = a^i$, $q_i = 1$; $a > 1$; $Y_a = [j\omega L]^{-1}$ and $Y_b = R^{-1}$.

$$Y^{(\infty)}(\omega) = [j\omega L]^{-1} + Y^{(\infty)}(\omega/a) \cdot [N + R\, Y^{(\infty)}(\omega/a)]^{-1}, \tag{21a}$$

$$a\, Y^{(\infty)}(a\omega) = [j\omega L]^{-1} + Y^{(\infty)}(\omega) \cdot [N + R\, Y^{(\infty)}(\omega)]^{-1}. \tag{21b}$$

By making use of the interchanges $Z \Leftrightarrow Y$, $R \Leftrightarrow R^{-1}$ and $L \Leftrightarrow C$, it is easy to show that the circuits YRC, YCR, YRL and YLR are the duals, respectively, of the circuits ZRL, ZLR, ZRC and ZCR.

Discussion

For the remainder of this paper, we will confine our discussion to the circuits ZRC and ZCR, whose scaling behavior are, respectively, identified by (8a, b) and (9a, b); furthermore, we shall drop the superscript (∞) on Z.

First, the circuit ZRC and a couple of its possible applications. Shown in Fig. 2 are the plots of the real and the imaginary parts of $Z^{(i)}$ as well as the phase angle $\varphi^{(i)} = \arctan\,[\mathrm{Im}\{Z^{(i)}\}/\mathrm{Re}\{Z^{(i)}\}]$ as functions of the frequency ω; the building blocks are $R = 1\,\mathrm{k}\Omega$ and $C = 1\,\mathrm{nF}$. To be noted is the fact that Z can be extrapolated from these graphs. It can be seen that in the low-frequency regime ($\omega RC \ll 1$), both the real and the imaginary parts of Z are proportional to $\omega^{-\zeta}$, where $\zeta = 1 - \ln(N)/\ln(a) = 1 - D$, D being the fractal dimension [12]; indeed $Z(\omega)$ is actually proportional to $(i\omega)^{-\zeta}$. As the frequency increases, then this law is no longer followed: for the high-frequency regime ($\omega RC \gg 1$), the real part of Z approaches the constant

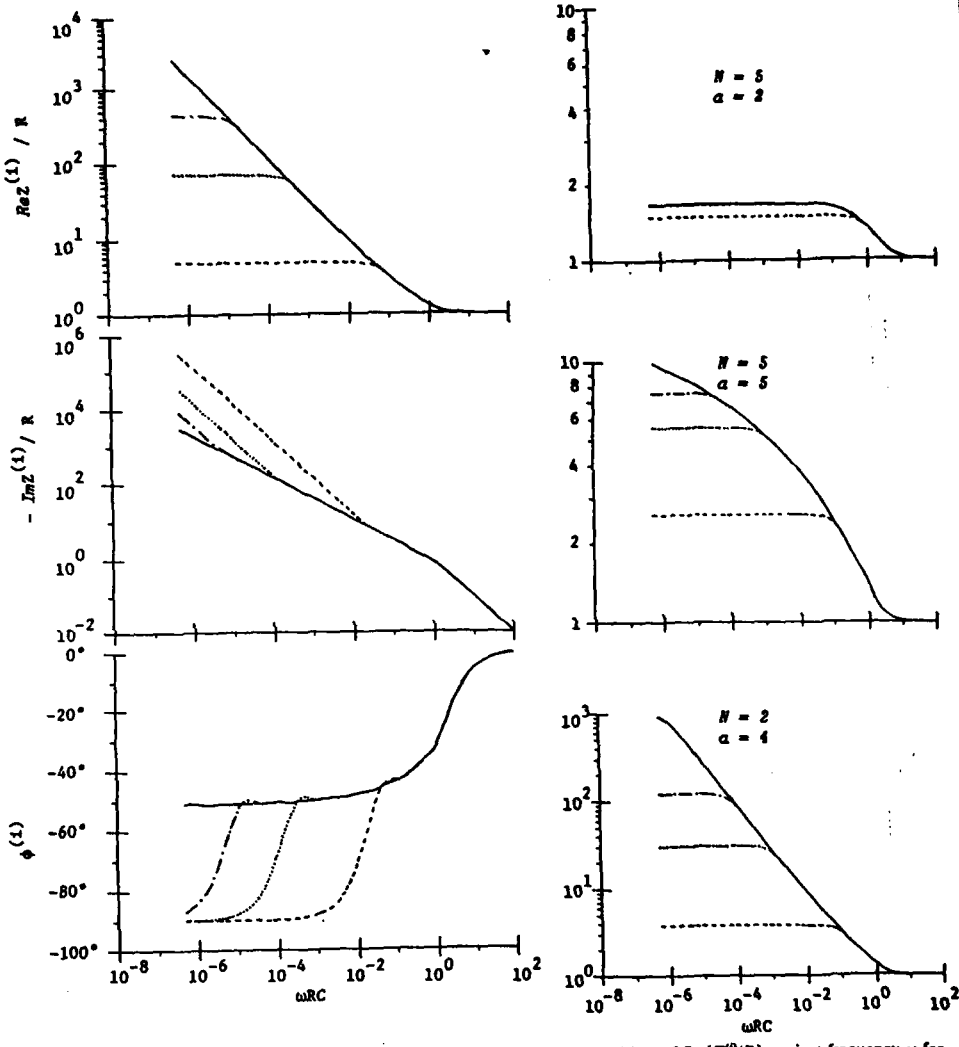

Fig. 2. Plots of $\mathrm{Re}\{Z^{(i)}/R\}$, $-\mathrm{Im}\{Z^{(i)}/R\}$ and phase angle $\varphi^{(i)} = \arctan\{\mathrm{Im}\{Z^{(i)}\}/\mathrm{Re}\{Z^{(i)}\}\}$ against frequency ω for the circuit ZRC. The building blocks $R = 1\,\mathrm{k}\Omega$ and $C = 1\,\mathrm{nF}$; the branch number $N = 2$ and the branching parameter $a = 5$, $i = 2$ (– – –), 5 (· · ·), 7 (–·–·–) and 10 (——). Note that $a > N^2$ and that for $\omega RC \ll 1$, $Z(\omega) \sim (i\omega)^{-\zeta}$, where $\zeta = 1 - \ln(N)/\ln(a)$.

Fig. 3. Plots of $\mathrm{Re}\{Z^{(i)}/R\}$ against frequency ω for the circuit ZRC. The building blocks $R = 1\,\mathrm{k}\Omega$ and $C = 1\,\mathrm{nF}$; $i = 2$ (– – –), 5 (· · ·), 7 (–·–·–) and 10 (——). Three cases have been considered: (a) $a = 2$, $N = 5$, (b) $a = N = 5$, and (c) $a = 4$, $N = 2$.

resistance R and the imaginary part of Z decays as ω^{-1}. But the imaginary part of Z is very small when compared to its real part; hence, Z is almost purely resistive at high frequencies. This behavior of the ZRC circuit was first noted by Liu [6] for $N = 2$, and the low-frequency, constant-phase-angle response of the ZRC circuit makes it a plausible model for some electrode surfaces [11, 13].

It should be noted that in the calculations of Fig. 2, $a > N$. Furthermore, $\ln(N)/\ln(a)$ is a fractal dimension of the ZRC circuit and lies between 0 and 0.5. Since the circuit has been used to encode in it the topography of an electrode surface, this consideration is justified [7]. From the point of view of circuit topology, however, there is no reason to confine $N < a$. In Figs. 3 and 4, the calculations of Fig. 2 are repeated for varying values of the ratio a/N. From these and other studies, it appears that the low-frequency, constant-phase-angle response of the circuit ZRC is confined to the regime $a \geq N^2$. When $N \gg a$, however, another interesting characteristic appears: whereas for $\omega RC \gg 1$, $Z \cong R$, even in the low-frequency regime Z is almost purely resistive. As the parameter a is increased relative to N^2, this behavior is supplanted by the "fractal" behavior observed for $a \geq N^2$.

As an application of the circuit ZRC, we now consider the reflection coefficient $\Re(\omega)$ when a planewave is normally incident on an infinite plane [14] whose impedance can be modelled by that of the ZRC circuit;

$$\Re(\omega) = [Z(\omega) - \eta_0][Z(\omega) + \eta_0]^{-1}. \qquad (22)$$

This reflection coefficient is plotted in Figs. 5 and 6 with $R = 200\,\Omega$ and $C = 100$ pF; the free space impedance, $\eta_0 = 120\pi\,\Omega > R$. In Fig. 5 the condition $a \geq N^2$ has been fulfilled. For this case, it appears that in the low-frequency range, the reflection coefficient is almost equal to $+1$, but in the high-frequency regime it acquires a constant negative value. Neither of these results is surprising because for $\omega RC \ll 1$, $|Z(\omega)| \gg \eta_0$, the free-space impedance; while for $\omega RC \gg 1$, $Z(\omega) \cong R < \eta_0$. In other words, at low frequencies the impedance plane behaves as if it were a perfect magnetic conductor (PMC), but becomes an insulator at higher frequencies. It is to be concluded, therefore, that the ZRC circuit with $a \geq N^2$ is a plausible model for PMC-insulator transition. When $a \ll N^2$, the circuit ZRC also provides a model for such transitions, but somewhat of a different kind. Shown in Fig. 6 is the case when $a = 2$ and $N = 5$. From this figure, it is to be noted that both in the low- and the high-frequency regimes, $\Re(\omega)$ is almost always a negative real number (except for the static case when it equals unity), which is because $Z(\omega)$ is almost purely resistive in these frequency ranges. Thus, this appears to be a case of

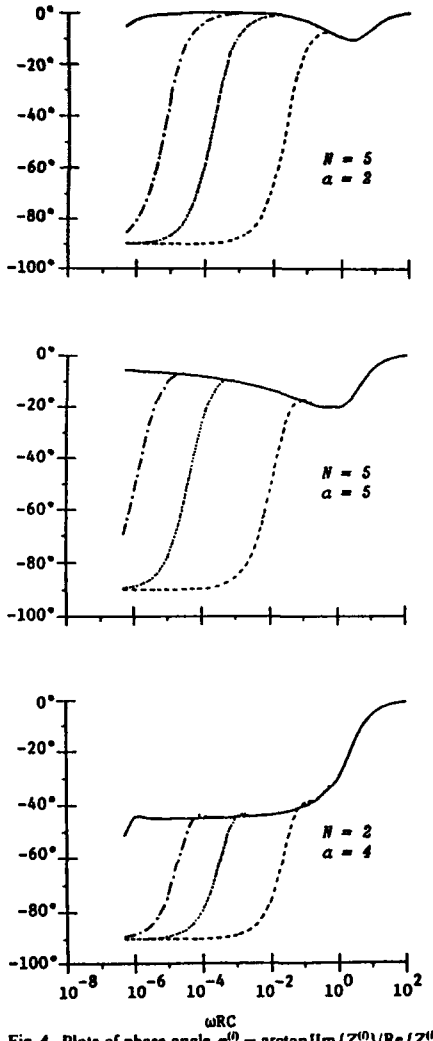

Fig. 4. Plots of phase angle $\varphi^{(i)} = \arctan[\mathrm{Im}\{Z^{(i)}\}/\mathrm{Re}\{Z^{(i)}\}]$ against frequency ω for the circuit ZRC. See Fig. 3 for other details.

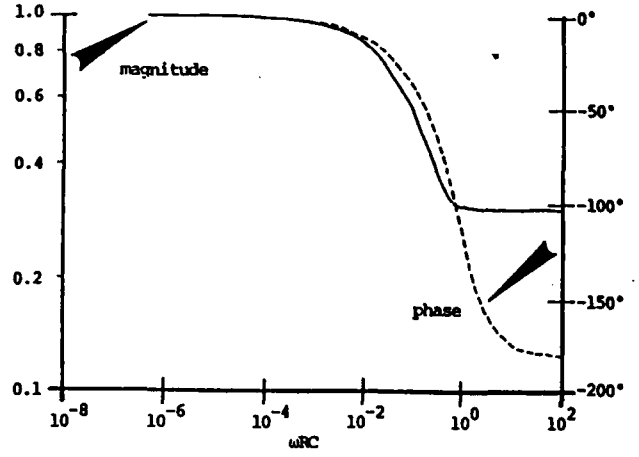

Fig. 5. Magnitude and phase of the reflection coefficient $\Re(\omega)$ given as a function of ω by (22). The impedance $Z(\omega)$ of the ZRC circuit is approximated by $Z^{(10)}$, no difference being observed when $Z^{(7)}$ was used in place of $Z(\omega)$. The parameters $R = 200\,\Omega$, $C = 100$ pF, $a = 5$, and $N = 2$.

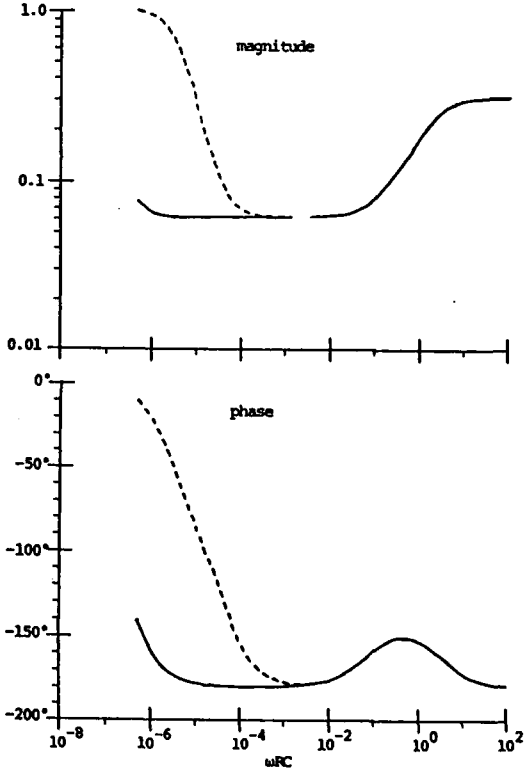

Fig. 6. Magnitude and phase of $\Re(\omega)$ given as a function of ω by (22). The impedance $Z(\omega)$ of the circuit ZRC was approximated by $Z^{(7)}$(– – –) and $Z^{(10)}$(——). The parameters $R = 200\,\Omega$, $C = 100$ pF, $a = 2$, and $N = 5$.

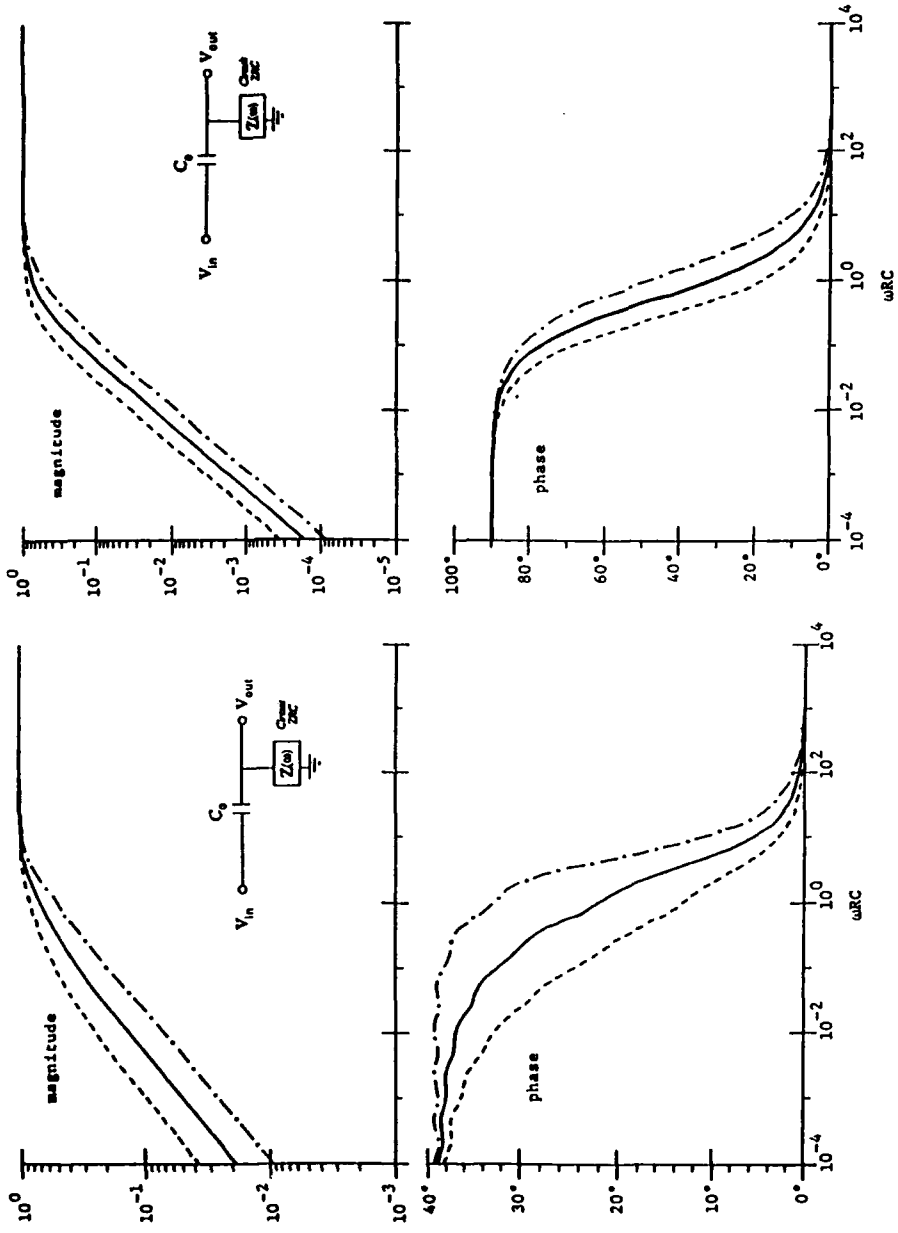

Fig. 7. Magnitude and phase of $G(\omega)$ given as a function of ω by (23). The impedance $Z(\omega)$ of the circuit ZRC was approximated by $Z^{(10)}$ with $R = 1\,k\Omega$, $C = 100\,pF$, $a = 5$ and $N = 2$. The capacitance $C_0 = C/2$ (— · — · —), C (— —) and $2C$ (— — —).

Fig. 8. Same as Fig. 7, except $a = 2$ and $N = 5$.

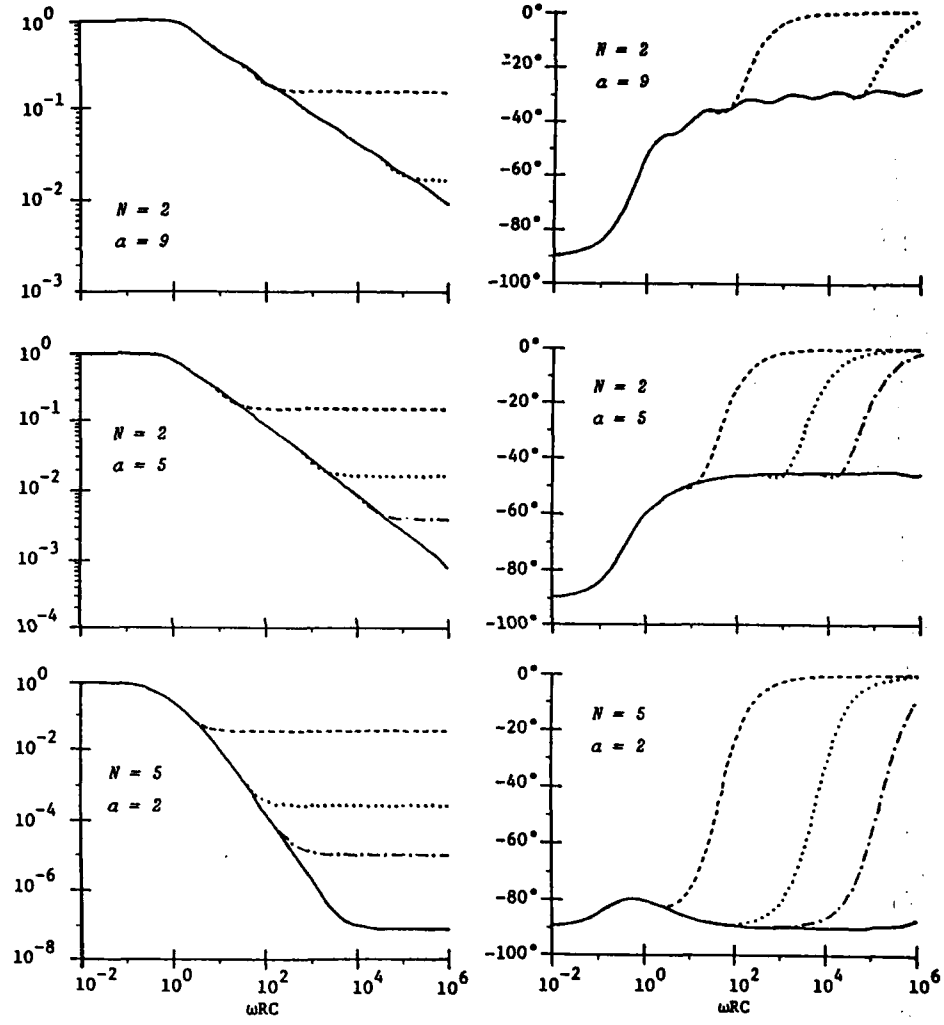

Fig. 9. Plots of $\mathrm{Re}\{Z^{(i)}/R\}$ against frequency ω for the circuit ZCR. The building blocks $R = 1\,k\Omega$ and $C = 1\,nF$; $i = 2$ (— — —), 5 (· · ·), 7 (— · — · —) and 10 (——). Three cases have been considered: (a) $a = 9$, $N = 2$, (b) $a = 5$, $N = 2$, and (c) $a = 2$, $N = 5$.

Fig. 10. Plots of phase angle $\varphi^{(i)} = \arctan[\mathrm{Im}\{Z^{(i)}\}/\mathrm{Re}\{Z^{(i)}\}]$ against frequency ω for the circuit ZCR. See Fig. 9 for other details.

insulator-insulator transition, perhaps typifying a curious (relaxation?) mechanism in which the dielectric constant changes from a low value to a higher value as the frequency increases [15, 16]. Parenthetically, it should be noted that this second case can also be interpreted to be symptomatic of a relaxation in which the (magnetic) permeability changes from a high value to a lower one with the increase in frequency [17]. Both of these impedance plane models merit further attention. It must also be noted that the scattering plane need not be planar: it is possible to think of a rough, bimaterial interface as a perfectly smooth plane possessed with a space-dependent impedance [18]. This impedance is not only a function of the geometry of the actual (rough) surface, but also of the frequency ω and the field incident on the surface.

Finally, the circuit ZRC may be used as part of a filter, as shown in the insets of Figs. 7 and 8. For these two figures, the open-circuit voltage gain was computed via

$$G(\omega) = Z(\omega)\,[Z(\omega) + (j\omega C_0)^{-1}], \qquad (23)$$

in which $Z(\omega)$ was approximated by $Z^{(10)}(\omega)$, $R = 1\,\mathrm{k}\Omega$ and $C = 100\,\mathrm{pF}$. The capacitance C_0 was assumed to have three values: $C_0 = C/2$, C and $2C$. In Fig. 7, $a = 5$ and $N = 2$, so that $a > N^2$; and in the latter figure, $a = 2$ and $N = 5$ so that $a \ll N^2$. It is to be noted that for either case, $G(\omega) \cong 1$ when $\omega RC \gg 1$, so that the high frequencies are passed on by the filters without any distortion. The low frequencies ($\omega RC \ll 1$) are, however, attenuated, so that these filters are essentially high pass; furthermore, the roll-off appears to be rather insensitive to the capacitance ratio C_0/C. But the roll-off in Fig. 7 is about 8.4 dB/decade, and in Fig. 8 it is about 20 dB/decade, which suggests that as an element of these filters, the circuit ZRC with $a \ll N^2$ is certainly the more efficient one. This is because, as evinced by Fig. 3, the circuit ZRC with $a \ll N^2$ behaves much like a pure resistance in both the low- and the high-frequency ranges.

Just as the response of the circuit ZRC is dominated by its real (resistive) part, the circuit ZCR is dominated by its imaginary (capacitative) part. Shown in Figs. 9 and 10 are the plots of the real part and the

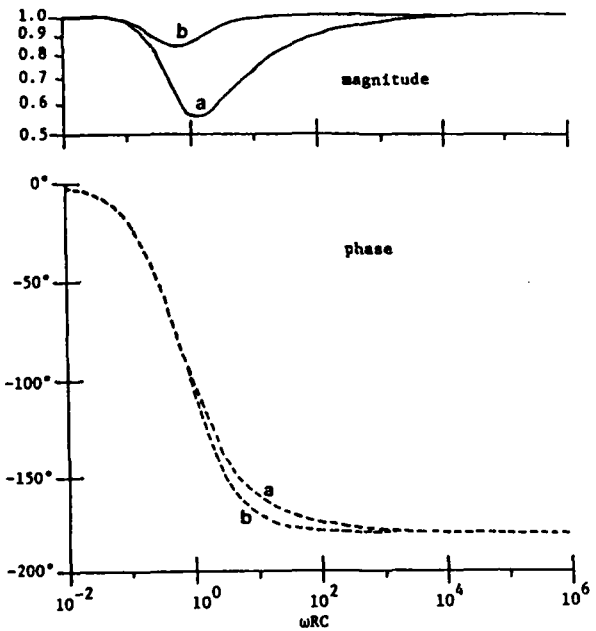

Fig. 11. Magnitude and phase of the reflection coefficient $\mathfrak{R}(\omega)$ given as a function of ω by (22). The impedance $Z(\omega)$ of the ZCR circuit is approximated by $Z^{(10)}$, no difference being observed when $Z^{(7)}$ was used in place of $Z(\omega)$; $R = 200\,\Omega$, $C = 100\,\mathrm{pF}$. The branching parameters are (a) $a = 5$, $N = 2$, and (b) $a = 2$, $N = 5$.

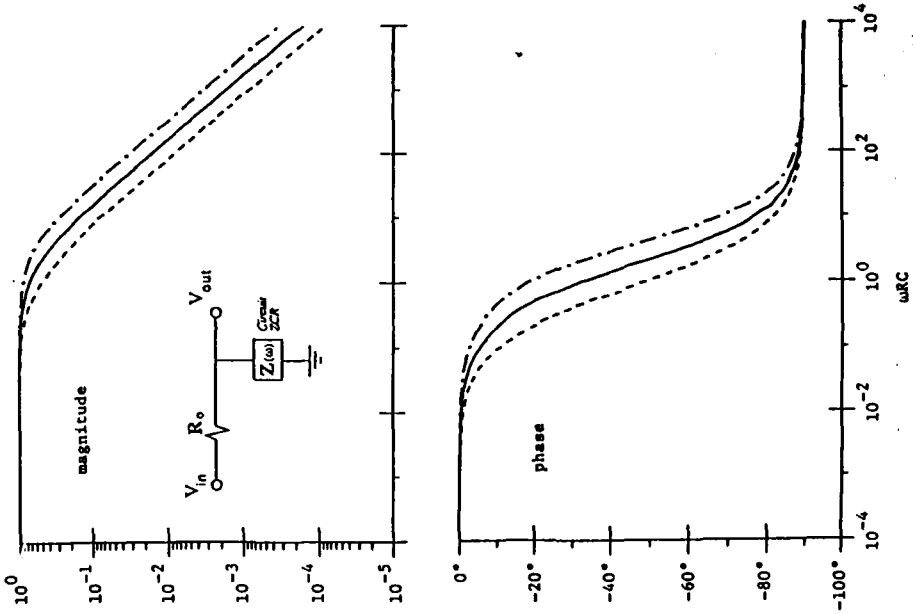

Fig. 13. Same as Fig. 12, except $a = 2$ and $N = 5$.

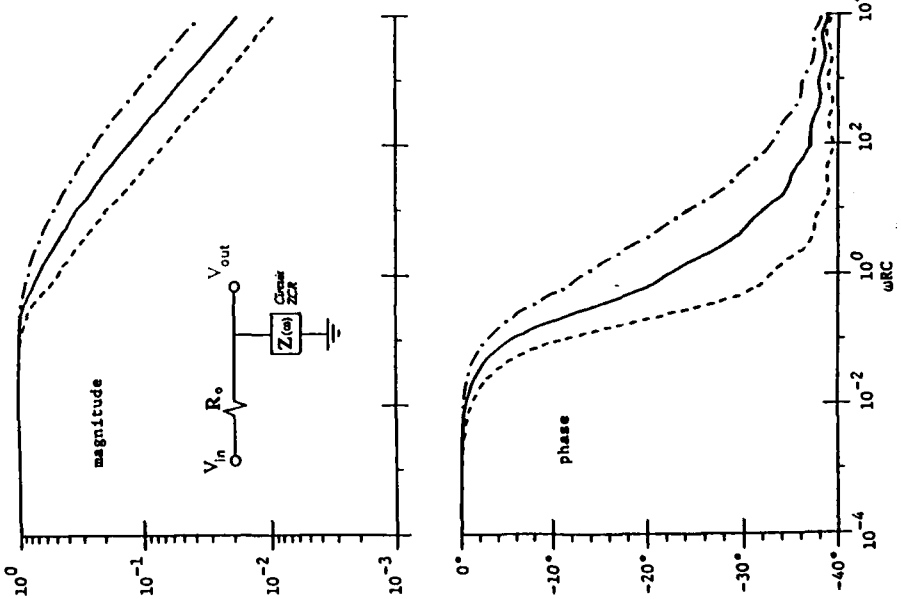

Fig. 12. Magnitude and phase of $G(\omega)$ given as a function of ω by (23). The impedance $Z(\omega)$ of the circuit ZCR was approximated by $Z^{(10)}$ with $R = 1\,\mathrm{k}\Omega$, $C = 100\,\mathrm{pF}$, $a = 5$ and $N = 2$. The resistance $R_o = R/2$ (- - - -), R ( ) and $2R$ (— —).

phase, respectively, of the approximants $Z^{(l)}$ for some circuits ZCR; the building blocks are $R = 1\,\text{k}\Omega$ and $C = 1\,\text{nF}$. To be noted is the fact that in the static limit $\omega \to \infty$, $Z(\omega)$ is almost purely capacitative. Furthermore, $\text{Re}\,Z(\omega) = R$ at low frequencies ($\omega RC \ll 1$), but for $\omega RC \gg 1$, it appears that $\text{Re}\,Z(\omega)$ is proportional to $\omega^{-\zeta}$. When $a \geq N^2$, then $\zeta = \ln(N)/\ln(a)$, which is a number less than 0.5; as the ratio N/a increases, however, ζ does so too and achieves values higher than unity. For $a \geq N^2$, the impedance of the circuit ZCR also scales as $(i\omega)^{-\zeta}$ for $\omega RC \gg 1$, but this relationship becomes slightly imprecise in its phase when $a \gg N^2$. On the other hand, when $a \ll N^2$, then both in the low and the high frequency limits, $Z(\omega)$ is almost purely capacitative.

Using (22), the reflection coefficient $\Re(\omega)$ is computed in Fig. 11 for a planewave normally incident on an infinite plane whose impedance is modelled by the circuit ZCR; $R = 200\,\Omega$ and $C = 100\,\text{pF}$. It is apparent from this figure that, qualitatively speaking, there is no difference between the cases (a) $a \geq N^2$ and (b) $a \ll N^2$. In the low frequency range, $\Re(\omega)$ tends towards $+1$; and in the high frequency regime, $\Re(\omega)$ is approximately equal to negative unity. Both of these observations are consistent with the capacitative nature of the circuit ZCR. Also, it appears that the impedance plane behaves as a perfect electric conductor (PEC) for $\omega RC \gg 1$, so that the circuit ZCR models PMC-PEC transitions, regardless of the specific values of the branching parameters a and N. Pertinent to the scattering of acoustic waves, this can also be interpreted as a transition from an acoustically hard surface to an acoustically soft one.

The open-circuit voltage gain $G(\omega)$ of the filter, shown in the insets of Figs. 12 and 13, has been computed via the relationship (23). For these calculations, $Z(\omega)$ of the circuit ZCR was approximated by $Z^{(10)}(\omega)$, $R = 1\,\text{k}\Omega$ and $C = 100\,\text{pF}$. The resistance R_0 was assumed to have three values: $R_0 = R/2$, R and $2R$. In Fig. 12, $a = 5$ and $N = 2$, so that $a > N^2$; while in Fig. 13, $a \ll N^2$ and $a = 2$ with $N = 5$. It is to be noted that for either case, $G(\omega) \cong 1$ when $\omega RC \ll 1$: this implies that the low frequencies are passed on by the filters without any significant distortion. On the other hand, the high frequencies ($\omega RC \gg 1$) are attenuated, the attenuation being rather insensitive to the ratio R_0/R. But this roll-off rate in Fig. 12 is about 8.5 dB/decade, while in Fig. 13 it is almost 20 dB/decade. This suggests that the use of the circuit ZCR with $a \ll N^2$ is certainly more efficient for these low-pass filters.

There are several envisioned applications of this mathematical formalism to the modelling of real thin film materials. First, it has already been shown that the ZRC circuit is a plausible model for the interfacial impedances of rough electrode surfaces in electrochemical cells [6].

Second, cermet films are mixtures of metallic and insulating materials which form a fractal [19–21] sponge-like connected network of either the metallic or the insulator phase, depending upon the concentration of the metal. A test for whether such materials are analogous would be to measure the reflection coefficient of thin ($\sim$100–500 Å) cermet films when a planewave is normally incident and compare the results with applicable formulas [14] similar to (22). The use of the ZRC and the ZCR circuit impedances to simulate the impedance of an infinite plane should turn out to be analogous to the metallic and the insulating cermet states [20], respectively.

Lastly, for thicker films (1–100 μ) of essentially a single-phase material prepared under conditions of low adatom mobility, it has been demonstrated that the top surface is cauliflower-like and is directly related to a conical void network structure [22]. Although these void networks appear fractal, there has been no quantitative description of them [23]. The present work suggests ways to test and measure the fractal nature of such films. The impedances of the void regions and that of the "bulk" conical regions are certainly different; the film properties should have analogy to both the ZRC (ionic diffusion and electrical conductivity) as well as the ZCR (permittivity) circuits.

Acknowledgement

This work was supported in part by the United States Air Force Office of Scientific Research.

Appendix: Generalized Continued Fractions

Rigorously speaking, a continued fraction should be defined [24] through an ordered set of numbers $\{a_n\}$, $\{b_n\}$ and $\{\zeta_n\}$, where $a_0, a_1, a_2, \ldots$ and $b_1, b_2, \ldots$ are complex numbers with all $b_n \neq 0$, and where $\{\zeta_n\}$ is a sequence in the extended complex plane. The numbers ζ_n approximate the continued fraction z, and assuming that the continued fraction is infinitely long,

$$z = \lim_{n \to \infty} \zeta_n, \tag{A1}$$

where

$$\zeta_n = a_0 + \cfrac{b_1}{a_1 + \cfrac{b_2}{a_2 + \cfrac{\ddots}{\ddots + b_n/a_n}}}. \tag{A2}$$

The convergence (A1) is subject to some conditions, which have been discussed in detail in Chaps. 3 and 4 of the book by Jones and Thron [24]. It will suffice for the present purposes to indicate here that the sequence $\{\zeta_n\}$ does converge to z, provided

$$|a_n| \geq |b_n| + 1; \quad n = 1, 2, 3, \ldots. \tag{A3}$$

For the sake of computational tractability, it is convenient to express the nth approximant as

$$\zeta_n = B_n/A_n, \tag{A4}$$

where

$$B_{-1} = A_0 = 1, \quad B_0 = a_0, \quad A_{-1} = 0, \tag{A5a}$$

$$A_n = a_n A_{n-1} + b_n A_{n-2}, \quad n = 1, 2, 3\ldots, \tag{A5b}$$

$$B_n = a_n B_{n-1} + b_n B_{n-2}, \quad n = 1, 2, 3\ldots. \tag{A5c}$$

[1] P. M. Chirlian, Basic Network Theory, McGraw-Hill, New York, 1969, p. 494.
[2] M. Ya. Azbel, Phys. Rev. Lett. 43, 1954 (1979).
[3] F. D. M. Haldane, Phys. Rev. Lett. 51, 605 (1983).
[4] K. A. Chao, J. Phys. A 19, 2907 (1986).
[5] K. Ikeda, M. Mizuno, Phys. Rev. Lett. 53, 1340 (1984).
[6] S. H. Liu, Phys. Rev. Lett. 55, 529 (1985).
[7] T. Kaplan, S. H. Liu, and L. J. Gray, Phys. Rev. B 34, 4870 (1986).
[8] M. R. Schroeder, Number Theory in Science and Communication, Springer-Verlag, Berlin, Chapter 5 (1986).
[9] N. H. McCoy, The Theory of Numbers, MacMillan, New York, p. 99 (1971).
[10] C. D. Olds, Continued Fractions, Math. Assoc. America, p. 56 (1963).
[11] P. H. Bottelberghs and G. H. J. Broers, J. Electroanal. Chem. 67, 155 (1976).
[12] A. Lakhtakia, R. Messier, V. V. Varadan, and V. K. Varadan, Phys. Lett. A 118, 54 (1986).
[13] J. R. MacDonald, J. Electroanal. Chem. 223, 25, (1987).
[14] J. D. Kraus, Electromagnetics, McGraw-Hill, New York 1984, Sect. 10–16.
[15] V. K. Farkya and D. Kumar, Ind. J. Pure Appl. Phys. 24, 592 (1986).
[16] A. Ramsamugh and F. Brouers, Phil. Mag. Lett. 55, 301 (1987).
[17] R. Barrue, J. C. Perron, and J. Robert, Rev. Phys. Appl. (Paris) 22, 399 (1987).
[18] A. Hessel and A. A. Oliner, Appl. Opt. 4, 1275 (1965).
[19] A. Kapitulnik and G. Deutscher, Phys. Rev. Lett. 49, 1444 (1982).
[20] R. B. Laibowitz, E. I. Allessandrini, and G. Deutscher, Phys. Rev. B 25, 2965 (1982).
[21] R. F. Voss, R. B. Laibowitz, and E. I. Allessandrini, Phys. Rev. Lett. 49, 1441 (1982).
[22] R. Messier and J. E. Yehoda, J. Appl. Phys. 58, 3739 (1985).
[23] R. Messier, J. Vac. Sci. Technol. A 4, 490 (1986).
[24] W. B. Jones and W. J. Thron, Continued Fractions: Analytic Theory and Applications, Addison-Wesley, Reading, Mass. 1980.

EXCITATION OF A PLANAR ACHIRAL/CHIRAL INTERFACE BY NEAR FIELDS

A. LAKHTAKIA, V.K. VARADAN and V.V. VARADAN
Department of Engineering Science and Mechanics
and
Research Center for the Engineering of Electronic and Acoustic Materials
The Pennsylvania State University
University Park, PA 16802

ABSTRACT

The refraction of near fields by a planar achiral/chiral interface has been examined. A realistic source, a constant current line source, has been used here, as apart from the usual analyses involving incident planewaves only. Provided a planewave spectral decomposition of the incident field is possible, this procedure can be extended to include sources of other configurations and polarizations as well. Maps of the refracted field are drawn to elucidate the effect of both the near-zone irradiation as well as of the handedness of the chiral medium. Such an analysis would be of use to various researchers in the area so that the effect of the near fields of radiating sources may not be ignored.

1. INTRODUCTION

Ever since the discovery of optical activity early in the last century, there has been a great interest in measuring the circular dichroic (CD) and the optical rotatory dispersion (ORD) spectra of molecular aggregations [1]. Such measurements are routinely made, at frequencies down into the infra-red regime nowadays. The measurement procedures usually are variants of a simple technique: A planar slab of the optically active, or chiral, material is irradiated by a source, the polarization state of the irradiating field being known. On the other side of the slab, the rotation of the plane of polarization of the transmitted field with respect to that of the incident field is measured, and the CD and the ORD of the material determined. A good description of such an experiment conducted at frequencies around 10 GHz is available in [2], where Tinoco and Freeman describe the procedure for measuring the optical rotatory activity of a collection of oriented copper helices, each approximately 0.5 cm in diam and about 1 cm long.

However, this and other such measurement techniques usually ignore the proximity of the chiral slab to the source. If the source is far away from the exposed face of the slab, the illuminating field may be conveniently taken to be a planewave. But when that is not so, the slab lies in the near-zone of the source, where the irradiating field has reactive components of large magnitudes. In such circumstances, the planewave approximation of the source field can be quite gross. In this communication, the nature of the fields excited in a chiral half-space are examined. The source is taken to be a constant current line source, the field radiated by which source is decomposed into an infinite set of planewaves, some of which are propagating and the remaining ones are evanescent. It is to be emphasized here that any other source can be accommodated in this theoretical procedure, provided its field can be expressed by a planewave spectral (PWS) representation [3]. By mapping the field refracted into the chiral half-space, some understanding of the effect of near-field irradiation of achiral/chiral interfaces is obtained.

2. REFRACTION OF A TE-POLARIZED PLANEWAVE BY A PLANE ACHIRAL/CHIRAL INTERFACE

Let the space $z \leq 0$ be filled by a non-dissipative achiral medium (here taken to be free-space) in which the constitutive relations

$$\mathbf{D} = \varepsilon_o \mathbf{E} \quad , \quad \mathbf{B} = \mu_o \mathbf{H} \qquad (1a,b)$$

hold, and from which a TE-polarized planewave

$$\mathbf{E}_i(\kappa) = \mathbf{j} \exp[\mathrm{j}\{\kappa x + \beta_o(\kappa) z\}] \quad , \quad \mathbf{H}_i(\kappa) = (1/\mathrm{j}\omega\mu_o) \nabla \times \mathbf{E}_i(\kappa) \quad , \qquad (2a,b)$$

with

$$\beta_o(\kappa) = +[k_o^2 - \kappa^2]^{1/2} \quad , \quad k_o = \omega[\mu_o \varepsilon_o]^{1/2} \quad , \qquad (3a,b)$$

is incident on the interface $z = 0$, the harmonic time-dependence $\exp[-\mathrm{j}\omega t]$ being suppressed here and hereafter, and the unit vectors $\mathbf{i}$, $\mathbf{j}$, $\mathbf{k}$ having their usual meanings in a rectangular co-ordinate system.

The region above the $z = 0$ interface, $z \geq 0$, is occupied by a chiral medium in which the constitutive equations are given as [4,5]

$$\mathbf{D} = \varepsilon \{\mathbf{E} + \alpha \nabla \times \mathbf{E}\} \quad , \quad \mathbf{B} = \mu \{\mathbf{H} + \alpha \nabla \times \mathbf{H}\} \qquad (4a,b)$$

and in which it would be proper, because of Snell's law, to express the transmitted field as [6]:

$$\mathbf{E}_t(\kappa) = T_L(\kappa)\, \mathbf{Q}_L(\kappa) + a_R\, T_R(\kappa)\, \mathbf{Q}_R(\kappa) \quad ; \qquad (5a)$$

$$\mathbf{H}_t(\kappa) = a_L\, T_L(\kappa)\, \mathbf{Q}_L(\kappa) + T_R(\kappa)\, \mathbf{Q}_R(\kappa) \qquad (5b)$$

in which $T_{L,R}(\kappa)$ are to be determined by the boundary conditions on the interface $z = 0$, and the left- and the right-circularly polarized (LCP and RCP) wavefunctions, respectively, are given as

$$\mathbf{Q}_L(\kappa) = (1/k_L)\{-\beta_L(\kappa)\mathbf{i} - \mathrm{j}k_L\mathbf{j} + \kappa\mathbf{k}\} \exp[\mathrm{j}\{\kappa x + \beta_L(\kappa) z\}] \quad , \qquad (6a)$$

and

$$\mathbf{Q}_R(\kappa) = (1/k_R)\{-\beta_R(\kappa)\mathbf{i} - \mathrm{j}k_R\mathbf{j} + \kappa\mathbf{k}\} \exp[\mathrm{j}\{\kappa x + \beta_R(\kappa) z\}] \quad . \qquad (6b)$$

In Eqs. (5) and (6) the following definitions hold:

$$a_L = -\mathrm{j}[\varepsilon/\mu]^{1/2} \quad , \quad a_R = -\mathrm{j}[\mu/\varepsilon]^{1/2} \quad , \qquad (7a,b)$$

$$k_L = k[1 - k\alpha]^{-1} \quad , \quad k_R = k[1 + k\alpha]^{-1} \quad , \qquad (7c,d)$$

$$\beta_L(\kappa) = +[k_L^2 - \kappa^2]^{1/2} \quad , \quad \beta_R(\kappa) = +[k_R^2 - \kappa^2]^{1/2} \quad , \qquad (7e,f)$$

$$k = \omega[\mu\varepsilon]^{1/2} \quad . \qquad (7g)$$

The field reflected back into the achiral medium also has LCP and RCP components, and it can be expressed in the form [6]:

$$\mathbf{E}_r(\kappa) = R_R(\kappa)\, \mathbf{P}_R(\kappa) + R_L(\kappa)\, \mathbf{P}_L(\kappa) \quad , \quad \mathbf{H}_r(\kappa) = (1/\mathrm{j}\omega\mu_o) \nabla \times \mathbf{E}_r(\kappa) \quad , \qquad (8a,b)$$

where $R_{L,R}(\kappa)$ are to be determined and the wavefunctions,

$$\mathbf{P}_R(\kappa) = (1/k_o)\{\beta_o(\kappa)\mathbf{i} + \mathrm{j}k_o\mathbf{j} + \kappa\mathbf{k}\} \exp[\mathrm{j}\{\kappa x - \beta_o(\kappa) z\}] \quad , \qquad (9a)$$

and

$$\mathbf{P}_L(\kappa) = (1/k_o)\{\beta_o(\kappa)\mathbf{i} - \mathrm{j}k_o\mathbf{j} + \kappa\mathbf{k}\} \exp[\mathrm{j}\{\kappa x - \beta_o(\kappa) z\}] \quad . \qquad (9b)$$

By invoking the usual boundary conditions across the $z = 0$ interface, i.e.,

$$\mathbf{k} \times [\mathbf{E}_i(\kappa) + \mathbf{E}_r(\kappa) - \mathbf{E}_t(\kappa)] = 0 \quad , \quad \mathbf{k} \times [\mathbf{H}_i(\kappa) + \mathbf{H}_r(\kappa) - \mathbf{H}_t(\kappa)] = 0 \quad , \qquad (10a,b)$$

and using Eqs. (1), (5) and (8), it can be shown that

$$T_L(\kappa) = 2\mathrm{j}\,[S + a_R\, Q(\kappa)] / \Delta(\kappa) \quad , \qquad (11a)$$

$$T_R(\kappa) = 2j\,[a_L\,S - P(\kappa)] / \Delta(\kappa) \quad , \tag{11b}$$

$$R_L(\kappa) = -(1/4)\,[T_L(\kappa)\,\{P(\kappa)+1\}\,\{a_L\,S+1\} + T_R(\kappa)\,\{Q(\kappa)-1\}\,\{S+a_R\}] \quad , \tag{11c}$$

$$R_R(\kappa) = (1/4)\,[T_L(\kappa)\,\{P(\kappa)-1\}\,\{a_L\,S-1\} + T_R(\kappa)\,\{Q(\kappa)+1\}\,\{S-a_R\}] \quad , \tag{11d}$$

$$\Delta(\kappa) = [S + a_R\,Q(\kappa)]\,[1 - a_L\,P(\kappa)\,S] - [a_L\,S - P(\kappa)]\,[a_R + Q(\kappa)\,S] \quad , \tag{11e}$$

and

$$P(\kappa) = (k_o/k_L)\,[\beta_L(\kappa)/\beta_o(\kappa)] \quad , \quad Q(\kappa) = (k_o/k_R)\,[\beta_R(\kappa)/\beta_o(\kappa)] \quad , \quad S = -j\,[\mu_o/\varepsilon_o]^{1/2} \quad . \tag{11f,g,h}$$

It should be noted that if $\alpha = 0$, i.e., the medium above the $z = 0$ interface also becomes achiral, then

$$k_R = k_L = k \quad , \quad \beta_R(\kappa) = \beta_L(\kappa) = \beta(\kappa) = +\,[k^2 - \kappa^2]^{1/2} \quad , \tag{12a,b}$$

$$P(\kappa) = Q(\kappa) = (k_o/k)\,[\beta(\kappa)/\beta_o(\kappa)] \quad , \tag{12c}$$

$$T_L(\kappa) = -\,a_R\,T_R(\kappa) = j\,a_R\,[a_R + Q(\kappa)\,S]^{-1} \quad , \tag{12d}$$

and

$$R_R(\kappa) = -\,R_L(\kappa) = (1/2)j\,[a_R - Q(\kappa)\,S]\,[a_R + Q(\kappa)\,S]^{-1} \quad ; \tag{12e}$$

consequently, the familiar expressions available in any standard textbook [e.g., 7] on EM theory emerge:

$$E_t(\kappa) = j\,2a_R\,[a_R + Q(\kappa)\,S]^{-1}\,\exp[j\,\{\kappa x + \beta(\kappa)z\}] \quad , \tag{13a}$$

and

$$E_r(\kappa) = -\,j\,[a_R - Q(\kappa)\,S]\,[a_R + Q(\kappa)\,S]^{-1}\,\exp[j\,\{\kappa x - \beta_o(\kappa)z\}] \quad . \tag{13b}$$

3. REFRACTION OF THE FIELD OF A LINE SOURCE

Let now an isotropically radiating, y-directed current line source be located at $r_p = -kd_p$ in the achiral half-space, and its radiated field be set as [8]:

$$E_I = j\pi H_0\,(k|r - r_p|) \quad . \tag{14}$$

A planewave spectral (PWS) decomposition [3] of this field is possible, and is given by

$$E_I = j \int_{-\infty}^{\infty} [d\kappa/\beta_o(\kappa)]\,\exp[j\beta_o(\kappa)d_p]\,\exp[j\,\{\kappa x + \beta_o(\kappa)z\}] \quad , \quad z > -d_p \quad , \tag{15a}$$

and

$$E_I = j \int_{-\infty}^{\infty} [d\kappa/\beta_o(\kappa)]\,\exp[-j\beta_o(\kappa)d_p]\,\exp[j\,\{\kappa x - \beta_o(\kappa)z\}] \quad , \quad z < -d_p \quad . \tag{15b}$$

In view of the PWS decomposition, Eq. (15a) and the development of the preceding section, it is possible to write down the total field existing in the chiral half-space due to the line source as

$$E_T = \int_{-\infty}^{\infty} [d\kappa/\beta_o(\kappa)] \exp[j\beta_o(\kappa)d_p] \cdot \{T_L(\kappa)\, Q_L(\kappa) + a_R\, T_R(\kappa)\, Q_R(\kappa)\} \quad , \quad z>0 \ . \quad (16)$$

Likewise, provided it is assumed that the field reflected from the achiral/chiral interface does not influence the line source current, the total field existing in the space $z < -d_p$ can be set down as

$$E_R = \int_{-\infty}^{\infty} [d\kappa/\beta_o(\kappa)] \exp[j\beta_o(\kappa)d_p] \cdot \{R_R(\kappa)\, P_R(\kappa) + R_L(\kappa)\, P_L(\kappa)\} +$$

$$+ j \int_{-\infty}^{\infty} [d\kappa/\beta_o(\kappa)] \exp[-j\beta_o(\kappa)d_p] \exp[j\{\kappa x - \beta_o(\kappa)z\}] \quad , \quad z<-d_p \quad . \quad (17)$$

4. DISCUSSION

It is the function E_T which has to be mapped in the xz plane in order to understand the fields generated in the chiral half-space. It is obvious that the κ-domain poles can be extracted simply by solving the equation $\Delta(\kappa) = 0$. However, such poles are of little interest in the present analysis. Instead, the only recourse is to actually map E_T over an xz grid for a given set of parameters. It would certainly be useful then to exploit the x- and the κ-symmetries of the various parts of the integrands in Eq. (16), and it turns out that

$$E_T = 2 \int_0^{\infty} [d\kappa/k_L\beta_o(\kappa)] \exp[j\beta_o(\kappa)d_p] \exp[j\beta_L(\kappa)z]\, T_L(\kappa) \{-i\beta_L(\kappa)\cos\kappa x - jjk_L\cos\kappa x + kj\kappa\sin\kappa x\} +$$

$$+ 2a_R \int_0^{\infty} [d\kappa/k_R\beta_o(\kappa)] \exp[j\beta_o(\kappa)d_p] \exp[j\beta_R(\kappa)z]\, T_R(\kappa) \{-i\beta_R(\kappa)\cos\kappa x + jjk_R\cos\kappa x + kj\kappa\sin\kappa x\} \ , \quad z>0 \ , \quad (18)$$

whose cartesian components have either even or odd symmetries with respect to the x coordinate.

A computer program to calculate E_T was implemented on a DEC VAX 11/730 minicomputer via Eq. (18). The infinite κ-integral in Eq. (18) was truncated to hold over the range $0 \le \kappa/k_o \le 20.0$, it being observed that this truncation did not give rise to any errors for the selected values $\varepsilon/\varepsilon_o \le 5.0$, $\mu/\mu_o = 1.0$, $\alpha k \le 0.1$ and $k_o d_p = 2.0$. The magnitudes of the x-, y-, and z- directed components of the LCP and the RCP parts of E_T, as well as of the total E_T, are illustrated in Figs. 1 - 4 for several cases over the rectangular region $0 \le kx/d_p, kz/d_p \le 10.0$.

In Fig. 1, $E_T = E_I$ since $\varepsilon/\varepsilon_o = 1.0$ and $\alpha k = 0.0$. This illustration, therefore, simply shows the field radiated by the line source in the specified xz domain when all space is covered by the non-dissipative achiral medium. As was expected and can be observed from this figure, the magnitudes of the RCP and the LCP parts of E_T are identical, but E_T is only y-directed. In Fig. 2, the ratio $\varepsilon/\varepsilon_o$ was increased to 5.0 with αk still equal to zero. Again, E_T turns out to have only a y-directed component, the x- and the z- directed components of its LCP and RCP parts having cancelled themselves out. These two figures are then simply symbolic of what can be expected when the refracting half-space is also achiral [8].

This cancellation of the x- and the z- directed components of the LCP and the RCP parts of E_T does not occur in Fig. 3 where $\varepsilon/\varepsilon_o = 5.0$ and $\alpha k = 0.01$. The magnitudes of the LCP and the RCP parts of E_T are still equal by virtue of the fact that all possible values of κ (positive as well as negative) are included in Eq. (18). However, the sum of these parts still shows the presence of the x- and the z- directed components, which had cancelled out in Figs. 1 and 2 where $\alpha k = 0.0$. The effect of handedness in the half-space $z \ge 0$ is betrayed, thus, by the presence of a transmitted electric field E_T which is not TE polarised like the source field E_I. This tendency is even more marked in Fig. 4 where $\varepsilon/\varepsilon_o = 5.0$ and $\alpha k = 0.1$. Furthermore, in Fig. 4, E_T records well-defined extrema, which are not as prominent in Fig. 3. It becomes possible to state,

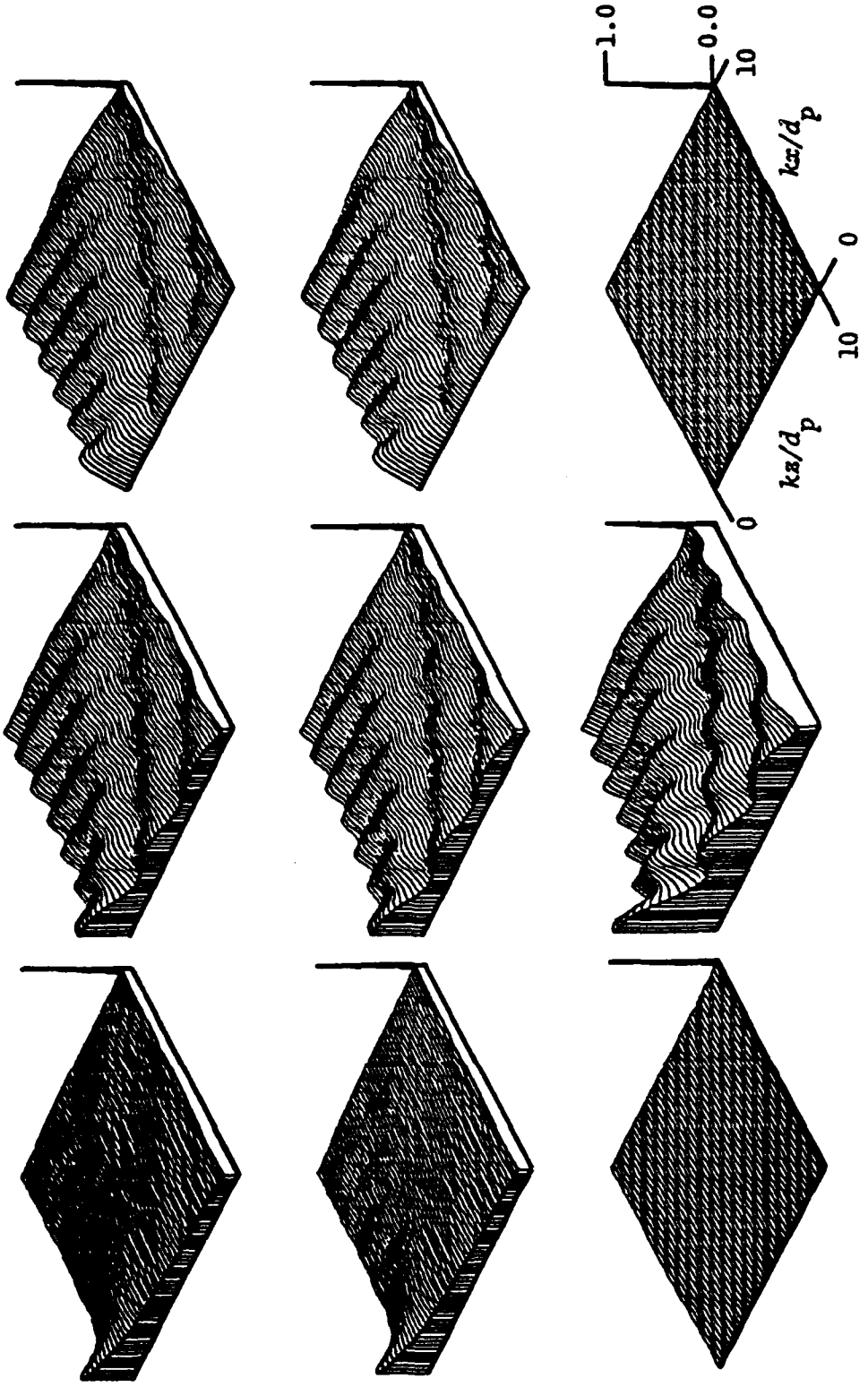

Figure 1 Magnitudes of the various components of E_T of Eq. (18) when E_I is given by Eq. (14). From left to right in each row: magnitudes of the x-, y- and z- directed components. From top to bottom: LCP part of E_T, RCP part of E_T, and E_T itself. The parameters $k_0 d_p = 2.0$, $\varepsilon/\varepsilon_0 = 1.0$, $\mu/\mu_0 = 1.0$ and $\alpha k = 0.0$. The field maps are drawn on the xz domain $0 \leq kx/d_p, kz/d_p \leq 10.0$.

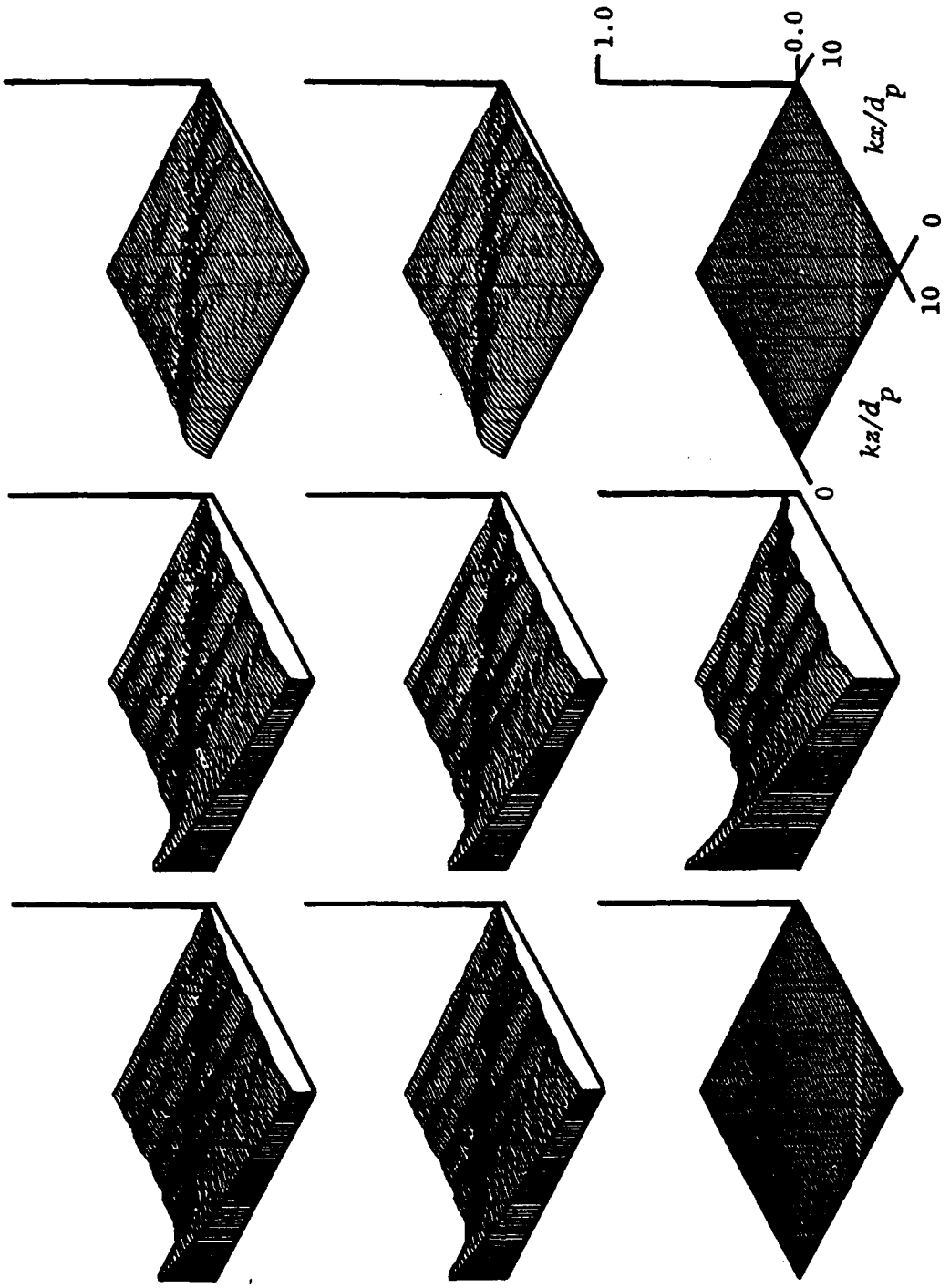

Figure 2 Same as Fig. 1, except $\varepsilon/\varepsilon_0 = 5.0$.

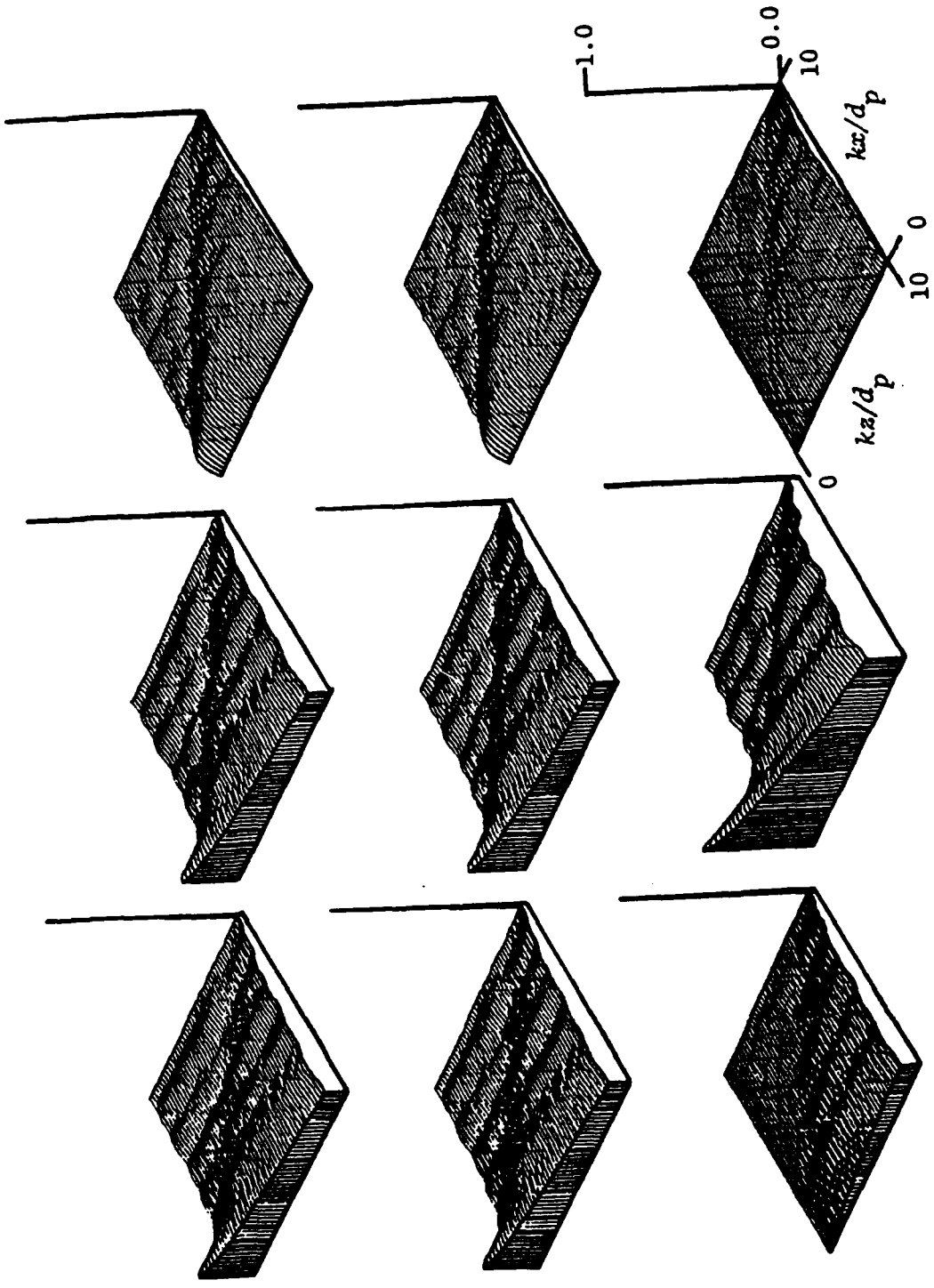

Figure 3 Same as Fig. 1, except $\varepsilon/\varepsilon_0 = 5.0$ and $\alpha k = 0.01$.

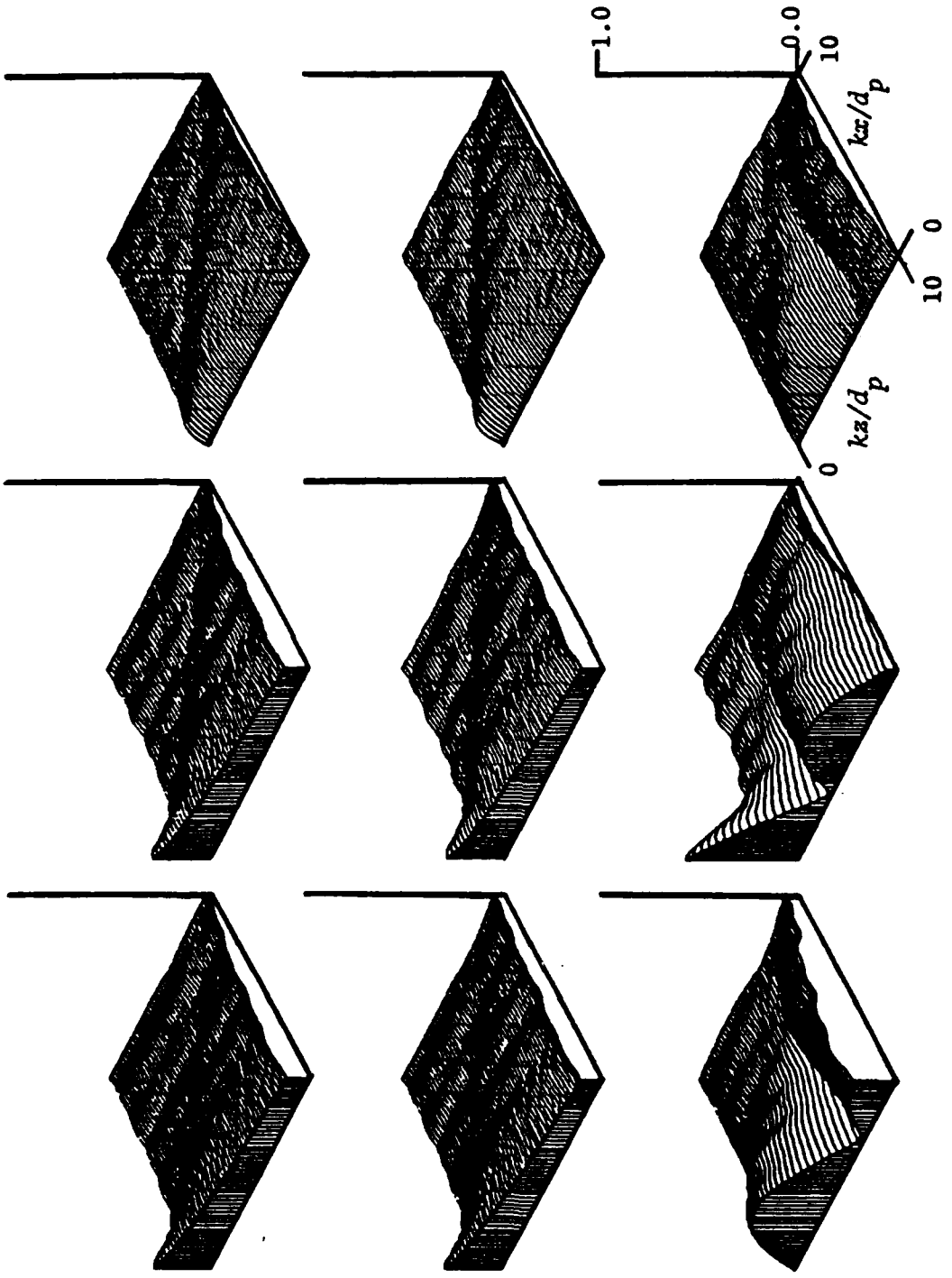

Figure 4 Same as Fig. 1, except $\varepsilon/\varepsilon_0 = 5.0$ and $\alpha k = 0.1$.

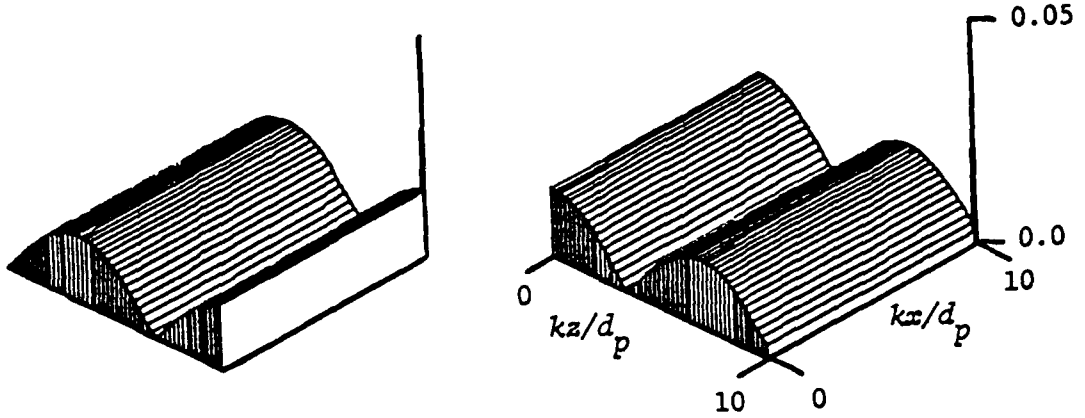

Figure 5 Magnitudes, from left to right, of the x- and y- directed components of $\mathbf{E}_T$ when $\mathbf{E}_I$ is given by Eq. (19). The parameters $k_o d_p = 2.0$, $\varepsilon/\varepsilon_o = 5.0$, $\mu/\mu_o = 1.0$ and $\alpha k = 0.1$. The field maps are drawn on the xz domain $0 \le kx/d_p, kz/d_p \le 10.0$.

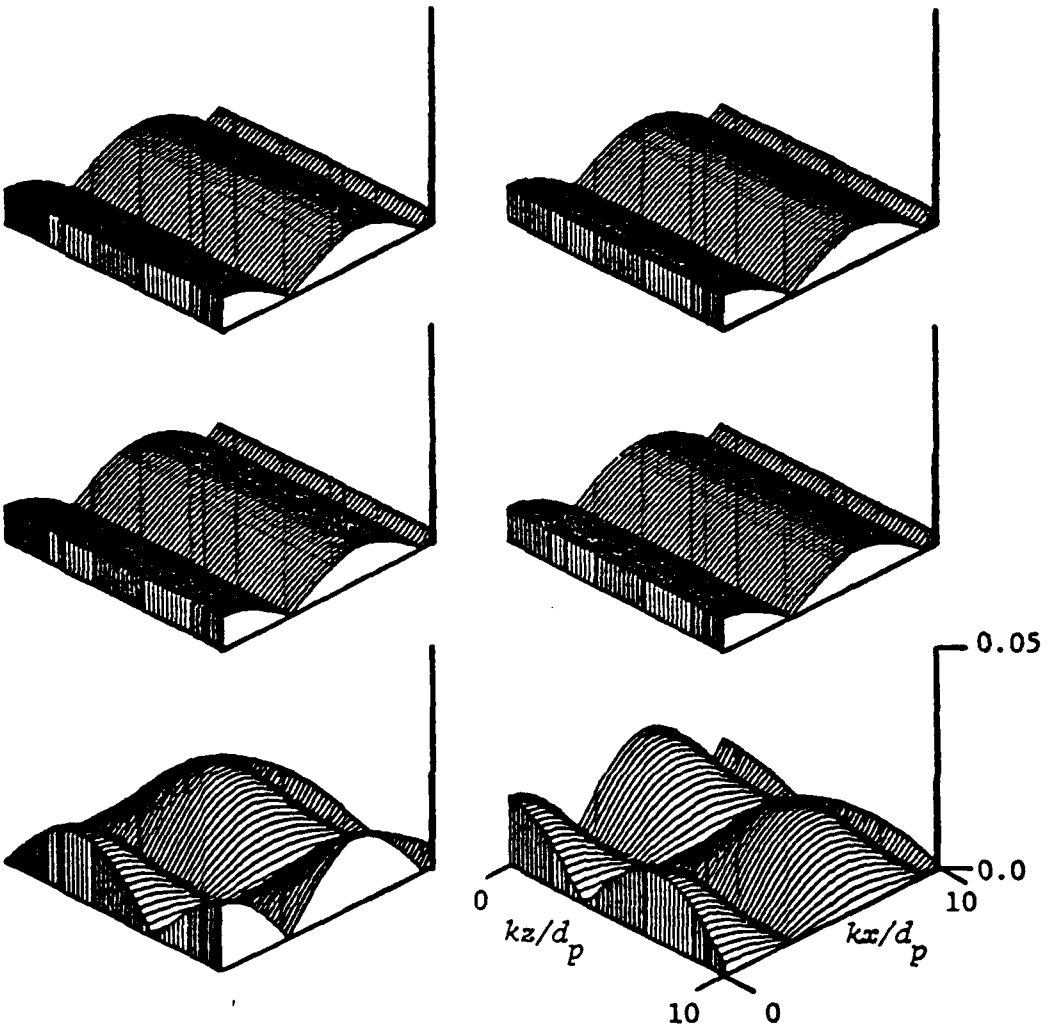

Figure 6 Magnitudes of the various components of $\mathbf{E}_T$ when $\mathbf{E}_I$ is given by Eq. (21). From left to right in each row: magnitudes of the x- and y- directed components. From top to bottom: LCP part of $\mathbf{E}_T$, RCP part of $\mathbf{E}_T$, and $\mathbf{E}_T$ itself. The parameters $k_o d_p = 2.0$, $\varepsilon/\varepsilon_o = 5.0$, $\mu/\mu_o = 1.0$ and $\alpha k = 0.1$. The field maps are drawn on the xz domain $0 \le kx/d_p, kz/d_p \le 10.0$.

therefore, that if $\alpha k << 1.0$, then $k_R \approx k_L \approx k$ and the effect of the chirality parameter α is slight on the field E_T as can be seen from comparing Fig. 3 with Fig. 2. But as αk increases, then k_R and k_L differ widely from k [9], and the interference of the LCP and the RCP parts of E_T is all too visible.

Some idea of this interference can be drawn from considering only specific values of κ in Eq. (18]) or, equivalently, by modifying the line source field E_I of Eq. (14) to

$$E_I = j\pi H_0(k|r - r_p|)\, \delta(\kappa) \quad , \tag{19}$$

where $\delta(\cdot)$ is the Dirac delta function. Shown in Fig. 5 are the magnitudes of the x- and the y- directed components of E_T, with $\varepsilon/\varepsilon_0 = 5.0$ and $\alpha k = 0.1$, there being no z-directed component of E_T. If Eq. (19])is used as the incident field, then, from the preceding theoretical analysis, it is easy to see that

$$E_T = [2/k_o(S + a_R)] \exp[j(kz - k_o d_p)]\ \{-i \sin(k^2 \alpha z) + j \cos(k^2 \alpha z)\} \quad , \tag{20a}$$

provided $\alpha k < 1$ and the approximations

$$k_L \approx k\,[1 + \alpha k] \quad ; \quad k_R \approx k\,[1 - \alpha k] \tag{20b,c}$$

are valid. Fig. 5 vindicates Eq. (20a) very well and it also becomes easy to observe the mutual interference of the LCP and the RCP parts of E_T in deriving this equation.

Finally, in Fig. 6, the incident field is modified to

$$E_I = j\pi H_0(k|r - r_p|)\, \delta(\kappa - k_o/4) \quad , \tag{21}$$

and E_T is computed; $\varepsilon/\varepsilon_0 = 5.0$ and $\alpha k = 0.1$. It turns out that $P(k_o/4) \approx Q(k_o/4)$, while $\beta_L(k_o/4)/k_L \approx \beta_R(k_o/4)/k_R$. Consequently, $T_L(k_o/4) \approx -a_R T_R(k_o/4)$. Hence, the RCP and the LCP parts of E_T are virtually identical in magnitude, their z-directed components are negligible, and their x- and y- directed components have a $\cos(k_o x/4)$ dependence on the x coordinate. When, the LCP and the RCP parts are added up, the cartesian components of E_T have well-defined extrema in the xz plane. In view of Figs. 5 and 6, then, the variations of E_T in Fig. 4 can be easily explained.

It should be noted that $E_T(x,y)$ in Figs. 1 - 4 tends to decay away as one goes farther from the source at r_p. This is natural since E_I, in the vicinity of the source, has reactive components with large magnitudes. As one moves farther and farther away from the source, these reactive, near-zone field components tend to die out. This behavior of E_I is replicated qualitatively by E_T as well, a phenomenon which has been noted in other electromagnetic scattering problems also [10].

In summary, it has been shown here that the fields refracted into a chiral half-space are markedly different when αk is substantially different from zero, i.e., when αk is of the order of 0.1. A realistic source has been used here, as apart from the usual analyses involving incident planewaves only [6]. Provided a PWS decomposition [3] of the incident field is possible, this procedure can be extended to include sources of other configurations and polarizations as well. Such an analysis would be of use to various researchers in the area so that the effect of the near fields [10] of radiating sources may not be ignored.

REFERENCES

1. E. Charney, "The Molecular Basis of Optical Activity," Wiley, New York, 1979.

2. I. Tinoco, Jr. and M.P. Freeman, *J. Phys. Chem.* **61**, 1196 (1957).

3. D.M. Kearns, "Plane-Wave Scattering Matrix Theory of Antennas and Antenna-Antenna Interactions," National Bureau of Standards Rept. No. NBSIR 78-890, Boulder, Colo., 1978.

4. C.F. Bohren, *J. Coll. Interface Sci.* **66**, 105 (1978).

5. A. Lakhtakia, V.V. Varadan and V.K. Varadan, *J. Opt. Soc. Am.* **A5**, 175 (1988).

6. A. Lakhtakia, V.K. Varadan and V.V. Varadan, *IEEE Trans. Electromagn. Compat.* **28**, 90 (1986).

7. J.A. Stratton, "Electromagnetic Theory," p. 490, McGraw-Hill, New York, 1941.

8. J.R. Wait, "Electromagnetic Waves in Stratified Media," p. 21, Macmillan, New York, 1962.

9. A. Lakhtakia, V.K. Varadan and V.V. Varadan, *Appl. Opt.* **24**, 4146 (1985).

10. A. Lakhtakia and M.F. Iskander, *IEEE Trans. Antennas Propagat.* **31**, 111 (1983).

What happens to plane waves at the planar interfaces of mirror-conjugated chiral media

Akhlesh Lakhtakia, Vasundara V. Varadan, and Vijay K. Varadan

Department of Engineering Science and Mechanics, The Pennsylvania State University, University Park, Pennsylvania 16802

Received May 23, 1988; accepted September 21, 1988

The plane-wave reflection and transmission characteristics of bimaterial interfaces between chiral and chiral–achiral interfaces have been extensively explored. We report on the curious characteristics of the interface formed by two chiral half-spaces, one of which is the mirror image of the other; this is referred to as problem 1. It is shown that these characteristics are related to the reflection of plane waves on the interface of a chiral half-space and a perfectly conducting one, which constitutes problem 2.

INTRODUCTION

The lack of geometric symmetry between an object and its mirror image is referred to as chirality,[1,2] and the mirror image of a chiral object cannot be made to coincide with the object itself by any operation involving only rotations and/or translations. The most commonly investigated chiral objects are the L- and the D-type stereoisomers, which are familiar to organic chemists. The basis for the difference in the physical properties of the mirror conjugates lies in the handedness, or the chirality, possessed by their molecular configurations. When an electromagnetic disturbance travels through a medium consisting of chiral molecules, it is forced to adapt to the handedness of the molecules. In other words, linearly polarized plane waves cannot be made to propagate through such a medium, whereas left-circularly polarized (LCP) and right-circularly polarized (RCP) plane waves, traveling with different phase velocities, are perfectly acceptable solutions of the vector wave equation for this class of medium.

The usual constitutive equations $\mathbf{D} = \epsilon\mathbf{E}$ and $\mathbf{B} = \mu\mathbf{H}$ do not hold for chiral media; instead, the equations[1,2]

$$\mathbf{D} = \epsilon E + \beta\epsilon\nabla \times \mathbf{E}, \qquad \mathbf{B} = \mu\mathbf{H} + \beta\mu\nabla \times \mathbf{H} \tag{1}$$

are deemed applicable, with β being the chirality parameter. The regular time-harmonic Maxwell equations [$\exp(-j\omega t)$] are now utilized along with Eqs. (1), and, following Bohren,[3] the electric and the magnetic fields are transformed into

$$\mathbf{E} = \mathbf{Q}_L + a_R\mathbf{Q}_R, \qquad \mathbf{H} = \mathbf{Q}_R + a_L\mathbf{Q}_L, \tag{2}$$

where the LCP and the RCP fields, $\mathbf{Q}_L$ and $\mathbf{Q}_R$, respectively, must satisfy the conditions

$$\begin{aligned} (\nabla^2 + k_1^2)\mathbf{Q}_L = 0, \qquad (\nabla^2 + k_2^2)\mathbf{Q}_R = 0, \\ \nabla \times \mathbf{Q}_L = k_1\mathbf{Q}_L, \qquad \nabla \cdot \mathbf{Q}_L = 0, \\ \nabla \times \mathbf{Q}_R = -k_2\mathbf{Q}_R, \qquad \nabla \cdot \mathbf{Q}_R = 0. \end{aligned} \tag{3}$$

In these equations, $k_1 = k/(1 - k\beta)$ and $k_2 = k/(1 + k\beta)$, while $k = \omega(\epsilon\mu)^{1/2}$ is a convenient abbreviation; $a_R = -j(\mu/\epsilon)^{1/2}$ is an impedance, and $a_L = -j(\epsilon/\mu)^{1/2}$ is an admittance.

The plane-wave reflection and transmission characteristics of bimaterial interfaces between chiral and chiral–achiral interfaces have been extensively explored recently.[4–6] Here we report on the curious characteristics of the interface formed by two chiral half-spaces, one of which is the mirror image of the other; this is referred to as problem 1. We show that these characteristics are related to the reflection of plane waves on the interface of a chiral half-space and a perfectly conducting one; this constitutes problem 2.

PROBLEM 1

Let the space $z \leq 0$ be occupied by the chiral medium (ϵ, μ, β), while the half-space $z \geq 0$ is occupied by the mirror-conjugate medium (ϵ, μ, $-\beta$). Either a LCP or a RCP plane wave is incident upon the interface $z = 0$ from the zone $z \leq 0$. It is appropriate to express the fields in the zone $z \leq 0$ by the fields

$$\begin{aligned} \mathbf{Q}_L = A_L[\mathbf{e}_y + j(-\mathbf{e}_x\alpha_1 + \mathbf{e}_z\kappa)/k_1]\exp[j(\kappa x + \alpha_1 z)] \\ + B_L[\mathbf{e}_y + j(\mathbf{e}_x\alpha_1 + \mathbf{e}_z\kappa)/k_1]\exp[j(\kappa x - \alpha_1 z)], \\ z \leq 0, \end{aligned} \tag{4a}$$

$$\begin{aligned} \mathbf{Q}_R = A_R[\mathbf{e}_y + j(\mathbf{e}_x\alpha_2 - \mathbf{e}_z\kappa)/k_2]\exp[j(\kappa x + \alpha_2 z)] \\ + B_R[\mathbf{e}_y - j(\mathbf{e}_x\alpha_2 + \mathbf{e}_z\kappa)/k_2]\exp[j(\kappa x - \alpha_2 z)], \\ z \leq 0. \end{aligned} \tag{4b}$$

In these equations, A_L and A_R represent the incident plane waves, while B_L and B_R are the amplitudes of the reflected ones; κ is the horizontal wave number required by Snell's laws to satisfy the phase-matching condition on the interface $z = 0$; $\alpha_1 = +(k_1^2 - k^2)^{1/2}$ and $\alpha_2 = +(k_2^2 - k^2)^{1/2}$; and $\mathbf{e}_x$, etc. are the unit Cartesian vectors.

The half-space $z \geq 0$ is occupied by the mirror-conjugate medium; this means that phase velocities of the LCP and the RCP plane waves here are, respectively, those of the RCP and the LCP plane waves in the medium of incidence. Consequently, an acceptable representation of the fields in the medium of transmission is given by

0740-3232/89/010023-04$02.00

$$\mathbf{Q}_L = C_L[\mathbf{e}_y + j(-\mathbf{e}_x\alpha_2 + \mathbf{e}_z\kappa)/k_2]\exp[j(\kappa x + \alpha_2 z)], \quad z \geq 0, \quad (5a)$$

$$\mathbf{Q}_R = C_R[\mathbf{e}_y + j(\mathbf{e}_x\alpha_1 - \mathbf{e}_z\kappa)/k_1]\exp[j(\kappa x + \alpha_1 z)], \quad z \geq 0, \quad (5b)$$

with C_L and C_R being the transmission coefficients.

The solution of the boundary-value problem is sought in the convenient matrix forms

$$\begin{bmatrix} B_L \\ B_R \end{bmatrix} = \begin{bmatrix} R_{LL} & R_{LR} \\ R_{RL} & R_{RR} \end{bmatrix} \begin{bmatrix} A_L \\ A_R \end{bmatrix}, \quad (6a)$$

$$\begin{bmatrix} C_L \\ C_R \end{bmatrix} = \begin{bmatrix} T_{LL} & T_{LR} \\ T_{RL} & T_{RR} \end{bmatrix} \begin{bmatrix} A_L \\ A_R \end{bmatrix}, \quad (6b)$$

with the R's constituting the reflection matrix and the T's constituting the transmission matrix. The utilization of Eqs. (2), (4), and (5) in ensuring that there are no discontinuities in the tangential E fields and the tangential H fields across the interface $z = 0$ yields

$$\begin{aligned} R_{LL} &= -R_{RR} = (\alpha_1 k_2 - \alpha_2 k_1)/(\alpha_1 k_2 + \alpha_2 k_1), \\ T_{LL} &= 2\alpha_1 k_2/(\alpha_1 k_2 + \alpha_2 k_1), \\ T_{RR} &= 2\alpha_2 k_1/(\alpha_1 k_2 + \alpha_2 k_1), \\ R_{LR} &= R_{RL} = T_{LR} = T_{RL} = 0. \end{aligned} \quad (7)$$

This curious result should be noted: If the incident plane wave is LCP (RCP), then the reflected and the transmitted waves are also LCP (RCP). There are no waves of the opposite handedness generated at the planar boundaries between mirror-conjugated chiral media. Thus, the arrangement of problem 1 acts somewhat like a beam splitter; an incident LCP (RCP) plane wave is broken into two LCP (RCP) plane waves, which leave the interface in opposite z directions with different amplitudes and phase velocities.

PROBLEM 2

Let the medium in the zone $z \geq 0$ be perfectly conducting. Then a solution of the form

$$\begin{bmatrix} B_L \\ B_R \end{bmatrix} = \begin{bmatrix} r_{LL} & r_{LR} \\ r_{RL} & r_{RR} \end{bmatrix} \begin{bmatrix} A_L \\ A_R \end{bmatrix} \quad (8)$$

is to be sought. For this purpose, Eqs. (2) and (4) are utilized to ensure the nulling of the tangential E field at the impenetrable surface $z = 0$, and the result obtained is

$$\begin{aligned} r_{LL} &= -r_{RR} = (\alpha_1 k_2 - \alpha_2 k_1)/(\alpha_1 k_2 + \alpha_2 k_1), \\ r_{RL} &= 2a_L\alpha_1 k_2/(\alpha_1 k_2 + \alpha_2 k_1), \\ r_{LR} &= -2a_R\alpha_2 k_1/(\alpha_1 k_2 + \alpha_2 k_1). \end{aligned} \quad (9)$$

We observe, therefore, that when a LCP or a RCP plane wave hits a perfectly conducting surface, the reflected field

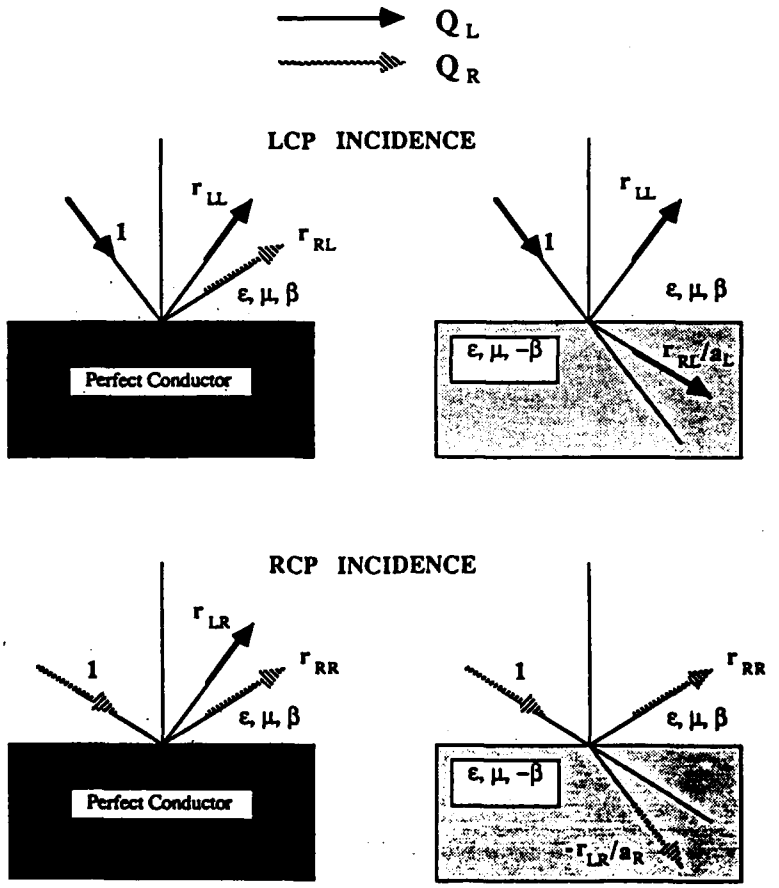

Fig. 1. Illustration of the correspondence between problems 1 and 2 in accordance with Eqs. (10). Problem 1 considers the interface of a chiral medium and a perfect conductor, while in problem 2 the two chiral media on either side of the interface are mirror conjugates.

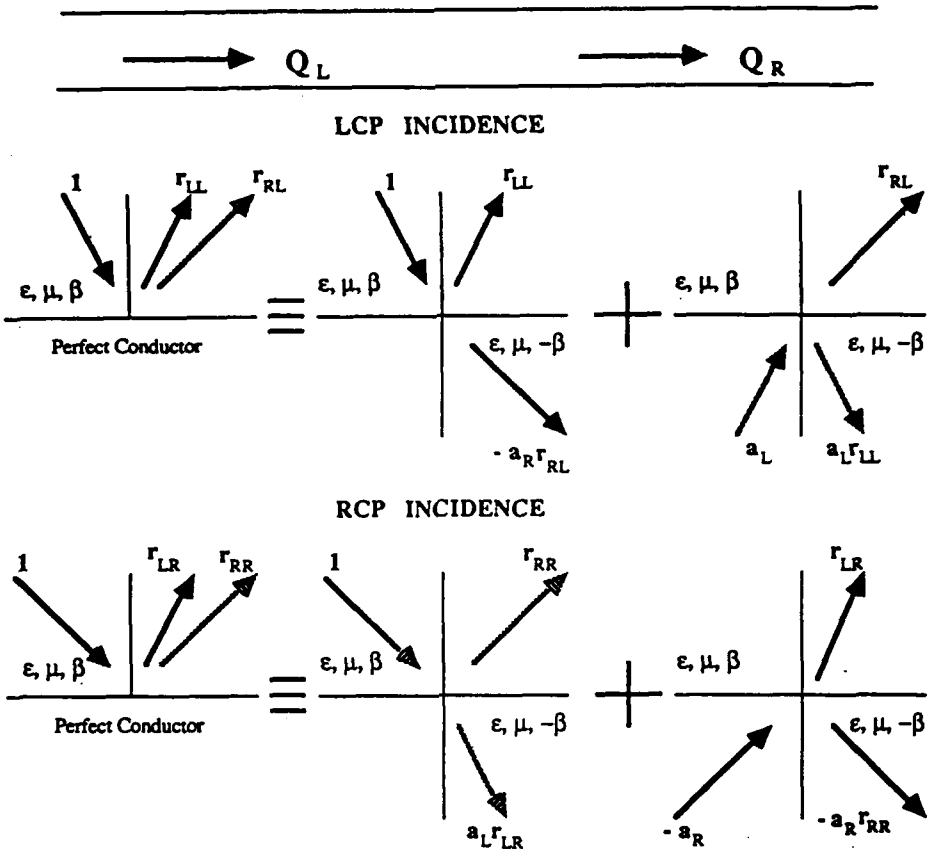

Fig. 2. Illustration of the imaging concept for problem 2 by using two specializations of problem 1. See Fig. 1 for the descriptions of problems 1 and 2.

consists of components of both circular polarization states. However, when $\kappa = k_1$, then $r_{RL} = 0$, $r_{LL} = -1$, $r_{LR} = -2a_R$, and $r_{RR} = 1$, which gives rise to the trivial case of no reflection for the grazing LCP incidence. Likewise, when $\kappa = k_2$, then $r_{LR} = 0$, $r_{RR} = -1$, $r_{RL} = 2a_L$, and $r_{LL} = 1$.

DISCUSSION

The correspondence between the solutions [Eqs. (7) and (9)] of problems 1 and 2 should be noted. That is,

$$R_{LL} = r_{LL}, \qquad R_{RR} = r_{RR},$$
$$T_{LL} = r_{RL}/a_L, \qquad T_{RR} = -r_{LR}/a_R. \tag{10}$$

For illustration, let us consider the case of LCP incidence. In problems 1 and 2, r_{LL} is the amplitude of the reflected LCP wave that travels with a phase velocity ω/k_1. In problem 2, r_{RL} is the amplitude of the *reflected* RCP wave with a phase velocity ω/k_2, but in problem 1, r_{RL}/a_L is the amplitude of the *transmitted* LCP wave, which also travels with a phase velocity ω/k_2 because the medium of transmission is the mirror conjugate of the medium of incidence and reflection. Analogous comments also apply to the case of RCP plane-wave incidence, and both cases are schematically illustrated in Fig. 1. It should be noted that Fermat's principle is equally well satisfied in problems 1 and 2, and in identical fashion.

The correspondences given in Eqs. (10), coupled with the complementary relations

$$r_{LL}(-\beta) = r_{RR}(\beta), \qquad r_{RR}(-\beta) = r_{LL}(\beta),$$
$$r_{LR}(-\beta) = a_R{}^2 r_{RL}(\beta), \qquad r_{RL}(-\beta) = a_L{}^2 r_{LR}(\beta) \tag{11}$$

point to the imaging concept. Consider problem 2 again with an incident LCP plane wave of unit amplitude. Relevant to the zone $z \leq 0$, this problem is equivalent to the superposition of two problems, each of which is a specialization of problem 1. These two problems are (i) a problem 1 in which a LCP plane wave is incident upon the interface from the zone $z \leq 0$ with unit amplitude and (ii) a problem 1 in which a RCP plane wave is incident upon the interface from the zone $z \geq 0$ with an amplitude equal to a_L. The case of an incident RCP plane wave in problem 2 can also be handled in this way, and both cases are schematically illustrated in Fig. 2. However, as becomes clear from Fig. 2, the use of an imaging theory for chiral media is complicated for scattering problems in general: not only do the sources get imaged but the medium does also.

The authors are also with the Center for the Engineering of Electronic and Acoustic Materials, The Pennsylvania State University, University Park, Pennsylvania.

REFERENCES

1. C. F. Bohren and D. R. Huffman, *Absorption and Scattering of Light by Small Particles* (Wiley, New York, 1983).
2. A. Lakhtakia, V. V. Varadan, and V. K. Varadan, "Field equations, Huygens's principle, integral equations, and theorems for

radiation and scattering of electromagnetic waves in isotropic chiral media," J. Opt. Soc. Am. A 5, 175–184 (1988).
3. C. F. Bohren, "Light scattering by an optically active sphere," Chem. Phys. Lett. 29, 458–462 (1974).
4. A. Lakhtakia, V. V. Varadan, and V. K. Varadan, "A parametric study of microwave reflection characteristics of a planar achiral-chiral interface," IEEE Trans. Electromag. Compat. EC-28, 90–95 (1986).
5. M. P. Silverman, "Reflection and refraction at the surface of a chiral medium: comparison of gyrotropic constitutive relations invariant or noninvariant under a duality transformation," J. Opt. Soc. Am. A 3, 830–837 (1986).
6. V. K. Varadan, V. V. Varadan, and A. Lakhtakia, "On the possibility of designing anti-reflection coatings using chiral composites," J. Wave Mater. Interact. 2, 71–81 (1987).

Green's functions for propagation of sound in a simply moving fluid

Akhlesh Lakhtakia, Vijay K. Varadan, and Vasundara V. Varadan
The Center for the Engineering of Electronic and Acoustic Materials and Department of Engineering Science and Mechanics, The Pennsylvania State University, University Park, Pennsylvania 16802

(Received 25 February 1988; accepted for publication 16 January 1989)

Two approaches involving the spatial and temporal Fourier transforms have been used to derive time- and space-dependent Green's functions pertinent to the propagation of sound waves in a fluid that is moving with a constant velocity $\mathbf{v}$. The two approaches give rise to differing interpretations of the observations made by a stationary observer *vis-à-vis* those made by an observer moving with the fluid. The properties of the causal and the noncausal Green's functions are analyzed, and are shown to be equivalent.

PACS numbers: 43.20.Rz, 43.30.Es

INTRODUCTION

It is readily apparent that, at the point of observation, the acoustic frequency spectrum of a radiating source is altered by the flow of the fluid in which the source and the observer are embedded; this phenomenon has been the subject of intense investigation.[1–4] In spite of the widespread interest, particularly in the area of fluid mechanics,[5–7] we have not been able to come across a systematic derivation of the pertinent Green's function; although, it should be noted that, for the corresponding problem in electromagnetic field theory, Green's functions are commonly available.[8–10]

Here, we will utilize spatial as well as temporal Fourier transforms in order to derive two separate expressions for the Green's function pertinent to the radiation and propagation of sound waves in an ideal fluid flowing with a constant velocity $\mathbf{v}$. These two approaches involve interchanging the order in which the spatial and the temporal transforms, and correspond to Doppler shifts in either spatial or temporal frequencies. Thus the two approaches give rise to differing interpretations of the observations made by a stationary observer *vis-à-vis* those made by an observer moving with the fluid. It is shown that the causal Green's functions derived from the two approaches are identical.

I. PRELIMINARIES

As per Morse and Ingard,[11] in a fluid moving with a velocity $\mathbf{v}$, the acoustic pressure $p(\mathbf{r},t)$ satisfies the wave equation

$$\left[\nabla^2 - c^{-2}\left(\frac{\partial}{\partial t} + \mathbf{v}\cdot\nabla\right)^2\right] p(\mathbf{r},t) = 0 \tag{1}$$

within a source-free region, c being the speed of sound in the medium at rest (i.e., when $\mathbf{v} = 0$); this equation is valid in a coordinate system that is moving with a velocity $-\mathbf{v}$ with respect to a parallel coordinate frame affixed to the fluid. The first coordinate system (x,y,z,t) is called *stationary*, while another coordinate system (x,y,z',t'), to be discussed later, will be referred to as the *auxiliary* system; the velocity $\mathbf{v} = v\mathbf{e}_z$ in the stationary system, $\mathbf{e}_z$ being the unit vector. The corresponding Green's function, therefore, must be the solution of the inhomogeneous wave equation

$$\left[\nabla^2 - c^{-2}\left(\frac{\partial}{\partial t} + \mathbf{v}\cdot\nabla\right)^2\right] g(\mathbf{r},t) = -\delta(\mathbf{r})\delta(t), \tag{2}$$

$\delta(\cdot)$ being the Dirac delta function.

As Jackson[12] has pointed out, (1) is not invariant under Galilean transformations, and no kinematic transformation of $p(\mathbf{r},t)$ can eliminate the term $\mathbf{v}\cdot\nabla$ in (1). The solution of (2) can, however, be very easily attempted if the term $(\partial/\partial t + \mathbf{v}\cdot\nabla)$ can be simplified, and Fourier analysis comes in very useful for that purpose. We define two sets of Fourier transform pairs: one in the time $\Leftrightarrow$ *temporal* frequency domains specified by the twin sets of relations[13]

$$a(t) = (2\pi)^{-1}\int_{-\infty}^{\infty} d\omega \exp(-i\omega t)a(\omega), \tag{3a}$$

$$a(\omega) = \int_{-\infty}^{\infty} dt \exp(i\omega t)a(t), \tag{3b}$$

ω being the temporal frequency; and the second in the space $\Leftrightarrow$ *spatial* frequency domains given as[14]

$$a(\mathbf{r}) = (2\pi)^{-3}\int_{-\infty}^{\infty}\int\int d^3\mathbf{q} \exp(i\mathbf{q}\cdot\mathbf{r})a(\mathbf{q}), \tag{4a}$$

$$a(\mathbf{q}) = \int_{-\infty}^{\infty}\int\int d^3\mathbf{r} \exp(-i\mathbf{q}\cdot\mathbf{r})a(\mathbf{r}), \tag{4b}$$

in which $\mathbf{q}$ is the (vector) three-dimensional spatial frequency variable. Armed with these two sets of Fourier transform pairs, we can solve (2) via any one of the two approaches possible.

II. DOPPLER SHIFT IN THE TEMPORAL FREQUENCY

The first approach involves taking the temporal Fourier transform of (2), which yields the relation

$$[\nabla^2 - c^{-2}(-i\omega + \mathbf{v}\cdot\nabla)^2]g(\mathbf{r},\omega) = -\delta(\mathbf{r}), \tag{5}$$

after using the integral representation of $\delta(t)$ given as

 0001-4966/89/051852-05$00.80

$$\delta(t) = (2\pi)^{-1} \int_{-\infty}^{\infty} d\omega \exp(-i\omega t). \quad (6)$$

Next, we employ the factorization[4,15–17]

$$g(\mathbf{r},\omega) = h(\mathbf{r},\omega)\exp[-i(\omega/c)M\gamma^2 z], \quad (7)$$

which is nothing but an expression of the Doppler shift in the temporal frequency domain. In (7), the Mach number $M = v/c$, and $\gamma^2(1-M^2) = 1$; we restrict $M < 1$.

As a consequence of (7), (5) simplifies to

$$[\nabla^2 - (M\mathbf{e}_z\cdot\nabla)^2 + (\gamma\omega/c)^2]h(\mathbf{r},\omega) = -\delta(\mathbf{r})\exp[i(\omega/c)M\gamma^2 z]. \quad (8)$$

Utilization of (4a) and (4b), along with the representation

$$\delta(\mathbf{r}) = (2\pi)^{-3} \int_{-\infty}^{\infty}\int\int d^3\mathbf{q} \exp(i\mathbf{q}\cdot\mathbf{r}) \quad (9)$$

for the Dirac delta function $\delta(\mathbf{r})$, in (8) then gives rise to the algebraic relation

$$h(\mathbf{q},\omega) = -(c/\gamma)^2/\{\omega^2 - (c/\gamma)^2[\mathbf{q}\cdot\mathbf{q} - M^2(\mathbf{e}_z\cdot\mathbf{q})^2]\}. \quad (10)$$

As a first step towards obtaining $h(\mathbf{r},t)$, we take the inverse temporal Fourier transform of (10); the application of (3a) to (10) yields[13]

$$h(\mathbf{q},t) = (2\pi)^{-1}(c/\gamma)[\pi\,\mathrm{sgn}(t)] \times [\mathbf{q}\cdot\mathbf{q} - M^2(\mathbf{e}_z\cdot\mathbf{q})^2]^{-1/2} \times \sin\{(ct/\gamma)\sqrt{[\mathbf{q}\cdot\mathbf{q} - M^2(\mathbf{e}_z\cdot\mathbf{q})^2]}\}, \quad (11)$$

whence, on taking the inverse spatial Fourier transform also, we get

$$h(\mathbf{r},t) = (2\pi)^{-4}(c/\gamma)[\pi\,\mathrm{sgn}(t)]I(M;\mathbf{r},t), \quad (12)$$

in which the signum function $\mathrm{sgn}(\xi) = 2U(\xi) - 1$, whereas the Heaviside function $U(\xi) = 1\,\forall\,\xi > 0$ and $U(\xi) = 0\,\forall\,\xi < 0$.

On expanding $\mathbf{q}$ in a cylindrical coordinate space (q_ρ, φ_q, q_z), $q_z = \mathbf{q}\cdot\mathbf{e}_z$, the integral $I(M;\mathbf{r},t)$ in (12) can be given as

$$I(M;\mathbf{r},t) = \int_{-\infty}^{\infty} dq_z \exp(iq_z z)\int_0^{\infty} dq_\rho\, q_\rho \times\left[q_\rho^2 + \left(\frac{q_z}{\gamma}\right)^2\right]^{-1/2} \times\sin\left[\left(\frac{ct}{\gamma}\right)\sqrt{q_\rho^2 + \left(\frac{q_z}{\gamma}\right)^2}\right] \times\int_0^{2\pi} d\varphi_q \exp(iq_\rho\rho\cos\varphi_q). \quad (13)$$

The integral on the azimuthal angle φ_q is easily implemented via an integral representation of the cylindrical Bessel function $J_0(\xi)$:

$$J_0(\xi) = (2\pi)^{-1}\int_0^{2\pi} d\alpha \exp(i\xi\cos\alpha); \quad (14a)$$

and the consequent integral on q_ρ can be calculated through Sonine's discontinuous integral[18]:

$$\int_0^{\infty} d\xi\,\xi J_0(c\xi)\sin(a\sqrt{\xi^2+b^2})(\xi^2+b^2)^{-1/2} = \cos(b\sqrt{a^2-c^2})(a^2-c^2)^{-1/2}U(a-c), \quad c>0. \quad (14b)$$

As a result,

$$I(M;\mathbf{r},t) = (2\pi)U\left(\frac{ct}{\gamma}-\rho\right)\left(\frac{1}{t_0}\right)\int_{-\infty}^{\infty} dq_z \times\exp(iq_z z)\cos(\gamma^{-1}q_z t_0), \quad (15a)$$

$$= 4\pi^2 U\left(\frac{ct}{\gamma}-\rho\right)\left(\frac{1}{t_0}\right)\left(\frac{1}{2}\right) \times\left[\delta\left(z+\frac{t_0}{\gamma}\right)+\delta\left(z-\frac{t_0}{\gamma}\right)\right], \quad (15b)$$

on utilizing (6); in these equations,

$$t_0 = \sqrt{(ct/\gamma)^2 - \rho^2}, \quad (16a)$$

$$\rho = +\sqrt{x^2+y^2}. \quad (16b)$$

Further simplification is afforded by the fact that

$$2|\alpha|\delta(\xi^2-\alpha^2) = \delta(\xi+\alpha)+\delta(\xi-\alpha), \quad (17)$$

and that $ct/\gamma > \rho$ due to the Heaviside function; consequently,

$$I(M;\mathbf{r},t) = (4\pi^2/\gamma)U(ct/\gamma-\rho)\delta(z^2-\gamma^{-2}t_0^2), \quad (18a)$$

and

$$h(\mathbf{r},t) = (c/4\gamma^2\pi^2)[\pi\,\mathrm{sgn}(t)]U(ct/\gamma-\rho) \times\delta(z^2-\gamma^{-2}t_0^2), \quad (18b)$$

From (3) and (7), it is easy to see that

$$g(\mathbf{r},t) = h(\mathbf{r},t+Mc^{-1}\gamma^2 z); \quad (19)$$

hence, a solution of (2), to be subscripted t for later use, is given as

$$g_t(\mathbf{r},t) = (c/4\pi^2)[\pi\,\mathrm{sgn}(t+Mc^{-1}\gamma^2 z)] \times U[c(t+Mc^{-1}\gamma^2 z)/\gamma-\rho] \times\delta(r^2-2zvt-c^2\gamma^{-2}t^2). \quad (20)$$

To be noted is the fact that the inversion (13) of (12) had not assumed causality; if causality is to be incorporated when the inverse temporal Fourier transform of (11) is taken,[13,19] then the signum function $\mathrm{sgn}(t+Mc^{-1}\gamma^2 z)$ in (20) should be replaced by the $2U(t+Mc^{-1}\gamma^2 z)$. Here and hereafter, the term causal should be interpreted as *causal with respect to time.*

III. DOPPLER SHIFT IN THE SPATIAL FREQUENCY

The second approach mirrors the first one in that the order of taking the *temporal* and the *spatial* Fourier transforms is reversed. Thus, on using (4) and (9) in (2), we obtain

$$\left[-\mathbf{q}\cdot\mathbf{q} - c^{-2}\left(\frac{\partial}{\partial t}+iv\cdot\mathbf{q}\right)^2\right]g(\mathbf{q},t) = -\delta(t). \quad (21$$

The introduction of the factorization

$$g(\mathbf{q},t) = f(\mathbf{q},t)\exp(-i\mathbf{e}_z\cdot\mathbf{q}vt) \quad (22$$

in (21) results in

$$\left(-\mathbf{q}\cdot\mathbf{q}-c^{-2}\frac{\partial^2}{\partial t^2}\right)f(\mathbf{q},t)=-\delta(t)\exp(i\mathbf{e}_z\cdot\mathbf{q}vt). \tag{23}$$

It should be noted that (22) tantamounts to a Doppler shift in the spatial frequency domain.

The temporal Fourier transform of (23) gives rise to the algebraic expression for $f(\mathbf{q},\omega)$ given by

$$f(\mathbf{q},\omega)=-c^2/(\omega^2-\mathbf{q}\cdot\mathbf{q}c^2). \tag{24}$$

As a first step towards deriving $f(\mathbf{r},t)$, the inverse temporal Fourier transform is taken; hence,[13]

$$f(\mathbf{q},t)=(2\pi)^{-1}c^2[\pi\,\mathrm{sgn}(t)](qc)^{-1}\sin(qct), \tag{25}$$

from where, on taking the inverse spatial Fourier transform also, we get

$$f(\mathbf{r},t)=(2\pi)^{-4}c[\pi\,\mathrm{sgn}(t)]J(M;\mathbf{r},t), \tag{26}$$

in which the integral $J(M;\mathbf{r},t)$ is given by

$$J(M;\mathbf{r},t)=\int_{-\infty}^{\infty}dq_z\exp(iq_zz)\int_0^{\infty}dq_\rho\,q_\rho(q_\rho^2+q_z^2)^{-1/2}\times\sin(ct\sqrt{q_\rho^2+q_z^2})\times\int_0^{2\pi}d\varphi_q\exp(iq_\rho\rho\cos\varphi_q). \tag{27}$$

The use of (14a), (14b) and (17) in (27) finally yields

$$J(M;\mathbf{r},t)=4\pi^2U(ct-\rho)\delta(r^2-c^2t^2), \tag{28a}$$

whence

$$f(\mathbf{r},t)=(c/4\pi^2)[\pi\,\mathrm{sgn}(t)]U(ct-\rho)\delta(r^2-c^2t^2). \tag{28b}$$

Finally, by applying (22) in (4), it can be shown that

$$g(\mathbf{r},t)=f(\mathbf{r}-\mathbf{v}t,t), \tag{29}$$

and the use of this relationship in (28b) gives the Green's function

$$g_r(\mathbf{r},t)=(c/4\pi^2)\times[\pi\,\mathrm{sgn}(t)]U(ct-\rho)\delta(r^2-2zvt-c^2\gamma^{-2}t^2); \tag{30}$$

the subscript r on g in (30) is for later use. Again, we note that g_r derived above is noncausal; for causality to be incorporated, $\mathrm{sgn}(t)$ should be replaced by $2U(t)$.

IV. DISCUSSION

The two Green's functions derived above share one important feature, i.e., they possess the same singularities. The singularities of both $g_t(\mathbf{r},t)$ and $g_r(\mathbf{r},t)$ are embedded in the delta function that can be expanded as

$$\delta(r^2-2zvt-c^2\gamma^{-2}t^2)=(2\gamma\sqrt{R^2+2zvt+c^2\gamma^{-2}t^2})^{-1}\times[\delta(z+\gamma^{-1}\sqrt{R^2+2zvt+c^2\gamma^{-2}t^2})+\delta(z-\gamma^{-1}\sqrt{R^2+2zvt+c^2\gamma^{-2}t^2})], \tag{31a}$$

where

$$R^2=M^2\gamma^2z^2-\rho^2. \tag{31b}$$

In this respect, therefore, there is nothing to distinguish between $g_t(\mathbf{r},t)$ and $g_r(\mathbf{r},t)$. In addition, it should be noted that if $v=0$, then both g_t and g_r reduce to the familiar expression

$$g_t(\mathbf{r},t)|_{v=0}=g_r(\mathbf{r},t)|_{v=0}=(1/4\pi^2r)[\pi\,\mathrm{sgn}(t)]U(ct-\rho)\times[\delta(t-rc^{-1})+\delta(t+rc^{-1})], \tag{32}$$

which too can be made causal if $\mathrm{sgn}(t)$ is replaced by $2U(t)$ and the second delta function is omitted. However, the switching functions, i.e., the signum and the Heaviside functions, included in (20) and (30) have different arguments.

The major reason for the difference between $g_r(\mathbf{r},t)$ and $g_t(\mathbf{r},t)$ appears to be due to the specific factorizations (7) and (22), respectively. As stated earlier, while (7) expresses a Doppler shift for time-harmonic waves, (22) gives rise to a Doppler shift for space-harmonic fields. However, it is easy to show that

$$g_t(\mathbf{r},t)=(2\pi)^{-4}\int_{-\infty}^{\infty}d\omega\exp(-i\omega t)\exp\left(\frac{-i\omega M\gamma^2z}{c}\right)\times\int_{-\infty}\iiint^{\infty}d^3\mathbf{q}\exp(i\mathbf{q}\cdot\mathbf{r})h(\mathbf{q},\omega) \tag{33}$$

is a proper solution of (2) by substituting (33) in (2) and noting that the differential operators of the left side of (2) will act only on the exponential terms of (33). Moreover, it is also possible to show similarly that

$$h(\mathbf{r},t)=(2\pi)^{-4}\int_{-\infty}^{\infty}d\omega\exp(-i\omega t)\times\int_{-\infty}\iiint^{\infty}d^3\mathbf{q}\exp(i\mathbf{q}\cdot\mathbf{r})h(\mathbf{q},\omega) \tag{34a}$$

satisfies the differential equation

$$\left[\nabla^2-M\frac{\partial^2}{\partial z^2}-\left(\frac{\gamma}{c}\right)^2\frac{\partial^2}{\partial t^2}\right]h(\mathbf{r},t)=-\delta(\mathbf{r})\delta(t). \tag{34b}$$

It should be noted that by using (19) in (2), it is observed that

$$\left[\left(\frac{\partial^2}{\partial x^2}\right)+\left(\frac{\partial^2}{\partial y^2}\right)+\gamma^{-2}\left(\frac{\partial^2}{\partial z'^2}\right)-\left(\frac{\gamma}{c}\right)^2\left(\frac{\partial^2}{\partial t'^2}\right)\right]h(x,y,z',t')=-\delta(\mathbf{r})\delta(t), \tag{34c}$$

where $t'=t+M\gamma^2z/c$, $z'=z$, and it is assumed that the stationary and the auxiliary frames coincide at $t=t'=0$. Likewise, it can also be shown that

$$g_r(\mathbf{r},t)=(2\pi)^{-4}\int_{-\infty}\iiint^{\infty}d^3\mathbf{q}\exp(i\mathbf{q}\cdot\mathbf{r})\exp(-i\mathbf{q}\cdot\mathbf{v}t)\times\int_{-\infty}^{\infty}d\omega\exp(-i\omega t)f(\mathbf{q},\omega) \tag{35}$$

is also a proper solution of (2) by substituting (35) in (2). In addition,

$$f(\mathbf{r},t)=(2\pi)^{-4}\int_{-\infty}\iiint^{\infty}d^3\mathbf{q}\exp(i\mathbf{q}\cdot\mathbf{r})\times\int_{-\infty}^{\infty}d\omega\exp(-i\omega t)f(\mathbf{q},\omega) \tag{36a}$$

satisfies the differential equation

$$\left(\nabla^2 - c^{-2}\frac{\partial^2}{\partial t^2}\right) f(\mathbf{r},t) = -\delta(\mathbf{r})\delta(t). \tag{36b}$$

Again, it is to be noted that by substituting (29) in (2), and assuming that the stationary and the auxiliary frames coincide at $z = z' = 0$, that

$$\left[\left(\frac{\partial^2}{\partial x^2}\right) + \left(\frac{\partial^2}{\partial y^2}\right) + \left(\frac{\partial^2}{\partial z'^2}\right) - c^{-2}\left(\frac{\partial^2}{\partial t'^2}\right)\right] f(x, y, z', t') = -\delta(\mathbf{r})\delta(t), \tag{36c}$$

where $z' = z - vt$ and $t' = t$. Thus the proprieties of the two procedures are in good standing.

The equivalence of $g_r(\mathbf{r},t)$ and $g_t(\mathbf{r},t)$ is now demonstrated. Using the relations (4b) and (7), it can be shown that

$$g_t(\mathbf{q},\omega) = h(\mathbf{q} + \omega\gamma^2\mathbf{v}/c^2, \omega), \tag{37a}$$

while, from (3b) and (22),

$$g_r(\mathbf{q},\omega) = f(\mathbf{q}, \omega - \mathbf{q}\cdot\mathbf{v}). \tag{37b}$$

However, the right sides of (37a) and (37b) are identical as can be seen by utilizing (10) and (24). Therefore, in the temporal-spatial-frequency domain, $g_r(\mathbf{q},\omega)$ and $g_t(\mathbf{q},\omega)$ are identical, as should be expected.[20] As a result of the uniqueness theorem for the inverse Fourier transforms,[21] it follows that $g_r(\mathbf{r},t) = g_t(\mathbf{r},t)$ except *perhaps* at their singularities. It is obvious that everywhere except at their (common) singularities, $g_r(\mathbf{r},t) = g_t(\mathbf{r},t) = 0$ as a consequence of the delta functions in (20) and (30).

Finally, we show that the two *causal* Green's functions have identical values at their singularities. Analyzing, first, for the causal $g_t(\mathbf{r},t)$, it should be noted that

$$r^2 - 2zvt - c^2\gamma^{-2}t^2 = \rho^2 + \gamma^2 z^2 - (c/\gamma)^2(t + M\gamma^2 z/c)^2 \tag{38}$$

and $\rho \geq 0$. Therefore, at the singularities $\rho^2 + \gamma^2 z^2 = (c/\gamma)^2 \times (t + M\gamma^2 z/c)^2$; together with $\rho \geq 0$, this implies that $(c/\gamma) \times (t + M\gamma^2 z/c) \geq \rho$. As a result, at its singularities, the causal $g_t(\mathbf{r},t) = c/2\pi$. Next, for the causal $g_r(\mathbf{r},t)$ it should be noted that

$$r^2 - 2zvt - c^2\gamma^{-2}t^2 = \rho^2 + (z - vt)^2 - c^2t^2. \tag{39}$$

Therefore, at the singularities, $\rho^2 + (z - vt)^2 = c^2t^2$; together with $\rho \geq 0$, this implies that $ct \geq \rho$. Consequently, at its singularities, the causal $g_r(\mathbf{r},t) = c/2\pi$. Hence, the causal $g_r(\mathbf{r},t)$ and $g_t(\mathbf{r},t)$ are equal for all r and $t \geq 0$. Similar reasoning also gives the noncausal $g_t(\mathbf{r},t) = g_r(\mathbf{r},t) = c/4\pi$ at their singularities, consequently, the noncausal $g_t(\mathbf{r},t)$ and $g_r(\mathbf{r},t)$ are also equal everywhere.

From the available literature, it is observed that

$$g_t(\mathbf{r},\omega) = \left(\frac{\gamma}{4\pi}\right)\exp\left[i\left(\frac{\gamma\omega}{c}\right)\sqrt{(x^2 + y^2 + \gamma^2 z^2)}\right] \times \exp\left[-i\left(\frac{\omega}{c}\right)M\gamma^2 z\right](x^2 + y^2 + \gamma^2 z^2)^{-1/2} \tag{40}$$

has been commonly utilized for solving time-harmonic problems.[4,15-17] On the other hand, $g_r(\mathbf{r},t)$ is in a form more amenable to interpretation for time-dependent problems. In order to illustrate the utility of these Green's functions, we consider a source pressure which acts on a ring of radius a.

First, let the time-harmonic problem be considered, i.e., the source pressure

$$p_s(\mathbf{r},\omega) = (P/a)\delta(\rho - a)\delta(z)\exp(-i\omega t), \tag{41}$$

P being some constant. The radiated pressure will be isotropic in the x-y plane; hence, in the x-z plane it will be given, using (40) and (41), as

$$p_{\text{rad}}(x,0,z,\omega) = \left(\frac{P\gamma}{4\pi}\right)\exp(-i\omega t)\exp\left[-i\left(\frac{\omega}{c}\right)M\gamma^2 z\right]\int_0^{2\pi} d\varphi_0 \times \exp[i(\gamma\omega/c)\sqrt{x^2 + a^2 - 2ax\cos\varphi_0 + \gamma^2 z^2}] \times (x^2 + a^2 - 2ax\cos\varphi_0 + \gamma^2 z^2)^{-1/2}, \quad x \neq a. \tag{42}$$

The evaluation of this integral must be done numerically; however Fraunhoffer-type approximations[14] can be made to obtain the far-zone pressure quite easily. If $(x^2 + \gamma^2 z^2)^{1/2} \to \infty$, then the integrand can be simplified to

$$\exp[i(\gamma\omega/c)(x^2 + \gamma^2 z^2)^{1/2}](x^2 + \gamma^2 z^2)^{-1/2} \times \exp[-i(\gamma\omega/c)ax\cos\varphi_0(x^2 + \gamma^2 z^2)^{-1/2}].$$

In which case, (42) simplifies to

$$p_{\text{rad}}(x,0,z,\omega) = (P\gamma/2)\exp(-i\omega t)\exp[-i(\omega/c)M\gamma^2 z] \times \exp[i(\gamma\omega/c)(x^2 + \gamma^2 z^2)^{1/2}](x^2 + \gamma^2 z^2)^{-1/2} \times J_0[(\gamma\omega/c)ax(x^2 + \gamma^2 z^2)^{-1/2}]. \tag{43}$$

To illustrate the use of $g_r(\mathbf{r},t)$, we consider the same ring source with an impulse excitation; i.e.

$$p_s(\mathbf{r},t) = (P/a)\delta(\rho - a)\delta(z)\delta(t). \tag{44}$$

In the equatorial plane $z = 0$, the radiation is isotropic. Hence, from the causal version of (30), the radiated pressure will be given by

$$p_{\text{rad}}(x,0,0,t) = \left(\frac{Pc\gamma}{2\pi}\right)\int_0^{\pi} d\varphi_0 \times \delta(ct \mp \gamma\sqrt{x^2 + a^2 - 2ax\cos\varphi_0}) \times (x^2 + a^2 - 2ax\cos\varphi_0)^{-1/2}, \quad t > 0. \tag{45}$$

Thus $p_{\text{rad}}(x,0,0,t)$ exists only for $\gamma(x - a) < ct < \gamma(x + a)$ and has a magnitude of $(P\gamma^2/2\pi)/t$ during that interval. On the other hand, along the z axis, the radiated pressure is

$$p_{\text{rad}}(0,0,z,t) = Pc\gamma^2\,\delta(ct + zM\gamma^2 - \sqrt{z^2M^2\gamma^4 + \gamma^2 z^2 + \gamma^2 a^2}). \tag{46}$$

It should be noted that the time of arrival at the origin from (46) equals $t = (\gamma/c)a$; thus the radiated pulse arrives there later in a moving fluid than in a stationary fluid. Also, $t = a/c$ is time of arrival at $z = Ma$, while $t = (a/c)\gamma^2(1 + M^2)$ is the time of arrival at $z = -Ma$ on the z axis, which conclusions correspond, respectively, to the upstream and the downstream velocities of z-directed plane waves derived by Ingard and Singhal for moving fluids.[20]

ACKNOWLEDGMENTS

It is a pleasure to acknowledge some discussions with our colleague, Professor S. I. Hayek of Penn State.

[1]H. P. Greenspan, *The Theory of Rotating Fluids* (Cambridge U.P., Cambridge, England, 1968), Chap. 4.
[2]F. P. Bretherton and C. J. R. Garrett, "Wavetrains in inhomogeneous moving media," Proc. R. Soc. London Ser. A 302, 529–544 (1969).
[3]M. J. Lighthill, "The fourth annual Fairey lecture: The propagation of sound through moving fluids," J. Sound Vib. 24, 471–492 (1972).
[4]D. Censor, "Propagation and scattering of sound waves in moving media," Isr. J. Tech. 9, 7–17 (1971).
[5]D. G. Crighton and J. E. Ffowcs-Williams, "Real space-time Green's functions applied to plate vibration induced by turbulent flow," J. Fluid Mech. 38, 305–313 (1969).
[6]J. E. Ffowcs-Williams and D. J. Lovely, "Sound radiation into uniformly flowing fluid by compact surface vibrations," J. Fluid Mech. 71, 689–700 (1975).
[7]M. S. Howe, "The generation of sound by aerodynamic sources in an inhomogeneous steady flow," J. Fluid Mech. 67, 597–610 (1975).
[8]C. T. Tai, "The dyadic Green's function for a moving isotropic medium," IEEE Trans. Antennas Propag. AP-13, 322–323 (1965).
[9]R. T. Compton, Jr., "The time-dependent Green's function for electromagnetic waves in moving simple media," J. Math. Phys. 7, 2145–2152 (1966).
[10]H. C. Chen, *Theory of Electromagnetic Waves* (McGraw-Hill, New York, 1983), Chaps. 8 and 11.
[11]P. M. Morse and K. U. Ingard, *Theoretical Acoustics* (McGraw-Hill, New York, 1968), Chap. 11.
[12]J. D. Jackson, *Classical Electrodynamics* (Wiley, New York, 1975), Sec. 11.1.
[13]B. P. Lathi, *Communication Systems* (Wiley, New York, 1968), Chap. 1.
[14]J. W. Goodman, *Introduction to Fourier Optics* (McGraw-Hill, New York, 1968).
[15]J. W. Miles, "On the reflection of sound at an interface of relative motion," J. Acoust. Soc. Am. 29, 226–228 (1957).
[16]C. Yeh, "Reflection and transmission of sound waves by a moving fluid layer," J. Acoust. Soc. Am. 41, 817–821 (1967).
[17]C. Yeh, "Diffraction of sound waves by a moving fluid cylinder," J. Acoust. Soc. Am. 44, 1216–1219 (1968).
[18]I. S. Gradshteyn and I. W. Ryzhik, *Table of Integrals, Series, and Products* (Academic, New York, 1965), p. 761.
[19]H. C. Chen, *Theory of Electromagnetic Waves* (McGraw-Hill, New York, 1983), Chap. 9.
[20]K. U. Ingard and V. K. Singhal, "Upstream and downstream sound radiation into a moving fluid," J. Acoust. Soc. Am. 54, 1343–1346 (1973).
[21]W. Kaplan, *Operational Methods for Linear Systems* (Addison-Wesley, Reading, MA, 1962), Chap. 5.

Reprinted from Applied Optics

Time-harmonic and time-dependent dyadic Green's functions for some uniaxial gyro-electromagnetic media

Akhlesh Lakhtakia, Vasundara V. Varadan, and Vijay K. Varadan

Pennsylvania State University, College of Engineering, University Park, Pennsylvania 16802.

Received 17 June 1988.
0003-6935/89/061049-04$02.00/0.

Time-harmonic and time-dependent Green's functions are derived for a lossless, uniaxial gyroelectromagnetic medium whose permeability tensor is a scalar multiple of its permittivity tensor, and their properties are nvestigated.

The derived Green's functions can be used for the solution of initial and boundary value problems, as well as for obtaining the electromagnetic fields radiated by electric and magnetic sources.

Researchers have begun to focus attention on the electromagnetic theory of anisotropic media because of the recent proliferation in the use of such materials for a variety of applications. Post[1] laid the foundation of the constitutive equations of a general, linear, bianisotropic, homogeneous medium around a quarter of a century ago; and his work was later extended by several workers (see, e.g., Refs. 2–8). In that vein, the dyadic formalism promoted by Chen[9] in connection with his work on the time-harmonic electric Green's function[10] for uniaxial dielectrics has recently been utilized to compute the corresponding magnetic Green's function also[11]; furthermore, time-dependent Green's functions have been derived for the same media.[12]

Gyroelectromagnetic media have not been given much attention. Ray optics of crystals such as calcite and rutile is well known,[13] and some work on radiation due to Chow[14] is also available. Some results can be obtained by appropriate simplifications of the extant results pertaining to bianisotropic media.[2–8] In general, however, a systematic electrodynamic theory of such media is not well-developed, particularly with respect to the infinite medium Green's functions. In the sequel we have derived the time-harmonic as well as the time-dependent Green's functions for a homogeneous, uniaxial gyroelectromagnetic medium whose permeability tensor is a scalar multiple of its permittivity tensor, and we have explored the characteristics of the derived Green's functions. Following a proposal due to Rumsey[15] for constructing artificial uniaxial gyromagnetic materials, it is conjectured that materials of the type studied here can be constructed by embedding parallel ferrite and dielectric fibers in some host medium. It is to be noted that while boldface English letters represent vectors, the German letters denote tensors or dyads; in addition, all vector operations have been ordered to proceed from right to left.

Uniaxial gyroelectromagnetic media possess a single optic axis for both their electric and magnetic properties; in addition, we assume that the permeability tensor is a scalar multiple of the permittivity tensor. Thus, the appropriate constitutive equations are given as

$$\mathbf{D} = \epsilon_0 \mathfrak{a} \cdot \mathbf{E}; \qquad \mathbf{B} = \mu_0 q \mathfrak{a} \cdot \mathbf{H}, \tag{1a,b}$$

in which the uniaxial tensor $\mathfrak{a}$ is specified by[9]

$$\mathfrak{a} = a_\perp \mathfrak{A} + (a_\parallel - a_\perp)\mathbf{e}_c\mathbf{e}_c, \tag{2}$$

$\mathbf{e}_c$ being the unit vector parallel to the optic axis, and $\mathfrak{A}$, the idempotent; $a_\perp$, $a_\parallel$, and q are scalar constitutive parameters assumed constant; and ϵ_0 and μ_0 refer to free space. Substitution into the time-dependent Maxwell's equations yields the field equations

$$(\nabla \times \mathfrak{A}) \cdot \mathfrak{a}^{-1} \cdot (\nabla \times \mathfrak{A}) \cdot \mathbf{E} + \epsilon_0\mu_0 q \mathfrak{a} \cdot \{\partial^2 \mathbf{E}/\partial t^2\} = -\mu_0 q\{\partial \mathbf{J}/\partial t\} - \nabla \times (\mathfrak{a}^{-1} \cdot \mathbf{K}), \tag{3a}$$

$$(\nabla \times \mathfrak{A}) \cdot \mathfrak{a}^{-1} \cdot (\nabla \times \mathfrak{A}) \cdot \mathbf{H} + \epsilon_0\mu_0 q \mathfrak{a} \cdot \{\partial^2 \mathbf{H}/\partial t^2\} = -\epsilon_0\{\partial \mathbf{K}/\partial t\} + \nabla \times (\mathfrak{a}^{-1} \cdot \mathbf{J}). \tag{3b}$$

Likewise, substitution into the time-harmonic Maxwell's equations, with an $\exp[-i\omega t]$ dependence, gives rise to the differential equations

$$(\nabla \times \mathfrak{A}) \cdot \mathfrak{a}^{-1} \cdot (\nabla \times \mathfrak{A}) \cdot \mathbf{E} - k^2 \mathfrak{a} \cdot \mathbf{E} = i\omega\mu_0 q \mathbf{J} - \nabla \times (\mathfrak{a}^{-1} \cdot \mathbf{K}), \tag{4a}$$

$$(\nabla \times \mathfrak{A}) \cdot \mathfrak{a}^{-1} \cdot (\nabla \times \mathfrak{A}) \cdot \mathbf{H} - k^2 \mathfrak{a} \cdot \mathbf{H} = i\omega\epsilon_0 \mathbf{K} + \nabla \times (\mathfrak{a}^{-1} \cdot \mathbf{J}), \tag{4b}$$

in which $k = \omega\sqrt{(\epsilon_0\mu_0 q)}$ has been used for convenience. It should be noted that in Eqs. (3a,b) and (4a,b), as well as hereafter, $\mathbf{J}$ and $\mathbf{K}$, respectively, denote the electric and the magnetic source current densities.

The solutions of Eqs. (3a,b) and (4a,b) are now sought in the forms of the infinite-domain Green's functions, beginning with the time-harmonic solutions.

For the time-harmonic case, by direct substitution in Eqs. (4a,b) it can be easily verified that the solutions

$$\mathbf{E}(\mathbf{r}|\omega) = \int\int\int d^3\mathbf{r}_s [i\omega\mu_0 q \mathfrak{B}_e(\mathbf{R}|\omega) \cdot \mathbf{J}(\mathbf{r}_s|\omega) - \mathfrak{B}_m(\mathbf{R}|\omega) \cdot \{\mathfrak{a}^{-1} \cdot \mathbf{K}(\mathbf{r}_s|\omega)\}], \tag{5a}$$

$$\mathbf{H}(\mathbf{r}|\omega) = \int\int\int d^3\mathbf{r}_s [i\omega\epsilon_0 \mathfrak{B}_e(\mathbf{R}|\omega) \cdot \mathbf{K}(\mathbf{r}_s|\omega) + \mathfrak{B}_m(\mathbf{R}|\omega) \cdot \{\mathfrak{a}^{-1} \cdot \mathbf{J}(\mathbf{r}_s|\omega)\}] \tag{5b}$$

hold, provided the Green's functions $\mathfrak{B}_e$ and $\mathfrak{B}_m$ satisfy, respectively, the equations

$$[(\nabla \times \mathfrak{A}) \cdot \mathfrak{a}^{-1} \cdot (\nabla \times \mathfrak{A}) - k^2 \mathfrak{a}] \cdot \mathfrak{B}_e(\mathbf{R}|\omega) = \mathfrak{A}\delta(\mathbf{R}), \tag{6a}$$

$$[(\nabla \times \mathfrak{A}) \cdot \mathfrak{a}^{-1} \cdot (\nabla \times \mathfrak{A}) - k^2 \mathfrak{a}] \cdot \mathfrak{B}_m(\mathbf{R}|\omega) = \nabla \times \mathfrak{A}\delta(\mathbf{R}), \tag{6b}$$

$\delta(\cdot)$ being the Dirac delta function. It should be noted that the appearance of $\mathbf{R} = \mathbf{r} - \mathbf{r}_s$ in Eqs. (6a,b) signifies the spatial invariance of the uniaxial gyroelectromagnetic medium considered here, with $\mathbf{r}_s$ being the source point and $\mathbf{r}$, the field point.

To solve Eq. (6a), its 3-D spatial Fourier transform is taken, as has been done elsewhere for uniaxial dielectrics.[9–11] It turns out that

$$\mathfrak{B}_e(\mathbf{R}|\omega) = (2\pi)^{-3} \int\int\int_{-\infty}^{\infty} d^3\mathbf{p} \exp[i\mathbf{p} \cdot \mathbf{R}] \mathfrak{W}_e^{-1}(\mathbf{p}|\omega), \tag{7}$$

in which the dyadic

$$\mathfrak{W}_e(\mathbf{p}|\omega) = -(\mathbf{p} \times \mathfrak{A}) \cdot \mathfrak{a}^{-1} \cdot (\mathbf{p} \times \mathfrak{A}) - k^2 \mathfrak{a}, \tag{8}$$

and $\mathbf{p}$ is the 3-D spatial frequency vector. Using dyadic algebra,[9] the inverse $\mathfrak{W}_e^{-1}(\mathbf{p}|\omega)$ can be derived as

$$\mathfrak{W}_e^{-1}(\mathbf{p}|\omega) = [a_\perp^2 a_\parallel \mathfrak{a}^{-1} - \mathbf{pp}/k^2]/[\mathbf{p} \cdot \mathfrak{a} \cdot \mathbf{p} - k^2 a_\perp^2 a_\parallel]. \tag{9}$$

By substituting Eq. (9) into Eq. (7) and evaluating the resulting integral, the Green's dyadic $\mathfrak{B}_e(\mathbf{R}|\omega)$ is calculated to be

$$\mathfrak{B}_e(\mathbf{R}|\omega) = [a_\perp^2 a_\parallel \mathfrak{a}^{-1} + \nabla\nabla/k^2] \exp[ikR_e]/4\pi R_e, \tag{10}$$

in which

$$R_e = \sqrt{[a_\perp^2 a_\parallel \mathbf{R} \cdot \mathfrak{a}^{-1} \cdot \mathbf{R}]}. \tag{11}$$

Similarly, by taking the Fourier transform of Eq. (6b), it can be shown that

$$\mathfrak{B}_m(\mathbf{R}|\omega) = (2\pi)^{-3} \int\int\int_{-\infty}^{\infty} d^3\mathbf{p} \exp[i\mathbf{p} \cdot \mathbf{R}][\mathfrak{W}_e^{-1}(\mathbf{p}|\omega) \cdot i\mathbf{p} \times \mathfrak{A}], \tag{12}$$

whence,

$$\mathfrak{B}_m(\mathbf{R}|\omega) = [a_\perp^2 a_\parallel \mathfrak{a}^{-1}] \cdot \nabla \times \mathfrak{A} \exp[ikR_e]/4\pi R_e = a_\perp^2 a_\parallel \mathfrak{a}^{-1} \times \nabla\{\exp[ikR_e]/4\pi R_e\}. \tag{13}$$

From Eqs. (10) and (13), it is quite clear that the uniaxial gyroelectromagnetic media considered in this paper are singly refringent, as opposed to uniaxial dielectrics which are birefringent. Additionally, all waves in these uniaxial gyroelectromagnetic media are of the extraordinary type, whereas both ordinary and extraordinary waves can propagate in uniaxial dielectrics.[9-12]

Coordinate-free forms[9] of $\mathcal{B}_e(\mathbf{R}|\omega)$ and $\mathcal{B}_m(\mathbf{R}|\omega)$ can be easily obtained from Eqs. (10) and (13), and are, respectively, given as

$$\mathcal{B}_e(\mathbf{R}|\omega) = (a_\perp^2 a_\parallel \exp[ikR_e]/4\pi R_e)([1-(ikR_e)^{-1}+(ikR_e)^{-2}]\mathbf{a}^{-1} - [1-3(ikR_e)^{-1}+3(ikR_e)^{-2}] (\mathbf{a}^{-1}\cdot\mathbf{R})(\mathbf{a}^{-1}\cdot\mathbf{R})/[\mathbf{R}\cdot\mathbf{a}^{-1}\cdot\mathbf{R}]), \quad (14a)$$

$$\mathcal{B}_m(\mathbf{R}|\omega) = (k^2 a_\perp^4 a_\parallel^2 \exp[ikR_e]/4\pi R_e) ([(ikR_e)^{-2}-(ikR_e)^{-1}]\mathbf{a}^{-1}\times[\mathbf{a}^{-1}\cdot\mathbf{R}]). \quad (14b)$$

These forms may be of use when solving radiation and scattering problems using numerical techniques which call for the discretization of surfaces and/or volumes.

The reciprocal nature[4] of these uniaxial gyroelectromagnetic media is reflected by the symmetry properties

$$\mathcal{B}_e(\mathbf{R}|\omega) = \mathcal{B}_e(-\mathbf{R}|\omega); \qquad \mathcal{B}_m(\mathbf{R}|\omega) = -\mathcal{B}_m(-\mathbf{R}|\omega); \quad (15a,b)$$

in addition, the following transpose properties also hold:

$$[\mathcal{B}_e(\mathbf{R}|\omega)]^{tr} = \mathcal{B}_e(\mathbf{R}|\omega); \quad (16a)$$

$$[\mathcal{B}_m(\mathbf{R}|\omega)\cdot\mathbf{a}^{-1}]^{tr} = -\mathcal{B}_m(\mathbf{R}|\omega)\cdot\mathbf{a}^{-1}. \quad (16b)$$

These relationships can be verified very easily from the coordinate-free forms (14a,b). Furthermore, using Eq. (10) it can be shown that $\mathcal{B}_e(\mathbf{R}|\omega)$ and $\mathcal{B}_m(\mathbf{R}|\omega)$ are connected through the relationship

$$\mathcal{B}_m(\mathbf{R}|\omega) = \mathbf{a}^{-1}\cdot[\nabla\times\mathcal{B}_e(\mathbf{R}|\omega)]\cdot\mathbf{a}; \quad (17a)$$

and the combination of Eqs. (6a) and (17a) gives

$$\nabla\times\mathcal{B}_m(\mathbf{R}|\omega) - k^2\mathbf{a}\cdot\mathcal{B}_e(\mathbf{R}|\omega)\cdot\mathbf{a} = \mathbf{a}\delta(\mathbf{R}). \quad (17b)$$

Correct to the order R_e^{-3}, the near-zone approximations of the Green's dyadics can be obtained from Eqs. (14a,b) as

$$\mathcal{B}_e(\mathbf{R}|\omega) = (a_\perp^2 a_\parallel \exp[ikR_e]/4\pi R_e)(ikR_e)^{-2} \times(\mathbf{a}^{-1}-3(\mathbf{a}^{-1}\cdot\mathbf{R})(\mathbf{a}^{-1}\cdot\mathbf{R})/[\mathbf{R}\cdot\mathbf{a}^{-1}\cdot\mathbf{R}]), \quad (18a)$$

$$\mathcal{B}_m(\mathbf{R}|\omega) = 0. \quad (18b)$$

The far-zone approximations, correct to order R_e^{-1}, are derived from Eqs. (14a,b) as

$$\mathcal{B}_e(\mathbf{R}|\omega) = (a_\perp^2 a_\parallel \exp[ikR_e]/4\pi R_e) \times(\mathbf{a}^{-1}-(\mathbf{a}^{-1}\cdot\mathbf{R})(\mathbf{a}^{-1}\cdot\mathbf{R})/[\mathbf{R}\cdot\mathbf{a}^{-1}\cdot\mathbf{R}]), \quad (19a)$$

$$\mathcal{B}_m(\mathbf{R}|\omega) = -(k^2 a_\perp^4 a_\parallel^2 \exp[ikR_e]/4\pi R_e) \times(ikRe)^{-1}(\mathbf{a}^{-1}\times[\mathbf{a}^{-1}\cdot\mathbf{R}]). \quad (19b)$$

As a by-product of the foregoing analysis, the propagation characteristics of plane waves in the uniaxial gyroelectromagnetic media considered here can be obtained. Consider a plane wave traveling in the direction $\mathbf{e}_p$ with the phase velocity ω/p. The wavenumber $p(\mathbf{e}_p)$ can be calculated from the relation

$$p^2(\mathbf{e}_p) = k^2 a_\perp^2 a_\parallel/[a_\perp(\mathbf{e}_p\times\mathbf{e}_c)\cdot(\mathbf{e}_p\times\mathbf{e}_c)+a_\parallel(\mathbf{e}_p\cdot\mathbf{e}_c)^2]. \quad (20)$$

When $\mathbf{e}_p$ is parallel to the optic axis, the associated $\mathbf{E}$ and $\mathbf{H}$ fields are mutually orthogonal, and are orthogonal to $\mathbf{e}_p$ as well, and any polarization can be chosen subject to the restrictions imposed by the time-harmonic Maxwell's equations. On the other hand, if $\mathbf{e}_p$ is not collinear with $\mathbf{e}_c$, two well-defined polarizations are possible. Respectively, these are given as

$$\text{(i) } \mathbf{E}_1 = \mathbf{e}_p\times\mathbf{e}_c; \qquad \mathbf{H}_1 = -[k^2 a_\perp/\omega\mu_0 qp]\mathbf{E}_2; \quad (21a,b)$$

$$\text{(ii) } \mathbf{E}_2 = \mathbf{e}_c - \mathbf{e}_p(\mathbf{e}_p\cdot\mathbf{e}_c)(p/ka_\perp)^2; \quad \mathbf{H}_2 = -[\omega\varepsilon_0 p^2/k^2 a_\perp]\mathbf{E}_1. \quad (22a,b)$$

It should be noted that the first polarization, Eqs. (21a,b), is TE-to-$\mathbf{e}_p$; while the second one, Eqs. (22a,b), is TH-to-$\mathbf{e}_p$; in either case, the $\mathbf{B}$ and $\mathbf{D}$ fields are orthogonal to $\mathbf{e}_p$.

The solutions of Eqs. (3a,b) are also sought for in the forms

$$\mathbf{E}(\mathbf{r}|t) = \iiint d^3\mathbf{r}_s \int dt_s[\mu_0 q\mathcal{B}_1(\mathbf{R}|\tau)\cdot\mathbf{J}(\mathbf{r}_s|t_s) + \mathcal{B}_2(\mathbf{R}|\tau)\cdot\mathbf{a}^{-1}\cdot\mathbf{K}(\mathbf{r}_s|t_s)], \quad (23a)$$

$$\mathbf{H}(\mathbf{r}|t) = \iiint d^3\mathbf{r}_s \int dt_s[-\mathcal{B}_2(\mathbf{R}|\tau)\cdot\mathbf{a}^{-1}\cdot\mathbf{J}(\mathbf{r}_s|t_s) + \varepsilon_0\mathcal{B}_1(\mathbf{R}|\tau)\cdot\mathbf{K}(\mathbf{r}_s|t_s)], \quad (23b)$$

in which the use of $\tau = t - t_s$ is in accordance with the temporal invariance of the medium, with $\tau \geq 0$ demanded by the consideration of causality[9]; t is the time associated with the field point, while t_s is associated with the source point. By substituting Eqs. (23a,b) into Eqs. (3a,b), and then taking the (causal) temporal Fourier transform of the resulting equations, it can be shown that

$$\mathcal{B}_1(\mathbf{R}|\tau) = (2\pi)^{-1}\int_{-\infty+\Delta}^{\infty+\Delta} d\omega(i\omega)\exp[-i\omega t]\mathcal{B}_e(\mathbf{R}|\omega), \quad (24a)$$

$$\mathcal{B}_2(\mathbf{R}|\tau) = -(2\pi)^{-1}\int_{-\infty+\Delta}^{\infty+\Delta} d\omega\exp[-i\omega t]\mathcal{B}_m(\mathbf{R}|\omega). \quad (24b)$$

Causality is obtained by invoking analytic continuation from real to complex ω by moving the integration path above the real axis in the complex ω plane; therefore, $\Delta > 0$ in Eqs. (23a,b) so as to ensure avoiding the pole singularities.[16,17]

Finally, by using the unit step function $u(t)$ defined as[18]

$$u(t) = \left(\frac{1}{2}\right) + (1/\pi)\int_0^\infty (d\omega/\omega)\sin\omega t, \quad t \geq 0$$
$$= 0, \quad t < 0, \quad (25)$$

as well as the Dirac delta function, the integrals involved on the right-hand sides of Eqs. (23a,b) are evaluated out to yield

$$\mathcal{B}_1(\mathbf{R}|\tau) = (a_\perp^2 a_\parallel/4\pi R_e)([-\delta'(\tau_e)+(c_e/R_e)\delta(\tau_e) - (c_e/R_e)^2 u(\tau_e)]\mathbf{a}^{-1} - [-\delta'(\tau_e)+3(c_e/R_e)\delta(\tau_e) - 3(c_e/R_e)^2 u(\tau_e)](\mathbf{a}^{-1}\cdot\mathbf{R})(\mathbf{a}^{-1}\cdot\mathbf{R})/[\mathbf{R}\cdot\mathbf{a}^{-1}\cdot\mathbf{R}]), \quad (26)$$

$$\mathcal{B}_2(\mathbf{R}|\tau) = (a_\perp^4 a_\parallel^2/4\pi c_e R_e^2)([\delta'(\tau_e) + (c_e/R_e)\delta(\tau_e)]\mathbf{a}^{-1}\times[\mathbf{a}^{-1}\cdot\mathbf{R}]), \quad (27)$$

in which $\delta'(\cdot)$ is the unit doublet impulse[17],

$$c_e = [\mu_0\varepsilon_0]^{-1/2}, \qquad \tau_e = \tau - R_e/c_e, \quad (28a,b)$$

τ_e being the retarded time in the direction $\mathbf{R}/R$. The time-domain Green's dyadics, Eqs. (26) and (27), once again show that the media being considered here are singly refringent, as opposed to uniaxial dielectric or uniaxial magnetic materials which are birefringent.[12]

The reciprocal nature of these uniaxial gyroelectromagnetic media is reaffirmed by the symmetry properties

$$\mathfrak{B}_1(\mathbf{R}|\tau) = \mathfrak{B}_1(-\mathbf{R}|\tau); \qquad \mathfrak{B}_2(\mathbf{R}|\tau) = -\mathfrak{B}_2(-\mathbf{R}|\tau); \quad (29a,b)$$

and the following transpose properties also hold:

$$[\mathfrak{B}_1(\mathbf{R}|\tau)]^{tr} = \mathfrak{B}_1(\mathbf{R}|\tau); \qquad [\mathfrak{B}_2(\mathbf{R}|\tau)\cdot\mathfrak{a}^{-1}]^{tr} = -\mathfrak{B}_2(\mathbf{R}|\tau)\cdot\mathfrak{a}^{-1}. \quad (30a,b)$$

The wavehead is established by the condition $\tau_e = 0$ and is dependent on the direction relative to the optic axis; while at large times such that $\tau_e > 0$, the Green's functions of Eqs. (26) and (27) can be reduced to

$$\mathfrak{B}_1(\mathbf{R}|\tau) = (\alpha_\perp^2\alpha_\parallel/4\pi R_e)(c_e/R_e)^2(-\mathfrak{a}^{-1} + 3(\mathfrak{a}^{-1}\cdot\mathbf{R})(\mathfrak{a}^{-1}\cdot\mathbf{R})/[\mathbf{R}\cdot\mathfrak{a}^{-1}\cdot\mathbf{R}]); \quad \tau_e > 0, \quad (31)$$

$$\mathfrak{B}_2(\mathbf{R}|\tau) = 0; \quad \tau_e > 0. \quad (32)$$

In summary, time-harmonic and time-dependent dyadic Green's functions have been derived for a lossless, uniaxial gyroelectromagnetic medium whose permeability tensor is a scalar multiple of its permittivity tensor, and their properties are investigated. The derived Green's functions can be used for the solution of initial and boundary value problems, as well as for obtaining the electromagnetic fields radiated by electric and magnetic sources.

This work was supported in part by the Ben Franklin Partnership Program of the Commonwealth of Pennsylvania. Additional support from the industrial sponsors of the Center for the Engineering of Electronic and Acoustic Materials is also acknowledged.

References

1. E. J. Post, *Formal Structure of Electromagnetics* (North-Holland, Amsterdam, 1962).
2. D. K. Cheng and J. A. Kong, "Covariant Descriptions of Bianisotropic Media," Proc. IEEE **56**, 248 (1968).
3. J. A. Kong, "Theorems of Bianisotropic Media," Proc. IEEE **60**, 1036 (1972).
4. C. M. Krowne, "Electromagnetic Theorems for Complex Anisotropic Media," IEEE Trans. Antennas Propag. **AP-32**, 1224 (1984).
5. C. Altman, A. Schatzberg, and K. Suchy, "Symmetry Transformations and Reversal of Currents and Fields in Bounded (Bi)anisotropic Media," IEEE Trans. Antennas Propag. **AP-32**, 1204 (1984).
6. K. K. Mei, "On the Perturbational Solution to the Dyadic Green's Function of Maxwell's Equations in Anisotropic Media," IEEE Trans. Antennas Propag. **AP-19**, 665 (1971).
7. S. Przezdziecki and R. A. Hurd, "A Note on Scalar Hertz Potentials for Gyrotropic Media," Appl. Phys. **20**, 313 (1979).
8. W. Weiglhofer, "Scalarization of Maxwell's Equations in General Inhomogeneous Bianisotropic Media," Proc. Inst. Electr. Eng. Part H **134**, 357 (1987).
9. H. C. Chen, *Theory of Electromagnetic Waves* (McGraw-Hill, New York, 1983).
10. H. C. Chen, "Dyadic Green's Function and Radiation in a Uniaxially Anisotropic Medium," Int. J. Electron. **35**, 633 (1975).
11. A. Lakhtakia, V. K. Varadan, and V. V. Varadan, "Radiation and Canonical Sources in Uniaxial Dielectric Media," Int. J. Electron. **65**, 1171 (1988).
12. A. Lakhtakia, V. V. Varadan, and V. K. Varadan, "Time-Dependent Dyadic Green's Functions for Uniaxial Dielectric Media," J. Wave-Mater. Interact. **3**, 1 (1988).
13. J. F. Nye, *Physical Properties of Crystals* (Clarendon, Oxford, 1972), Chap. 3.
14. Y. Chow, "A Note on Radiation in a Gyro-Electric-Magnetic Medium—An Extension of Bunkin's Calculations," IRE Trans. Antennas Propag. **AP-10**, 464 (1962).
15. V. H. Rumsey, "Propagation in Generalized Gyrotropic Media," IEEE Trans. Antennas Propag. **AP-12**, 83 (1964).
16. L. B. Felsen, "Propagation and Diffraction of Transient Fields in Non-Dispersive and Dispersive Media," in *Transient Electromagnetic Fields*, L. B. Felsen, Ed. (Springer-Verlag, Berlin, 1976).
17. D. S. Jones, *Methods in Electromagnetic Wave Propagation* (Clarendon, Oxford, 1979).
18. Y. H. Ku, *Transient Circuit Analysis* (Van Nostrand, Princeton, NJ, 1961).

J. Phys. D: Appl. Phys. 22 (1989) 825–828. Printed in the UK

Eigenmodes of a chiral sphere with a perfectly conducting coating

Akhlesh Lakhtakia, Vijay K Varadan and Vasundara V Varadan

Department of Engineering Science and Mechanics, and Center for the Engineering of Electronic and Acoustic Materials, The Pennsylvania State University, University Park, PA 16802, USA

Received 23 September 1988, in final form 23 December 1988

Abstract. The eigenmodes of a spherical resonator, with a perfectly conducting wall and filled with a homogeneous isotropic chiral medium, have been identified and studied. In particular, the roots of the dispersion equation have been given as functions of β/a, where a is the cavity radius and β is the chirality parameter. Application as a microwave circuit element is suggested.

1. Introduction and preliminaries

Though the phenomenon of chirality is known chiefly at the molecular level, and therefore, at frequencies in or above the ultraviolet range, it has been suggested (Lakhtakia *et al* 1988) that particles endowed with chirality can exist at even lower frequencies, say, in the GHz range. This is because chirality, or handedness, is a geometric property; for example, the electromagnetic (EM) response of a right-handed helix is different from that of a left-handed one (Varadan *et al* 1988). Furthermore, by embedding such chiral particles in a low-loss dielectric medium, the resulting composite medium too will possess handedness. With advances in polymer science, it is becoming increasingly possible that such artificial materials can be manufactured with ease, and their properties tailored by altering the sizes and concentration of the embedded chiral particles.

Significant advances have taken place recently in the formulation of a frequency-domain electromagnetic theory for chiral media; we have summarised these elsewhere (Lakhtakia *et al* 1988). With these developments, it is time that aspects relating to the application of chiral media for practical problems be explored. To that end, we consider here the eigenmodes of a perfectly conducting sphere filled with a homogeneous, isotropic, chiral medium. Such an arrangement constitutes a microwave resonator, an important circuit element (Harrington 1964).

Consider a source-free region occupied by an isotropic chiral medium in which the usual constitutive relations $\boldsymbol{D} = \varepsilon\boldsymbol{E}$ and $\boldsymbol{B} = \mu\boldsymbol{H}$ are not adequate because of their incompatibility with the handedness of the medium. Instead, the relations

$$\boldsymbol{D} = \varepsilon\boldsymbol{E} + \beta\varepsilon\nabla\times\boldsymbol{E} \qquad \boldsymbol{B} = \mu\boldsymbol{H} + \beta\mu\nabla\times\boldsymbol{H} \tag{1}$$

hold, and satisfy the requirements of time-reversal symmetry and reciprocity; here β is the chirality parameter measured in units of length. Following Bohren (1974), the EM field is transformed to

$$\boldsymbol{E} = \boldsymbol{Q}_1 + a_R\boldsymbol{Q}_2 \qquad \boldsymbol{H} = \boldsymbol{Q}_2 + a_L\boldsymbol{Q}_1 \tag{2}$$

where the left- and the right-circularly polarised (LCP and RCP) fields, $\boldsymbol{Q}_1$ and $\boldsymbol{Q}_2$, respectively, must satisfy the Helmholtz equations

$$(\nabla^2 + \gamma_1^2)\boldsymbol{Q}_1 = 0 \qquad (\nabla^2 + \gamma_2^2)\boldsymbol{Q}_2 = 0 \tag{3}$$

along with the rotational conditions†

$$\nabla\times\boldsymbol{Q}_1 = \gamma_1\boldsymbol{Q}_1 \qquad \nabla\times\boldsymbol{Q}_2 = -\gamma_2\boldsymbol{Q}_2. \tag{4}$$

Needless to say, these fields are also divergence-free i.e.

$$\nabla\cdot\boldsymbol{Q}_1 = 0 \qquad \nabla\cdot\boldsymbol{Q}_2 = 0. \tag{5}$$

In these equations, the two wavenumbers are given by

$$\gamma_1 = k/(1 - k\beta) \qquad \gamma_2 = k/(1 + k\beta) \tag{6}$$

and

$$a_L = -\mathrm{i}(\varepsilon/\mu)^{1/2} \qquad a_R = -\mathrm{i}(\mu/\varepsilon)^{1/2}. \tag{7}$$

An $\exp(-\mathrm{i}\omega t)$ time dependence has been assumed throughout this work, while $k = \omega(\mu\varepsilon)^{1/2}$ is simply a short-hand notation.

2. Fields inside the spherical resonator

Consider now the spherical resonator $r = a$ which is bounded by perfectly conducting walls and is wholly filled with a chiral medium. Using a representation due to Bohren (1974) and justified by us elsewhere

† We are indebted to an anonymous referee for pointing out that $\boldsymbol{Q}_1$ and $\boldsymbol{Q}_2$ are Beltrami fields (Caraman 1974).

0022-3727/89/060825 + 04 $02.50

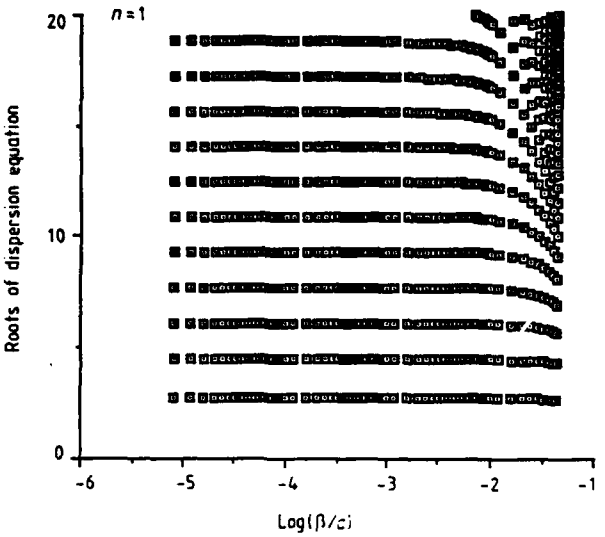

Figure 1. Roots ($x = ka$) of the dispersion equation $F(x; n) = 0$ as functions of β/a for $n = 1$. Computations for figures 1–4 were performed on a MAC II minicomputer using Absoft MACFORTRAN/020.

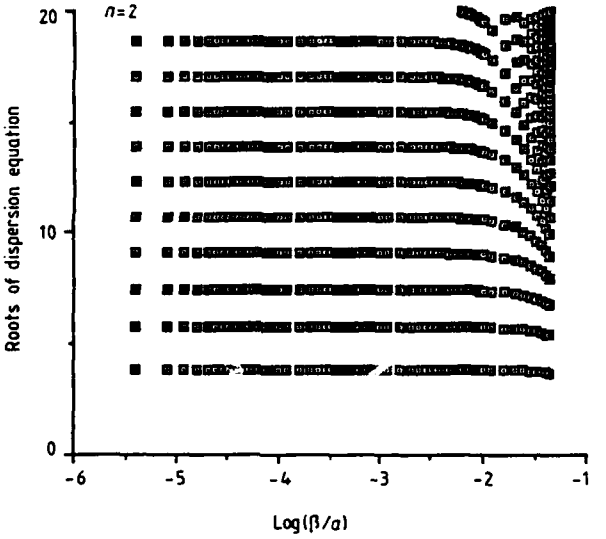

Figure 2. Roots ($x = ka$) of the dispersion equation $F(x; n) = 0$ as functions of β/a for $n = 2$.

(Lakhtakia *et al* 1987), the field inside the cavity can be adequately expressed by

$$Q_1(r) = \sum_{\nu=smn} A_\nu L_\nu^{(1)}(\gamma_1 r)$$
$$Q_2(r) = \sum_{\nu=smn} B_\nu R_\nu^{(1)}(\gamma_2 r). \tag{8}$$

In these equations, the functions

$$L_\nu^{(1)}(\gamma_1 r) = M_\nu^{(1)}(\gamma_1 r) + N_\nu^{(1)}(\gamma_1 r) \tag{9a}$$
$$R_\nu^{(1)}(\gamma_2 r) = M_\nu^{(1)}(\gamma_2 r) - N_\nu^{(1)}(\gamma_2 r) \tag{9b}$$

are left- and right-circularly polarised, respectively. The subscript ν is a triple index—the index s can be even or odd, the index n varies from 1 to ∞, and the index m assumes values from 0 to n; the well known vector spherical wavefunctions $M_\nu^{(1)}(\sigma r)$ and $N_\nu^{(1)}(\sigma r)$

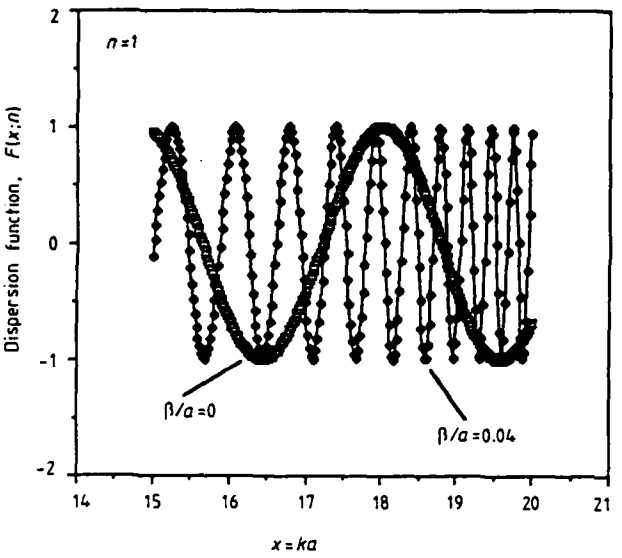

Figure 3. Function $F(x; n = 1)$ for $\beta/a = 0$ and $\beta/a = 0.04$.

have been defined by Morse and Feshbach (1953), while A_ν and B_ν are the unknown expansion coefficients.

The determination of the expansion coefficients can be accomplished using the boundary conditions $e_r \times E = 0$ on the surface $r = a$, where E can be synthesised using (2) and (8), and e_r is the unit radial vector. On taking the inner product† of E_θ with $(m'\pi_{n'}^{m'}(\cos\theta)\ \sin m'\varphi)$ and that of E_φ with $(\tau_{n'}^{m'}(\cos\theta)\cos m'\varphi)$ on $r = a$, and adding the two results, it is easy to see that

$$A_{emn} j_n(x_1) + a_R B_{emn} j_n(x_2) = 0. \tag{10a}$$

In these equations $j_n(\sigma r)$ is the spherical Bessel function of order n, $\pi_n^m(\cos\theta) = P_n^m(\cos\theta)/\sin\theta$, $\tau_n^m(\cos\theta) = \mathrm{d}P_n^m(\cos\theta)/\mathrm{d}\theta$, $P_n^m(\cos\theta)$ is the associated Legendre function of order n and degree m, and $x_p = \gamma_p a$ for $p = 1, 2$. Likewise, after taking the inner product of E_θ with $(m'\pi_{n'}^{m'}(\cos\theta)\cos m'\varphi)$ and that of E_φ with $(-\tau_{n'}^{m'}(\cos\theta)\sin m'\varphi)$ on $r = a$, the equation

$$A_{omn} j_n(x_1) + a_R B_{omn} j_n(x_2) = 0 \tag{10b}$$

can be obtained. Furthermore, from the inner products of E_θ with $(\tau_{n'}^{m'}(\cos\theta)\ \cos m'\varphi)$ and of $-E_\varphi$ with $(m'\pi_{n'}^{m'}(\cos\theta)\ \sin m'\varphi)$ on $r = a$, one can obtain

$$A_{emn} x_2 \partial\psi_n(x_1) - a_R B_{emn} x_1 \partial\psi_n(x_2) = 0 \tag{10c}$$

in which $\psi_n(\xi) = \xi j_n(\xi)$ is the Riccatti–Bessel function and $\partial\psi_n(\xi) \equiv \mathrm{d}\psi_n(\xi)/\mathrm{d}\xi$. Finally, adding the inner product of E_θ with $(\tau_{n'}^{m'}(\cos\theta)\ \sin m'\varphi)$ to that of E_φ with $(m'\pi_{n'}^{m'}(\cos\theta)\ \cos m'\varphi)$ on $r = a$ yields

$$A_{omn} x_2 \partial\psi_n(x_1) - a_R B_{omn} x_1 \partial\psi_n(x_2) = 0. \tag{10d}$$

Is it obvious from (10) that azimuthal parity in terms of the indices s and m is conserved for the present problem, which contributes to the degeneracy of the eigenvalues.

† The inner product of two functions $f(\theta, \varphi)$ and $g(\theta, \varphi)$, as used here, is defined as the integral

$$\int_0^{2\pi} \mathrm{d}\varphi \int_0^{\pi} \mathrm{d}\theta \sin\theta f(\theta, \varphi) g(\theta, \varphi).$$

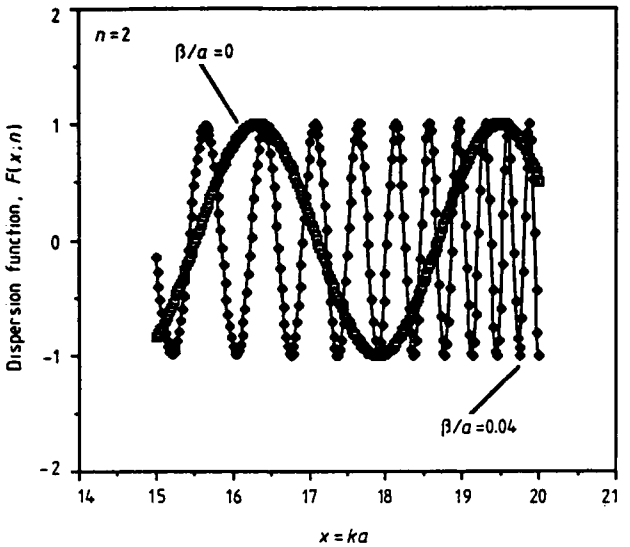

Figure 4. Function $F(x; n = 2)$ for $\beta/a = 0$ and $\beta/a = 0.04$.

The dispersion equation for the chiral-filled resonator is simply obtained by the simultaneous solution of (10*a*)–(10*d*); consequently, each solution of the equation

$$F(x; n) = \psi_n(x_1)\,\partial\psi_n(x_2) + \partial\psi_n(x_1)\psi_n(x_2) = 0 \qquad x = ka \tag{11a}$$

adds yet another index q (for its qth zero), represented jointly by x_{nq}, x_{1nq} and x_{2nq}. Corresponding to this qth solution of (11*a*), the ratio

$$A_{smnq}/a_R B_{smnq} = -j_n(x_{2nq})/j_n(x_{1nq}). \tag{11b}$$

Thus, mode-ordering for the chiral-filled spherical resonator requires four separate indices, of which s, m and n are as before, and q denotes the qth zero of (11*a*) for a given n. The eigenmodes of this cavity are

$$\boldsymbol{E}_{smnq} = -j_n(x_{2nq})\boldsymbol{L}_\nu^{(1)}(\gamma_{1nq}r) + j_n(x_{1nq})\boldsymbol{R}_\nu^{(1)}(\gamma_{2nq}r) \tag{12}$$

$$a_R\boldsymbol{H}_{smnq} = j_n(x_{2nq})\boldsymbol{L}_\nu^{(1)}(\gamma_{1nq}r) + j_n(x_{1nq})\boldsymbol{R}_\nu^{(1)}(\gamma_{2nq}r) \tag{13}$$

and the field inside the chiral-filled resonator can be expressed in terms of these modes:

$$\boldsymbol{E} = \sum_{smnq} F_{smnq}\boldsymbol{E}_{smnq} \qquad \boldsymbol{H} = \sum_{smnq} F_{smnq}\boldsymbol{H}_{smnq} \tag{14}$$

with the usual restriction that the $m = 0$, $s =$ odd mode is non-existent. In these equations $x_{pnq} = \gamma_{pnq}a$ for $p = 1, 2$; and $\omega_{nq} = (\varepsilon\mu)^{1/2}/k_{nq}$ are the resonance frequencies, with

$$x_{nq}^{-1} = (k_{nq}a)^{-1} = \tfrac{1}{2}(x_{1nq}^{-1} + x_{2nq}^{-1}). \tag{15}$$

The stored energy in a given eigenmode can be computed in either of two ways (Lakhtakia *et al* 1988): using the relation

$$W_{smnq} = \tfrac{1}{2}\mathrm{Re}(\boldsymbol{E}_{smnq}\cdot\boldsymbol{D}^*_{smnq} - \boldsymbol{H}_{smnq}\cdot\boldsymbol{B}^*_{smnq}) \tag{16a}$$

or equivalently through the expression

$$W_{smnq} = \tfrac{1}{2}\mathrm{Re}(\varepsilon^{-1}\boldsymbol{D}_{smnq}\cdot\boldsymbol{D}^*_{smnq} - \mu^{-1}\boldsymbol{B}_{smnq}\cdot\boldsymbol{B}^*_{smnq}). \tag{16b}$$

In either case, it can be shown that

$$W_{smnq} = -j_n(x_{1nq})j_n(x_{2nq})4\varepsilon(\gamma_{1nq}\gamma_{2nq}/k_{nq}^2) \times \int_0^{2\pi} \mathrm{d}\varphi \int_0^{\pi} \mathrm{d}\theta \sin\theta \times \int_0^{a} \mathrm{d}r\, r^2 \boldsymbol{L}_{smn}^{(1)}(\gamma_{1nq}r)\cdot\boldsymbol{R}_{smn}^{(1)}(\gamma_{2nq}r) \tag{17a}$$

provided ε, μ and β are all assumed real. The angular integrals can be evaluated analytically to yield

$$W_{smnq} = -j_n(x_{1nq})j_n(x_{2nq})4\varepsilon(\gamma_{1nq}\gamma_{2nq}/k_{nq}^2) \times [(2n+1)(n-m)!]^{-1}[2\pi(1+\delta_{m0}) \times n(n+1)(n+m)!]I_{nq} \tag{17b}$$

in which $\delta_{mm'}$ is the Dirac delta, and the integral

$$I_{nq} = \int_0^{a} \mathrm{d}r\, r^2\{j_n(\gamma_{1nq}r)j_n(\gamma_{2nq}r) \times [1 - n(n+1)/\gamma_{1nq}\gamma_{2nq}r^2] - \partial\psi_n(\gamma_{1nq}r)\partial\psi_n(\gamma_{1nq}r)/\gamma_{1nq}\gamma_{2nq}r^2\} \tag{17c}$$

may have to be evaluated numerically due to its significant complexity.

It is well known that although LCP and RCP waves can propagate independently in an unbounded chiral region, at a bimaterial interface mode-conversion occurs (Lakhtakia *et al* 1985). Therefore, pure LCP or RCP modes cannot exist within a bound chiral volume, as is also apparent from (12) and (13). Moreover, in view of the definitions (6), the solutions x_{nq} of (11*a*) do not depend on the sign of the chirality parameter β; if β changes its sign then x_{1nq} and x_{2nq} are simply interchanged. In the sequel it is assumed that β is real and positive.

3. Results and discussion

Returning to (11*a*), it is clear that with $\beta/a = 0$, i.e., when the medium is non-chiral, this equation reduces to

$$\psi_n(x)\,\partial\psi_n(x) = 0 \qquad x = ka \tag{18a}$$

in which case the TE-to-r eigenvalues come from the zeros of the equation (Harrington 1964)

$$j_n(x) = 0 \qquad x = ka \tag{18b}$$

and yield the transverse electric modes with $\boldsymbol{e}_r\cdot\boldsymbol{E} = 0$. On the other hand, the TM-to-r eigenvalues are the solutions of the equation (Harrington 1964)

$$\partial\psi_n(x) = 0 \qquad x = ka \tag{18c}$$

and give the transverse magnetic modes with $\boldsymbol{e}_r\cdot\boldsymbol{H} =$

0. Furthermore, when $x\beta/a \ll 1$, then the Riccatti–Bessel functions in (11*a*) can be expanded around x to first order in $x^2\beta/a$ using a Taylor series expansion; with this approximation (11*a*) consequently reduces to

$$\psi_n(x)\partial\psi_n(x) - (x^2\beta/a)^2\,\partial\psi_n(x)\,\partial^2\psi_n(x) = 0. \tag{19a}$$

But

$$x^2\partial^2\psi_n(x) = [n(n+1) - x^2]\psi_n(x)$$

so that (19*a*) further simplifies to

$$\psi_n(x)\,\partial\psi_n(x)[1 - x^2\beta^2a^{-2}n(n+1) + x^4\beta^2a^{-2}] = 0$$

$$x = ka \tag{19b}$$

suggesting that the eigenvalues for $x\beta/a \ll 1$ do not appreciably differ from the case $\beta/a = 0$. The third factor on the right side of (19*b*), however, suggests additional roots (due to chirality) which will be significant when $x\beta/a$ is larger.

The roots (x) of (11*a*) are plotted in figures 1 and 2 for $n = 1$ and $n = 2$, respectively, as functions of the parameter β/a, and these figures confirm the deductions of the previous paragraph. Only those roots have been given for which both x_{1nq} and x_{2nq} are non-negative. There is considerable deviation from the achiral values, however, when β/a becomes larger than about 10^{-2}. In fact, the roots are extremely crowded around $\beta/a = 10^{-3/2}$. In order to bring out this crowding further, shown in figures 3 and 4, respectively, are the plots of $F(x; n)$ as functions of x for $n = 1$ and $n = 2$; the normalised chirality parameter $\beta/a = 0$ and $\beta/a = 0.04$ in these two diagrams. The increase in the numbers of zeros of $F(x; n)$ for $\beta/a = 0.04$ and should be noted. As $x\beta/a \to 1$, $x_1 \to \infty$ very rapidly; consequently the cavity becomes electrically large for the LCP components (and constant but small for the RCP components), creating conditions thereby for the accommodation for an increasingly larger number of eigenmodes.

It is well known that resonators find use as the microwave analogues of LC circuits. For fixed n and $\beta = 0$, the resonance frequencies are spaced far apart, as is obvious also from figures 1 and 2; thus, non-chiral resonators are essentially narrow-band. On the other hand, when β/a is large in the present context, the resonance frequencies are closely spaced. Therefore, chiral resonators may be utilised for 'wide-band' purposes, and, in particular, to replace the multicavity staggered turning arrangements (Gewartowski and Watson 1965) in klystron amplifiers.

References

Bohren C F 1974 Light scattering by an optically active sphere *Chem. Phys. Lett.* **29** 458

Caraman P 1974 *n-Dimensional Quasiconformal (QCF) Mappings* (Tunbridge Wells, Kent: Abacus)

Gewartowski J W and Watson H A 1965 *Principles of Electron Tubes* (Princeton: Van Nostrand)

Harrington R F 1964 *Time-Harmonic Electromagnetic Fields* (New York: McGraw-Hill)

Lakhtakia A, Varadan V K and Varadan V V 1985 Scattering and absorption characteristics of lossy dielectric, chiral, nonspherical objects *Appl. Opt.* **24** 4146

—— 1987 Regarding the sources of radiation fields in an isotropic chiral medium *J. Wave–Mater. Interact.* **2** 183

Lakhtakia A, Varadan V V and Varadan V K 1988 Field equations, Huygens's principle, integral equations, and theorems for radiation and scattering of electromagnetic waves in isotropic chiral media *J. Opt. Soc. Am.* A **5** 175

Morse P M and Feshbach H 1953 *Methods of Theoretical Physics* vol. II (New York: McGraw-Hill)

Varadan V V, Lakhtakia A and Varadan V K 1988 Equivalent dipole moments of helical arrangements of small, isotropic, point-polarizable scatterers: Application to chiral polymer design *J. Appl. Phys.* **63** 280

JOURNAL OF MODERN OPTICS, 1989, VOL. 36, NO. 10, 1385–1392

Influence of impedance mismatch between a chiral scatterer and the surrounding chiral medium

AKHLESH LAKHTAKIA, VIJAY K. VARADAN
and VASUNDARA V. VARADAN

Department of Engineering Science and Mechanics and Center for the Engineering of Electronic and Acoustic Materials, Pennsylvania State University, University Park, Pennsylvania 16802, U.S.A.

(*Received 15 March 1989 and accepted 18 March 1989*)

Abstract. In a homogeneous isotropic chiral medium, the electromagnetic field has to be described in terms of left-circularly and right-circularly polarized (LCP and RCP) components, each of which has a different wavenumber associated with it. In general, when a wave propagating in a homogeneous isotropic chiral medium encounters a homogeneous isotropic chiral scatterer, both the scattered and the internally induced fields contain LCP and RCP components regardless of the state of polarization of the incident field. It is proved here that the scattered as well as the internal fields have the same state of polarization as the incident field, if the scatterer and the surrounding medium are impedance-matched; this conclusion holds regardless of the two chiral parameters involved as well as the geometry of the scatterer. Two examples are also given.

1. Introduction and preliminaries

Homogeneous isotropic chiral media are circularly birefringent [1, 2]: the electromagnetic field in such a medium has to be described in terms of left-circularly and right-circularly polarized components, each of which has a different wavenumber associated with it. Either of the two components is capable of independent propagation in an unbounded homogeneous region. However, when either a left-circularly polarized (LCP) or a right-circularly polarized (RCP) wave hits an isotropic obstacle, then the scattered field is composed of both LCP and RCP components; in addition, if any field can be induced inside the obstacle, it too is composed of both components.

Chiral media can come in two forms, one being the mirror-conjugate of the other; this is commonly exemplified by L-type and D-type enantiomorphs of many organic molecules [3]. A homogeneous, isotropic, reciprocal chiral medium can be described by the constitutive equations

$$\mathbf{D} = \varepsilon[\mathbf{E} + \beta\nabla\times\mathbf{E}], \qquad \mathbf{B} = \mu[\mathbf{H} + \beta\nabla\times\mathbf{H}], \tag{1 a, b}$$

in which ε and μ have their usual meaning, while β is the chirality parameter. Two media having the same ε, μ and $|\beta|$, but with their chirality parameters differing in sign, are mirror-conjugates of each other. In a recent paper [4], it was shown that when a plane wave is scattered by the planar interface between two mirror-conjugated chiral media, the reflected as well as the refracted plane waves are of the same circular polarization state as the incident plane wave. This phenomenon will be generalized here, and shown to exist at the interface of any two homogeneous isotropic chiral media, provided that they are impedance-matched.

Following the pioneering work of Bohren [2], the electromagnetic field in a chiral medium is transformed by the prescription of a LCP field $\mathbf{Q}_1$ and a RCP field $\mathbf{Q}_2$, defined as per the following relations:

$$\mathbf{E}=\mathbf{Q}_1+a_R\mathbf{Q}_2, \qquad \mathbf{H}=a_L\mathbf{Q}_1+\mathbf{Q}_2, \tag{2a,b}$$

with

$$a_R=-i\left(\frac{\mu}{\varepsilon}\right)^{1/2}=-\frac{1}{a_L}. \tag{3}$$

It should be noted that a_R has the units of an impedance and a_L, that of an admittance. In an unbounded chiral medium LCP and RCP fields can exist independent of each other, while linearly polarized fields are not allowed [5]. From the aforementioned transformation, it follows that $\mathbf{E}=i(\mu/\varepsilon)^{1/2}\mathbf{H}$ for a LCP field, and $\mathbf{E}=-i(\mu/\varepsilon)^{1/2}\mathbf{H}$ for a RCP field; consequently, the ratio $(\mu/\varepsilon)^{1/2}$ may be considered as the intrinsic wave impedance of a chiral medium, just as in the case of achiral media [6].

Substitution of equations (2a,b) into source-free Maxwell's equations, with a harmonic time-dependence $\exp[-i\omega t]$, leads to the circulation equations

$$\nabla\times\mathbf{Q}_1=\gamma_1\mathbf{Q}_1, \qquad \nabla\times\mathbf{Q}_2=-\gamma_2\mathbf{Q}_2, \tag{4a,b}$$

both $\mathbf{Q}_1$ and $\mathbf{Q}_2$ are solenoidal. The wavenumbers corresponding to the LCP and the RCP fields are given as

$$\gamma_1=\frac{k}{1-k\beta}, \qquad \gamma_2=\frac{k}{1+k\beta}, \tag{5}$$

in which $k=\omega(\varepsilon\mu)^{1/2}$ is simply a shorthand notation and does not represent any wavenumber except when $\beta=0$.

2. Analysis

In an unbounded source-free region occupied by an isotropic chiral medium, it can be shown that $\mathbf{E}$ and $\mathbf{H}$ satisfy the same homogeneous *governing* differential equations,

$$\nabla^2\mathbf{E}+2\gamma_1\gamma_2\beta\nabla\times\mathbf{E}+\gamma_1\gamma_2\mathbf{E}=0, \qquad \nabla\cdot\mathbf{E}=0, \tag{6}$$

$$\nabla^2\mathbf{H}+2\gamma_1\gamma_2\beta\nabla\times\mathbf{H}+\gamma_1\gamma_2\mathbf{H}=0, \qquad \nabla\cdot\mathbf{H}=0. \tag{7}$$

For this isotropic chiral medium, the *infinite medium* Green function $\mathbb{G}(\mathbf{r},\mathbf{r}_o)$ satisfies the dyadic inhomogeneous relation [5]

$$[\nabla\nabla-\nabla^2\mathbb{I}-\gamma_1\gamma_2\mathbb{I}-2\gamma_1\gamma_2\beta\nabla\times\mathbb{I}]\cdot\mathbb{G}(\mathbf{r},\mathbf{r}_o)=\mathbb{I}\,\delta(\mathbf{r}-\mathbf{r}_o), \tag{8}$$

$\mathbb{I}$ being the unit dyadic. Its solution is given by the decomposition

$$\mathbb{G}(\mathbf{r},\mathbf{r}_o)=\mathbb{G}_1(\mathbf{r},\mathbf{r}_o)+\mathbb{G}_2(\mathbf{r},\mathbf{r}_o), \tag{9a}$$

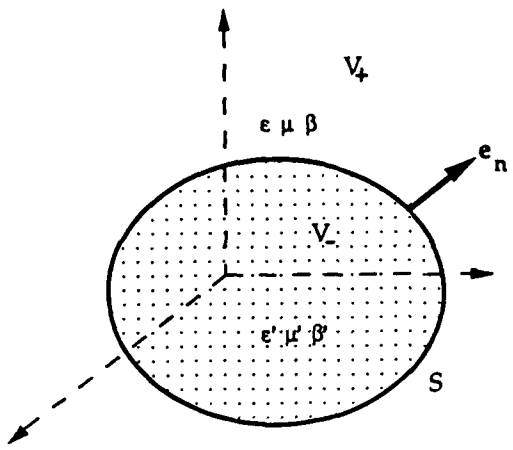

Quantities of relevance to the scattering analysis.

with

$$\mathfrak{G}_1(\mathbf{r},\mathbf{r}_o)=\frac{k}{8\pi\gamma_1\gamma_2}[\gamma_1\mathfrak{I}+\gamma_1^{-1}\nabla\nabla+\nabla\times\mathfrak{I}]g(\gamma_1;|\mathbf{r}-\mathbf{r}_o|), \tag{9b}$$

$$\mathfrak{G}_2(\mathbf{r},\mathbf{r}_o)=\frac{k}{8\pi\gamma_1\gamma_2}[\gamma_2\mathfrak{I}+\gamma_2^{-1}\nabla\nabla-\nabla\times\mathfrak{I}]g(\gamma_2;|\mathbf{r}-\mathbf{r}_o|), \tag{9c}$$

while $g(\sigma;R)=\exp[i\sigma R]/R$ is a scalar Green's function.

Consider the region V_+ shown in the figure, which is occupied by a chiral medium (ε,μ,β). The obstacle volume V_- is occupied by another chiral medium $(\varepsilon',\mu',\beta')$, no restriction being placed on the chirality parameters of either medium. Let an electromagnetic field, $\{\mathbf{E}^{inc},\mathbf{H}^{inc}\}$, be incident on the obstacle, it being understood that the source of the incident field lies outside the circumscribing sphere of V_-. As per Huygens's principle and the extinction theorem [5, 7] applied to V_+, it turns out that

$$-\mathbf{E}^{inc}(\mathbf{r})=(\gamma_1\gamma_2k^{-2})\int\int_S d^2\mathbf{r}_o\,\mathfrak{G}_1(\mathbf{r},\mathbf{r}_o)\cdot[i\omega\mu\mathbf{e}_n\times\mathbf{H}_+(\mathbf{r}_o)+k\mathbf{e}_n\times\mathbf{E}_+(\mathbf{r}_o)]$$
$$+(\gamma_1\gamma_2k^{-2})\int\int_S d^2\mathbf{r}_o\mathfrak{G}_2(\mathbf{r},\mathbf{r}_o)\cdot[i\omega\mu\mathbf{e}_n\times\mathbf{H}_+(\mathbf{r}_o)-k\mathbf{e}_n\times\mathbf{E}_+(\mathbf{r}_o)],$$
$$\mathbf{r}\in V_-, \tag{10a}$$

$$-\mathbf{H}^{inc}(\mathbf{r})=(\gamma_1\gamma_2k^{-2})\int\int_S d^2\mathbf{r}_o\mathfrak{G}_1(\mathbf{r},\mathbf{r}_o)\cdot[k\mathbf{e}_n\times\mathbf{H}_+(\mathbf{r}_o)-i\omega\varepsilon\mathbf{e}_n\times\mathbf{E}_+(\mathbf{r}_o)]$$
$$-(\gamma_1\gamma_2k^{-2})\int\int_S d^2\mathbf{r}_o\mathfrak{G}_2(\mathbf{r},\mathbf{r}_o)\cdot[k\mathbf{e}_n\times\mathbf{H}_+(\mathbf{r}_o)+i\omega\varepsilon\mathbf{e}_n\times\mathbf{E}_+(\mathbf{r}_o)],$$
$$\mathbf{r}\in V_-. \tag{10b}$$

In these equations, $\mathbf{e}_n$ is the unit outward normal to the bimaterial interface S; and $\{\mathbf{E}_+,\mathbf{H}_+\}$ denote the electromagnetic field on the exterior side of S. The Green functions used above also refer to the medium in V_+.

Equations (10 *a*, *b*) form the bedrock of the *T*-matrix method [7, 8]. Once these have been solved, the scattered field, $\{\mathbf{E}^{sc}, \mathbf{H}^{sc}\}$, can be easily determined via the relations

$$\mathbf{E}^{sc}(\mathbf{r}) = (\gamma_1\gamma_2 k^{-2}) \int\int_S d^2\mathbf{r}_o \, \mathbb{G}_1(\mathbf{r}, \mathbf{r}_o) \cdot [i\omega\mu \mathbf{e}_n \times \mathbf{H}_+(\mathbf{r}_o) + k\mathbf{e}_n \times \mathbf{E}_+(\mathbf{r}_o)]$$
$$+ (\gamma_1\gamma_2 k^{-2}) \int\int_S d^2\mathbf{r}_o \mathbb{G}_2(\mathbf{r}, \mathbf{r}_o) \cdot [i\omega\mu \mathbf{e}_n \times \mathbf{H}_+(\mathbf{r}_o) - k\mathbf{e}_n \times \mathbf{E}_+(\mathbf{r}_o)], \quad \mathbf{r} \in V_+, \qquad (11\,a)$$

$$\mathbf{H}^{sc}(\mathbf{r}) = (\gamma_1\gamma_2 k^{-2}) \int\int_S d^2\mathbf{r}_o \, \mathbb{G}_1(\mathbf{r}, \mathbf{r}_o) \cdot [k\mathbf{e}_n \times \mathbf{H}_+(\mathbf{r}_o) - i\omega\varepsilon \mathbf{e}_n \times \mathbf{E}_+(\mathbf{r}_o)]$$
$$- (\gamma_1\gamma_2 k^{-2}) \int\int_S d^2\mathbf{r}_o \, \mathbb{G}_2(\mathbf{r}, \mathbf{r}_o) \cdot [k\mathbf{e}_n \times \mathbf{H}_+(\mathbf{r}_o) + i\omega\varepsilon \mathbf{e}_n \times \mathbf{E}_+(\mathbf{r}_o)], \quad \mathbf{r} \in V_+. \qquad (11\,b)$$

Let the transformation (2 *a*, *b*) be applied to both the incident and the scattered fields. As a consequence, equations (10 *a*, *b*) and (11 *a*, *b*) can be respectively rewritten in the forms

$$-\mathbf{Q}_1^{inc}(\mathbf{r}) = (\gamma_1\gamma_2 k^{-1}) \int\int_S d^2\mathbf{r}_o \, \mathbb{G}_1(\mathbf{r}, \mathbf{r}_o) \cdot [\mathbf{e}_n \times \mathbf{E}_+(\mathbf{r}_o) - a_R \mathbf{e}_n \times \mathbf{H}_+(\mathbf{r}_o)], \quad \mathbf{r} \in V_-, \qquad (12\,a)$$

$$\mathbf{Q}_2^{inc}(\mathbf{r}) = (\gamma_1\gamma_2 k^{-1}) \int\int_S d^2\mathbf{r}_o \, \mathbb{G}_2(\mathbf{r}, \mathbf{r}_o) \cdot [\mathbf{e}_n \times \mathbf{H}_+(\mathbf{r}_o) - a_L \mathbf{e}_n \times \mathbf{E}_+(\mathbf{r}_o)], \quad \mathbf{r} \in V_-, \qquad (12\,b)$$

$$\mathbf{Q}_1^{sc}(\mathbf{r}) = (\gamma_1\gamma_2 k^{-1}) \int\int_S d^2\mathbf{r}_o \, \mathbb{G}_1(\mathbf{r}, \mathbf{r}_o) \cdot [\mathbf{e}_n \times \mathbf{E}_+(\mathbf{r}_o) - a_R \mathbf{e}_n \times \mathbf{H}_+(\mathbf{r}_o)], \quad \mathbf{r} \in V_+, \qquad (13\,a)$$

$$-\mathbf{Q}_2^{sc}(\mathbf{r}) = (\gamma_1\gamma_2 k^{-1}) \int\int_S d^2\mathbf{r}_o \, \mathbb{G}_2(\mathbf{r}, \mathbf{r}_o) \cdot [\mathbf{e}_n \times \mathbf{H}_+(\mathbf{r}_o) - a_L \mathbf{e}_n \times \mathbf{E}_+(\mathbf{r}_o)], \quad \mathbf{r} \in V_+. \qquad (13\,b)$$

The boundary conditions on the interface S are the continuity of the tangential components of the $\mathbf{E}$ and $\mathbf{H}$ fields across S. Consequently, equations (12 *a*, *b*) and (13 *a*, *b*) can be re-expressed to bring in the field, $\{\mathbf{E}^{int}, \mathbf{H}^{int}\}$, induced inside V_- [5, 8] as

$$-\mathbf{Q}_1^{inc}(\mathbf{r}) = (\gamma_1\gamma_2 k^{-1}) \int\int_S d^2\mathbf{r}_o \, \mathbb{G}_1(\mathbf{r}, \mathbf{r}_o) \cdot [\mathbf{e}_n \times \mathbf{E}^{int}(\mathbf{r}_o) - a_R \mathbf{e}_n \times \mathbf{H}^{int}(\mathbf{r}_o)], \quad \mathbf{r} \in V_-, \qquad (14\,a)$$

$$\mathbf{Q}_2^{inc}(\mathbf{r}) = (\gamma_1\gamma_2 k^{-1}) \int\int_S d^2\mathbf{r}_o \, \mathbb{G}_2(\mathbf{r}, \mathbf{r}_o) \cdot [\mathbf{e}_n \times \mathbf{H}^{int}(\mathbf{r}_o) - a_L \mathbf{e}_n \times \mathbf{E}^{int}(\mathbf{r}_o)], \quad \mathbf{r} \in V_-, \qquad (14\,b)$$

$$\mathbf{Q}_1^{sc}(\mathbf{r}) = (\gamma_1\gamma_2 k^{-1}) \int\int_S d^2\mathbf{r}_o\, \mathbb{G}_1(\mathbf{r}, \mathbf{r}_o) \cdot [\mathbf{e}_n \times \mathbf{E}^{int}(\mathbf{r}_o) - a_R \mathbf{e}_n \times \mathbf{H}^{int}(\mathbf{r}_o)], \qquad \mathbf{r} \in V_+, \tag{15a}$$

$$-\mathbf{Q}_2^{sc}(\mathbf{r}) = (\gamma_1\gamma_2 k^{-1}) \int\int_S d^2\mathbf{r}_o\, \mathbb{G}_2(\mathbf{r}, \mathbf{r}_o) \cdot [\mathbf{e}_n \times \mathbf{H}^{int}(\mathbf{r}_o) - a_L \mathbf{e}_n \times \mathbf{E}^{int}(\mathbf{r}_o)], \qquad \mathbf{r} \in V_+. \tag{15b}$$

But, Bohren's decomposition (2 *a*, *b*) also applies to the medium inside V_-, albeit with the primed constitutive parameters. In strict analogy with expression (3), the quantities

$$a_R' = -i\left(\frac{\mu'}{\varepsilon'}\right)^{1/2} = -\frac{1}{a_L'}, \tag{16}$$

can also be defined. Consequently, the foregoing sets of integral equations are transformed to

$$-\mathbf{Q}_1^{inc}(\mathbf{r}) = \gamma_1\gamma_2 k^{-1}[1 + a_R/a_R'] \int\int_S d^2\mathbf{r}_o\, \mathbb{G}_1(\mathbf{r}, \mathbf{r}_o) \cdot [\mathbf{e}_n \times \mathbf{Q}_1^{int}(\mathbf{r}_o)]$$
$$+ \gamma_1\gamma_2 k^{-1}[a_R' - a_R] \int\int_S d^2\mathbf{r}_o\, \mathbb{G}_1(\mathbf{r}, \mathbf{r}_o) \cdot [\mathbf{e}_n \times \mathbf{Q}_2^{int}(\mathbf{r}_o)], \qquad \mathbf{r} \in V_-, \tag{17a}$$

$$\mathbf{Q}_1^{sc}(\mathbf{r}) = \gamma_1\gamma_2 k^{-1}[1 + a_R/a_R'] \int\int_S d^2\mathbf{r}_o\, \mathbb{G}_1(\mathbf{r}, \mathbf{r}_o) \cdot [\mathbf{e}_n \times \mathbf{Q}_1^{int}(\mathbf{r}_o)]$$
$$+ \gamma_1\gamma_2 k^{-1}[a_R' - a_R] \int\int_S d^2\mathbf{r}_o\, \mathbb{G}_1(\mathbf{r}, \mathbf{r}_o) \cdot [\mathbf{e}_n \times \mathbf{Q}_2^{int}(\mathbf{r})], \qquad \mathbf{r} \in V_+, \tag{17b}$$

$$-\mathbf{Q}_2^{inc}(\mathbf{r}) = \gamma_1\gamma_2 k^{-1}[a_L - a_L'] \int\int_S d^2\mathbf{r}_o\, \mathbb{G}_2(\mathbf{r}, \mathbf{r}_o) \cdot [\mathbf{e}_n \times \mathbf{Q}_1^{int}(\mathbf{r}_o)]$$
$$- \gamma_1\gamma_2 k^{-1}[1 + a_R'/a_R] \int\int_S d^2\mathbf{r}_o\, \mathbb{G}_2(\mathbf{r}, \mathbf{r}_o) \cdot [\mathbf{e}_n \times \mathbf{Q}_2^{int}(\mathbf{r}_o)], \qquad \mathbf{r} \in V_-, \tag{18a}$$

$$\mathbf{Q}_2^{sc}(\mathbf{r}) = \gamma_1\gamma_2 k^{-1}[a_L - a_L'] \int\int_S d^2\mathbf{r}_o\, \mathbb{G}_2(\mathbf{r}, \mathbf{r}_o) \cdot [\mathbf{e}_n \times \mathbf{Q}_1^{int}(\mathbf{r}_o)]$$
$$- \gamma_1\gamma_2 k^{-1}[1 + a_R'/a_R] \int\int_S d^2\mathbf{r}_o\, \mathbb{G}_2(\mathbf{r}, \mathbf{r}_o) \cdot [\mathbf{e}_n \times \mathbf{Q}_2^{int}(\mathbf{r}_o)], \qquad \mathbf{r} \in V_+. \tag{18b}$$

As was expected, equations (17 *a*, *b*) and (18 *a*, *b*) show that both the scattered and the internally induced fields contain LCP and RCP components regardless of the state of polarization of the incident field. It should be noted that in deriving equations (17 *a*, *b*) and (18 *a*, *b*), the chiral parameters of either medium were not explicitly used; nor do equations (2 *a*, *b*) need them. In fact, these equations are applicable whether both, any one or neither of the two materials are chiral.

$$\mathbf{Q}_1^{sc}(\mathbf{r}) = (\gamma_1\gamma_2 k^{-1}) \int\int_S d^2\mathbf{r}_o\, \mathbb{G}_1(\mathbf{r}, \mathbf{r}_o) \cdot [\mathbf{e}_n \times \mathbf{E}^{int}(\mathbf{r}_o) - a_R \mathbf{e}_n \times \mathbf{H}^{int}(\mathbf{r}_o)], \qquad \mathbf{r} \in V_+, \tag{15a}$$

$$-\mathbf{Q}_2^{sc}(\mathbf{r}) = (\gamma_1\gamma_2 k^{-1}) \int\int_S d^2\mathbf{r}_o\, \mathbb{G}_2(\mathbf{r}, \mathbf{r}_o) \cdot [\mathbf{e}_n \times \mathbf{H}^{int}(\mathbf{r}_o) - a_L \mathbf{e}_n \times \mathbf{E}^{int}(\mathbf{r}_o)], \qquad \mathbf{r} \in V_+. \tag{15b}$$

But, Bohren's decomposition (2 *a*, *b*) also applies to the medium inside V_-, albeit with the primed constitutive parameters. In strict analogy with expression (3), the quantities

$$a'_R = -i\left(\frac{\mu'}{\varepsilon'}\right)^{1/2} = -\frac{1}{a'_L}, \tag{16}$$

can also be defined. Consequently, the foregoing sets of integral equations are transformed to

$$-\mathbf{Q}_1^{inc}(\mathbf{r}) = \gamma_1\gamma_2 k^{-1}[1 + a_R/a'_R] \int\int_S d^2\mathbf{r}_o\, \mathbb{G}_1(\mathbf{r}, \mathbf{r}_o) \cdot [\mathbf{e}_n \times \mathbf{Q}_1^{int}(\mathbf{r}_o)]$$
$$+ \gamma_1\gamma_2 k^{-1}[a'_R - a_R] \int\int_S d^2\mathbf{r}_o\, \mathbb{G}_1(\mathbf{r}, \mathbf{r}_o) \cdot [\mathbf{e}_n \times \mathbf{Q}_2^{int}(\mathbf{r}_o)], \qquad \mathbf{r} \in V_-, \tag{17a}$$

$$\mathbf{Q}_1^{sc}(\mathbf{r}) = \gamma_1\gamma_2 k^{-1}[1 + a_R/a'_R] \int\int_S d^2\mathbf{r}_o\, \mathbb{G}_1(\mathbf{r}, \mathbf{r}_o) \cdot [\mathbf{e}_n \times \mathbf{Q}_1^{int}(\mathbf{r}_o)]$$
$$+ \gamma_1\gamma_2 k^{-1}[a'_R - a_R] \int\int_S d^2\mathbf{r}_o\, \mathbb{G}_1(\mathbf{r}, \mathbf{r}_o) \cdot [\mathbf{e}_n \times \mathbf{Q}_2^{int}(\mathbf{r})], \qquad \mathbf{r} \in V_+, \tag{17b}$$

$$-\mathbf{Q}_2^{inc}(\mathbf{r}) = \gamma_1\gamma_2 k^{-1}[a_L - a'_L] \int\int_S d^2\mathbf{r}_o\, \mathbb{G}_2(\mathbf{r}, \mathbf{r}_o) \cdot [\mathbf{e}_n \times \mathbf{Q}_1^{int}(\mathbf{r}_o)]$$
$$- \gamma_1\gamma_2 k^{-1}[1 + a'_R/a_R] \int\int_S d^2\mathbf{r}_o\, \mathbb{G}_2(\mathbf{r}, \mathbf{r}_o) \cdot [\mathbf{e}_n \times \mathbf{Q}_2^{int}(\mathbf{r}_o)], \qquad \mathbf{r} \in V_-, \tag{18a}$$

$$\mathbf{Q}_2^{sc}(\mathbf{r}) = \gamma_1\gamma_2 k^{-1}[a_L - a'_L] \int\int_S d^2\mathbf{r}_o\, \mathbb{G}_2(\mathbf{r}, \mathbf{r}_o) \cdot [\mathbf{e}_n \times \mathbf{Q}_1^{int}(\mathbf{r}_o)]$$
$$- \gamma_1\gamma_2 k^{-1}[1 + a'_R/a_R] \int\int_S d^2\mathbf{r}_o\, \mathbb{G}_2(\mathbf{r}, \mathbf{r}_o) \cdot [\mathbf{e}_n \times \mathbf{Q}_2^{int}(\mathbf{r}_o)], \qquad \mathbf{r} \in V_+. \tag{18b}$$

As was expected, equations (17 *a*, *b*) and (18 *a*, *b*) show that both the scattered and the internally induced fields contain LCP and RCP components regardless of the state of polarization of the incident field. It should be noted that in deriving equations (17 *a*, *b*) and (18 *a*, *b*), the chiral parameters of either medium were not explicitly used; nor do equations (2 *a*, *b*) need them. In fact, these equations are applicable whether both, any one or neither of the two materials are chiral.

One notable case stands out: let the scatterer be impedance-matched with the surrounding medium; $\mu'/\varepsilon' = \mu/\varepsilon$. In that case, equations (17 *a*, *b*) and (18 *a*, *b*) simplify to

$$-\mathbf{Q}_1^{inc}(\mathbf{r}) = 2\gamma_1\gamma_2 k^{-1} \int\int_S d^2\mathbf{r}_o \, \mathbb{G}_1(\mathbf{r}, \mathbf{r}_o) \cdot [\mathbf{e}_n \times \mathbf{Q}_1^{int}(\mathbf{r}_o)], \qquad \mathbf{r} \in V_-, \tag{19a}$$

$$\mathbf{Q}_1^{sc}(\mathbf{r}) = 2\gamma_1\gamma_2 k^{-1} \int\int_S d^2\mathbf{r}_o \, \mathbb{G}_1(\mathbf{r}, \mathbf{r}_o) \cdot [\mathbf{e}_n \times \mathbf{Q}_1^{int}(\mathbf{r}_o)], \qquad \mathbf{r} \in V_+, \tag{19b}$$

$$\mathbf{Q}_2^{inc}(\mathbf{r}) = 2\gamma_1\gamma_2 k^{-1} \int\int_S d^2\mathbf{r}_o \, \mathbb{G}_2(\mathbf{r}, \mathbf{r}_o) \cdot [\mathbf{e}_n \times \mathbf{Q}_2^{int}(\mathbf{r}_o)], \qquad \mathbf{r} \in V_-, \tag{20a}$$

$$-\mathbf{Q}_2^{sc}(\mathbf{r}) = 2\gamma_1\gamma_2 k^{-1} \int\int_S d^2\mathbf{r}_o \, \mathbb{G}_2(\mathbf{r}, \mathbf{r}_o) \cdot [\mathbf{e}_n \times \mathbf{Q}_2^{int}(\mathbf{r}_o)], \qquad \mathbf{r} \in V_+. \tag{20b}$$

Equations (19 *a*, *b*) and (20 *a*, *b*) clearly show that the scattered as well as the internal fields have the same state of polarization as the incident field, if the scatterer and the surrounding medium are impedance-matched. This conclusion is not affected by the value of the chirality parameter in either of the two media, and forms the major result of this paper.

3. Scattering by planar interface

As an example of the analysis given above, let the reflection and refraction of plane waves at bimaterial interfaces be considered. Let V_+ be the half space $z \leqslant 0$; and V_-, the half space $z \geqslant 0$. The interface S is the plane $z = 0$.

In V_+, the unprimed constitutive parameters are used, and the incident fields can be represented by [9]

$$\mathbf{Q}_1^{inc}(\mathbf{r}) = A_1[\mathbf{e}_y + i(-\alpha_1\mathbf{e}_x + \kappa\mathbf{e}_z)/\gamma_1] \exp[i(\kappa x + \alpha_1 z)], \qquad \mathbf{r} \in V_+, \tag{21a}$$

$$\mathbf{Q}_2^{inc}(\mathbf{r}) = A_2[\mathbf{e}_y + i(\alpha_2\mathbf{e}_x - \kappa\mathbf{e}_z)/\gamma_2] \exp[i(\kappa x + \alpha_2 z)], \qquad \mathbf{r} \in V_+, \tag{21b}$$

while the scattered (i.e. reflected) fields are given by

$$\mathbf{Q}_1^{sc}(\mathbf{r}) = R_1[\mathbf{e}_y + i(\alpha_1\mathbf{e}_x + \kappa\mathbf{e}_z)/\gamma_1] \exp[i(\kappa x - \alpha_1 z)], \qquad \mathbf{r} \in V_+, \tag{22a}$$

$$\mathbf{Q}_2^{sc}(\mathbf{r}) = R_2[\mathbf{e}_y - i(\alpha_2\mathbf{e}_x + \kappa\mathbf{e}_z)/\gamma_2] \exp[i(\kappa x - \alpha_2 z), \qquad \mathbf{r} \in V_+. \tag{22b}$$

The fields induced in V_- (i.e. the refracted fields) are to be given as

$$\mathbf{Q}_1^{int}(\mathbf{r}) = T_1[\mathbf{e}_y + i(-\alpha_1'\mathbf{e}_x + \kappa\mathbf{e}_z)/\gamma_1'] \exp[i(\kappa x + \alpha_1' z)], \qquad \mathbf{r} \in V_-, \tag{23a}$$

$$\mathbf{Q}_2^{int}(\mathbf{r}) = T_2[\mathbf{e}_y + i(\alpha_2'\mathbf{e}_x - \kappa\mathbf{e}_z)/\gamma_2'] \exp[i(\kappa x + \alpha_2' z)], \qquad \mathbf{r} \in V_-, \tag{23b}$$

in which the primed constitutive parameters have been used. In these equations, κ is the (common) horizontal wavenumber required to satisfy Snell's laws at the interface S; $\mathbf{e}_x, \ldots$ are the unit Cartesian vectors; while $\alpha_1 = +(\gamma_1^2 - \kappa^2)^{1/2}$, $\alpha_2 = +(\gamma_2^2 - \kappa^2)^{1/2}$, $\alpha_1' = -(\gamma_1'^2 - \kappa^2)^{1/2}$ and $\alpha_2' = +(\gamma_2'^2 - \kappa^2)^{1/2}$.

The x-directed and y-directed components of the $\mathbf{E}$ and the $\mathbf{H}$ fields have to be continuous across S; in addition, the two media are impedance-matched, namely $\mu'/\varepsilon' = \mu/\varepsilon$. Use of these conditions leads to the solutions

$$T_1 = 2\gamma_1'\alpha_1[\gamma_1'\alpha_1 + \alpha_1'\gamma_1]^{-1} A_1, \qquad R_1 = T_1 - A_1, \tag{24}$$

$$T_2 = 2\gamma_2'\alpha_2[\gamma_2'\alpha_2 + \alpha_2'\gamma_2]^{-1} A_2, \qquad R_2 = T_2 - A_2. \tag{25}$$

This illustrates the observation that the incident, the reflected, and the refracted plane waves are of the same circular-polarization state whenever the two chiral media on either side of a planar interface are impedance-matched. Given that $\mu'/\varepsilon' = \mu/\varepsilon$, it should also be noted from equations (24) and (25) that $T_1/A_1 = T_2/A_2 = 1$ for the case of normal incidence ($\kappa = 0$); further, if $\beta = 0$, then the case of normal incidence trivially satisfies the Brewster condition [10].

4. Scattering by a sphere

The second, and the last, example involves the scattering characteristics of a sphere. Let V_- be a sphere of radius a. The incident field can be expanded as

$$\mathbf{Q}_1^{\text{inc}}(\mathbf{r}) = \sum_{\nu = smn} A_\nu [\mathbf{M}_\nu^{(1)}(\gamma_1 \mathbf{r}) + \mathbf{N}_\nu^{(1)}(\gamma_1 \mathbf{r})], \tag{26a}$$

$$\mathbf{Q}_2^{\text{inc}}(\mathbf{r}) = \sum_{\nu = smn} B_\nu [\mathbf{M}_\nu^{(1)}(\gamma_2 \mathbf{r}) - \mathbf{N}_\nu^{(1)}(\gamma_2 \mathbf{r})]. \tag{26b}$$

The subscript ν is a triple-index—the index s can be even or odd, the index n varies from 1 to ∞, and the index m assumes values from 0 to n; the well known vector spherical wavefunctions, $\mathbf{M}_\nu^{(j)}(\sigma \mathbf{r})$ and $\mathbf{N}_\nu^{(j)}(\sigma \mathbf{r}, j = 1, 3$, have been defined by Morse and Feshbach [11], while A_ν and B_ν are the expansion coefficients.

The scattered field is likewise expressed in terms of the vector wavefunctions as

$$\mathbf{Q}_1^{\text{sc}}(\mathbf{r}) = \sum_\nu F_\nu [\mathbf{M}_\nu^{(3)}(\gamma_1 \mathbf{r}) + \mathbf{N}_\nu^{(3)}(\gamma_1 \mathbf{r})], \qquad \mathbf{r} \in V_+, \tag{27a}$$

$$\mathbf{Q}_2^{\text{sc}}(\mathbf{r}) = \sum_\nu G_\nu [\mathbf{M}_\nu^{(3)}(\gamma_2 \mathbf{r}) - \mathbf{N}_\nu^{(3)}(\gamma_2 \mathbf{r})], \qquad \mathbf{r} \in V_+, \tag{27b}$$

while the field induced inside V_- has the representation

$$\mathbf{Q}_1^{\text{int}}(\mathbf{r}) = \sum_\nu C_\nu [\mathbf{M}_\nu^{(1)}(\gamma_1' \mathbf{r}) + \mathbf{N}_\nu^{(1)}(\gamma_1' \mathbf{r})], \qquad \mathbf{r} \in V_-, \tag{28a}$$

$$\mathbf{Q}_2^{\text{int}}(\mathbf{r}) = \sum_\nu D_\nu [\mathbf{M}_\nu^{(1)}(\gamma_2' \mathbf{r}) - \mathbf{N}_\nu^{(1)}(\gamma_2' \mathbf{r})], \qquad \mathbf{r} \in V_-. \tag{28b}$$

After enforcing the continuity of the tangential components of the **E** and the **H** fields across the sphere $r = a$, utilizing the orthogonalities of the spherical harmonics [11], and recognizing that the two media are impedance-matched (i.e. $\mu'/\varepsilon' = \mu/\varepsilon$), one obtains the following solution:

$$F_\nu = -A_\nu [\hat{c} \psi_n(\gamma_1 a) \psi_n(\gamma_1' a) - \psi_n(\gamma_1 a) \partial \psi_n(\gamma_1' a)][\partial \xi_n(\gamma_1 a) \psi_n(\gamma_1' a) - \xi_n(\gamma_1 a) \partial \psi_n(\gamma_1' a)]^{-1}, \tag{29a}$$

$$C_\nu = A_\nu \left(i \frac{\gamma_1'}{\gamma_1} \right) [\partial \xi_n(\gamma_1 a) \psi_n(\gamma_1' a) - \xi_n(\gamma_1 a) \partial \psi_n(\gamma_1' a)]^{-1}, \tag{29b}$$

$$G_\nu = -B_\nu [\partial \psi_n(\gamma_2 a) \psi_n(\gamma_2' a) - \psi_n(\gamma_2 a) \partial \psi_n(\gamma_2' a)][\partial \xi_n(\gamma_2 a) \psi_n(\gamma_2' a) - \xi_n(\gamma_2 a) \partial \psi_n(\gamma_2' a)]^{-1}, \tag{30a}$$

$$D_\nu = B_\nu \left(i \frac{\gamma_2'}{\gamma_2} \right) [\partial \xi_n(\gamma_2 a) \psi_n(\gamma_2' a) - \xi_n(\gamma_2 a) \partial \psi_n(\gamma_2' a)]^{-1}. \tag{30b}$$

In these expressions $\psi_n(x)=xj_n(x)$ and $\xi_n(x)=xh_n^{(1)}(x)$ are the Riccati–Bessel functions [12]; and $\partial\psi_n(x)=d\psi_n(x)/dx$, and so on. Again, the major result of this paper has been exemplified by equations (29 *a*, *b*) and (30 *a*, *b*).

Acknowledgments

This work was partially supported by the US Office of Naval Research under contract N00014-87-K-0031. Additional support from the industrial members and sponsors of the Center for the Engineering of Electronic and Acoustic Materials is also acknowledged.

References

[1] CHARNEY, E., 1979, *The Molecular Basis of Optical Activity* (Malabar: Kreiger).
[2] BOHREN, C. F., 1974, *Chem. Phys. Lett.*, **29**, 458.
[3] EYRING, H., WALTER, J., and KIMBALL, G. E., 1944, *Quantum Chemistry* (New York: John Wiley).
[4] LAKHTAKIA, A., VARADAN, V. V., and VARADAN, V. K., 1989, *J. opt. Soc. Am.* A, **6**, 23.
[5] LAKHTAKIA, A., VARADAN, V. V., and VARADAN, V. K., 1988, *J. opt. Soc. Am.* A, **5**, 175.
[6] JOHNK, C. T. A., 1975, *Engineering Electromagnetic Fields and Waves* (New York: John Wiley).
[7] WATERMAN, P. C., 1969, *Alta Freq.*, **38**, (Speciale), 348.
[8] LAKHTAKIA, A., VARADAN, V. K. and VARADAN, V. V., 1985, *Appl. Optics*, **24**, 4146.
[9] LAKHTAKIA, A., VARADAN, V. V., and VARADAN, V. K., 1986, *IEEE Trans. Electromagn. Compat.*, **28**, 90.
[10] CHEN, H. C., 1983, *Theory of Electromagnetic Waves* (New York: McGraw-Hill), p. 246.
[11] MORSE, P. M., and FESHBACH, H., 1953, *Methods of Theoretical Physics II* (New York: McGraw-Hill), chap. 13.
[12] ABRAMOWITZ, M., and STEGUN, I. A., 1980, *Handbook of Mathematical Functions* (New York: Dover), p. 445.

EFFECTIVE PROPERTIES OF MICROWAVE COMPOSITES

YUSHIEH MA, VIJAY K. VARADAN and VASUNDARA V. VARADAN
Research Center for the Engineering of Electronic and Acoustic Materials
and
Department of Engineering Science and Mechanics
The Pennsylvania State University
University Park, PA 16802

ABSTRACT

We employ the multiple scattering formalism to obtain two independent expressions for the effective permittivity $< \varepsilon >$ and permeability $< \mu >$ of microwave composite materials. These two expressions are required, but not provided in the literature, in the investigation of the reflection and transmission characteristics for a layer of microwave composite materials in response to incident millimeter-waves and microwaves. In order to check the validity of the expressions, several cases involving lossy/lossless matrix and inclusion materials are discussed.

1. INTRODUCTION

It is well known that when waves propagate through a medium containing scatterers, the entrained energy (intensity) is going to be either redistributed in various directions by scattering or absorbed by intrinsic absorption mechanisms. This suggests the well known idea that to achieve a high attenuation of the incident wave energy, the geometry and material properties of the scatterers as well as physical mechanisms for scattering and absorption should be carefully selected. The selection is not an easy task and it depends on different applications, civilian as well as military considerations and advancements in material technology.

In many applications involving microwaves, it is desirable to design materials that will have prescribed reflection and transmission characteristics as a function of frequency (narrow or wide band) and at the same time conform to restrictions on weight, structural properties, thickness, etc. Microwave composite materials that contain a distribution of inclusions of specific concentration, distribution, geometry and material properties can often achieve such goals. Since the actual response of microwave composite materials to the incident wave of low to high gigahertz frequency is quite diverse, it becomes very expensive and time consuming to actually prepare samples of such materials and test them experimentally. However, an optimal design through theoretical analysis of such materials is relatively efficient and the parameters involved are tractable.

When particles are dispersed in a host medium to form a composite, depending on the volume fraction of particles, single or multiple scattering dominates the scattered energy when waves are incident on them. Multiple scattering effect cannot be ignored when the concentration of particles is considerable as in the case of microwave composites. In this theoretical investigation, we employ the multiple scattering formalism, which has been previously applied to get the effective propagation constant for the ferrite composites [1], to obtain two independent expressions for the effective permittivity $< \varepsilon >$ and permeability $< \mu >$ of microwave composite materials. These two expressions are required, but not provided in the literature, in the investigation of the reflection and transmission characteristics for a layer of microwave composite materials in response to incident millimeter-waves and microwaves. In order to check the validity of the expressions, several cases involving lossy/lossless matrix and inclusion materials are discussed.

2. MULTIPLE SCATTERING FORMALISM

Consider the propagation of a plane harmonic electromagnetic wave in a medium referred to as the matrix characterized by complex values of the dielectric function $\varepsilon_2 = \varepsilon_2' + j\,\varepsilon_2''$ and magnetic permeability $\mu_2 = \mu_2' + j\,\mu_2''$. Embedded in the matrix is a random distribution of uniform size spherical scatterers whose permittivity $\varepsilon_1 = \varepsilon_1' + j\,\varepsilon_1''$ and permeability $\mu_1 = \mu_1' + j\,\mu_1''$. The matrix of volume V contains N scatterers such that $N \to \infty$, $V \to \infty$ but n_0 (= N/V) the number density is finite.

Let $\mathbf{E}$, $\mathbf{E}^o$, $\mathbf{E}_i^e$ and $\mathbf{E}_i^s$ be respectively the total electromagnetic field, the incident wave field, the field exciting the ith scatterer and the field scattered by the ith scatterer. All the fields have implicit $\exp(-i\omega t)$ time dependence and satisfy vector Helmholtz equation. Let $\mathrm{Re}\,\phi_n$ and $\mathrm{Ou}\,\phi_n$ denote the basis of orthogonal functions which are eigenfunctions of the vector Helmholtz equation. The qualifiers Re and Ou denote functions which are regular at the origin and outgoing at infinity [2]. Thus, we can write the following set of self-consistent equations:

$$\mathbf{E} = \mathbf{E}^o + \sum_{i=1}^{N} \mathbf{E}_i^s \tag{1}$$

$$\mathbf{E}^o = \Sigma_n a_n^i \,\mathrm{Re}\,\phi_n(\mathbf{r} - \mathbf{r}_i) \tag{2}$$

$$\mathbf{E}_i^e = \Sigma_n \alpha_n^i \,\mathrm{Re}\,\phi_n(\mathbf{r} - \mathbf{r}_i) \quad ; \quad a < |\mathbf{r} - \mathbf{r}_i| < 2a \tag{3}$$

$$\mathbf{E}_i^s = \Sigma_n f_n^i \,\mathrm{Ou}\,\phi_n(\mathbf{r} - \mathbf{r}_i) \quad ; \quad |\mathbf{r} - \mathbf{r}_i| > a \tag{4}$$

where $\alpha_n{}^i$ and $f_n{}^i$ are unknown expansion coefficients and $a_n{}^i$ are known incident field coefficients. We observe in (3) and (4) that a is the radius of the sphere and that all expansions are with respect to a coordinate origin located in a particular scatterer.

The T-matrix by definition simply relates the expansion coefficients of $\mathbf{E}_i^e$ and $\mathbf{E}_i^s$ provided the sum of them is the total field. Thus [2],

$$f_n^i = \Sigma_{n'} T_{nn'} \alpha_{n'}^i \tag{5}$$

and the following addition theorem for the basis functions is invoked

$$\mathrm{Ou}\,\phi_n(\mathbf{r} - \mathbf{r}_j) = \Sigma_{n'} \sigma_{nn'}(\mathbf{r}_i - \mathbf{r}_j)\,\mathrm{Re}\,\phi_{n'}(\mathbf{r} - \mathbf{r}_i) \quad . \tag{6}$$

Substituting (2) - (6) in (1), and using the orthogonality of the basis functions we obtain

$$\alpha^i = a^i + \sum_{j \neq i}^{N} T^j \sigma(\mathbf{r}_i - \mathbf{r}_j)\,\alpha^j \quad . \tag{7}$$

This is a set of coupled algebraic equations for the exciting field coefficients which can be iterated and leads to a multiple scattering series.

For randomly distributed scatterers, an ensemble average can be performed on (7) leading to

$$\langle \alpha^i \rangle_i = a^i + \langle \sigma(\mathbf{r}_i - \mathbf{r}_j)\, T^j \langle \alpha^j \rangle_{ij} \rangle_i \tag{8}$$

where the angle brackets and their subscripts i and ij denote conditional averages. Equation (8) when iterated is an infinite hierarchy and usually the hierarchy is truncated by use of the *quasi-crystalline approximation* (QCA) [3]. The QCA states as

$$\langle \alpha^j \rangle_{ij} \approx \langle \alpha^j \rangle_j \quad . \tag{9}$$

Then, (8) simplifies to

$$\langle \alpha^i \rangle_i = a^j + \langle \sigma(\mathbf{r}_i - \mathbf{r}_j)\, T^j \langle \alpha^j \rangle_j \rangle_i \tag{10}$$

an integral equation for $\langle \alpha^i \rangle_i$ which in principle can be solved. We observe that the ensemble average in (10) only requires $P(\mathbf{r}_j|\mathbf{r}_i)$, the joint probability distribution function. In particular, the homogeneous solution of (10) leads to a dispersion equation for the effective medium in the quasi-crystalline approximation. Defining the spatial Fourier transform of $\langle \alpha^i \rangle_i$ as

$$\langle \alpha^i \rangle_i = \int e^{i\mathbf{K}\cdot\mathbf{r}_i}\, X^i(\mathbf{K})\, d\mathbf{K} \tag{11}$$

and substituting in (10), we obtain for the homogeneous solution

$$X^i(K) = \sum_{j \neq i} \int \sigma(r_i - r_j)\, T^j\, p(r_j|r_i) \times e^{iK\cdot(r_i - r_j)}\, X^j(K)\, dr_j \quad . \tag{12}$$

If the scatterers are identical

$$X^i(K) = X^j(K) = X(K) \tag{13}$$

and thus for a nontrivial solution to $< \alpha^i >_i$, we require

$$\left| I - \sum_{j \neq i}^{N} \int \sigma(r_i - r_j)\, T^j\, p(r_j|r_i)\, e^{iK\cdot(r_i - r_j)}\, dr_j \right| = 0 \quad . \tag{14}$$

In (14), $P(r_j|r_i)$ is the joint probability distribution function and I is an identity matrix. For isotropic or spherical statistics,

$$P(r_j|r_i) = \begin{cases} 0\,; & |r_i - r_j| < 2\alpha \\ g(|r_i - r_j|)/V \;; & |r_i - r_j| > 2a \end{cases} \tag{15}$$

where we have assumed that the scatterers are impenetrable with a minimum separation between the centers, and in (15), 2a could be the diameter of the circumscribing sphere. For spherical scatterers, the joint probability distribution depends only on the interparticle distance and not on the orientation of the vector joining the centers; and the function $g(|r_i - r_j|)$ is called the radial distribution function.

3. DISPERSION EQUATION IN THE LONG WAVELENGTH LIMIT

The objective of the self-consistent multiple scattering formalism derived for the problem is to obtain an analytical expression for the dispersion equation (14) of a wave propagating in the random medium. By solving the dispersion equation, we can obtain an effective propagation constant of the random medium. However, this is a forbidden task and can only be done numerically when the size of the scatterers is large compared with the incident wavelength.

Fortunately, for most microwave composite materials, the scatterers are much smaller than a millimeter in size. Therefore, at frequencies in the gigahertz range, the wavelength in the matrix material is much larger than the size a of particles and make the nondimensional frequency ka fall in the Rayleigh region . Thus, one can solve the dispersion equation in the long wavelength regime and obtain a closed form solution.

Retaining only the dipole terms, we have the following dispersion equation [1]

$$\begin{vmatrix} T^1(JH_0 + JH_2/2) - 1 & 3\,JH_1\,T^2/2 \\ 3\,JH_1\,T^2/2 & T^2(JH_0 + JH_2/2) - 1 \end{vmatrix} = 0 \tag{16}$$

$$JH_0 = 3\,j\,\Omega/X_2^3 + w$$

$$JH_1 = 3\,j\,\Omega\,(K/k_2)/X_2^3$$

$$JH_2 = 3\,j\,\Omega\,(K/k_2)^2/X_2^3$$

$$\Omega = c/[1 - (K/k_2)^2]$$

$$T^1 = j\,(2X_2^3/3)\,[(\mu_1 - \mu_2)/(2\mu_2 + \mu_1)]$$

$$T^2 = j\,(2X_2^3/3)\,[(\varepsilon_1 - \varepsilon_2)/(2\varepsilon_2 + \varepsilon_1)]$$

$$w = (1-c)^4/(1+2c)^2$$

$$X_2 = \mathrm{Re}\,(k_2 a)$$

$$\mu_1 = \mu_1' + j\mu_1''$$

$$\varepsilon_1 = \varepsilon_1' + j\varepsilon_1''$$

$$\mu_2 = \mu_2' + j\mu_2''$$

$$\varepsilon_2 = \varepsilon_2' + j\varepsilon_2''$$

$$k_2 = \omega\,(\mu_2\varepsilon_2)^{1/2}/c_o$$

$$K = \text{Effective propagation constant} = \omega\,(\langle\mu\rangle\langle\varepsilon\rangle)^{1/2}/c_o$$

$$c_o = \text{Light speed in vacuum}$$

$$c = \text{Volume fraction of scatterers}$$

The effective dielectric constant $\langle\varepsilon\rangle$ and permeability $\langle\mu\rangle$ can be easily obtained from Eq. (16) due to the fact that T^1 and T^2 are uncoupled and the effective propagation constant K is polarization independent in the Rayleigh region. This approach can also be applied to the study of electromagnetic scattering by a periodic array of particles.

For randomly distributed lossy/lossless scatterers with a high concentration in a lossy/lossless matrix, the effective permeability and permittivity are, respectively,

$$\langle\mu\rangle/\mu_2 = \{1 - [\beta w - (c\gamma - cj)/(1+\gamma^2)]\,(B + jA)\}/\{1 - [\beta w + (c\gamma - cj)/2(1-\gamma^2)]\,(B + jA)\}$$

$$\langle\varepsilon\rangle/\varepsilon_2 = \{1 - [\beta w - (c\gamma - cj)/(1+\gamma^2)]\,(C + jD)\}/\{1 - [\beta w + (c\gamma - cj)/2(1-\gamma^2)]\,(C + jD)\} \tag{17}$$

where,

$$A = 2\,(B\gamma + A) \qquad B = 2\,(A\gamma - B)$$

$$C = 2\,(C\gamma - D) \qquad D = 2\,(D\gamma + C)$$

$$A = [(\mu_1' - \mu_2')(2\mu_2' + \mu_1') + (\mu_1'' - \mu_2'')(2\mu_2'' + \mu_1'')]/\Delta$$

$$B = [(\mu_1'' - \mu_2'')(2\mu_2' + \mu_1') + (\mu_1' - \mu_2')(2\mu_2'' + \mu_1'')]/\Delta$$

$$C = [(\varepsilon_1' - \varepsilon_2')(2\varepsilon_2' + \varepsilon_1') + (\varepsilon_1'' - \varepsilon_2'')(2\varepsilon_2'' + \varepsilon_1'')]/\Delta'$$

$$D = [(\varepsilon_1'' - \varepsilon_2'')(2\varepsilon_2' + \varepsilon_1') + (\varepsilon_1' - \varepsilon_2')(2\varepsilon_2'' + \varepsilon_1'')]/\Delta'$$

$$\Delta = (2\mu_2' + \mu_1')^2 + (2\mu_2'' + \mu_1'')^2$$

$$\Delta' = (2\varepsilon_2' + \varepsilon_1')^2 + (2\varepsilon_2'' + \varepsilon_1'')^2$$

$$\gamma = (X_2^3 - 3X_2^2 X_2')/(X_2^3 - 3X_2 X_2''^2)$$

$$\beta = (X_2^3 - 3X_2 X_2''^2)/3$$

$$X_2' = \mathrm{Im}\,(k_2 a)$$

4. RESULTS AND DISCUSSION

Different from various equations, which are quite popularly used, such as Maxwell-Garnett equation, Clausius-Mosotti equation, and other equations like Lichtenecker logarithmic equation, our equations for independent permittivity and permeability can be used in either purely scattering domain or absorption domain. In other words, the matrix as well as the inclusion materials can both be lossy and lossless or combinations of the two. Furthermore, a rigorous multiple scattering theory has been employed in the derivations accounted for high concentrations of the inclusion phase while none of the mentioned equations has considered multiple scattering.

In the following, we discuss some limiting cases when (17) is applied to compute the effective properties of microwave composite materials. Because the effective permittivity and permeability bear the same form. For simplicity, we use only the expressions for the effective permittivity. However, all the following discussion are exactly those for the effective permeability when all the ε's are replaced by the μ's in the statements.

Case 1. Pure Scattering

If neither the scatterers nor the matrix material are lossy, i.e. $\varepsilon_1'' = \varepsilon_2'' = 0$, only scattering contributes to the imaginary part of the effective dielectric constant $< \varepsilon >$.

$$< \varepsilon > / \varepsilon_2' = (1 + 2cT)/(1 - cT) + j\,6\beta w c T^2/(1 - cT)^2 \qquad (18)$$

where $T = (\varepsilon_1' - \varepsilon_2')/(\varepsilon_1' + 2\varepsilon_2')$. The effective dielectric constant $< \varepsilon >$ becomes ε_2' and ε_1', respectively, when c equals to 0 (no scatterer) and 1 (matrix material totally occupied by scatterers). Meanwhile, the imaginary part of $< \varepsilon >$ vanishes due to the disappearance of scatterers.

Case 2. Lossy scatterers in a lossless matrix

This is a common case happened in various problems, e.g. suspensions in fluids. For this case, $\varepsilon_2'' = 0$ but ε_1'' is not. Equation (17) can be reduced to the form as follows

$$< \varepsilon > / \varepsilon_2' = \{1 + 2(\beta w + cj)(D - jC)\}/\{1 + 2[\beta w - cj/2](D - jC)\} \quad . \qquad (19)$$

Again, $< \varepsilon >$ becomes ε_2' when $c = 0$. However, when $c = 1$,

$$< \varepsilon > / \varepsilon_2' = (1 + 2C + 2jD)/(1 - C - jD) = (\varepsilon_1' + j\varepsilon_1'')/\varepsilon_2' \quad . \qquad (20)$$

It is easy to see that the effective dielectric constant becomes that of the lossy scatterers.

Case 3. Lossless scatterers in a lossy matrix

Although this problem has seldom been considered for electromagnetic case , e.g. particles in a viscous fluid, it is useful to check the validity of the formalism. For this case, $\varepsilon_1'' = 0$ and ε_2'' is finite. It is easy to

show using (17), for c = 0, $< \varepsilon > = \varepsilon_2 = \varepsilon_2' + j\,\varepsilon_2''$. For c = 1, (17) reduces to

$$< \varepsilon > / \varepsilon_2 = (1 + 2C + 2\,jD) / (1 - C - jD) = \varepsilon_1' / (\varepsilon_2' + j\,\varepsilon_2'') \quad , \tag{21}$$

which means the effective dielectric constant becomes that of the scatterers and is real.

Case 4. Lossy scatterers in a lossy matrix

For this case, the complete form of (17) must be considered. As for the relative contribution form scattering and absorption towards $< \varepsilon >$, one can easily show by using case 2 that

$$< \varepsilon > / \varepsilon_2' = [(1 + 2\,c\,C)\,(1 - c\,C) - 2\,c^2 D^2] / [(1 - c\,C)^2 + c^2 D^2]$$
$$+ j\,[3\,c\,D + 6\,\beta\,w\,c\,(C^2 + D^2)] / [(1 - c\,C)^2 + c^2 D^2] \quad . \tag{22}$$

If $\varepsilon_1'' = 0$ then D = 0, the above equation becomes that for case 1. Therefore, the scattering contribution to the imaginary part of $< \varepsilon >$ has a β dependence. Because β is of the order of $(k_2 a)^3$, which is much less than one for the long wavelength limit, we know the scattering contribution is fairly small when compared with the absorption contribution which is frequency independent if ε_1 and ε_2 are also frequency independent. The real part of the effective dielectric constant is less affected by the absorption due to the fact that ε_1'' is, in general, fairly small.

REFERENCES

1. V.K. Varadan, V.V. Varadan, Y. Ma and W.F. Hall, *IEEE Trans. Microwave Theory Tech. MIT-34*, 251 (1986).

2. V.K. Varadan and V.V. Varadan, (eds.) *Acoustic, Electromagnetic and Elastic Wave Scattering: Focus on the T-Matrix Approach*, Pergamon, New York (1980).

3. M. Lax, *Phys. Rev.* **85**, 621 (1952).

PROPAGATION IN A PARALLEL-PLATE WAVEGUIDE WHOLLY FILLED WITH A CHIRAL MEDIUM

VIJAY K. VARADAN, AKHLESH LAKHTAKIA *and* VASUNDARA V. VARADAN
Department of Engineering Science and Mechanics
and
Center for the Engineering of Electronic and Acoustic Materials
The Pennsylvania State University
University Park, PA 16802.

ABSTRACT

Propgation of electromagnetic waves in a parallel-plate waveguide wholly filled with a chiral medium is examined. The dispersion equation derived leads to two sets of modes. Propagation constants for the two sets have been numerically obtained.

1. INTRODUCTION

Although the phenomenon of chirality is known chiefly at the molecular level, it has been suggested [1] that particles endowed with chirality can exist at even lower frequencies, say, in the GHz range. This is because chirality, or handedness, is a geometric property: for example, the electromagnetic response of a right-handed helix is different from that of a left-handed one [2]. Furthermore, by embedding such chiral particles in a low-loss dielectric medium, that medium too will possess handedness. With advances in polymer science, it is becoming increasingly possible that such artificial materials can be manufactured with ease, and their properties tailored by altering the sizes and concentration of the embedded chiral particles.

Significant advances have taken place recently in the formulation of a frequency-domain electromagnetic theory for chiral media, and these have been summarised by us elsewhere [1]. With these developments, it is time that aspects relating to the application of chiral media for practical problems be explored. To that end, we have already obtained the eigenmodes of a perfectly conducting sphere filled with a homogeneous, isotropic, chiral medium [3]. In continuation of our aim, we study here the modes of a parallel-plate waveguide filled with a chiral material. It is our conjecture that this geometry will be of use in the development of integrated circuitry with chiral substrates.

Consider a source-free region occupied by an isotropic chiral medium in which the usual constitutive relations $\mathbf{D} = \varepsilon\mathbf{E}$ and $\mathbf{B} = \mu\mathbf{H}$ do not hold due to their incompatibility with the handedness of the medium. Instead, the relations

$$\mathbf{D} = \varepsilon\mathbf{E} + \beta\varepsilon\,\nabla\times\mathbf{E} \quad ; \quad \mathbf{B} = \mu\mathbf{H} + \beta\mu\,\nabla\times\mathbf{H} \tag{1}$$

hold, and satisfy the requirements of time-reversal symmetry and reciprocity. Following [4], the electromagnetic field is transformed to

$$\mathbf{E} = \mathbf{Q}_1 + a_R\,\mathbf{Q}_2 \quad ; \quad \mathbf{H} = \mathbf{Q}_2 + a_L\,\mathbf{Q}_1 \quad , \tag{2}$$

where the left- (LCP) and the right- (RCP) circularly polarized fields, $\mathbf{Q}_1$ and $\mathbf{Q}_2$, respectively, must satisfy the Helmholtz equations

$$\{\nabla^2 + \gamma_1^2\}\,\mathbf{Q}_1 = 0 \quad ; \quad \{\nabla^2 + \gamma_2^2\}\,\mathbf{Q}_2 = 0 \quad , \tag{3}$$

along with the rotational conditions

$$\nabla\times\mathbf{Q}_1 = \gamma_1\,\mathbf{Q}_1 \quad ; \quad \nabla\times\mathbf{Q}_2 = -\gamma_2\,\mathbf{Q}_2 \quad . \tag{4}$$

Needless to say, these fields are also divergence-free, *vide*

$$\nabla\cdot\mathbf{Q}_1 = 0 \quad ; \quad \nabla\cdot\mathbf{Q}_2 = 0 \quad . \tag{5}$$

In these equations, the two wavenumbers are given by

$$\gamma_1 = k/\{1-k\beta\} \quad ; \quad \gamma_2 = k/\{1+k\beta\} \quad , \tag{6}$$

and

$$a_L = -i\,(\varepsilon/\mu)^{1/2} \quad ; \quad a_R = -i\,(\mu/\varepsilon)^{1/2} \quad . \tag{7}$$

An exp[−iωt] time dependence has been assumed throughout this work, while $k = \omega\{\mu\varepsilon\}^{1/2}$ is simply a shorthand notation.

2. MODAL ANALYSIS

Consider the region bounded by the perfectly conducting plates z = ±d, which is wholly filled with a chiral medium. It is well-known that although LCP and RCP waves can propagate independently in an unbounded chiral region, at a bimaterial interface mode-conversion occurs [4]. Therefore, pure LCP or RCP modes cannot exist within a bounded chiral volume. Using a representation given by us earlier [5], the electromagnetic field inside the parallel-plate waveguide can be adequately expressed by

$$Q_1 = \left[A_{1+}\gamma_1^{-1}\{-\alpha_1 e_x + \kappa e_z - i\gamma_1 e_y\}\exp[i\alpha_1 z]\right.$$

$$\left. + A_{1-}\gamma_1^{-1}\{\alpha_1 e_x + \kappa e_z - i\gamma_1 e_y\}\exp[-i\alpha_1 z]\right]\exp[i\kappa x] \quad , \tag{8a}$$

$$Q_2 = \left[A_{2+}\gamma_2^{-1}\{-\alpha_2 e_x + \kappa e_z + i\gamma_2 e_y\}\exp[i\alpha_2 z]\right.$$

$$\left. + A_{2-}\gamma_2^{-1}\{\alpha_2 e_x + \kappa e_z + i\gamma_2 e_y\}\exp[-i\alpha_2 z]\right]\exp[i\kappa x] \quad , \tag{8b}$$

which satisfy the phase-matching conditions *via* the horizontal wavenumber κ. In these equations, $\alpha_1 = +\sqrt{(\gamma_1^2 - \kappa^2)}$ and $\alpha_2 = +\sqrt{(\gamma_2^2 - \kappa^2)}$, while $A_{1\pm}$ and $A_{2\pm}$ are the unknown field coefficients.

The boundary conditions require that the tangential components of the electric field be identically zero on the surfaces z = ±d. The use of (2) and (8) along with the boundary conditions leads to the dispersion equation

$$0 = \left[\{\alpha_1\gamma_1^{-1} + \alpha_2\gamma_2^{-1}\}\{1-\exp[i2(\gamma_1+\gamma_2)d]\} + \{\alpha_1\gamma_1^{-1} - \alpha_2\gamma_2^{-1}\}\{\exp[i2\gamma_1 d]\} - \exp[i2\gamma_2 d]\}\right] \times$$

$$\left[\{\alpha_1\gamma_1^{-1} + \alpha_2\gamma_2^{-1}\}\{1-\exp[i2(\gamma_1+\gamma_2)d]\} - \{\alpha_1\gamma_1^{-1} - \alpha_2\gamma_2^{-1}\}\{\exp[i2\gamma_1 d]\} - \exp[i2\gamma_2 d]\}\right]. \tag{9}$$

Since (9) contains two factors on its right hand side, it is clear that two kinds of modes can exist. The dispersion equation for the *first* set of modes is given by

$$0 = \left[\{\alpha_1\gamma_1^{-1} + \alpha_2\gamma_2^{-1}\}\{1-\exp[i2(\gamma_1+\gamma_2)d]\} + \{\alpha_1\gamma_1^{-1} - \alpha_2\gamma_2^{-1}\}\{\exp[i2\gamma_1 d]\} - \exp[i2\gamma_2 d]\}\right] , \tag{10a}$$

and for these modes it is easily seen that

$$A_{1+}/A_{1-} = A_{2+}/A_{2-} = -1 \quad , \tag{10b}$$

$$a_R A_{2+}/A_{1+} = \sin(\alpha_1 d)/\sin(\alpha_2 d) \quad . \tag{10c}$$

As a consequence the field components E_x and H_x are *even* with respect to z, whereas the field components E_y, H_y, E_z and H_z are *odd* with respect to z.

On the other hand, the dispersion equation for the *second* set of modes is given by

$$0 = \left[\{\alpha_1 \gamma_1^{-1} + \alpha_2 \gamma_2^{-1}\} \{1 - \exp[i2 (\gamma_1 + \gamma_2) d]\} - \{\alpha_1 \gamma_1^{-1} - \alpha_2 \gamma_2^{-1}\} \{\exp[i2\gamma_1 d]\} - \exp[i2\gamma_2 d]\} \right] , \tag{11a}$$

and for these modes it can be shown that

$$A_{1+} / A_{1-} = A_{2+} / A_{2-} = 1 , \tag{11b}$$

$$a_R A_{2+} / A_{1+} = \cos(\alpha_1 d) / \cos(\alpha_2 d) \quad . \tag{11c}$$

As a consequence the field components E_x and H_x are *odd* with respect to z, whereas the field components E_y, H_y, E_z and H_z are *even* with respect to z.

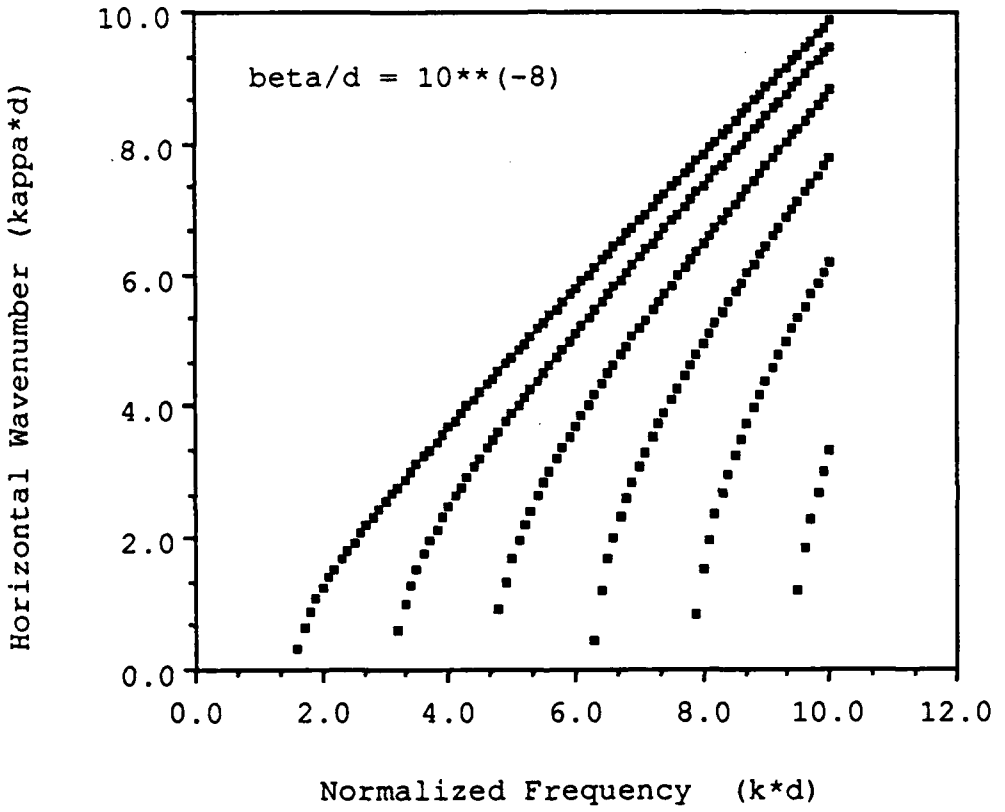

Figure 1. Solutions κd of the dispersion equations (12c) and (13c) are virtually identical for $\beta/d \leq 10^{-4}$. They also correspond (almost exactly) to the TE- and TM- polarised fields when $\beta/d = 0$.

3. NUMERICAL RESULTS

With the developments of the previous section, the modal fields of the *first* set can be compactly set down as

$$Q_1 = \exp[i\kappa x]\, \gamma_1^{-1} \{-\alpha_1 \cos(\alpha_1 z)\, e_x + i\kappa \sin(\alpha_1 z)\, e_z + \gamma_1 \sin(\alpha_1 z)\, e_y\} , \tag{12a}$$

$$a_R Q_2 = \exp[i\kappa x]\, \gamma_2^{-1} \{-\alpha_2 \cos(\alpha_2 z)\, e_x + i\kappa \sin(\alpha_2 z)\, e_z - \gamma_2 \sin(\alpha_2 z)\, e_y\} \sin(\alpha_1 d) / \sin(\alpha_2 d) \quad ; \tag{12b}$$

the horizontal wavenumber κ can be determined for this set by solving the equation

$$\alpha_1\gamma_2 / \alpha_2\gamma_1 + \tan(\alpha_1 d) / \tan(\alpha_2 d) = 0 \quad . \tag{12c}$$

In a similar vein, the modal fields of the *second* set can be written as

$$Q_1 = \exp[i\kappa x]\, \gamma_1^{-1} \{-\alpha_1 \sin(\alpha_1 z)\, e_x + \kappa \cos(\alpha_1 z)\, e_z - i\gamma_1 \cos(\alpha_1 z)\, e_y\} \ , \tag{13a}$$

$$a_R\, Q_2 = \exp[i\kappa x]\, \gamma_2^{-1} \{-i\alpha_2 \sin(\alpha_2 z)\, e_x + \kappa \cos(\alpha_2 z)\, e_z + i\gamma_2 \cos(\alpha_2 z)\, e_y\} \cos(\alpha_1 d) / \cos(\alpha_2 d) \ ; \tag{13b}$$

the horizontal wavenumber κ can be determined for this set by solving the equation

$$\alpha_1\gamma_2 / \alpha_2\gamma_1 + \cot(\alpha_1 d) / \cot(\alpha_2 d) = 0 \quad . \tag{13c}$$

The solutions κd of the dispersion equations (12c) and (13c) were obtained numerically on a Macintosh II minicomputer as functions of the normalized frequency $kd \leq 10.0$ for various values of β/d; while $\kappa \leq \min[\gamma_1, \gamma_2]$, $k\beta$ was kept less than 0.5 for Figs. 1-3, it is less than 0.99 for Figs. 4 and 5. Fig.1 shows the calculations for $\beta/d = 10^{-8}$. For $\beta/d \leq 10^{-4}$, the roots for the two sets of modes did not appreciably differ from each other; furthermore $\alpha_1 d$ and $\alpha_2 d$ were approximately equal to integral multiples of $\pi/2$. The effect of chirality became numerically appreciable, however, at $\beta/d = 10^{-3}$, although the differences between the roots for the two sets are still small enough to be appreciated on a graph.

Shown in Figs. 2 and 3 are the roots κd of the dispersion equations (12c) and (13c), respectively, for $\beta/d = 10^{-2}$. The root structures are now different for the two sets, and particularly so when kd is high. When β/d increases even further, the differences are even more telling, as illustrated in Figs. 4 and 5. Thus it is only at the higher frequencies, and for a higher degree of chirality as characterised by larger values of $|\beta|$, that the effect of the chirality of the medium becomes significant.

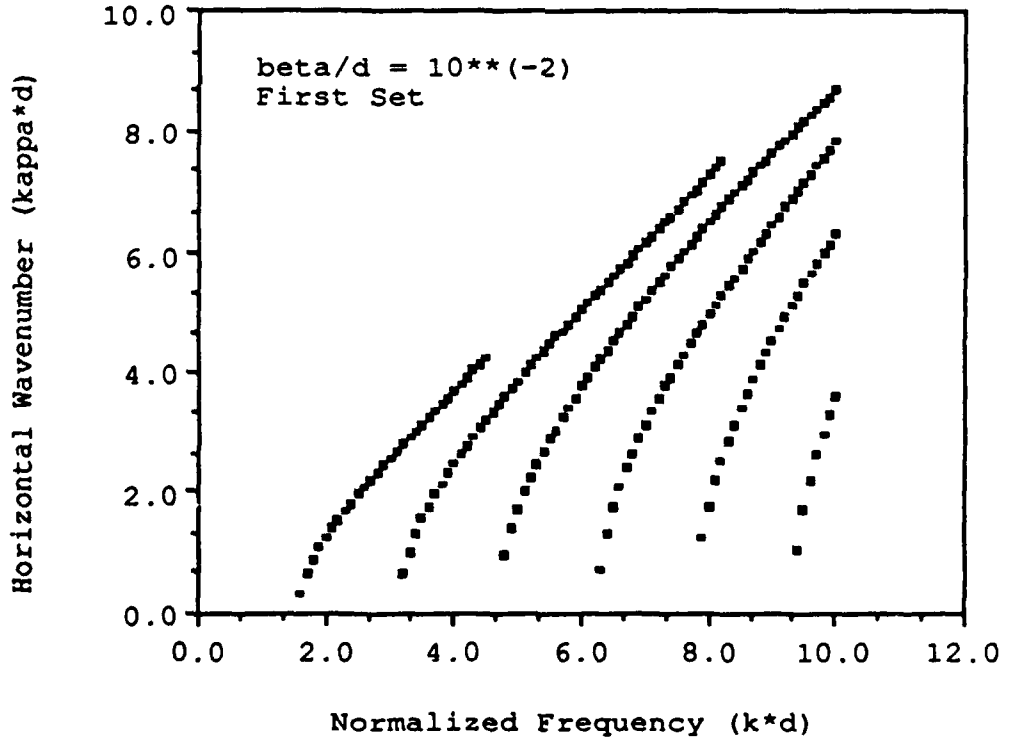

Figure 2. Solutions κd of the dispersion equation (12c) of the first set at $\beta/d = 10^{-2}$; $k\beta \leq 0.5$.

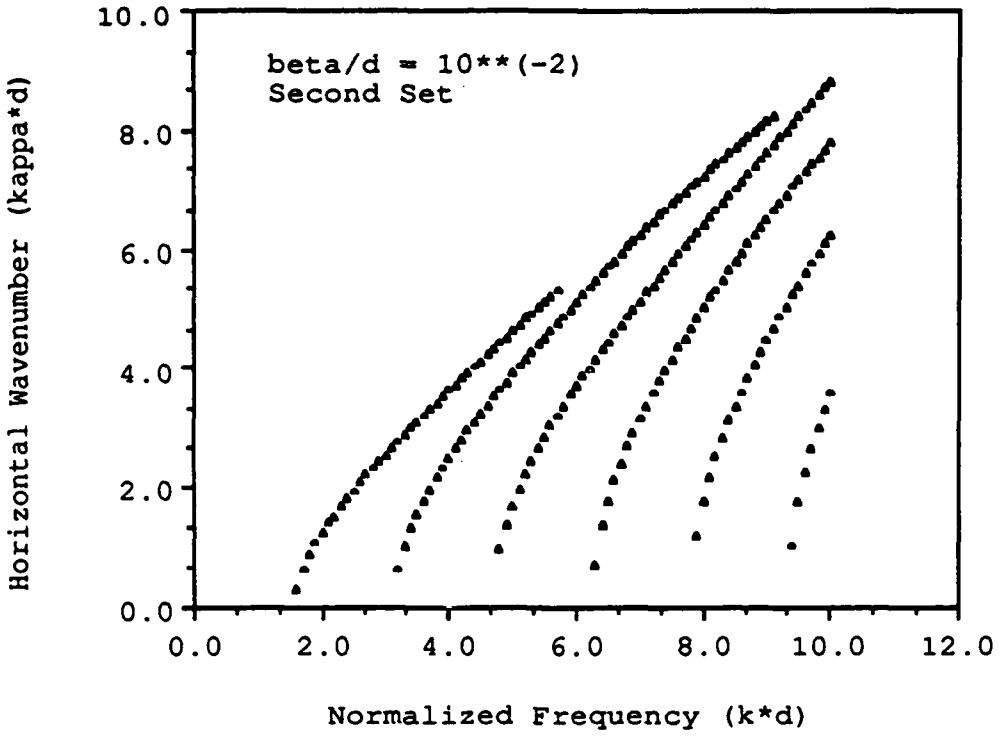

Figure 3. Solutions κd of the dispersion equation (13c) of the second set at $\beta/d = 10^{-2}$; $k\beta \leq 0.5$.

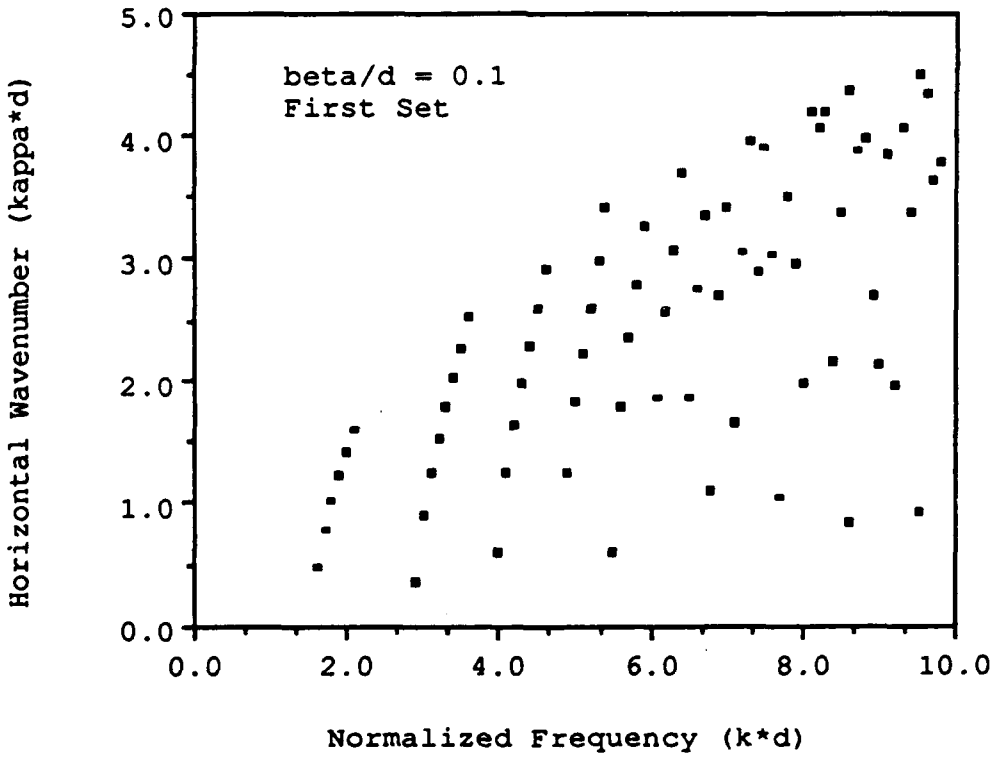

Figure 4. Solutions κd of the dispersion equation (12c) of the first set at $\beta/d = 10^{-1}$; $k\beta \leq 0.99$.

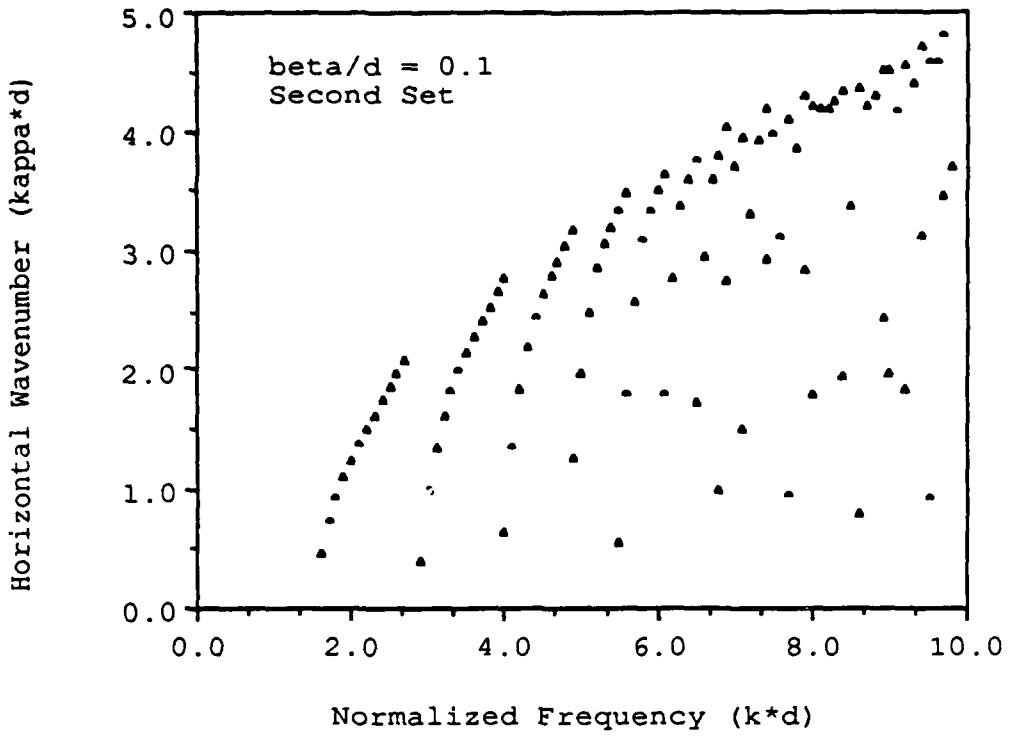

Figure 5. Solutions κd of the dispersion equation (13c) of the second set at $\beta/d = 10^{-1}$; $k\beta \leq 0.99$.

ACKNOWLEDGEMENTS

This work was partially supported by the U.S. Office of Naval Research. Additional support from the industrial members and sponsors of the Center for the Engineering of Electronic and Acoustic Materials is also acknowledged.

REFERENCES

1. A. Lakhtakia, V.V. Varadan and V.K. Varadan, 'Field equations, Huygens's principle, integral equations, and theorems for radiation and scattering of electromagnetic waves in isotropic chiral media', *J. Opt. Soc. Am. A* **5**, 175 (1988).

2. V.V. Varadan, A. Lakhtakia and V.K. Varadan, 'Equivalent dipole moments of helical arrangements of small, isotropic, point-polarizable scatterers: Application to chiral polymer design', *J. Appl. Phys.* **63**, 280 (1988).

3. A. Lakhtakia, V.K. Varadan and V.V. Varadan, 'Eigenmodes of a chiral sphere with a perfectly conducting coating', *J. Phys. D* (submitted for publication, 1988).

4. A. Lakhtakia, V.K. Varadan and V.V. Varadan, 'Regarding the sources of radiation fields in an isotropic chiral medium, *J. Wave-Mater. Interact.* **2**, 183 (1987).

5. V.K. Varadan, V.V. Varadan and A. Lakhtakia, 'On the possibility of designing anti-reflection coatings using chiral composites, *J. Wave-Mater. Interact.* **2**, 71 (1987).

Errata:

PROPAGATION IN A PARALLEL-PLATE WAVEGUIDE WHOLLY FILLED WITH A CHIRAL MEDIUM

VIJAY K. VARADAN, AKHLESH LAKHTAKIA *and* VASUNDARA V. VARADAN
Department of Engineering Science and Mechanics
and
Center for the Engineering of Electronic and Acoustic Materials
The Pennsylvania State University
University Park, PA 16802.

Equations (9), (10a), (11a) and (13a) of the subject paper [1] contained typographical errors. The correct versions are as follows:

$$0 = \left[\{\alpha_1\gamma_1^{-1} + \alpha_2\gamma_2^{-1}\}\{1 - \exp[i2(\alpha_1 + \alpha_2)d]\} + \{\alpha_1\gamma_1^{-1} - \alpha_2\gamma_2^{-1}\}\{\exp[i2\alpha_1 d]\} - \exp[i2\alpha_2 d]\}\right]\times$$
$$\left[\{\alpha_1\gamma_1^{-1} + \alpha_2\gamma_2^{-1}\}\{1 - \exp[i2(\alpha_1 + \alpha_2)d]\} - \{\alpha_1\gamma_1^{-1} - \alpha_2\gamma_2^{-1}\}\{\exp[i2\alpha_1 d]\} - \exp[i2\alpha_2 d]\}\right]. \quad (9)$$

$$0 = \left[\{\alpha_1\gamma_1^{-1} + \alpha_2\gamma_2^{-1}\}\{1 - \exp[i2\,(\alpha_1 + \alpha_2)d]\} + \{\alpha_1\gamma_1^{-1} - \alpha_2\gamma_2^{-1}\}\{\exp[i2\alpha_1 d]\} - \exp[i2\alpha_2 d]\}\right], \quad (10a)$$

$$0 = \left[\{\alpha_1\gamma_1^{-1} + \alpha_2\gamma_2^{-1}\}\{1 - \exp[i2\,(\alpha_1 + \alpha_2)d]\} - \{\alpha_1\gamma_1^{-1} - \alpha_2\gamma_2^{-1}\}\{\exp[i2\alpha_1 d]\} - \exp[i2\alpha_2 d]\}\right], \quad (11a)$$

$$Q_1 = \exp[i\kappa x]\,\gamma_1^{-1}\{-i\alpha_1\sin(\alpha_1 z)\,e_x + \kappa\cos(\alpha_1 z)\,e_z - i\gamma_1\cos(\alpha_1 z)\,e_y\}, \quad (13a)$$

REFERENCE

1. V.K. Varadan, V.V. Varadan and A. Lakhtakia, 'Propagation in a parallel-plate waveguide wholly filled with a chiral medium', *J. Wave-Mater. Interact.* 3, 267 (1988).

Scattering by Three-Dimensional Anisotropic Scatterers

VASUNDARA V. VARADAN
AKHLESH LAKHTAKIA
VIJAY K. VARADAN

Reprinted from
IEEE TRANSACTIONS ON ANTENNAS AND PROPAGATION
Vol. 37, No. 6, 1989

Scattering by Three-Dimensional Anisotropic Scatterers

VASUNDARA V. VARADAN, MEMBER, IEEE, AKHLESH LAKHTAKIA, AND VIJAY K. VARADAN, MEMBER, IEEE

Abstract—**The coupled dipole approximation method has been extended in order to compute the scattering characteristics of three-dimensional, homogeneous, lossless, anisotropic objects. Numerical results are given for uniaxial spheres made of titanium dioxide.**

Introduction and Theory

The Mie formulation [1] of scattering by a homogeneous, isotropic sphere has enjoyed an enormous amount of popularity ever since its inception in 1909, but no formulation of comparable magnitude exists for anisotropic spheres. Recently, Graglia and Uslenghi [2] have formulated integral equations for scattering by anisotropic objects using microscopic arguments; however, they have been successful in the numerical implementation of their formulation only for two-dimensional problems [3]. A method for the solution of electromagnetic scattering by transversely isotropic cylinders due to Monzon and Damaskos [4] should also be mentioned, as should Moon's formalism [5] for the scattering of elastic waves by uniaxial, piezoelectric cylinders made of barium titanate.

The oscillations of a small gyrotropic sphere have been handled by Walker [6] by considering quasistatic electric and magnetic modes. For the electric modes the internal **E**-field was expressed as $\nabla\psi_e$, and for the magnetic modes the internal **H**-field was modeled as $\nabla\psi_m$. Walker's method was iteratively refined by Yan'-Shen [7], [8], but remained valid for very small spheres. This work was extended by Pistol'kors [9] who considered the self-oscillation modes with no azimuthal dependence of a small ferrite sphere. Further research using similar approximations has also been reported in two papers by Wolff [10], [11]. A more comprehensive approach [12], published in Russian, on scattering by ferrite spheres appears to be flawed in its selection of the basis functions for representing fields in the spherical coordinate system.

A semimicroscopic approach [15], in which the scatterer is modeled by mutually interacting point-polarizable groups, has gained popularity in the last few years (e.g., [16], [17]). This technique, dubbed the coupled dipole approximation procedure, has been successfully applied to compute the scattering characteristics of nonspherical, lossless dielectric objects. This procedure has also been successful in predicting the Perrin matrix for scattering by bacteria [18]. Here we report, for the first time, the application of this method for the computation of the scattering by homogeneous, anisotropic scatterers with a relative permittivity dyadic ϵ. Numerical results will be presented for spheres made of titanium dioxide, which is an uniaxial medium.

Detailed discussions of the presented method as applicable to isotropic scatterers are available elsewhere [15]–[17]; therefore, here we shall mention only its features arising due to the anisotropic properties of the scatterer. The scatterer is modeled by a three-dimensional array of point-polarizable groups arranged on a cartesian lattice embedded in free space. Each one of these groups is characterised by a polarizability tensor $\wp$, such that when an electric field **E** hits it, the scattered field can be adequately expressed as being due to an electric dipole moment **p**, with

$$\mathbf{p} = \wp \cdot \mathbf{E}. \tag{1}$$

It has been shown by Bedeaux and Mazur [19] that the polarizability of a small volume v and dielectric dyadic $(\epsilon_0\epsilon)$ immersed in free space is given by

$$\wp = 3v\epsilon_0[\epsilon - \mathcal{I}] \cdot [\epsilon + 2\mathcal{I}]^{-1}. \tag{2}$$

For our purposes we set $v = V/N$, in which V is the volume of the scatterer and N is the total number of point-polarizable groups it has been modeled by. It is to be emphasized that from a geometric viewpoint, the polarizability $\wp$ could be that of an equivoluminal sphere. Still, for our purposes, each sphere is to be visualized solely as a point-polarizable group located at the center of the sphere; hence, any discussion of intersecting spheres is moot. It is hoped that with a sufficiently large N, a convergent result would be obtained (as is the case with the method of moments), and which would be checked with experimental results for adequacy and accuracy.

It also needs be mentioned that the term $[\epsilon - \mathcal{I}]\cdot[\epsilon + 2\mathcal{I}]^{-1}$ has not been obtained through a simple-minded extension of the Clausius–Mossotti relation for small, isotropic, dielectric spheres [20]. Instead, Bedeaux and Mazur [19] invoked a statistical theory for the wave vector and the frequency-dependent dielectric tensor for their treatment of a nonpolar fluid. Hence, their theory is not restricted to small values of the polarizability per unit volume. The only restriction here is that the medium not be lossy, for it is not clear if a lossy spherical unit can be adequately represented by a complex electric dipole.

The electric field, $\mathbf{E}_{ex,m}$ exciting the mth spherical subunit is composed of the incident field $\mathbf{E}_{inc}(\mathbf{r}_m)$ as well as the scattered fields due to all the other subunits evaluated at $\mathbf{r}_m$, the location of the mth

Manuscript received March 4, 1988; revised August 12, 1988.

The authors are with the Department of Engineering Science and Mechanics and the Center for the Engineering of Electronic and Acoustic Materials, Pennsylvania State University, University Park, PA 16802.

IEEE Log Number 8927252.

0018-926X/89/0600-0800$01.00

subunit. Thus

$$\mathbf{E}_{inc}(\mathbf{r}_m) = \sum_{n=1,2,\cdots,M} \mathcal{Q}_{mn} \cdot \mathbf{E}_{ex,n};\ m = 1, 2, \cdots, M, \quad (3a)$$

where

$$\mathcal{Q}_{mn} = \mathcal{J}\delta_{mn} - (1-\delta_{mn})(k^2/4\pi\epsilon_0 R_{mn}) \cdot \exp[ikR_{mn}]\{g_{mnP} \cdot \mathbf{e}_{mn}\mathbf{e}_{mn} - h_{mnP}\}. \quad (3b)$$

In these equations, δ_{mn} is the Kronecker delta, $k = \omega\sqrt{[\epsilon_0\mu_0]}$ is the free-space wavenumber, $\mathbf{R}_{mn} = \mathbf{r}_m - \mathbf{r}_n$, $\mathbf{e}_{mn} = \mathbf{R}_{mn}/R_{mn}$, $g_{mn} = 3[kR_{mn}]^{-2} - 3i[kR_{mn}]^{-1} - 1$ and $3h_{mn} = g_{mn} - 2$. Equation (4b) can be so[illegible] for the exciting fields, whence the far-zone scattered field due to the anisotropic scatterer can be easily derived as

$$\mathbf{F}_{sc}(r) = \lim_{kr\to\infty}\{kr \exp[-ikr]\mathbf{E}_{sc}(r)\} = (k^3/4\pi\epsilon_0) \sum_{m=1,2,\cdots,M} \exp[-ik\mathbf{r}_m \cdot \mathbf{r}/r]_P \cdot [I - r^{-2}\mathbf{rr}] \cdot \mathbf{E}_{ex,m}. \quad (4)$$

Equations (3) give the procedure its name. The exciting field is determined at the location of each point-polarizable group via the second term in (3b), which permits interactions between the groups. These interactions are exact, given that the groups are dipolar.

Numerical Results and Discussion

Equations (3b) and (4) were programmed and solved, for a uniaxial sphere, on a DEC VAX 11/730 minicomputer using single precision complex arithmetic. Uniaxial dielectric media are characterized by an anisotropic permittivity, with the relative permittivity stated in dyadic notation as

$$\epsilon = \epsilon_\perp \mathcal{J} + (\epsilon_\parallel - \epsilon_\perp)\mathbf{cc}, \quad (5)$$

where $\mathcal{J}$ is the unit dyadic and $\mathbf{c}$ is the unit vector along the optic axis; without loss of generality it can be assumed that $\mathbf{c} = \mathbf{e}_z$. We chose the scatterer to be a sphere of radius a (i.e., $V = 4\pi a^3/3$) made up of titanium dioxide ($\epsilon_\perp = 0.913$, $\epsilon_\parallel = 7.197$) on which plane waves are incident at a normalized frequency $ka = 0.5$. We compared the scattering pattern $\mathbf{F}_{sc}$ for a dielectric sphere of relative permittivity 7.2 with rigorous calculations made using the Mie theory, and observed agreement within 5 percent when 179 spherical subunits were utilized; see Fig. 1. For the results presented in the sequel, therefore, 179 spherical subunits were used to model the uniaxial spheres.

Shown in Fig. 2 are computations made for the titanium dioxide sphere when a plane wave, $\mathbf{E}_{inc} = \mathbf{e}_x \exp[ikz]$ is incident on it. The scattering pattern in the x-z plane turns out be predominantly θ-polarized, whereas in the y-z plane it is φ-polarized. For comparison, the data from Mie theory for isotropic spheres of relative permittivities 5.913 and 7.197 are also plotted. The depolarized scattered fields (i.e., the φ-polarized one in the x-z plane and the θ-polarized one in the y-z plane), which are due to anisotropy of the scatterer, have not been plotted since they are several orders of magnitude smaller for the calculations pertaining Fig. 2.

In Fig. 3, the scattering pattern is plotted when the incident plane wave is given by $\mathbf{E}_{inc} = \mathbf{e}_z \exp[ikx]$; the depolarized component of the scattered field is φ-polarized in the x-y plane, and θ-polarized in the y-z plane. The scattering pattern in the x-z plane is still θ-polarized; but, in the y-z plane, the predominant component of the scattering pattern is also the θ-polarized one, not the φ-polarized one. This suggests the tremendous effect of the anisotropy when the incident electric vector is parallel to the optic axis. This understanding is further underscored in Fig. 4 where the scattering pattern is plotted for the incident plane wave $\mathbf{E}_{inc} = \mathbf{e}_y \exp[ikx]$; the depolarized component of the scattered field is θ-polarized in the x-z plane, and φ-polarized in the y-z plane. It should be noticed that the depolarized component manifests itself significantly only in the y-z plane, but its magnitude is small.

This coupled dipole approximation method is simple, and does not require the solution of any integrodifferential equation. As is apparent from (3), the presented method will work for any constitutive dyadic ϵ, provided it is lossless; furthermore, scatterers of any shape can be accommodated. Thus, this procedure will work well for any three-dimensional, lossless, anisotropic scatterer. With increasing frequency, however, the number of spherical subunits

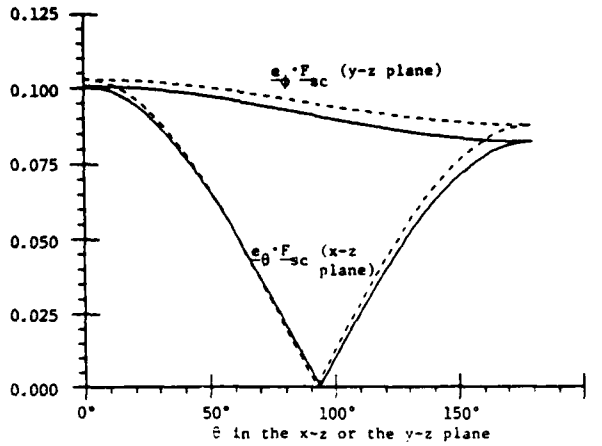

Fig. 1. Comparison of the scattering patterns of an isotropic sphere, of radius a and relative permittivity 7.2, using Mie theory (———) and the present method (——). The plane wave $\mathbf{E}_{inc} = \mathbf{e}_x \exp[ikz]$ is incident with $ka = 0.5$.

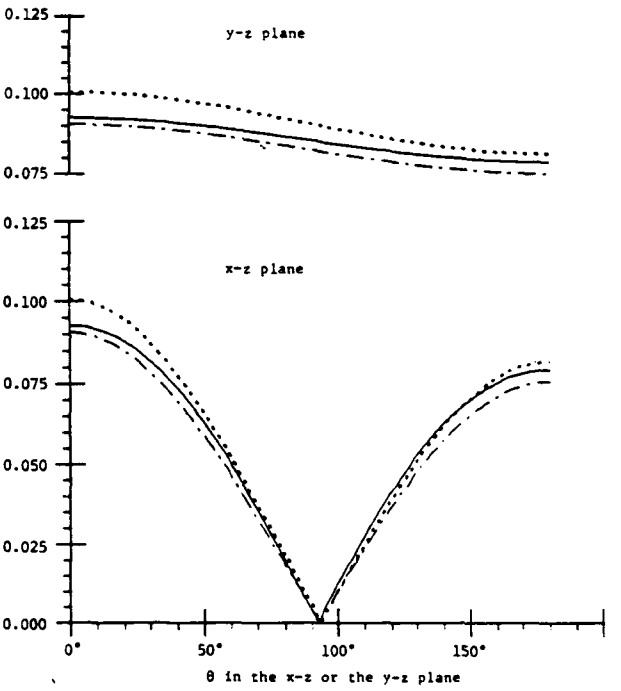

Fig. 2. Scattering pattern of a TiO_2 sphere (——) of radius a on which a planewave, $\mathbf{E}_{inc} = \mathbf{e}_x \exp[ikz]$ is incident with $ka = 0.5$. Top: $\mathbf{e}_\varphi \cdot \mathbf{F}_{sc}$ in the y-z plane. Bottom: $\mathbf{e}_\theta \cdot \mathbf{F}_{sc}$ in the x-z plane. For comparison, Mie theory calculations for isotropic spheres of relative permittivities 5.913 (– • – • –) and 7.197 (· · · ·) are also plotted.

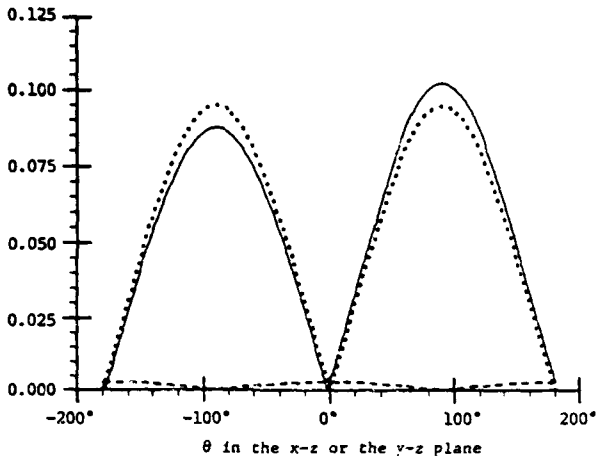

Fig. 3. Scattering pattern of TiO_2 sphere of radius a on which a plane wave, $\mathbf{E}_{inc} = \mathbf{e}_z \exp[ikx]$ is incident with $ka = 0.5$. Code: $\mathbf{e}_\theta \cdot \mathbf{F}_{sc}$ in the x-z plane (——), $\mathbf{e}_\theta \cdot \mathbf{F}_{sc}$ in the y-z plane (· · · ·), and $\mathbf{e}_\varphi \cdot \mathbf{F}_{sc}$ in the y-z plane (— — —).

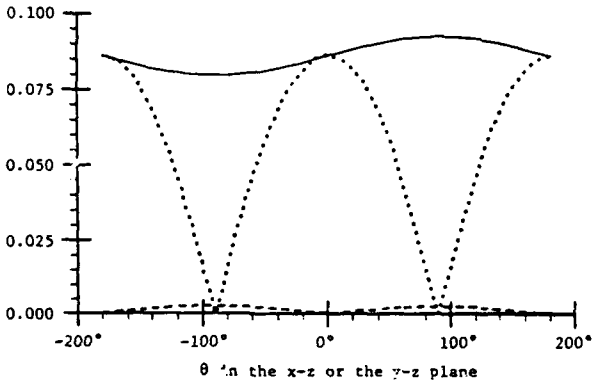

Fig. 4. Scattering pattern of a TiO_2 sphere of radius a on which a plane wave, $\mathbf{E}_{inc} = \mathbf{e}_y \exp[ikx]$ is incident with $ka = 0.5$. Code: $\mathbf{e}_\varphi \cdot \mathbf{F}_{sc}$ (——), $\mathbf{e}_\theta \cdot \mathbf{F}_{sc}$ in the y-z plane (· · · ·), and $\mathbf{e}_\varphi \cdot \mathbf{F}_{sc}$ in the y-z plane (— — —).

required for a convergent solution increases, thereby straining the memory resources of any computer. On the other hand, for aspherical objects, fewer spherical subunits will be needed, making this procedure very attractive. The danger of having to invert extremely large matrices can be surmounted by resorting to an *order of scattering* procedure, in which the interactions are built in through a Feynmann series, as has been done for isotropic particles by Singham and Bohren [21]. In addition, scattering by inhomogeneous objects, like coated spheres and spheroids, can also be handled as has been done for the isotropic case [16]. It should also be noted that this procedure works best when the internal field does not vary rapidly in space.

References

[1] J. A. Stratton, *Electromagnetic Theory*. New York: McGraw-Hill, 1941.

[2] R. D. Graglia and P. L. E. Uslenghi, "Electromagnetic scattering from anisotropic materials, Part I: General theory," *IEEE Trans. Antennas Propagat.*, vol. AP-32, pp. 867–869, 1984.

[3] ——, "Electromagnetic scattering from anisotropic materials, Part II: Computer code and numerical results in two dimensions," *IEEE Trans. Antennas Propagat.*, vol. AP-35, pp. 225–232, 1987.

[4] J. C. Monzon and N. J. Damaskos, "Two-dimensional scattering by a homogeneous anisotropic rod," *IEEE Trans. Antennas Propagat.*, vol. AP-34, pp. 1243–1249, 1986.

[5] F. C. Moon, "Scattering by piezoelectric inclusions," *J. Acoust. Soc. Am.*, vol. 48, pp. 254–262, 1972.

[6] L. R. Walker, "Magnetostatic modes in ferromagnetic resonance," *Phys. Rev.*, vol. 105, pp. 390–395, 1957.

[7] S. Yan'-Shen, "Methods for solving the problem on the oscillations of a small gyrotropic sphere. Part I," *Radio Eng. Electron. Phys.*, vol. 5, no. 12, pp. 109–121, 1960.

[8] S. Yan'-Shen, "Some methods for the solution of a problem concerning the oscillations of a small gyrotropic sphere. Part II," *Radio Eng. Electron. Phys.*, vol. 6, no. 1, pp. 88–94, 1961.

[9] A. A. Pistol'kors, "Axial-symmetric self-oscillations of a gyrotropic sphere sphere of small radius," *Radio Eng. Electron. Phys.*, vol. 7, no. 1, pp. 53–62, 1962.

[10] I. Wolff, "Über die axialsymmetrischen Eigenschwingungen eines kugelförmigen, mit Ferritmaterial gefüllten Hohlraumresonators," *Arch. Elektrisch. Über.*, vol. 22, pp. 19–26, 1968.

[11] I. Wolff, "Die elektromagnetischen Eigenschwingungen einer offenen Ferritkugel," *Arch. Elektrisch. Über.*, vol. 23, pp. 561–569, 1969.

[12] S. S. Hovhannessian and V. A. Baregamian, "The diffraction of a plane electromagnetic wave on an anisotropic sphere," *Izvest. Akad. Nauk. Armenian SSR Phys.*, vol. 16, pp. 37–43, 1981. (Compare (7), (5), (6a) for their spherical wave expansion of $\mathbf{e}_z \exp[ikz]$ in free space with Stratton's expansion to find that the expansions of these authors are erroneous. In addition, no justification appears to be given for the expansions (8) of the internal fields; it appears to be doubtful that these expansions, based on a single scalar potential, shall suffice. For a more rigorous treatment on scalar potentials for anisotropic media, see [13] and [14].)

[13] S. Przezdziecki and R. A. Hurd, "A note on scalar Hertz potentials for gyrotropic media," *Appl. Phys.*, vol. 20, pp. 313–317, 1979.

[14] W. Weiglhofer, "Scalarisation of Maxwell's equations in general inhomogeneous bianisotropic media," *Proc. Inst. Elec. Eng.*, pt. H, vol. 134, pp. 357–360, 1987.

[15] E. M. Purcell and C. R. Pennypacker, "Scattering and absorption of light by non-spherical dielectric grains," *Astrophys. J.*, vol. 186, pp. 705–714, 1973.

[16] S. B. Singham and G. C. Salzman, "Evaluation of the scattering matrix of an arbitrary particle using the coupled dipole approximation," *J. Chem. Phys.*, vol. 84, pp. 2658–2667, 1986.

[17] V. V. Varadan, A. Lakhtakia, and V. K. Varadan, "Equivalent dipole moments of helical arrangements of small, isotropic, point-polarizable scatterers: Application to chiral polymer design," *J. Appl. Phys.*, vol. 63, pp. 280–284, 1988.

[18] R. A. Harris and W. M. McClain, "On the manifestation of retarding effects in diagonally polarized light scattering," *J. Chem. Phys.*, vol. 82, pp. 658–663, 1985.

[19] D. Bedeaux and P. Mazur, "On the critical behaviour of the dielectric constant for a nonpolar fluid," *Physica*, vol. 67, pp. 23–54, 1973.

[20] C. Kittel, *Introduction to Solid State Physics*, 4th ed., New Delhi: Wiley Eastern, 1974, p. 459.

[21] S. B. Singham and C. F. Bohren, "Light scattering by an arbitrary particle: a physical reformulation of the couple dipole method," *Opt. Lett.*, vol. 12, pp. 10–12, 1988.

Lecture Notes in Physics

335

A. Lakhtakia
V.K. Varadan
V.V. Varadan

Time-Harmonic Electromagnetic Fields in Chiral Media

Springer-Verlag

MICROWAVE SINTERING OF CERAMICS

VIJAY K. VARADAN, YUSHIEH MA, AKHLESH LAKHTAKIA
AND VASUNDARA V. VARADAN

Department of Engineering Science & Mechanics, and The Center for Engineering of Electronic and Acoustic Materials,
Pennsylvania State University, University Park, PA 16802.

ABSTRACT

Theoretical considerations regarding microwave sintering of ceramics are discussed. It is shown how the rigorous application of multiple scattering theory may permit a better understanding of this interesting process. The possibility of thermal runaway being chaotic is discussed. Experimental results, and a possible connection to percolation theory, are also given.

INTRODUCTION

Recent years have witnessed an exploration in the industrial use of microwaves for processing of ceramics, glasses and composites. Microwave heating has the potential for uniform, rapid sintering since microwave energy is absorbed directly inside the object contrary to the conventional infrared heating in which absorption starts at the surface. It has also been observed that there is substantial reduction of sintering time and reduction in the input energy. This is because the loss tangent of the object increases with temperature, thereby creating conditions for thermal runaway. Thermal runway depends on the dielectric properties and the porosity of the ceramic; and on the shapes and the sizes of ceramic particles, as well as those of the pores. Incidentally, the slope of temperature-time curve, which is a function of above parameters, is also a strong indicator of grain growth. By adjusting these parameters, grain growth may be controlled during microwave sintering and thus superior material characteristics may be achieved.

While research in this area seems promising, applications of microwave sintering have so far met with little success for many ceramics and composites. Ever since Tinga and Voss [1] showed the feasibility of sintering of ceramics in the mid-sixties, a significant amount of research [2,3] has been focused on identifying and understanding the problems associated with the sintering of various types of ceramics and composites. Many ceramics are transparent to microwaves at room temperature. Sintering of such ceramics has been achieved by some researchers [4] using a microwave plasma to couple the power into the ceramic which results in vary rapid heating rates (thermal runaway) of the order of 100 °C/s. In this case, the energy is conducted into the ceramic, rather than being absorbed inside it.

Ceramics such as mullite, alumina and zirconia have, however, been sintered using conventional 2.0-4.5 GHz traveling wave tubes without the use of plasma. Composites, on the other hand, lend themselves very well to microwave sintering if the inclusions or fibers are microwave absorbers. It is not very well understood how the parameters, such as shapes, size etc., of ceramics in green samples, affect sintering. Experimental verification is very time consuming since various types of samples have to be made and sintered. This suggests theoretical research involving computer simulation using various mixtures and approximations.

In this paper we begin addressing the problems associated with mixture theories and propose a rigorous multiple scattering theory involving correlation function, shape and size effects which might help us understand the basic mechanisms involved in sintering. Thermal runaway conditions may then be studied using the heat-diffusion equation with appropriate initial and boundary conditions. SEM pictures of sintered alumina, strontium titanate are also presented to show that the grain growth is not excessive.

Mat. Res. Soc. Symp. Proc. Vol. 124. © 1988 Materials Research Society

MULTIPLE SCATTERING FORMULATION

Ceramics as well as composites can be modeled as multi-phase random media. In the study of waves propagating through such random media, we are able to retrieve various valuable dynamic properties which describe the average characteristics of random media. For most practical problems, random media are modeled as particles or fibers (discrete inclusion phase) of one or various kinds randomly dispersed in a host medium (connected matrix phase). Although the modeling can consider a number of details of both phases as mentioned in the introduction, for clarity we try to avoid these complexities and present a simpler model for microwave sintering.

The average dielectric constants of materials (random media) to be sintered, which are complex in the microwave frequency band, usually play key roles in the whole sintering process. The imaginary part of the dielectric constant which is an indicator of the material absorbing capability of microwave energy, increases with increasing temperature. This increase is mainly due to the collapse of pore concentrations and the enlargement of pore sizes which in turn directly relates to the change of the temperature. Nevertheless, there is a critical temperature at which the heating rate (degree Celsius per second) is dramatically raised. This is the well known temperature runaway phenomenon and a similar case also occurs for a critical pore concentration known as the concentration threshold. The mechanisms coupling thermodynamics and the concentrations and sizes of pores are, unfortunately, not very clear to the materials research community. The change of dielectric constants due to the change of concentrations and sizes of pores may be predicted by the following model and, as a result, our understanding of the microwave sintering process is improved.

The average dielectric constant can be, in general, obtained for any microwave composites through multiple scattering theory. The role of the imaginary part of the effective dielectric constant is generally neglected in mixture theory but plays an important part in the sintering process. The complex average dielectric constant can be directly calculated from the effective wavenumber using multiple scattering theory [5,6,7]. Nevertheless, in most applications involving multiple scattering, the discrete and continuous phases are well defined and the physical sizes of the discrete phase remains unchanged no matter how the concentration is varied. Due to the selection of the models, results by switching the phases will be different. Therefore, the choice of the appropriate phases in the model becomes critical especially when a phase transition is involved. But the selection of the phases becomes unimportant in modeling ceramic sintering which will be shown in this paper.

In microwave sintering, both sizes of grains and pores vary with either the concentration of grains or pores. With increasing temperature, the concentration of the pores (grains) decreases (increases) and a direct but an implicit relationship between the sizes of particles and the sintering temperature can be visualized but remains to be explored.

Generally speaking, the average field in the random medium is written as a partial summation of a multiple scattering series. By assuming that the average field to be a plane wave with an effective wavenumber K (for a nonmagnetic random composite, its average dielectric constant ϵ is directly proportional to K^2), the resulting dispersion equation is solved. The formalism is general and applicable to any types of wave. Only the most important details that lead to the dispersion equation involving the pair correlation are presented and for all intermediate steps, we refer the reader to Varadan et al [6]. Vector notation is dispensed with, but the formalism is equally applicable to acoustic fields satisfying the scalar Helmholtz equation, or the electromagnetic field satisfying the vector Helmholtz equation.

Let the medium contain N randomly distributed scatterers (grains or pores depending on the model chosen) in a volume V ($n_0 = N/V$ the number density), see Figure 1. Let u, u^0, u^c_i, u^s_i be respectively the total field; the incident or primary plane, harmonic wave of frequency ω; the field incident or exciting the ith scatterer; and the field which is in turn scattered by the ith scatterer. The time dependence $\exp(-i\omega t)$ of all fields is the same and not written explicitly.

These fields are defined at a point r which is not occupied by one of the scatterers. In general, these fields or potentials, which can be used to describe them, satisfy the scalar or vector wave equation. Let Re ϕ_n and Ou ϕ_n denote the basis of orthogonal functions which are eigenfunctions of the vector Helmholtz equation. The qualifiers Re and Ou denote functions which are regular at the origin and outgoing at infinity which are, respectively, appropriate for

expanding the field which is incident on a scatterer and that which it scatters which in turn must satisfy outgoing or radiation conditions. Thus, we can write the following set of self-consistent equations:

$$u = u^0 + \sum_{i=1} u^s_i = u^c_i + u^s_i = u^0 + \sum_{j\neq i} u^s_j + u^s_i \tag{1}$$

$$u^0(r) = p \exp(ikk_0 \cdot r) = \sum_n a_n{}^i \ \mathrm{Re}\ \phi_n(r - r_i) \tag{2}$$

$$u^c_i = \sum_n \alpha_n{}^i \ \mathrm{Re}\ \phi_n(r - r_i);\ a < |r - r_i| < 2a \tag{3}$$

$$u^s_i = \sum_n f_n{}^i \ \mathrm{Ou}\ \phi_n(r - r_i); \qquad |r - r_i| > a \tag{4}$$

where $\alpha_n{}^i$ and $f_n{}^i$ are unknown expansion coefficients. We observe in Eqs.(3) and (4) that a is the radius of the sphere circumscribing the scatterer and that all expansions are with respect to a coordinate origin located in a particular scatterer.

The T-matrix by definition [5] simply relates the expansion coefficients of u^c_i and u^s_i provided $u^c_i + u^s_i$ is the total field which is consistent with the definitions in Eq. (1). Thus,

$$f_n{}^i = \sum_{n'} \langle\langle T_{nn'} \rangle\rangle \ \alpha_{n'}{}^i \tag{5}$$

where $\langle\langle T_{nn'} \rangle\rangle$ is the T matrix averaged over all possible orientations of the scatterer if the scatterer is nonspherical and all scatterers are randomly oriented. Otherwise the regular T matrix is used. If the addition theorem for the basis functions is invoked, we have

$$\mathrm{Ou}\ \phi_n(r - r_j) = \sum_{n'} \sigma_{nn'}(r_i - r_j)\, \mathrm{Re}\phi_{n'}(r - r_i) \tag{6}$$

Substituting Eqs. (2) - (6) in Eq. (1), and using the orthogonality of the basis functions we obtain

$$\alpha^i = a^i + \sum_{j\neq i} \langle\langle T^j \rangle\rangle\ \sigma(r_i - r_j)\ \alpha^j \tag{7}$$

This is a set of coupled algebraic equations for the exciting field coefficients which can be iterated and leads to a multiple scattering series.

For randomly distributed scatterers, an ensemble average can be performed on Eq. (7) leading to

$$\langle \alpha^i \rangle_i = a^i + \langle \sigma\ (r_i - r_j) \langle\langle T^j \rangle\rangle \langle \alpha^j \rangle_{ij} \rangle_i \tag{8}$$

where angle brackets and ijk... denotes a conditional average and Eq.(8) when iterated is an infinite hierarchy involving higher and higher conditional expectations of the exciting field coefficients. In actual engineering applications, a knowledge of higher order correlation functions is difficult to obtain, and usually the hierarchy is truncated so that at most only the two body positional correlation function is required.

To achieve this simplification the quasi-crystalline approximation (QCA), first introduced by Lax [8] is invoked, which is stated as

$$\langle \alpha^j \rangle_{ij} = \langle \alpha^j \rangle_j \tag{9}$$

Then, Eq.(8) simplifies to

$$\langle \alpha^i \rangle_i = a^i + \langle \sigma(r_i - r_j) \langle\langle T^j \rangle\rangle \langle \alpha^j \rangle \rangle_i \tag{10}$$

an integral equation for $\langle \alpha^i \rangle_i$ which in principle can be solved. We observe that the ensemble average in Eq.(10) only requires $P(r_j|r_i)$, the joint probability distribution function. In particular, the homogeneous solution of Eq.(10) leads to a dispersion equation for the effective medium in the quasi-crystalline approximation. Defining the spatial Fourier transform of $\langle \alpha^i \rangle_i$ as

$$\langle \alpha^i \rangle_i = \int e^{iK \cdot r_i} X^i(K)\, dK \tag{11}$$

and substituting in (10), we obtain for the homogeneous solution

$$X^i(K) = \Sigma_{j \neq i} \int \sigma(r_i - r_j) \langle\langle T^j \rangle\rangle\, p(r_j|r_i) \times e^{iK \cdot (r_i - r_j)}\, dr_j\, X^j(K) \tag{12}$$

If the scatterers are identical, then

$$X^i(K) = X^j(K) = X(K) \tag{13}$$

and for a nontrivial solution to $\langle \alpha^i \rangle_i$, we require

$$\left| I - \sum \int \sigma(r_i - r_j) \langle\langle T^j \rangle\rangle p(r_j|r_i)\, e^{iK \cdot (r_i - r_j)}\, dr_j \right| = 0 \tag{14}$$

In Eqs. (12) and (14), $P(r_j|r_i)$ is the joint probability distribution function. For isotropic or spherical statistics,

$$P(r_j|r_i) = \begin{cases} 0; & |r_i - r_j| < 2a \\ g(|r_i - r_j|)/V; & |r_i - r_j| > 2a \end{cases} \tag{15}$$

where we have assumed that the scatterers are impenetrable with a minimum separation between the centers, and in Eq.(15), 2a could be the diameter of the circumscribing sphere or of a sphere of equal volume. We observe that in Eq.(15), the joint probability distribution depends only on the interparticle distance and not on the orientation of the vector joining the centers and the function $g(|r_i - r_j|)$ is called the radial distribution function.

If the concentration of nonspherical particles is not small, then it is incorrect or at best approximate to assume that isotropic statistics are valid. In this case we assume that the radial distribution function depends not just on the magnitude of the vector joining the centers of two spheroids but also on the orientation of this vector. For aligned spheroids which are rotationally symmetric, the dependence is only on the angle θ between the separation vector and the

symmetry axis which is taken to be the z axis of the coordinate system, as shown in Figure 1. There is no dependence on the azimuthal angle ϕ. The joint probability distribution function is then written as

$$P(r_j|r_i) = \begin{cases} 0; & |r_i - r_j| < R(\theta) \\ G(r, \theta)/V; & |r_i - r_j| > R(\theta) \end{cases} \tag{16}$$

In the above equation, $G(r, \theta)$ is the pair correlation function for aligned spheroidal scatterers, and $R(\theta)$ is the minimum center to center distance when the spheroids just touch one another at one point, such that the line joining their centers subtends an angle θ with the symmetry or z-axis of the spheroids. In this case the statistics are not isotropic but are a function of direction.

For randomly oriented nonspherical scatterers, the joint probability distribution function becomes dependent on the variables describing the mutual orientation, in addition to the interparticle separation distance.

$$P(r_j|r_i) = \begin{cases} 0; & |r_i - r_j| < R(\theta_i, \theta_j, \phi_{ij}) \\ G(r_{ij}, \theta_i, \theta_j, \phi_{ij})/V; & |r_i - r_j| > R(\theta_i, \theta_j, \phi_{ij}) \end{cases} \tag{17}$$

In the above equation, $G(\,)$ is the pair correlation function for randomly oriented spheroidal scatterers, and $R(\,)$ is the minimum center to center distance when the spheroids just touch one another at one point. Here θ_i and θ_j are the angles made by the axial vector with the interparticle vector r_{ij} and ϕ_{ij} is the angle between the projections of the axial vectors onto the plane perpendicular to r_{12}.

Equation (14) is a determinantal equation, the roots of which can be solved for numerically to yield the values of the effective wave number $K = K_1 + iK_2$ as a function of the frequency via $k = \omega/c$, the shape, size and orientation of the scatterer via the T-matrix, and the statistics of the distribution via the joint probability distribution function. The effective wavenumber which describes wave propagation characteristics in the random composite medium also gives information of the effective properties.

In microwave sintering of ceramics, we are interested in the imaginary part of the dielectric constant ε'' ($\varepsilon = \varepsilon' + j\varepsilon''$) of ceramics which will be later used in the heat equation. The relation between K and ε is through the following equation for a nonmagnetic material

$$\varepsilon/\varepsilon_o = K^2/k_o^2 \tag{18}$$

in which ε_o and k_o are the permittivity and wavenumber of free space, respectively.

GRAIN- AND PORE- SIZES

Before sintering, the porous ceramic samples have definite grain as well as pore sizes which remain constant (or the change of size can be neglected) even after the start of sintering as long as the temperature runaway has not been triggered. A critical concentration c_{cr} which depends exclusively on the runaway temperature determines the start of the growth of grain and pore sizes. By microwave sintering, beyond the critical concentration, the green samples begin to densify much more effectively than by mechanical compaction or by conventional oven heating.

The size of grain particles, after the critical concentration, can be assumed to be a function of concentration and has the following form

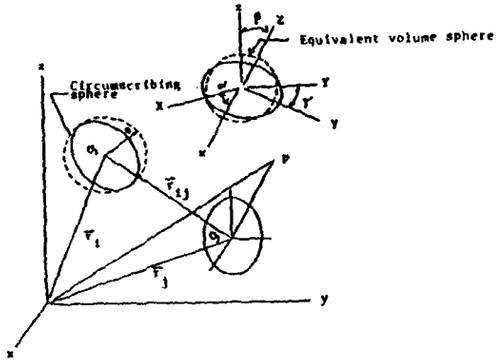

Figure 1. Geometry of the scattering problem.

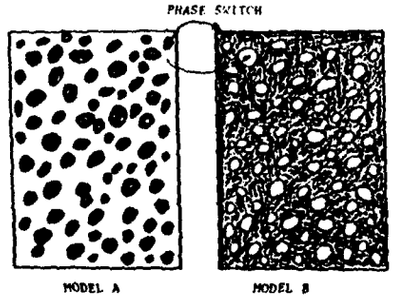

Figure 2. Schematic of two models considered in microwave sintering.

$$a = a_i (\varepsilon_r)(c - c_{cr})\,\alpha / (c_f - c_{cr}) \tag{19}$$

where $\alpha = \ln(\varepsilon_r) / (\ln a_f - \ln a_i)$, ε_r is the permittivity ratio between the grain and the pore. The parameters a_f and a_i are the sizes of particles after and before sintering, respectively. The final sintering concentration c_f is, in general, in the range of 0.95 to 0.98 or even higher which means the toal volume fraction occupied by the pores in the sintered ceramics has been reduced to about less than 2 to 5 percent of the total volume.

Although the purpose of sintering is to reduce the concentration of pores in ceramics, the pore sizes according to SEM increase with the decreasing concentration of pores. Therefore, we assume the pore size during sintering process is also a function of concentration and can be written as

$$b = b_i (\varepsilon_r)(c - c_{cr})\,\beta / (c_f - c_{cr}) \tag{20}$$

where $\beta = \ln(\varepsilon_r) / (\ln b_f - \ln b_i)$, b_f and b_i are the sizes of pores after and before sintering, respectively. In order to avoid confusion, c again is the concentration of grains as in Eq.(20) and the corresponding concentration of pores is simply 1- c. In sintering alumina, the grain grows from about one micron to about fifty microns. Meanwhile, the pore size is increased from about 0.05 micron to about one micron. This is simply a general description of the average sizes of grains and pores during sintering processes and we are not ambitious in putting detailed but complicated expressions, which may turn out to be totally empirical, in this preliminary model.

In order to predict the concentration threshold, a linear relationship between the grain size and the concentration is assumed to be

$$a = a_i + (c_f - c_i)\,\gamma \tag{21}$$

where $\gamma = (a_f - a_i) / (c_f - c_i)$. The concentration threshold is able to be predicted by finding the maximum attenuation through solving the dispersion equation.

Two models can be used for sintering ceramics and the choice of the continuous and discrete phases in the modeling becomes uncritical after reaching the concentration threshold. To explain this, we calculated the effective wavenumber K by solving the dispersion equation and used it to compute the imaginary part of the dielectric constant ε'' through Eq. (18). The magnitude of ε'' then was normalized to the frequency so that the results were irrespective with any specific microwave frequency. We were able to do this because both sizes of grains and pores were very small compared to the microwave wavelength. Besides, the details of the grain and pore geometry were not very sensitive at these frequencies so that we assumed them to be spherical in shape.

Figure 2 depicts the models considered in the calculations. Model A used air as the matrix material and the grains were dispersed in it while model B took the matrix having the properties of grains and the discrete phases were the randomly distributed pores. We selected three permittivity (dielectric constant) ratios between the scatterer and the matrix materials in order to show the material effects on microwave sintering. The ratio 9.5 happened to be that of alumina. In all the calculations, the imaginary part of the dielectric constant ε'' which determined the frequency dependent loss tangent of the samples to be sintered dramatically increased, after the concentration threshold, with the increasing (decreasing) volume fraction (concentration) of grains (pores). In other words, as mentioned in the previous section, the increasing sintering temperature followed by an increasing sample density and a reducing concentration of pores through the increasing ε''. The large ε'' not only made the heat distribution inside the sample more even but also enhanced the sample absorbing capability. This explained the effectiveness of microwave sintering.

Figures 4, 5, and 6 are numerical results of the normalized ε'' against the concentration of either the grains or the pores. In order to use Eqs. (19) and (20) which required critical

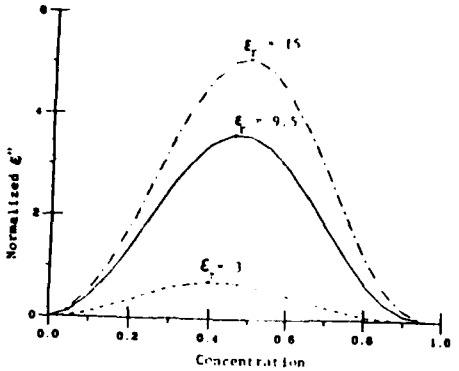

Figure 3. Critical concentrations for different materials to be sintered.

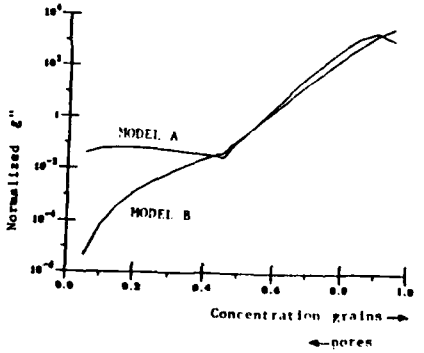

Figure 4. Normalized ε'' vs. Concentration for ε_r = 9.5.

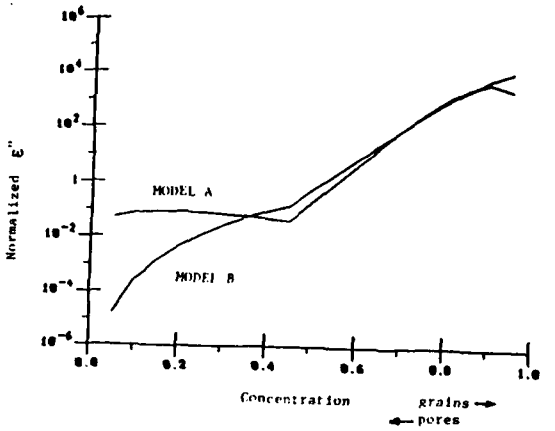

Figure 5. Normalized ε'' vs. concentration for ε_r = 15.

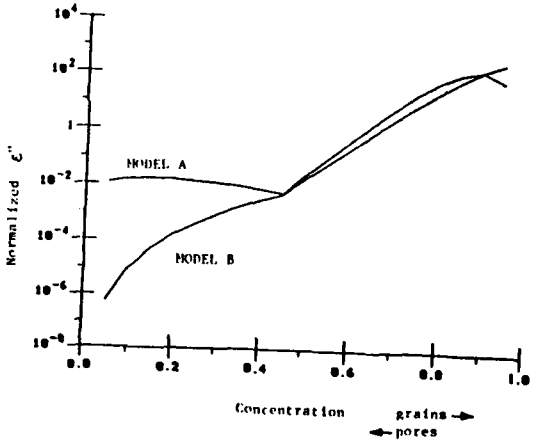

Figure 6. Normalized ε'' vs. concentration for ε_r = 3.

concentrations, we first used Eq. (21) to predict the concentration threshold for three different materials characterized by three different ε_r. As can be seen from Figure 3, the concentration threshold depended on the material properties which have also been observed in the experiments. The concentration threshold happened at the maximum ε'' in Figure 3. The appropriate choice of the discrete and continuous phases seemed to be important when the concentration was below its critical value but not for its beyond. One reason for this was the continuous phase switch through the interpenetration among grain particles during the sintering process which in turn indiscriminated between models A and B. However, this involved the size varying during the change of concentration which has not been considered in the earlier multiple scattering formalism.

CHAOS IN THE HEAT-DIFFUSION EQUATION

Once the profile of ε'' as a function of temperature and other parameters has been obtained through multiple scattering studies, it may be possible to study the thermal runaway conditions through the source-incorporated heat-diffusion equation. The diffusion of thermal energy in a homogeneous bounded volume V is determined by the partial differential equation

$$\rho \quad C_p \, \partial T/\partial t - K_h \, \nabla^2 T = F(r,t,T), \tag{22}$$

in which ρ is the mass density, C_p is the specific heat capacity, K_h is the thermal conductivity, F is a source term, and $T(r,t)$ is the temperature at a point r at time t. On the boundary S of the volume V, the boundary condition

$$K_h \; e_n \cdot \nabla T = H \, (T - T_O) \tag{23}$$

must hold, in which H is the convection heat coefficient, e_n is the unit inward normal to S, and T_O is the ambient temperature. The initial condition is, obviously,

$$T(r,0) = T_O. \tag{24}$$

it being assumed that the change in the temperature of the surroundings is negligibly small.

Pertinent to the problem of the microwave heating of the volume V, it can be safely stated that the long-wavelength condition may hold. In that case, if the microwave source creates a power density P in the space occupied by the sample were the sample to be absent, and if $\varepsilon''(\omega,T)$ is the imaginary part of the dielectric constant at the frequency ω and temperature T, the source term in Eq. (22) can be expressed as

$$F(r,t,T) = \varepsilon''(\omega,T) \, P/\varepsilon_O. \tag{25}$$

implicit in which is the fact that the temperature is a function of both r and t.

With the incorporation of Eq. (25) in Eq. (22), it can be seen that Eq. (22) is analogous to the forced Fisher equation

$$T_t = T_{XX} + G(T), \tag{26}$$

which is known to exhibit chaotic behavior for specific initial and boundary conditions [9,10].

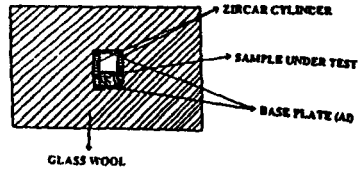

Figure 7. Schematic of the setup used for the microwave sintering of strontium titanate and α- alumina.

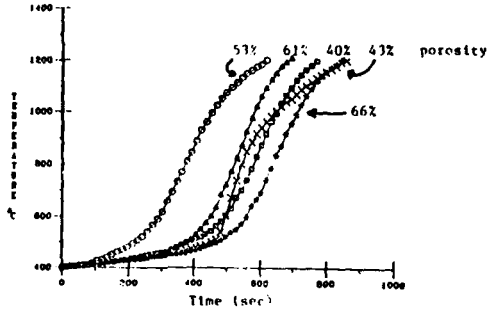

Figure 8. Temperature-time curves for strontium titanate samples with different initial porosities.

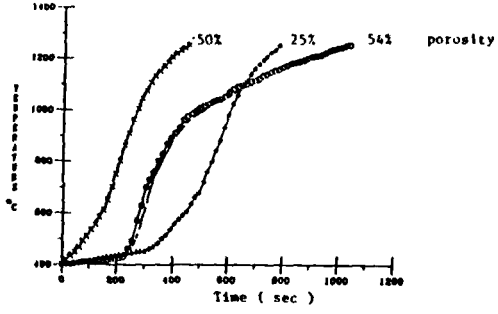

Figure 9. Temperature-time curves for α-alumina samples with different initial porosities.

MICROWAVE SINTERING OF $SrTiO_3$ AND Al_2O_3

$SrTiO_3$

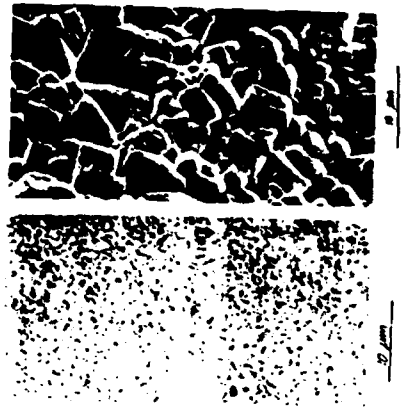

microwave sintering

density = 98% at 1300 °C

heating rate = 3 °C/sec.

conventional sintering

density = 80% at 1300 °C

heating rate = 0.08 °C/sec

Al_2O_3

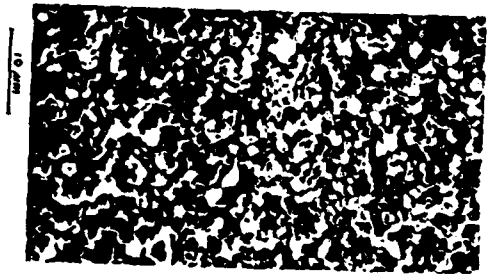

density = 95 % at 1500 °C

Figure 10. SEM micrographs of sintered strontium titanate and α-alumina samples.

Additional work on the chaotic response of the two-dimensional form is available in the work of Bruch and his colleagues [11,12]. Although further work is necessary, knowing that $\varepsilon''(\omega,T)$ is an increasing function of T for sinterable ceramics, it is conjectures that the chaos inherent in Eq. (22) gives rise to the temperature runaway conditions observed by Roussy et al [13] during the microwave irradiation of EPDM rubber.

TEMPERATURE RUNAWAY DURING MICROWAVE SINTERING

The phenomenon of temperature runaway during microwave sintering of ceramics was also experimentally investigated. For this purpose, strontium titanate and α-alumina samples were irradiated inside a microwave oven at 2450 MHz frequency. The schematic of the experimental set up is shown in Figure 7, and full details of the experimental setup will be reported shortly.

Consider Figures 8 and 9, respectively, for strontium titanate and α-alumina. Equivoluminal samples of both materials were made with different (initial) porosities. Shown in these figures are the sample temperatures versus time during the microwave irradiation process. It is quite clear from Fig. 8 that the temperature runaway is most pronounced in the strontium titanate sample of initial porosity 43%. Likewise, from Fig. 9 it is also observed that the temperature runaway is most pronounced in the α-alumina sample of initial porosity 54%. These two figures, along with the aforementioned observations suggest the criticality of percolation studies in the area of microwave sintering.

Shown in Fig. 10 are SEM micrographs of sintered strontium titanate and α-alumina samples. The low grain growth in the microwave-sintered samples is noteworthy. In particular, consider the strontium titanate samples shown in this figure: microwave heating gave an average temperature increase of 3 °C/s with 98% density at the the final temperature of 1300 °C, while conventional sintering gave an average heating rate of only 0.08 °C/s with only 80% density at the same final temperature.

We conclude here by saying that, although much needs to be done regarding the generation of acceptable theoretical models, the future of microwave sintering is extremely promising.

Acknowledgements: Microwave sintering experiments were performed by graduate student Fathi Selmi as part of his doctoral studies. A more detailed account will be published elsewhere. This work was supported by the industrial sponsors of the Center for the Engineering of Electronic and Acoustic Materials at Penn State.

REFERENCES

1. Tinga, W.R. and W.A.G. Voss, in *Microwave Power Engineering*, Academic Press, New York (1968).
2. Borom, M.P. and M. Lee, *Adv. Ceram. Mater.* 1, 335 (1986).
3. Meek, T.T., *J. Mater. Sci.* 6, 638 (1984).
4. See other papers in this volume.
5. Varadan, V.K. and V.V. Varadan (Eds.) *Acoustic, Electromagnetic and Elastic Wave Scattering: Focus on the T-Matrix Approach*, Pergamon, New York (1980).
6. Varadan, V.K., V.N. Bringi and V.V. Varadan, *Phys. Rev. D* 19, 2480 (1979).
7. Varadan, V.K., V.N. Bringi, V.V. Varadan and A. Ishimaru, *Radio Sci.* 18, 321 (1983).
8. Lax, M., *Phys. Rev.* 85, 621 (1952).
9. Fisher, R.A., *Ann. Eugenics* 7, 355 (1937).
10. Rothe, F., *Rocky Mt. J. Math.* 11, 617 (1981).
11. Mitchell, A.R. and J.C. Bruch, Jr., *Num. Methods P.D.E.* 1, 13 (1985).
12. Wachholz, J.J. and J.C. Bruch, Jr., *Num. Methods P.D.E.* 3, 139 (1987).
13. Roussy, G., A. Mercier, J.-M. Thiebaut and J.-P. Vaubourg, *J. Microwave Power* 20, 47 (1985).

PRINCIPLES OF MICROWAVE INTERACTION WITH POLYMERIC AND ORGANIC MATERIALS

VIJAY K. VARADAN, VASUNDARA V. VARADAN AND AKHLESH LAKHTAKIA

Department of Engineering Science & Mechanics, and The Center for Engineering of Electronic and Acoustic Materials,
Pennsylvania State University, University Park, PA 16802.

ABSTRACT

Electromagnetic waves can discriminate between objects of different handedness due to their transverse nature, which implies that the origin of chirality need not necessarily be molecular as in the case of optically active media. Effectively chiral composites may, therefore, be constructed by embedding chiral microstructures in non-chiral host media.

INTRODUCTION

Many organic molecules occur as stereoisomers in enantiomorphic pairs, i.e., one isomer is the mirror image of the other one, but the two of them are not congruent with each other. The basis for the difference in the physical properties of the mirror-conjugates lies in the handedness or the chirality possessed by their molecular configurations. When an electromagnetic disturbance travels through a medium consisting of chiral molecules, it is forced to adapt to the handedness of the molecules. Electromagnetic (EM) waves can recognize the handedness of a chiral object primarily due to their transverse nature, i.e., the applicable vector, infinite-medium Green's function contains the *vector* distance between the source and the field points. From a microscopic, not molecular, point of view, therefore, it is possible that an effectively chiral composite medium may be constructed by embedding macroscopic chiral objects, all of the same handedness, in a dielectric host. The microstructure size should be large enough that the EM wave in the matrix can appreciate the handedness of the microstructure; at the same time, the microstructure size should be small enough so that the composite medium, consisting of achiral phases, is effectively chiral. By varying the concentrations and the sizes of the chiral inclusions, the properties of the composite medium may be altered to suit desired polarization characteristics. It has been observed by us that the introduction of chirality in an otherwise achiral, dielectric scattering volume radically alters its scattering and absorption characteristics [1]. Particularly with the proliferation of research on novel polymers, it is possible that such materials can turn out to be of considerable importance for many electromagnetic applications It has been demonstrated [2,3] that it is possible to produce polymers which possess no true axisymmetric centers, and helical strands -- either left- or right-handed -- can be produced.

WHAT IS CHIRALITY?

In order to understand the characteristics of chiral media, one has to begin with the notions of the intrinsic polarization and the intrinsic magnetization vectors. Free space is vacuum, i.e., it does not contain any matter. The constitutive relations for the electromagnetic fields in free space can be adequately expressed in the form

$$\mathbf{D} = \epsilon_0 \mathbf{E}; \qquad \mathbf{B} = \mu_0 \mathbf{H}. \tag{1}$$

Fields in material media induce bound charges too. Collectively, the constitutive equations in material media have the form

Mat. Res. Soc. Symp. Proc. Vol. 124. © 1988 Materials Research Society

$$\mathbf{D} = \varepsilon_0\mathbf{E} + \mathbf{P}; \qquad \mathbf{B} = \mu_0\mathbf{H} + \mathbf{M}, \tag{2}$$

in which **P** and **M**, respectively, are the polarization and the magnetization. The polarization **P** is nothing but the average electric dipole moment per unit volume, while **M** is the average magnetic dipole moment per unit volume.

In non-magnetic dielectric media, a prominent contribution to **P** comes from the charge separation in the atom, and is designated as *electronic* polarization. This is because an applied electric field causes displacement of the electrons with respect to the atomic nucleus. *Atomic* or *ionic* polarization may be caused by the displacement of atoms or ions in a molecule by electric fields. Some media may also have permanent electric dipole moments because the centers of the negative and the positive charges are not co-incident. Without an applied electric field, these permanent dipoles are randomly aligned, and their effect is nulled on the average; however, when an electric field is applied, then these dipole moments line up to give rise to *orientational* polarization. In linear media, these various contributions can be summed up as

$$\mathbf{P} = \chi_e\varepsilon_0\mathbf{E}; \qquad \mathbf{D} = \varepsilon_0[1+\chi_e]\mathbf{E} = \varepsilon\mathbf{E} \tag{3}$$

χ_e being the electric susceptibility, and ε the (real) dielectric constant.

Each of the three types of polarizations are frequency-dependent; however, as the frequency increases the polarization may not be able to follow the oscillations of the applied field. Orientational polarization concerns itself with the most massive entities; hence, it is the first to be unable to reach its equilibrium value. The loss of orientational polarization occurs at lower frequencies for macromolecules and large-chain polymers, and it occurs at higher frequencies for small molecules. As the frequency increases even further, first the atomic, and then the electronic, polarizations also fall off. Typically, the times for orientational, atomic, and electronic polarizations to reach their equilibrium values are 10^{-9} s, 10^{-13} s and 10^{-15} s, respectively. Highly elongated and aligned molecules tend to give rise to anisotropic properties.

Electronic polarizability is due to the bound electrons. Therefore, it increases when the atomic radius also increases. This implies that polymers with delocalized electrons will have larger electronic polarizations; for example, conducting polymers with electron-withdrawing groups. On the other hand, polymers possessing highly asymmetric positive and negative charge densities will have large orientational polarizabilities. Too some extent, these considerations permit one to tailor the frequency-dependent dielectric constants of polymers.

Under the influence of the externally applied field, the polar molecules rotate towards an equilibrium distribution. If the polar molecules are massive, or if the frequency is very high, the rotatory motion lags behind the applied field and equilibrium is never attained. Thus, the polarization is no longer in sync with the applied field, giving rise to a conduction current density. This results in thermal dissipation of energy. Thus, ohmic losses in dielectric media give rise to a conductivity σ, which is incorporated in the time-harmonic constitutive equations by making ε complex, i.e.

$$\mathbf{D} = \varepsilon\mathbf{E}, \qquad \varepsilon = \varepsilon_0[1+\chi_e] + \sigma/\omega, \tag{4}$$

$\omega = 2\pi f$ being the circular frequency. It would also follow that conduction losses increase with temperature, since the conduction charges have enhance mobilities at higher temperatures. Furthermore, more massive molecules are less able to follow the applied field, which means that the ratio $\tan\delta_\varepsilon = \mathrm{Im}\{\varepsilon\}/\mathrm{Re}\{\varepsilon\}$ is generally higher for such substances. Unsaturated polymers will also have higher $\tan\delta_\varepsilon$ because of the increased availability of electrons for conduction. It should also be noted that while charge transport in metals takes place via electrons only, charge transport in polymers may even involve ions.

There are microscopic currents due to electron spin and the motion of electrons around the nucleus. These microscopic currents act as sources of macroscopic magnetic fields, thereby endowing the electrons and the atoms with magnetic dipole moments; but these currents do not produce macroscopic charge transport. In magnetic media, the effect of the magnetic dipole moments cannot be ignored, giving rise to the magnetization **M**. Again, for linear media, it can be stated that

$$\mathbf{M} = \chi_m\mu_0\mathbf{H}; \qquad \mathbf{B} = \mu_0[1+\chi_m]\mathbf{H} = \mu\mathbf{H} \tag{5}$$

χ_m being the magnetic susceptibility, and μ the (real) permeability. Magnetic ohmic losses can be incorporated by making μ complex in the same fashion as the electric ohmic losses.

Chirality was first observed as optical activity, which is the rotation of the plane of polarization in certain linear isotropic media. Pasteur interpreted the observations of Biot and Arago by imagining that the arrangement of atoms within an optically active material is mirror-asymmetric [4]. Phenomenological studies by Drude [5] indicated that the rotation of the plane of polarization is predicted by Maxwell's equations provide **P** has an additional term proportional to $\nabla\times\mathbf{E}$. Further studies [6,7] have shown that even **M** must have a term proportional to $\nabla\times\mathbf{H}$. Thus, the constitutive equations for homogeneous chiral media have the form

$$\mathbf{D} = \varepsilon[\mathbf{E} + \beta\nabla\times\mathbf{E}]; \qquad \mathbf{B} = \mu[\mathbf{H} + \alpha\nabla\times\mathbf{H}], \tag{6}$$

in which α and β are the chirality parameters. Since the curl is a pseudo-vector under a reflection of the coordinate system, the mirror-asymmetry of chiral media is immediately apparent in (6). The nonlocal character of (6) needs to be noticed, because the polarization **P** (resp. magnetization **M**) depends not only on **E** (resp. **H**) but also on the *circulation* of **E** (resp. **H**). In a not-too-rigorous manner, one may even observe that **P** (resp. **M**) has a component due to the time-rate of change of **H** (resp. **E**), *vide* Faraday and Ampere-Maxwell laws. Reciprocity demands that $\alpha = \beta$, a constraint which is generally obeyed by optically active media [8].

Thus, optically active media (mostly organic materials) are naturally chiral, at optical frequencies; interesting examples include the famous Watson-Crick double-helix representation of the DNA molecule. But the underlying principle behind chirality is the mirror-asymmetry of the constituent microstructure. Therefore, artificially chiral media can be constructed by embedding chiral microstructures in non-chiral host media, such composites being effectively chiral even at the sub-optical, and even in the high mm-wave, frequencies. The microstructure size should be large enough compared to the wavelength in the matrix medium so that the spatial variation of the EM field can sense its handedness; at the same time, it should be small enough so that, at least in some frequency range, the composite should appear to be effectively chiral.

In a non-chiral medium, the simplest EM waves that can propagate are linearly-polarized plane waves. But in chiral media the simplest waves are either left-circularly polarized, or they are right-circularly polarized, plane waves; it is important to note that the left- and the right-handed waves travel with different phase velocities [7]. Furthermore, when a linearly polarized wave hits a chiral scatterer embedded in a non-chiral medium, the scattered field has both LCP and RCP components. Now, let us envision the propagation of a plane wave in an artificial chiral medium which contains a certain density of chiral inclusions in a host phase. Multiple scattering [9] between the chiral inclusions will create LCP and RCP fields. In the right frequency range only LCP or RCP fields will be allowed to propagate in the forward direction, thereby rendering the composite effectively chiral.

ANTI-REFLECTION COATINGS

There is considerable interest in developing low-weight coatings which will reduce reflections from metallic surfaces. In view of our previous studies [1], it appeared that artificial chiral media may be just the thing to fill the bill. To further investigate this premise, we considered the planewave reflection characteristics of a chiral coating, of thickness d, on top of a perfectly conducting plane. The chiral layer has a permittivity ε, a permeability $\mu = \mu_0$, as well

the chirality parameter β, *vide* the constitutive relations [7]

$$\mathbf{D} = \varepsilon[\mathbf{E} + \beta\nabla\times\mathbf{E}]; \qquad \mathbf{B} = \mu_0[\mathbf{H} + \beta\nabla\times\mathbf{H}]. \tag{7}$$

The chiral dielectric medium is low-loss so that its relative permittivity $\varepsilon/\varepsilon_0$ is complex with $Im\{\varepsilon/\varepsilon_0\} << Re\{\varepsilon/\varepsilon_0\}$. The thickness d of the coating was assumed to be 2 mm for all of our numerical studies, and the reflection coefficients, R_{TE} and R_{TM} [10], were computed, respectively, for TE- and TM- polarized planewave incidence cases.

A design of a wideband anti-reflection chiral coating cannot afford to have both $\varepsilon/\varepsilon_0$ and β independent of frequency. Once it became clear from numerical experimentation that (i) chirality is ineffective in the reduction of the reflection efficiency if $\varepsilon/\varepsilon_0$ is purely real, and (ii) that either β or $\varepsilon/\varepsilon_0$ or both must be frequency dependent in order to obtain a wideband anti-reflection coating, the design of such a coating became more of an optimization problem. Shown in Figs. 1 - 3 is a sample design with $\varepsilon/\varepsilon_0$ assumed to be constant, whereas $\beta = \beta(f)$ assumed is shown in Fig. 1. In Figs. 2 and 3, the enhancement of the absorption efficiency of over a 50-300 GHz frequency range by incorporating this frequency dependent $\beta = \beta(f)$ is illustrated, for the TE- and TM- polarization incidence cases, respectively; θ_0 is the angle of incidence with respect to the normal. The relative permittivity $\varepsilon/\varepsilon_0$ is set at 5.0 + i0.05 for all frequencies considered. It should be noted from these two figures that whereas the design objective of achieving R_{TE} and R_{TM} less than 20% (or $50 \le f \le 300$ GHz and $0° \le \theta_0 \le 30°$ can be achieved using the β of Fig. 1, the reflection efficiencies hover around 92% if β were to be set equal to zero.

From our numerical studies, several conclusions can be drawn. Firstly, in reducing reflection if a larger constant β is used, then the values of $\varepsilon/\varepsilon_0$ tend to decrease over the entire frequency band of interest, a goal which appears to be desirable for a material scientist. However, this also tends to reduce the bandwidth over which the desired absorption efficiencies can be achieved. Secondly, chirality in the absence of a lossy ε is of no use whatsoever in reducing reflected power density: conducting polymers constitute feasible matrix media. Therefore, chirality serves only as an enhancement factor for absorption, but of itself it is not an absorbing mechanism. Thirdly, and very importantly, both $\varepsilon/\varepsilon_0$ and β should be frequency dependent. This last conclusion, however, was not verified here because of the complexities of multivariate optimization problems.

EQUIVALENT DIPOLE MOMENTS OF HELICAL ENSEMBLES

Thus, the significance of chiral media cannot be denied. As has been mentioned earlier, effectively chiral media can be constructed by embedding chiral microstructures in non-chiral host media. Such microstructures may be macromolecular polymers with helical conformations [2,3,11]. What is of interest for EM use is the optimization of the polymer's chirality: the parameters governing the helix geometry must be examined for their effect on an incident EM wave. We decided to model helical polymers by an arrangement of spherical beads (in themselves, large molecules for our purposes) suspended on a helical strand which is indistinguishable from the surrounding space. Whereas the spheres are also sufficiently small to be modeled as point electric dipoles, the overall size of the finite helical arrangement can be large enough to be in the high-frequency regime. The helix on which the tiny spheres are located is given, in a cartesian co-ordinate system, by the radius vector

$$\mathbf{r}(\xi) = a[\mathbf{u}_x \cos\xi + \mathbf{u}_y\, h \sin\xi] + \mathbf{u}_z\, P(\xi/2\pi); \quad \xi \in \{-\infty, \infty\}, \tag{8}$$

where a is the radius and P is the pitch of the helix; the handedness parameter h = +1 if the helix curls up in the +z direction according to the right-handed rule, and h = -1, if otherwise; and $\mathbf{u}_x$, $\mathbf{u}_y$, and $\mathbf{u}_z$ are the unit orthogonal vectors. Let the helix be finite in extent, having 2N+1 complete rotations, N being a positive integer or zero. On each of the 2N+1 rings of this finite helix, there are 2M+1 spheres arranged over equal-$\Delta\xi$ segments, M being a positive integer greater than zero. Each of the spheres in this arrangement has a radius b which is small enough

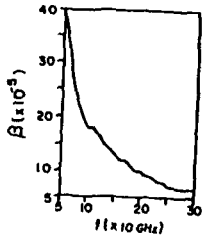

Figure 1 The frequency profile $\beta = \beta(f)$ used for the results shown in Figs. 2 and 3. The parameter β carries the unit of meter.

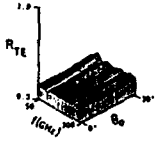

Figure 2 Reflection efficiency R_{TE} plotted as a function of θ_0 and frequency f for a 2 mm thick anti-reflection coating. The complex permittivity $\varepsilon/\varepsilon_0 = 5.0 + i0.05$. In the upper figure the $\beta = \beta(f)$ of Fig. 1 is used while in the lower figure β is set equal to 0.0 m.

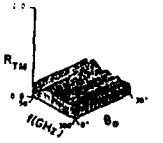

Figure 3 Same as Fig. 2, but R_{TM} is plotted.

that no two of them ever touch. The spheres possess a dielectric constant ε, and if a field $\boldsymbol{E}_m$ illuminates the m^{th} sphere, an electric dipole moment [12]

$$\mathbf{p}_m = \alpha\, \boldsymbol{E}_m = 4\pi\varepsilon_o b^3 (\varepsilon - \varepsilon_o)(\varepsilon + 2\varepsilon_o)^{-1}\ \boldsymbol{E}_m \qquad (9)$$

is induced on it, with α being the isotropic electric polarizability of the spheres.

The EM field incident on the helical ensemble, E_{inc}, can be any arbitrary field so long as its source is not located anywhere inside or on the minimum sphere circumscribing the helix. But the field $\boldsymbol{E}_m$ actually incident on the m^{th} sphere is not $E_{inc}(r_m)$ alone; it also consists of the fields re-radiated by all of the other spheres as well [9,13]. With this reasoning, the system of 3Q simultaneous equations,

$$\boldsymbol{E}_m = E_{inc}(r_m) + \alpha k^2 (4\pi\varepsilon_o)^{-1} \sum_{n,n\neq m} \{R_{mn}^{-1} \exp[jkR_{mn}] \cdot \cdot\{g_{mn}\mathbf{n}_{mn}(\mathbf{n}_{mn}\cdot\boldsymbol{E}_n) - (1/3)(g_{mn} - 2j)\,\boldsymbol{E}_n\}\}, \qquad (10)$$

must be solved, in order to obtain the various exciting fields $\boldsymbol{E}_m$. Here, $R_{mn} = |r_m - r_n|$, $\mathbf{n}_{mn} = (r_m - r_n)/R_{mn}$, $g_{mn} = 3(kR_{mn})^{-2} - 3j(kR_{mn})^{-1} - 1$, while the wavenumber $k = \omega\sqrt{(\varepsilon_o\mu_o)}$. Once the solution of (10) has been obtained, the total scattered field for $kr \to \infty$ can be computed from

$$4\pi\varepsilon_o E_{sc}(r) = \alpha\, k^2 r^{-1} \exp[jkr] \sum_m \{\exp[-jkr_m\cdot r/r]\,[\boldsymbol{E}_m - r(r\cdot\boldsymbol{E}_m)/r^2]\}. \qquad (11)$$

Multiple scattering between the spheres would ensure that $\boldsymbol{E}_m \neq E_{inc}(r_m)$. It is to be expected that the exciting fields should reflect the chirality of the helical ensemble, because the ensemble of unit vectors $\{\mathbf{n}_{mn}\}$ used in (10) is handed, even though the scalar distances $\{R_{mn}\}$ do not depend on h. This, indeed turned out to be the case. From our computations a very interesting conclusion can be drawn: Provided $\mathbf{k}_{inc} \parallel \mathbf{u}_x$ or $\mathbf{k}_{inc} \parallel \mathbf{u}_y$, then (i) only $\mathbf{u}_y\cdot\boldsymbol{E}_m$ changes sign with h when $\mathbf{u}_y\cdot\mathbf{E}_{inc} = 0$, and (ii) only $\mathbf{u}_y\times\boldsymbol{E}_m$ changes sign with h when $\mathbf{u}_y\times\mathbf{E}_{inc} = 0$. Symmetries of similar natures are also present when $\mathbf{k}_{inc} \parallel \mathbf{u}_y$, but they are not so easily describable.

Since the source of E_{sc} is not concentrated at any given location, it can be conveniently expressed as being due to a set of multipoles concentrated at the origin. The two lowest order multipoles would be an electric dipole, $\mathbf{p}_{eqvt}$ and a magnetic dipole, $\mathbf{m}_{eqvt}$. Since the helical ensembles are much smaller than the ambient wavelength, it appears that optimally chiral helical strands must have maximal values of $\mathbf{m}_{eqvt}$. The magnetic dipole moment can be calculated by taking the projection of $\mathbf{E}_{sc}$ or $\mathbf{E}_m$ in the limit $kr \to \infty$ as

$$0\int^{\pi} d\theta \sin\theta \int_0^{2\pi} d\varphi\ \mathbf{E}_m(r)\cdot\mathbf{E}_m^*(r) = 0\int^{\pi} d\theta \sin\theta \int_0^{2\pi} d\varphi\ \mathbf{E}_{sc}(r)\cdot\mathbf{E}_m^*(r), \qquad (12)$$

in which $\mathbf{E}_m$ is the electric field radiated by the equivalent magnetic dipole,

$$4\pi\varepsilon_o \mathbf{E}_m(r) = -k^2 [\mu_o\varepsilon_o]^{1/2} r^{-2} \exp[jkr]\,[r\times\mathbf{m}_{eqvt}]. \qquad (13)$$

Several studies were carried out for different planewave incidence conditions and the results of these investigations are summarized now. From studying the magnitude of $\mathbf{m}_{eqvt}$ as a function of the ratio a/P for several different incident plane waves, we observe that when a/P ~ 0.24, optimal chirality is achieved because $\mathbf{m}_{eqvt}$ is maximal. The computed *optimal* value of the ratio a/P is, interestingly enough, not far from values reported for various helical polymers [14,15]. It is important to realize that chirality will not be observed unless $a/P \neq 0$ or $P/a \neq 0$, because in these two respective limits, the ensemble of scatterers is either linear or circular, and, thus, devoid of handedness. On the other hand, the ratio a/P cannot be very large either, because polymers in the helical configuration deviate only slightly from their linear counterparts [16]. Thus, that the optimal value of a/P turns out to be 0.24 is quite satisfactory.

Furthermore, it is obvious that by increasing α, $\mathbf{m}_{eqvt}$ can also be enhanced: but the spheres are small and α is only weakly dependent on $\varepsilon/\varepsilon_o$. Even so, it is recommended that α be as large as possible. Next, it was also found that increasing the number of spheres per ring (i.e., increasing M) is also helpful in increasing chirality by enhancing the number of dipole-dipole interaction paths. Short helices appeared to be, however, preferable to large ones; in other words N should be as small as possible.

EXPERIMENTAL RESULTS

As part of our experimental effort to test the viability of chiral composites, we devised a free-space measurement method, using a dielectric-loaded horn antenna and the HP8510A network analyzer to determine the reflection from an artificially chiral slab which is backed by a metal plate. A 41.5 mm thick chiral slab was made of Eccogel 90, into which were put in a certain number of miniature right-handed metallic springs; the metal content of the exposed area due to the introduction of the springs was set at 3.2% v/v. The horn antenna was arranged so as to simulate a linearly polarized planewave normally incident on the slab. The full details of our experimental efforts will appear elsewhere [17], but, for the purpose of illustration, shown in Fig. 4 is the reflected power measured over the 14.5-17.5 GHz frequency range. As control, yet another sample with 3.2% metallic content, but with each spring replaced by an equi-voluminal steel sphere was used; the measurements with the control sample are also shown in Fig. 4. Almost over the whole frequency range, it appears that the chiral sample reduces the reflected power more than the control sample, thus illustrating the effect of chirality. It should be noted that the chiral slab is solid, in contrast to the extant absorbing coatings which are largely porous and brittle (e.g., the lining of anechoic chambers).

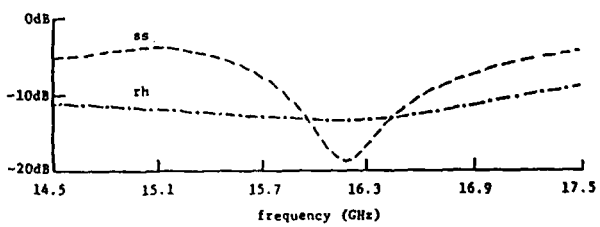

Figure 4 Measured reflected power when a linearly polarized planewave is normally incident on a chiral slab backed by a metal plate. The identifier 'rh' denotes 3.2% v/v metallic content in Eccogel 90 in the form of miniature right-handed metallic springs. The control sample has each spring replaced by a steel sphere ('ss').

When the concentration of metallic springs was found to exceed 4%, the reflected power density from the chiral sample started to increase. This was because the metallic springs made the chiral sample highly conducting, thereby giving rise to a big impedance mismatch at the air-sample interface. Therefore, we conjecture that the springs should be made up of dielectric media would be more appropriate, and helical polymers would be natural candidates for that role. Further experimental work, with dielectric springs instead of metallic ones, is in progress.

As has been mentioned earlier, it is necessary for the host material to be lossy in order for the composite to absorb EM radiation effectively. Therefore, we repeated the experiment described above with a 5mm thick chiral slab backed by a metallic plate. The matrix medium was a mixture of a silicone polymer and a non-silicone polymer; in particular, the non-silicone polymer was carbon-based with electron-withdrawing groups. The chiral inclusions were 40μ dia spheres made of Poly-γ-Benzyl-L-Glutamate, each PMG sphere coated with a 2-3μ coat of Poly(Methyl Methacrylate). Shown in Figure 5 is the measured reflected power from this sample over the 14.5-17.5 GHz frequency range, the inclusion concentration being about 1% v/v. This and other results lead us to believe that the use of chiral composites for absorption of microwave energy is very promising.

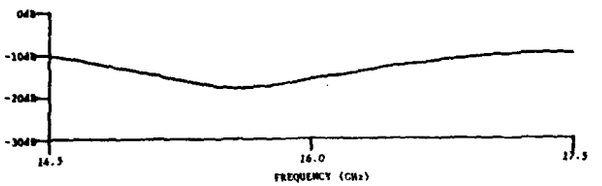

Figure 5 Measured reflected power when a linearly polarized planewave is normally incident on a 5mm thick chiral slab, backed by a metal plate. Microballoons made of PMG spheres coated with PMMA are immersed in a conducting polymer; the inclusion concentration is about 1% v/v.

REFERENCES

[1] A. Lakhtakia, V.K. Varadan and V.V. Varadan, *Appl. Opt.* 24, 4146-4154 (1985).
[2] L.S. Corley and O.Vogl, *Polymer Bull.* 3, 211-217 (1980).
[3] W.J. Harris and O. Vogl, *Polymer Preprints* 22, 309-312 (1981).
[4] J. Applequist, *Amer. Scientist* 75(1), 59-65 (1987).
[5] P. Drude, *Lehrbuch der Optik* (S. Hirzel, Leipzig, 1900).
[6] F.I. Fedorov, *Opt. Spectrosc. (USSR)* 6, 237-241 (159).
[7] A. Lakhtakia, V.V. Varadan and V.K. Varadan, *J. Opt. Soc. Am. A* 5, 175-184 (1988).
[8] R.A. Sutton, *J. Chem. Phys.* 28, 742-743 (1959).
[9] V.K. Varadan, in *Acoustic, Electromagnetic and Elastic Wave Scattering*, Eds.:V.K. and V.V. Varadan, (Pergamon, New York, 1980) 103-134.
[10] V.K. Varadan, V.V. Varadan and A. Lakhtakia, *J. Wave-Mater. Interact.* 2, 71-81 (1987).

[11] G. Heppke, D. Lötzsch and F. Oestricher, *Z. Naturforsch.* 41A, 1214-1218 (1986).
[12] J.D. Jackson, *Classical Electrodynamics* (McGraw-Hill, New York, 1975).
[13] V.V. Varadan, A. Lakhtakia and V.K. Varadan, *J. Appl. Phys.* 63, 280-284 (1988).
[14] T. Miyazawa, *J. Poly. Sci.* 55, 215-231 (1961).
[15] R.B. Setlow and E.C. Pollard, *Molecular Biophysics* (Addison-Wesley, Reading, MA, 1964).
[16] M.L. Elert and C.T. White, *Macromolecules* 20, 1411-1414 (1987).
[17] T. Guire, *Property Measurements of Chiral Composites at Microwave Frequencies*, MS Thesis, Pennsylvania State University (1988).

PRINCIPLES OF MICROWAVE INTERACTION WITH POLYMERIC AND ORGANIC MATERIALS

VIJAY K. VARADAN, VASUNDARA V. VARADAN AND AKHLESH LAKHTAKIA

Department of Engineering Science & Mechanics, and The Center for Engineering of Electronic and Acoustic Materials,
Pennsylvania State University, University Park, PA 16802.

ABSTRACT

Electromagnetic waves can discriminate between objects of different handedness due to their transverse nature, which implies that the origin of chirality need not necessarily be molecular as in the case of optically active media. Effectively chiral composites may, therefore, be constructed by embedding chiral microstructures in non-chiral host media.

INTRODUCTION

Many organic molecules occur as stereoisomers in enantiomorphic pairs, i.e., one isomer is the mirror image of the other one, but the two of them are not congruent with each other. The basis for the difference in the physical properties of the mirror-conjugates lies in the handedness or the chirality possessed by their molecular configurations. When an electromagnetic disturbance travels through a medium consisting of chiral molecules, it is forced to adapt to the handedness of the molecules. Electromagnetic (EM) waves can recognize the handedness of a chiral object primarily due to their transverse nature, i.e., the applicable vector, infinite-medium Green's function contains the *vector* distance between the source and the field points. From a microscopic, not molecular, point of view, therefore, it is possible that an effectively chiral composite medium may be constructed by embedding macroscopic chiral objects, all of the same handedness, in a dielectric host. The microstructure size should be large enough that the EM wave in the matrix can appreciate the handedness of the microstructure; at the same time, the microstructure size should be small enough so that the composite medium, consisting of achiral phases, is effectively chiral. By varying the concentrations and the sizes of the chiral inclusions, the properties of the composite medium may be altered to suit desired polarization characteristics. It has been observed by us that the introduction of chirality in an otherwise achiral, dielectric scattering volume radically alters its scattering and absorption characteristics [1]. Particularly with the proliferation of research on novel polymers, it is possible that such materials can turn out to be of considerable importance for many electromagnetic applications It has been demonstrated [2,3] that it is possible to produce polymers which possess no true axisymmetric centers, and helical strands -- either left- or right-handed -- can be produced.

WHAT IS CHIRALITY?

In order to understand the characteristics of chiral media, one has to begin with the notions of the intrinsic polarization and the intrinsic magnetization vectors. Free space is vacuum, i.e., it does not contain any matter. The constitutive relations for the electromagnetic fields in free space can be adequately expressed in the form

$$\mathbf{D} = \epsilon_0 \mathbf{E}; \qquad \mathbf{B} = \mu_0 \mathbf{H}. \tag{1}$$

Fields in material media induce bound charges too. Collectively, the constitutive equations in material media have the form

Mat. Res. Soc. Symp. Proc. Vol. 124. • 1988 Materials Research Society

$$\mathbf{D} = \varepsilon_o \mathbf{E} + \mathbf{P}; \qquad \mathbf{B} = \mu_o \mathbf{H} + \mathbf{M}, \tag{2}$$

in which **P** and **M**, respectively, are the polarization and the magnetization. The polarization **P** is nothing but the average electric dipole moment per unit volume, while **M** is the average magnetic dipole moment per unit volume.

In non-magnetic dielectric media, a prominent contribution to **P** comes from the charge separation in the atom, and is designated as *electronic* polarization. This is because an applied electric field causes displacement of the electrons with respect to the atomic nucleus. *Atomic* or *ionic* polarization may be caused by the displacement of atoms or ions in a molecule by electric fields. Some media may also have permanent electric dipole moments because the centers of the negative and the positive charges are not co-incident. Without an applied electric field, these permanent dipoles are randomly aligned, and their effect is nulled on the average; however, when an electric field is applied, then these dipole moments line up to give rise to *orientational* polarization. In linear media, these various contributions can be summed up as

$$\mathbf{P} = \chi_e \varepsilon_o \mathbf{E}; \qquad \mathbf{D} = \varepsilon_o [1 + \chi_e] \mathbf{E} = \varepsilon \mathbf{E} \tag{3}$$

χ_e being the electric susceptibility, and ε the (real) dielectric constant.

Each of the three types of polarizations are frequency-dependent; however, as the frequency increases the polarization may not be able to follow the oscillations of the applied field. Orientational polarization concerns itself with the most massive entities; hence, it is the first to be unable to reach its equilibrium value. The loss of orientational polarization occurs at lower frequencies for macromolecules and large-chain polymers, and it occurs at higher frequencies for small molecules. As the frequency increases even further, first the atomic, and then the electronic, polarizations also fall off. Typically, the times for orientational, atomic, and electronic polarizations to reach their equilibrium values are 10^{-9} s, 10^{-13} s and 10^{-15} s, respectively. Highly elongated and aligned molecules tend to give rise to anisotropic properties.

Electronic polarizability is due to the bound electrons. Therefore, it increases when the atomic radius also increases. This implies that polymers with delocalized electrons will have larger electronic polarizations; for example, conducting polymers with electron-withdrawing groups. On the other hand, polymers possessing highly asymmetric positive and negative charge densities will have large orientational polarizabilities. Too some extent, these considerations permit one to tailor the frequency-dependent dielectric constants of polymers.

Under the influence of the externally applied field, the polar molecules rotate towards an equilibrium distribution. If the polar molecules are massive, or if the frequency is very high, the rotatory motion lags behind the applied field and equilibrium is never attained. Thus, the polarization is no longer in sync with the applied field, giving rise to a conduction current density. This results in thermal dissipation of energy. Thus, ohmic losses in dielectric media give rise to a conductivity σ, which is incorporated in the time-harmonic constitutive equations by making ε complex, i.e.

$$\mathbf{D} = \varepsilon \mathbf{E}, \qquad \varepsilon = \varepsilon_o [1 + \chi_e] + j\sigma/\omega, \tag{4}$$

$\omega = 2\pi f$ being the circular frequency. It would also follow that conduction losses increase with temperature, since the conduction charges have enhance mobilities at higher temperatures. Furthermore, more massive molecules are less able to follow the applied field, which means that the ratio $\tan\delta_e = \mathrm{Im}\{\varepsilon\}/\mathrm{Re}\{\varepsilon\}$ is generally higher for such substances. Unsaturated polymers will also have higher $\tan\delta_e$ because of the increased availability of electrons for conduction. It should also be noted that while charge transport in metals takes place via electrons only, charge transport in polymers may even involve ions.

There are microscopic currents due to electron spin and the motion of electrons around the nucleus. These microscopic currents act as sources of macroscopic magnetic fields, thereby endowing the electrons and the atoms with magnetic dipole moments; but these currents do not

produce macroscopic charge transport. In magnetic media, the effect of the magnetic dipole moments cannot be ignored, giving rise to the magnetization M. Again, for linear media, it can be stated that

$$\mathbf{M} = \chi_m \mu_o \mathbf{H}; \qquad \mathbf{B} = \mu_o[1 + \chi_m]\mathbf{H} = \mu\mathbf{H} \tag{5}$$

χ_m being the magnetic susceptibility, and μ the (real) permeability. Magnetic ohmic losses can be incorporated by making μ complex in the same fashion as the electric ohmic losses.

Chirality was first observed as optical activity, which is the rotation of the plane of polarization in certain linear isotropic media. Pasteur interpreted the observations of Biot and Arago by imagining that the arrangement of atoms within an optically active material is mirror-asymmetric [4]. Phenomenological studies by Drude [5] indicated that the rotation of the plane of polarization is predicted by Maxwell's equations provide P has an additional term proportional to $\nabla\times\mathbf{E}$. Further studies [6,7] have shown that even M must have a term proportional to $\nabla\times\mathbf{H}$. Thus, the constitutive equations for homogeneous chiral media have the form

$$\mathbf{D} = \epsilon[\mathbf{E} + \beta\nabla\times\mathbf{E}]; \qquad \mathbf{B} = \mu[\mathbf{H} + \alpha\nabla\times\mathbf{H}], \tag{6}$$

in which α and β are the chirality parameters. Since the curl is a pseudo-vector under a reflection of the coordinate system, the mirror-asymmetry of chiral media is immediately apparent in (6). The nonlocal character of (6) needs to be noticed, because the polarization P (resp. magnetization M) depends not only on E (resp. H) but also on the *circulation* of E (resp. H). In a not-too-rigorous manner, one may even observe that P (resp. M) has a component due to the time-rate of change of H (resp. E), *vide* Faraday and Ampere-Maxwell laws. Reciprocity demands that $\alpha = \beta$, a constraint which is generally obeyed by optically active media [8].

Thus, optically active media (mostly organic materials) are naturally chiral, at optical frequencies; interesting examples include the famous Watson-Crick double-helix representation of the DNA molecule. But the underlying principle behind chirality is the mirror-asymmetry of the constituent microstructure. Therefore, artificially chiral media can be constructed by embedding chiral microstructures in non-chiral host media, such composites being effectively chiral even at the sub-optical, and even in the high mm-wave, frequencies. The microstructure size should be large enough compared to the wavelength in the matrix medium so that the spatial variation of the EM field can sense its handedness; at the same time, it should be small enough so that, at least in some frequency range, the composite should appear to be effectively chiral.

In a non-chiral medium, the simplest EM waves that can propagate are linearly-polarized plane waves. But in chiral media the simplest waves are either left-circularly polarized, or they are right-circularly polarized, plane waves; it is important to note that the left- and the right-handed waves travel with different phase velocities [7]. Furthermore, when a linearly polarized wave hits a chiral scatterer embedded in a non-chiral medium, the scattered field has both LCP and RCP components. Now, let us envision the propagation of a plane wave in an artificial chiral medium which contains a certain density of chiral inclusions in a host phase. Multiple scattering [9] between the chiral inclusions will create LCP and RCP fields. In the right frequency range only LCP or RCP fields will be allowed to propagate in the forward direction, thereby rendering the composite effectively chiral.

ANTI-REFLECTION COATINGS

There is considerable interest in developing low-weight coatings which will reduce reflections from metallic surfaces. In view of our previous studies [1], it appeared that artificial chiral media may be just the thing to fill the bill. To further investigate this premise, we considered the planewave reflection characteristics of a chiral coating, of thickness d, on top of a perfectly conducting plane. The chiral layer has a permittivity ϵ, a permeability $\mu = \mu_o$, as well

the chirality parameter ß, *vide* the constitutive relations [7]

$$\mathbf{D} = \varepsilon[\mathbf{E} + \beta\nabla\times\mathbf{E}]; \qquad \mathbf{B} = \mu_0[\mathbf{H} + \beta\nabla\times\mathbf{H}]. \tag{7}$$

The chiral dielectric medium is low-loss so that its relative permittivity $\varepsilon/\varepsilon_0$ is complex with $\mathrm{Im}\{\varepsilon/\varepsilon_0\} << \mathrm{Re}\{\varepsilon/\varepsilon_0\}$. The thickness d of the coating was assumed to be 2 mm for all of our numerical studies, and the reflection coefficients, R_{TE} and R_{TM} [10], were computed, respectively, for TE- and TM- polarized planewave incidence cases.

A design of a wideband anti-reflection chiral coating cannot afford to have both $\varepsilon/\varepsilon_0$ and β independent of frequency. Once it became clear from numerical experimentation that (i) chirality is ineffective in the reduction of the reflection efficiency if $\varepsilon/\varepsilon_0$ is purely real, and (ii) that either β or $\varepsilon/\varepsilon_0$ or both must be frequency dependent in order to obtain a wideband anti-reflection coating, the design of such a coating became more of an optimization problem. Shown in Figs. 1 - 3 is a sample design with $\varepsilon/\varepsilon_0$ assumed to be constant, whereas $\beta = \beta(f)$ assumed is shown in Fig. 1. In Figs. 2 and 3, the enhancement of the absorption efficiency of over a 50-300 GHz frequency range by incorporating this frequency dependent $\beta = \beta(f)$ is illustrated, for the TE- and TM- polarization incidence cases, respectively; θ_0 is the angle of incidence with respect to the normal. The relative permittivity $\varepsilon/\varepsilon_0$ is set at 5.0 + i0.05 for all frequencies considered. It should be noted from these two figures that whereas the design objective of achieving R_{TE} and R_{TM} less than 20% for $50 \le f \le 300$ GHz and $0° \le \theta_0 \le 30°$ can be achieved using the β of Fig. 1, the reflection efficiencies hover around 92% if β were to be set equal to zero.

From our numerical studies, several conclusions can be drawn. Firstly, in reducing reflection if a larger constant β is used, then the values of $\varepsilon/\varepsilon_0$ tend to decrease over the entire frequency band of interest, a goal which appears to be desirable for a material scientist. However, this also tends to reduce the bandwidth over which the desired absorption efficiencies can be achieved. Secondly, chirality in the absence of a lossy ε is of no use whatsoever in reducing reflected power density: conducting polymers constitute feasible matrix media. Therefore, chirality serves only as an enhancement factor for absorption, but of itself it is not an absorbing mechanism. Thirdly, and very importantly, both $\varepsilon/\varepsilon_0$ and β should be frequency dependent. This last conclusion, however, was not verified here because of the complexities of multivariate optimization problems.

EQUIVALENT DIPOLE MOMENTS OF HELICAL ENSEMBLES

Thus, the significance of chiral media cannot be denied. As has been mentioned earlier, effectively chiral media can be constructed by embedding chiral microstructures in non-chiral host media. Such microstructures may be macromolecular polymers with helical conformations [2,3,11]. What is of interest for EM use is the optimization of the polymer's chirality: the parameters governing the helix geometry must be examined for their effect on an incident EM wave. We decided to model helical polymers by an arrangement of spherical beads (in themselves, large molecules for our purposes) suspended on a helical strand which is indistinguishable from the surrounding space. Whereas the spheres are also sufficiently small to be modeled as point electric dipoles, the overall size of the finite helical arrangement can be large enough to be in the high-frequency regime. The helix on which the tiny spheres are located is given, in a cartesian co-ordinate system, by the radius vector

$$\mathbf{r}(\xi) = a[\mathbf{u}_x \cos\xi + \mathbf{u}_y\, h \sin\xi] + \mathbf{u}_z\, P(\xi/2\pi); \quad \xi \in (-\infty, \infty), \tag{8}$$

where a is the radius and P is the pitch of the helix; the handedness parameter $h = +1$ if the helix curls up in the +z direction according to the right-handed rule, and $h = -1$, if otherwise; and $\mathbf{u}_x$, $\mathbf{u}_y$, and $\mathbf{u}_z$ are the unit orthogonal vectors. Let the helix be finite in extent, having 2N+1 complete rotations, N being a positive integer or zero. On each of the 2N+1 rings of this finite helix, there are 2M+1 spheres arranged over equal-$\Delta\xi$ segments, M being a positive integer greater than zero. Each of the spheres in this arrangement has a radius b which is small enough

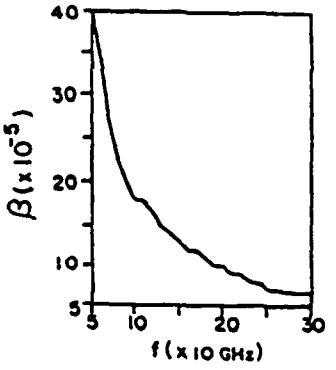

Figure 1 The frequency profile $\beta = \beta(f)$ used for the results shown in Figs. 2 and 3. The parameter β carries the unit of meter.

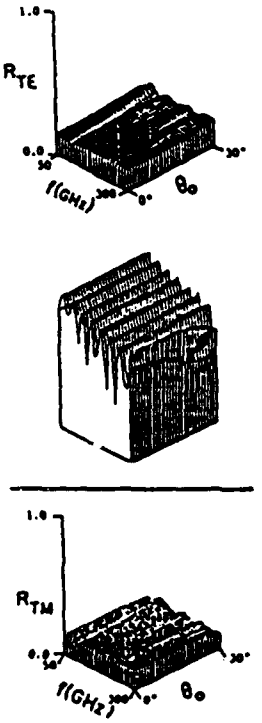

Figure 2 Reflection efficiency R_{TE} plotted as a function of θ_0 and frequency f for a 2 mm thick anti-reflection coating. The complex permittivity $\varepsilon/\varepsilon_0 = 5.0 + i0.05$. In the upper figure the $\beta = \beta(f)$ of Fig. 1 is used while in the lower figure β is set equal to 0.0 m.

Figure 3 Same as Fig. 2, but R_{TM} is plotted.

that no two of them ever touch. The spheres possess a dielectric constant ϵ, and if a field $\boldsymbol{E}_m$ illuminates the m^{th} sphere, an electric dipole moment [12]

$$p_m = \alpha\, \boldsymbol{E}_m = 4\pi\epsilon_o b^3\, (\epsilon - \epsilon_o)(\epsilon + 2\epsilon_o)^{-1}\ \ \boldsymbol{E}_m \tag{9}$$

is induced on it, with α being the isotropic electric polarizability of the spheres.

The EM field incident on the helical ensemble, E_{inc}, can be any arbitrary field so long as its source is not located anywhere inside or on the minimum sphere circumscribing the helix. But the field $\boldsymbol{E}_m$ actually incident on the m^{th} sphere is not $E_{inc}(r_m)$ alone; it also consists of the fields re-radiated by all of the other spheres as well [9,13]. With this reasoning, the system of 3Q simultaneous equations,

$$\boldsymbol{E}_m = E_{inc}(r_m) + \alpha k^2 (4\pi\epsilon_o)^{-1} \sum_{n,n\neq m} \left[R_{mn}^{-1} \exp[jkR_{mn}] \cdot \right.$$
$$\left. \cdot \{ g_{mn} n_{mn} (n_{mn} \cdot \boldsymbol{E}_n) - (1/3)[g_{mn} - 2]\, \boldsymbol{E}_n \} \right], \tag{10}$$

must be solved, in order to obtain the various exciting fields $\boldsymbol{E}_m$. Here, $R_{mn} = |r_m - r_n|$, $n_{mn} = (r_m - r_n)/R_{mn}$, $g_{mn} = 3(kR_{mn})^{-2} - 3j(kR_{mn})^{-1} - 1$, while the wavenumber $k = \omega\sqrt{(\epsilon_o\mu_o)}$. Once the solution of (10) has been obtained, the total scattered field for $kr \to \infty$ can be computed from

$$4\pi\epsilon_o\, E_{sc}(r) = \alpha\, k^2 r^{-1} \exp[jkr] \sum_m \left\{ \exp[-jkr_m \cdot r/r]\, [\boldsymbol{E}_m - r(r \cdot \boldsymbol{E}_m)/r^2] \right\}. \tag{11}$$

Multiple scattering between the spheres would ensure that $\boldsymbol{E}_m \neq E_{inc}(r_m)$. It is to be expected that the exciting fields should reflect the chirality of the helical ensemble, because the ensemble of unit vectors $\{n_{mn}\}$ used in (10) is handed, even though the scalar distances $\{R_{mn}\}$ do not depend on h. This, indeed turned out to be the case. From our computations a very interesting conclusion can be drawn: Provided $k_{inc} \parallel u_x$ or $k_{inc} \parallel u_z$, then (i) only $u_y \cdot \boldsymbol{E}_m$ changes sign with h when $u_y \cdot E_{inc} = 0$, and (ii) only $u_y \times \boldsymbol{E}_m$ changes sign with h when $u_y \times E_{inc} = 0$. Symmetries of similar natures are also present when $k_{inc} \parallel u_y$, but they are not so easily describable.

Since the source of E_{sc} is not concentrated at any given location, it can be conveniently expressed as being due to a set of multipoles concentrated at the origin. The two lowest order multipoles would be an electric dipole, p_{eqvt} and a magnetic dipole, m_{eqvt}. Since the helical ensembles are much smaller than the ambient wavelength, it appears that optimally chiral helical strands must have maximal values of m_{eqvt}. The magnetic dipole moment can be calculated by taking the projection of E_{sc} on E_m in the limit $kr \to \infty$ as

$$\int_0^{\pi} d\theta \sin\theta \int_0^{2\pi} d\varphi\, \boldsymbol{E}_m(r) \cdot \boldsymbol{E}_m^*(r) = \int_0^{\pi} d\theta \sin\theta \int_0^{2\pi} d\varphi\, E_{sc}(r) \cdot \boldsymbol{E}_m^*(r), \tag{12}$$

in which $\boldsymbol{E}_m$ is the electric field radiated by the equivalent magnetic dipole,

$$4\pi\epsilon_o \boldsymbol{E}_m(r) = -\, k^2\, [\mu_o\epsilon_o]^{1/2}\, r^{-2} \exp[jkr]\, (r \times m_{eqvt}). \tag{13}$$

Several studies were carried out for different planewave incidence conditions and the results of these investigations are summarized now. From studying the magnitude of m_{eqvt} as a function of the ratio a/P for several different incident plane waves, we observe that when $a/P \sim 0.24$, optimal chirality is achieved because m_{eqvt} is maximal. The computed *optimal* value of the ratio a/P is, interestingly enough, not far from values reported for various helical polymers [14,15]. It is

important to realize that chirality will not be observed unless $a/P \neq 0$ or $P/a \neq 0$, because in these two respective limits, the ensemble of scatterers is either linear or circular, and, thus, devoid of handedness. On the other hand, the ratio a/P cannot be very large either, because polymers in the helical configuration deviate only slightly from their linear counterparts [16]. Thus, that the optimal value of a/P turns out to be 0.24 is quite satisfactory.

Furthermore, it is obvious that by increasing α, m_{eqvl} can also be enhanced: but the spheres are small and α is only weakly dependent on ϵ/ϵ_0. Even so, it is recommended that α be as large as possible. Next, it was also found that increasing the number of spheres per ring (i.e., increasing M) is also helpful in increasing chirality by enhancing the number of dipole-dipole interaction paths. Short helices appeared to be, however, preferable to large ones; in other words N should be as small as possible.

EXPERIMENTAL RESULTS

As part of our experimental effort to test the viability of chiral composites, we devised a free-space measurement method, using a dielectric-loaded horn antenna and the HP8510A network analyzer to determine the reflection from an artificially chiral slab which is backed by a metal plate. A 41.5 mm thick chiral slab was made of Eccogel 90, into which were put in a certain number of miniature right-handed metallic springs; the metal content of the exposed area due to the introduction of the springs was set at 3.2% v/v. The horn antenna was arranged so as to simulate a linearly polarized planewave normally incident on the slab. The full details of our experimental efforts will appear elsewhere [17], but, for the purpose of illustration, shown in Fig. 4 is the reflected power measured over the 14.5-17.5 GHz frequency range. As control, yet another sample with 3.2% metallic content, but with each spring replaced by an equi-voluminal steel sphere was used; the measurements with the control sample are also shown in Fig. 4. Almost over the whole frequency range, it appears that the chiral sample reduces the reflected power more than the control sample, thus illustrating the effect of chirality. It should be noted that the chiral slab is solid, in contrast to the extant absorbing coatings which are largely porous and brittle (e.g., the lining of anechoic chambers).

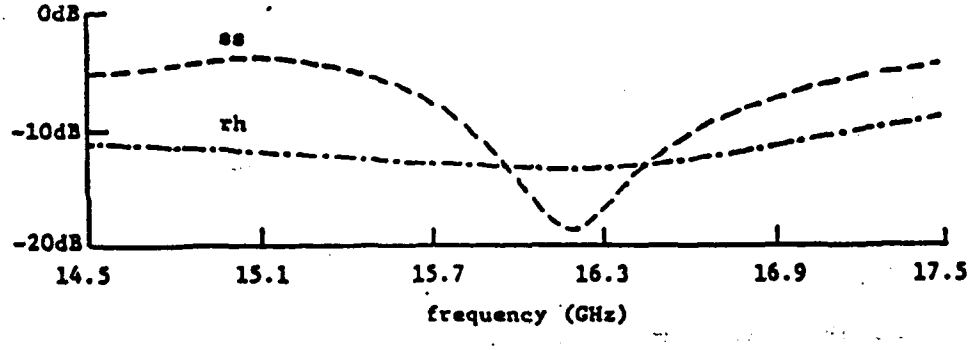

Figure 4 Measured reflected power when a linearly polarized planewave is normally incident on a chiral slab backed by a metal plate. The identifier 'rh' denotes 3.2% v/v metallic content in Eccogel 90 in the form of miniature right-handed metallic springs. The control sample has each spring replaced by a steel sphere ('ss').

[11] G. Heppke, D. Lötzsch and F. Oestricher, Z. *Naturforsch.* 41A, 1214-1218 (1986).
[12] J.D. Jackson, *Classical Electrodynamics* (McGraw-Hill, New York, 1975).
[13] V.V. Varadan, A. Lakhtakia and V.K. Varadan, *J. Appl. Phys.* 63, 280-284 (1988).
[14] T. Miyazawa, *J. Poly. Sci.* 55, 215-231 (1961).
[15] R.B. Setlow and E.C. Pollard, *Molecular Biophysics* (Addison-Wesley, Reading, MA, 1964).
[16] M.L. Elert and C.T. White, *Macromolecules* 20, 1411-1414 (1987).
[17] T. Guire, *Property Measurements of Chiral Composites at Microwave Frequencies*, MS Thesis, Pennsylvania State University (1988).